Preliminay Report
of
The Hakuho Maru Cruise KH-89-1

June 20 - July 13, 1989

Izu-Ogasawara, Shikoku Basin and Kashima Oki

(KAIKO-NANKAI, ODP)

1990
Ocean Research Institute
University of Tokyo

Preliminary Report of the Hakuho Maru Cruise KH-89-1

June 20 - July 13, 1989

Izu-Ogasawara, Shikoku Basin and Kashima Oki

(KAIKO-NANKAI, ODP)

by
The Scientific Members of the Cruise
Edited by
Jiro SEGAWA

Research Vessel HAKUHO-MARU

The Ocean Research Institute has two research vessels, **Tansei-maru** and **Hakuho-maru** for multi-disciplinary research activities in the ocean. **Tansei-maru** (257.69 tons) is engaged in 18 to 20 scientific cruises every year in the seas adjacent to the Japanese Islands.

The new **Hakuho-maru** was launched on October 28, 1988 and put in service on May 1, 1989. Its operating characteristics are listed below. Ten laboratories including multi-purpose dry, semi-dry and wet labs, a freezing lab and a clean room encompass 387.71m, accommodating Seabeam, NOAA-GMS-BS satellites receiver, isotope treatment facilities, acoustic biomass survey system, CTD, Doppler current meter, liquid N_2tank, multi-channel seismic profiler, 3.5 kHz subbottom profiler, SSBL acoustic transponder system, towed side-scan-sonar, gravimeter, high-precision gyro, and data processing system linked with navigation instruments by LAN and Ethernet. A research room equipped with word processors and meeting facilities is also installed. It was built to replace the old "Hakuho-maru" completed in March 1967 and operated until the end of the fiscal year 1988.

Operating Characteristics of R.V. Hakuho-Maru

Keel Laid : May 9, 1988
Launched : October 28, 1988
Completed : May 1, 1989
Gross Tonnage : 3,987 tons
Length (o.a.) : 100.00m
Length (b.p.) : 90.00m
Bredth (mld.) : 16.20m
Depth (mld.) : 6.35m
Draft (mld.) : 6.00m
Cruising Speed : 16 knots
Complement : 89 including 35 Scientists
Propulsion System : Diesel for cruising ;
Electric for slow speeds & dynamic positioning
Engine : 1,900ps x 720rpm x 4 Motor : 460KW x 12P (20~92/-20~-65 rpm) x 2
Propeller : 4-wing skewed CPP 3,700mm x 4,791 mm x 2
Twin shaft & twin rudder
Bow Thruster : 4-wing CPP, 187rpm x 2 Stern Thruster : 4-wing CPP, 251rpm x 1
Main Generator : for propulsion, 1,550 KVA (1,085 KW) x 2
for electric power, 893.75 KVA (715 KW) x 3
Electric power supply : AC 450V 3 phase 60Hz x 2 [main]
AC 100V 80KVA 60 Hz x 2, AC 115V 6KVA 400 Hz x 2 [precision]
Navigation : Gyro compass, Radar & ARPA, Auto-pilot device, Joystic control system, Auto-nav. system including Loran C, NNSS, GPS, Doppler Log, EM Log, Cs frequency standard, Data logger and track display
Deck Gears :

#1 Heavy duty winch with 15,000m of 14mm ϕ steel wire

#2 Armoured cabel winch with 12,000m of 8.15mm ϕ Ti-wire for CTD
Swell Compensator (1.5m strole) for the above 2 winches

#3 Hydrographic winch with 12,000m of 6.4mm ϕ Ti-wire

#4 Heavy duty winch with 7,000m of 9mm ϕ steel wire

#5 Rope winch for 6,000m x 14mm ϕ nylon rope

#6 BT winch with 1,000m x 3mm ϕ steel wire removable

#7 Nonmagnetic rubber-coated cable winch for magnetometer, 700m x 16mm ϕ

#8 BT winch with 1,500m x 3mm ϕ steel wire [bow starboard side]

A-shaped stern gantry : 7.0m (w) x 8.0m (H) x 1, 11ton max load
Side-beam for starboard deck work : 4m stroke, 11ton max load x 1
Deck crane : aft #2 deck with 3 tons max capacity x 1
Constructed by : Mitsubishi Heavy Industries Co., Ltd.
(Shimonoseki Shipyard & Engine Works)

HAKUHŌ MARU

GENERAL ARRANGEMENT

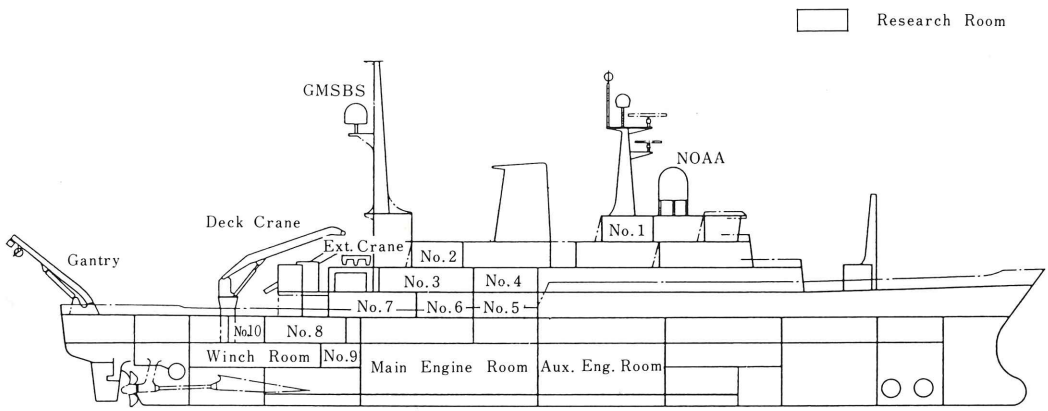

Preface

This is a preliminary report of the first research cruise KH-89-1 by the newly-built research vessel 'Hakuho-Maru' Junior of the Ocean Research Institute, the University of Tokyo.

The cruise was conducted from 20 June to 13 July 1989, starting from the Harumi Pier, Tokyo, and ending at the Yokosuka Harbor, Kanagawa Prefecture, with an intermediate break at Yokosuka for the exchange of participants and research equipments. In the first leg of this cruise between 20 June and 30 June, emphasis was laid upon detailed examinations of the research devices newly equipped as well as actual geophysical measurements. The operation/observations during the first leg included those of gravity, inertial navigation, acoustic positioning, sea beam mapping, three-component and total geomagnetic measurement, deep-towed geomagnetic measurement, controlled source electrical sounding, sea floor magnetotellurics and heat flow.

In the second leg between 4 July and 13 July the operation was focused on site surveys for the International Kaiko-Nankai Program which will be carried out in August this year. The site surveys were conducted at the Tenryu River Continental Slope over to the Nankai Trough, using a deep-towed TV camera and a side-scanning sonar. The seabeam mapping, gravity measurement and acoustic tomographic experiment were also conducted in this leg.

Taking advantage of this publication I would like to give a comment on and thank for the wholesale co-operation of the Japan Marine Science and Technology Center in the case of deep-tow photographing, which resulted in new findings of distribution and characteristic features of the sea floor sedimentation.

Jiro SEGAWA
Chief Scientist

CONTENTS

Preface

1. Scientists Aboard the R.V. Hakuho Maru for the Cruise KH-89-1 1

2. Time Table and Positions of Works 2

2.1 Index Maps of the Cruise KH-89-1 2

2.2 List of Research Stations in the Cruise KH-89-1 4

3. Topics 6

3.1 New Geophysical Equipments of the Hakuho Maru 6

3.2 Recent Techniques of the Sea Floor Study 7

3.3 ODP Techniques Involving Wide Applications 21

4. Geodetic and Geophysical Measurements 25

4.1 Gravity Measurements and Test of Inertial Navigator 25

4.2 Bathymetric Mapping Using the Sea Beam System 30

4.3 The Geomagnetic Total Force Measurement 41

4.4 Magnetic Measurement by Means of a Deep-Towed Proton magnetometer 44

4.5 Measurement of Three Component Geomagnetic Field by STCM 50

4.6 Electrical Sounding of the Sea Floor Using Controlled Electromagnetic Source Method (MOSES) 58

4.7 Magnetotelluric Study of the Sea Floor 80

4.8 Heat Flow Measurements Around the Zenisu Ridge 88

4.9 Heat Flow Measurement with Acoustic Digital Data Telemetry 100

4.10 A Super-Short-Baseline (SSBL) Transponder Navigation System 102

4.11 Report on ODP Nankai Downhole Observatory (ONDO) Tested on KH89-1 Cruise of Hakuho-maru 105

4.12 Measurement of Oceanic Current by Means of the IES (Inverted Echo Sounder) 128

5. Deep-towed TV and side-scanning sonar observation at the Kaiko-Nankai sites 134

5.1 Principal Purposes of Investigation 134

5.2 Brief Description of Instruments 137

5.2.1 JAMSTEC deep tow camera 137

5.2.2 JAMSTEC deep tow sonar 137

5.2.3 Deck Arrangement of the Apparatus 140

5.2.4 Position Fixing for Deep-Towed Survey 145

5.3 Brief Description of Observation 146

5.3.1 Tracks of Observation and Brief Description of Each Line 146

Line 1: South of Omaezaki (July 5) 150
(Camera : DT-1)

Line 2 : Across mud mound in the Nankai Trough (July 6) 156
(Camera : DT-2 and DT-3)

Line 3 : Tenryu canyon and canyon wall (July 7) 157
(Camera : DT-4, DT-5 and DT-6)

Line 4 : First deformation front (July 8) 159
(Camera : DT-7)

Line 5 : Along-contour on deformation front (July 9) 162
(Side Scan Sonar : DT-8 and DT-9)

Line 6 : Upper Nankai prism (July 10) 166
(Camera : DT-10)

Line 7 : East Zenisu thrust and mud volcano (July 12) 167
(Camera : DT-11 and DT-12)

5.3.2 Cross-Section with Time Table, and Table of Positions 168

5.4 Discussion and Comments 197

5.5 Summary 204

1. SCIENTISTS ABOARD THE R.V. HAKUHO MARU FOR THE CRUISE KH-89-1

SEGAWA, Jiro	[Chief Scientist] Ocean Research institute, University of Tokyo
FUJIMOTO, Hiromi	Ocean Research Institute, University of Tokyo
ASHI, Jun-ichiro	Ocean Research Institute, University of Tokyo
BAPAT, Vinit	Ocean Research Institute, University of Tokyo
BOULEGUE, Jacques	Universite Pierre et Marie Curie
CAMBRAY, Herve	Ocean Research Institute, University of Tokyo
CHAMOT-ROOKE, Nicolas	Department de Geologie, Ecole Normale Superieure
FURUTA, Toshio	Ocean Research Institute, University of Tokyo
ICHIKITA, Takao	Department of Earth Science, Kobe University
IIYAMA, Toshimichi	Department of Earth Sciences, Chiba University
KANAZAWA, Toshihiko	Department of Geophysics, University of Tokyo
KINOSHITA, Hajimu	Department of Earth Sciences, Chiba University
KINOSHITA, Masataka	Earthquake Research Institute, University of Tokyo
KOIZUMI, Kin-ichiro	Ocean Research Institute, University of Tokyo
KOIZUMI, Tooru	Department of Earth Sciences, Chiba University
KOBAYASHI, Kazuo	Ocean Research Institute, University of Tokyo
MITSUZAWA, Kyohiko	JAMSTEC
MONMA, Hiroyasu	JAMSTEC
MOTTA, Joaquim	Ocean Research Institute, University of Tokyo
MURAYAMA, Masashi	Ocean Research Institute, University of Tokyo
NAGAYA, Yoshiharu	Hydrographic Department
NAKAKUKI, Tomoeki	Department of Earth Sciences, Chiba University
NAKANISHI, Masao	Ocean Research Institute, University of Tokyo
NANBU, Hiroki	Department of Earth Sciences, Chiba University
OGAWA, Yujiro	Department of Geology, Kyushu University
OKADA, Makoto	Ocean Research Institue, University of Tokyo
OTSUKA, Kiyoshi	JAMSTEC
OSHIDA, Atsushi	Ocean Research Institute, University of Tokyo
OUBINA, Jose	Ocean Research institute, University of Tokyo
SAYANAGI, Keizo	Ocean Research Institute, university of Tokyo
SEAMA, Nobukazu	The Graduate School of Science & Technology, Kobe University
SOH, Wonn	Ocean Research institute, University of Tokyo
TAKEUCHI, Akira	College of General Education, Toyama University
TAKEUCHI, Tomoyoshi	University of Electro-Communications
TOH, Hiroaki	Ocean Research Institute, University of Tokyo
WATANABE, Masaharu	Ocean Research Institute, University of Tokyo
YAMAGATA, Takeshi	Department of Geology, Kyushu University
YAMANAKA, Masashi	University of Electro-Communications
YANG, Chul Soo	Ocean Research Institute, University of Tokyo

2. TIME TABLE AND POSITIONS OF WORKS

2.1 Index Maps of the Cruise KH-89-1

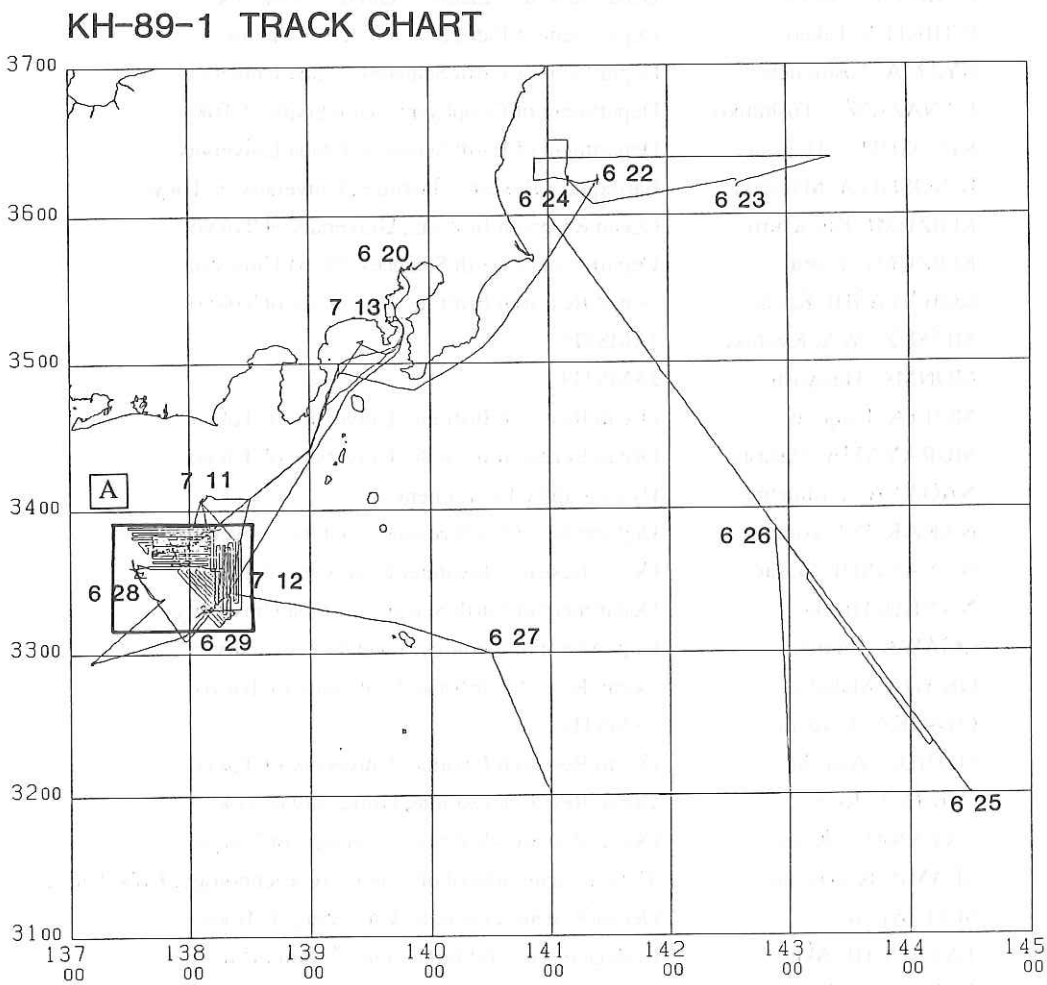

Fig. 2.1.1 Track chart of KH-89-1. Numerical figures indicate positions at 00:00 (GMT) of month-day.

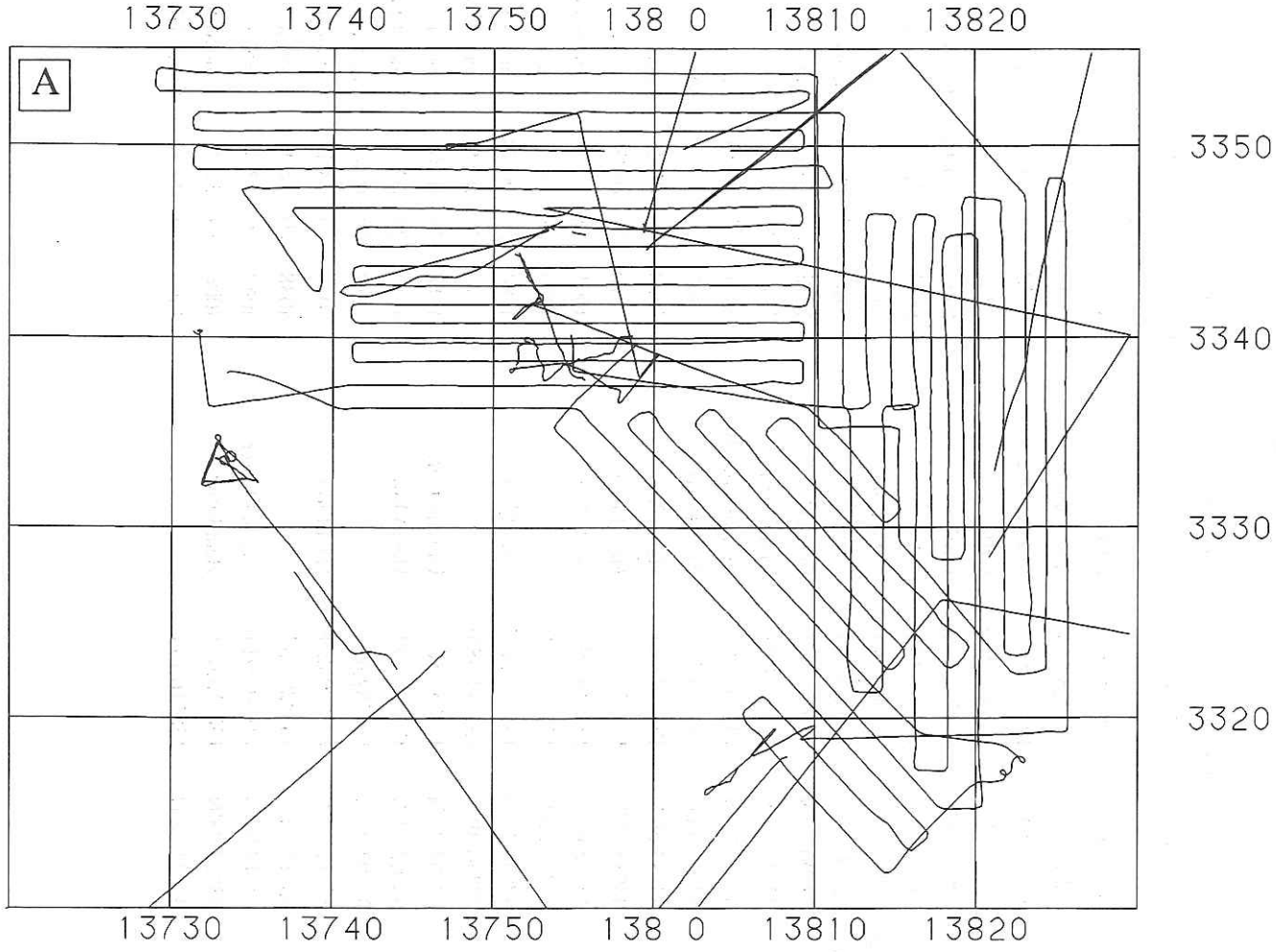

Fig. 2.1.2 Track chart of KH-89-1 in the Kaiko-Nankai site.

2.2 List of Research Stations in the Cruise KH 89-1

Site No.	Position Lat.	Long.	Investigation	Water Depth(m)	Date & Time(SST)		Remarks
Leg 1					June		
CS6	36°14.00'N	141°25.08'E	OBI	1286	21	20:14	Set
	36°13.97'N	141°25.65'E	Transponder	1317	21	20:28	Set
	36°12.60'N	142°35.84'E	ONDO Test	5633	23	08:06	Start
CS 4	36°14.30'N	141°09.99'E	OBI	764	23	16:16	Launch
JK19	32°22.06'N	144°11.97'E	OBEM	5432	25	10:18	Launch
JK20A	31°59.83'N	143°00.10'E	OBE	5674	26	15:09	Launch
JK20B	31°59.64'N	143°00.09'E	OBM S4	5693	26	15:26	Launch
JK21	32°00.03'N	140°59.93'E	OBM S5	2702	27	00:29	Launch
JK22	33°00.10'N	140°30.07'E	OBM C3	1218	27	08:12	Launch
	33°34.53'N	137°33.00'E	Transponder A	3813	27	21:47	Set
	33°32.36'N	137°32.00'E	Transponder B	3891	27	22:11	Set
	33°32.54'N	137°24.25'E	Transponder C	3792	27	22:34	Set
	33°33.69'N	137°32.94'E	Heat Flow	3828	28	04:25	Landed
	33°35.70'N	137°32.60'E	Heat Flow	3870	28	09:05	Landed
ST2	33°22.62'N	137°44.29'E	Heat Flow	4061	28	17:28	Landed 1st
ST2	33°22.86'N	137°44.26'E		4073	28	18:31	Landed 4th
ST10	32°56.27'N	137°11.30'E	Heat Flow	4184	29	00:53	Landed 1st
ST10	32°56.39'N	137°11.38'E		4190	29	01:46	Landed 3rd
ST1	33°07.76'N	137°56.80'E	Gravity Corer	4118	29	07:08	Landed
ST1	33°07.71'N	137°57.37'E	Heat Flow	4113	29	09:46	Landed 1st
ST1	33°07.83'N	137°57.43'E		4112	29	0:46	Landed 3rd
ST7	33°17.98'N	138°09.80'E	Heat Flow	4037	29	14:14	Landed 1st
	33°18.12'N	138°09.73'E		4038	29	14:46	Landed 3rd
ST7	33°17.97'N	138°07.91'E	Gravity Corer	4043	29	17:33	Landed
ST8	33°23.78'N	138°16.05'E	Heat Flow	4006	29	20:46	Landed 1st
	33°23.68'N	138°16.19'E		4007	29	22:10	Landed 4th

Site No.	Position Lat.	Long.	Investigation	Water Depth(m)	Date & Time(SST)		Remarks
Leg 2					July		
	34°04.98'N	138°07.85'E	IES C	2442	4	17:27	Launch
	34°04 26'N	138°07.05'E	IES A	2439	4	18:13	Launch
	34°03.47'N	138°06.11'E	IES B	2430	4	18:40	Launch
Line 1	33°49.77'N	137°55.17'E	Deep-tow Camera	2017	5	09:49	
	33°48.00'N	138°02.30'E		3679	5	16:35	DT-1 End
Line 2	33°45.25'N	137°54.70'E	Deep-tow Camera	3586	6	10:02	Start
	33°45.06'N	137°59.50'E		3720	6	14:16	DT-2.End
	33°47.08'N	137°57.42'E		3662	6	16:40	DT-3 End
Line 3	33°38.81'N	137°31.14'E	Deep-tow Camera	3544	7	09:41	Start
	33°35.23'N	137°32.22'E		3872	7	14:22	DT-4 End
	33°36.63'N	137°34.35'E		3146	7	16:20	DT-5 End
	33°37.61'N	137°34.44'E		2754	7	18:10	DT-6 End
Line 4	33°37.86'N	137°54.59'E	Deep-tow Camera	4027	8	10:05	Start
	33°43.66'N	137°51.65'E		3200	8	17:00	DT-7 End
Line 5	33°39.49'N	137°52.29'E	Deep-tow Sonar	3708	9	11:58	Start
	33°37.96'N	137°53.62'E		4014	9	14:30	DT-8 End
	33°38.90'N	137°56.93'E		3986	9	17:00	DT-9 End
Line 6	33°42.63'N	137°52.13'E	Deep-tow Camera	3512	10	10:21	Start
	33°49.06'N	137°49.06'E		2332	10	18:00	DT-10 End
HF1	33°45.88'N	137°59.06'E	TF Heat Flow	3722	11	14:12	Landed
Line 7	33°18.06'N	138°05.55'E	Deep-tow Camera	3625	12	10:19	Start
	33°18.91'N	138°09.19'E		4061	12	14:12	DT-11 End
	33°19.88'N	138°10.31'E		3785	12	16:00	DT-12 End

3. TOPICS

3.1 New geophysical equipments of the Hakuho Maru

K. Kobayashi

The research vessel we used for this cruise KH 89-1 is a brand new. It was built at the Simonoseki Ship Yard & Machinery Works of Mitsubishi Heavy Industries, Ltd. and delivered to the Ocean research Institute, University of Tokyo on May 1, 1989. This cruise is the first scientific voyage of this ship, after one trial cruise from June 1 to June 15, 1989.

This ship was designed to fulfil a high-level demand of the up-to-date scientific research in the wide world oceans. For a variety of geophysical measurement highly precise manueverability is required with various speeds ranging between 0 and 16 knots. For this purpose as well as for saving its cruising time and for safely moving in changeable meteorological conditions around Japan, it is facilitated with four 1,900 PS diesel engines for propulsion by two shafts of propellers with changeable pitch through reduction gears. During precise and quiet operation with speeds less than 10 knots the power of engines are transferred to two generators supplying electricity to two motors driving both propellers with a fixed pitch by thyrister-controlled revolutions. Three sets of diesel-driven generators supply 60Hz/100V & 220V electricity for general onboard use. In addition, two motor generators provide highly stable electric power with 60Hz/100V and 400Hz/115V for scientific instruments. Laboratories onboard are sufficiently air-conditioned and vibration-free to accomodate precise devices.

A number of research facilities are installed on this ship. Among them the following geophysical equipments are operated in the present cruise; (1) Gravimeter and inertia navigator, (2) Seabeam, (3) Differential proton magnetometer, (4) Deep-towed self-recording proton magnetometer, (5) SSBL acoustic transponder system. Results of operation of each equipment is described in the following chapters.

The ship is equipped with an integrated navigation system based on Magnavox Series5000 and much modified to fit to our demands. Most of navigation data such as the ship's position, heading, speed together with some geophysical data including vertical depth are logged and displayed in some laboratories by use of this system.

3.2 Recent Techniques of the Sea Floor Study

J. Segawa

The largest problem in scientific study at deep ocean bottom will be the deficiency of defined observatories and the long-term continuity of observations. This lasting problem has been causing uncertainty involved in marine observations which is often untolerably large so that they do not even deserve 'observation'. To solve this problem several new attempts to establish fixed observatories at deep-sea floor where precise scientific observations over a sufficiently long period are possible have been made recently both in Japan and abroad.

The most important innovation in scientific/industrial sea floor research may be based on three new movements, i.e., establishment of the sea floor observatory, development of ROV (Remotely Operated Vehicle) and manned submersible. In addition, a large scale and permanent sea floor station, in which the submersible is able to dock and man can stay for scientific works for a certain period, will be the future target for development towards higher quality investigations.

In this report the author will describe the recent progress and endeavour made in Japan for the sake of advanced study of the sea floor, particularly on the sea floor observatory and the unmanned submersible.

3.2.1 Sea Floor Observatory

There are diversified concepts on the sea floor observatory. The first idea which one imagines is a giant platform installed at the sea floor which is equipped with fundamental systems such as electric power generator, position indicator and communication devices. In this platform various kinds of observations may be made together for a long period of time. However, this sort of platform must be too huge a body to be handled easily, its weight being expected to be a hundred, thousand in tonnage. The second idea which may replace the first one is a group of platforms consisting of a few or many platforms with a small size, on each of which a single observation will be made.

The Ocean Research Institute (ORI) has so far established three ocean bottom bases (platform) in the Sagami Bay, which are based on the second concept.

The requirement of the ocean bottom base is that its position is fixed on the earth and relocatable from the surface ship whenever it is necessary and that either a manned or an unmanned submersible may have access to it and be able to install observation equipments.

The Ocean Bottom Base (OBB) designed by ORI is equipped with an acoustic transponder which makes it possible for a surface ship to locate the OBB acoustically. The transponder attached to OBB, together with an on-board control and commanding device is capable of giving a slant range between OBB and the surface ship with a resolution of one meter. When an OBB is to be installed at a new site its position relative to the earth has to be determined. To do so, a Long Base Line Positioning Method (LBL Method) is applied to OBB installation. Figure 3.2.1 shows a schematic view of the method (Fujimoto et al., 1988). Three acoustic transponders are first installed on the sea floor in such a way as the transponders are located at three vertices of a triangle whose central point approximately coincides with the point where the OBB is expected to settle. So, in case of installation of OBB four acoustic transponders are used at a time, i.e., one attached to OBB itself and the other three installed at the sea floor. The acoustic control and commanding device on board transmits acoustic signals to measure slant ranges between the surface ship, the transponder of OBB, and three transponders at the sea floor. The position of the surface ship is continuously determined by using Loran C, NNSS and GPS throughout the period when slant range measurements are made. By combining the slant ranges acoustically obtained in water with the change of the positions of the surface ship the position of OBB can be determined with the accuracy of a few meters. As this measurement is conducted while OBB with a transponder is suspended down from the ship and being lowered to the bottom the position of OBB can be monitored on the way. This is a kind of subnavigation technique. The OBB designed by ORI is made of carbon-fibre reenforced concrete with the size 110 x 110 x 50 cm3 and a weight 800kg in air (Fig. 3.2.2a, b). When it is launched the OBB is suspended by a winch wire and lowered into water, and when it comes close to the sea floor with the height 2 to 3 meters, the OBB is released off the wire and let go treely. Thios operation is executed by an acoustic release which is triggered by a command from a ship. The height of OBB off the bottom is measured by an acoustic pinger which is added to the bottom of the OBB acoustic transponder. The configuration of three OBB's installed at the Sagami Bay is shown in Figure 3.2.3.

There are some unique ideas in the design of OBB as seen from Figure 3.2.2. They are summarized as follows:

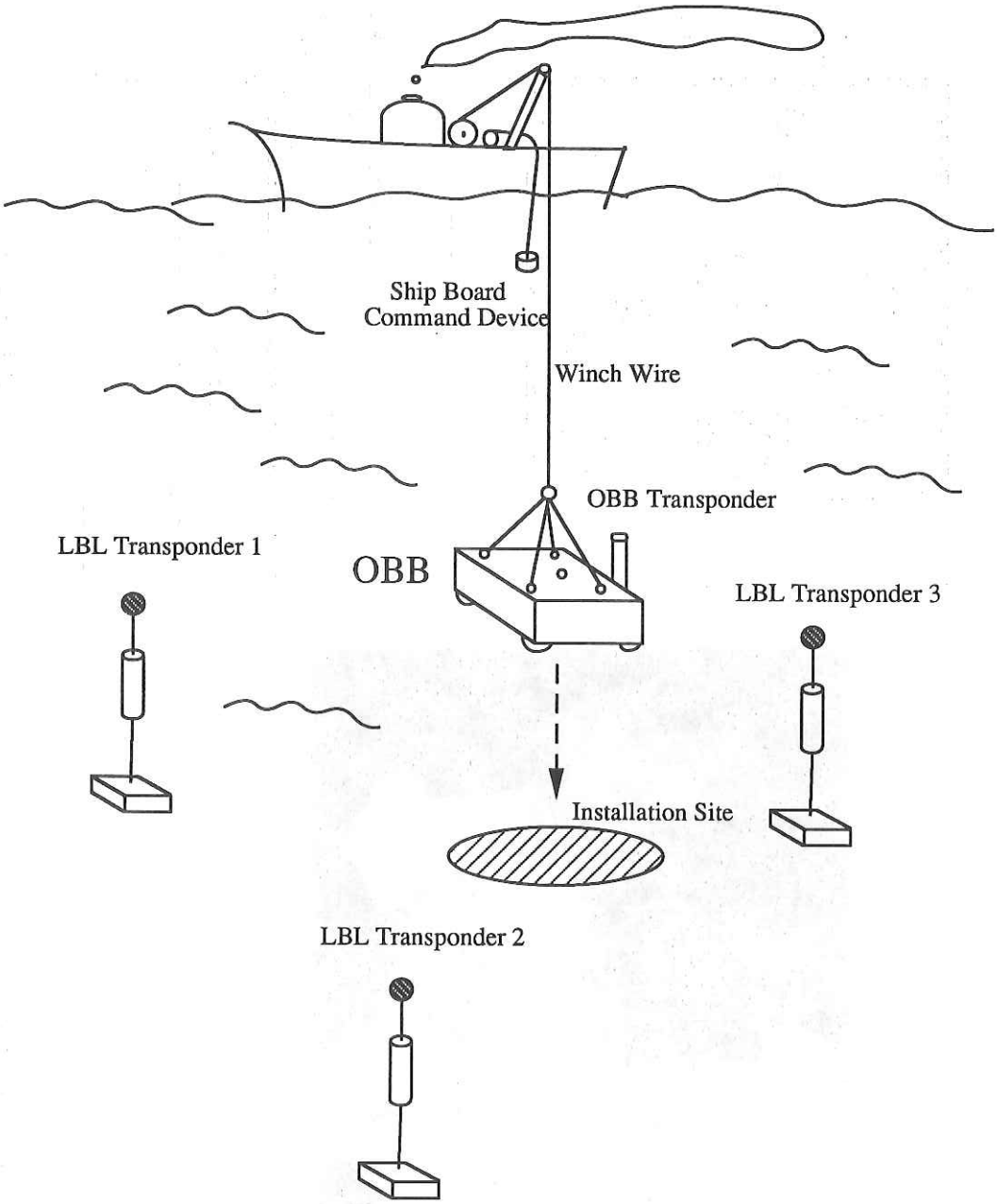

Fig. 3.2.1 A schematic illustration of Long Base Line Positioning Method and Subnavigation Method.

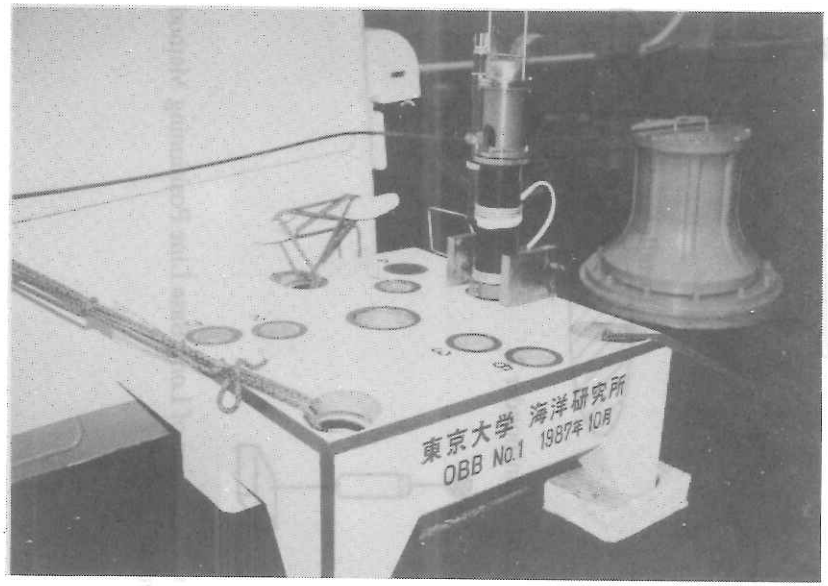

Fig. 3.2.2 a) A picture of OBB designed by ORI.

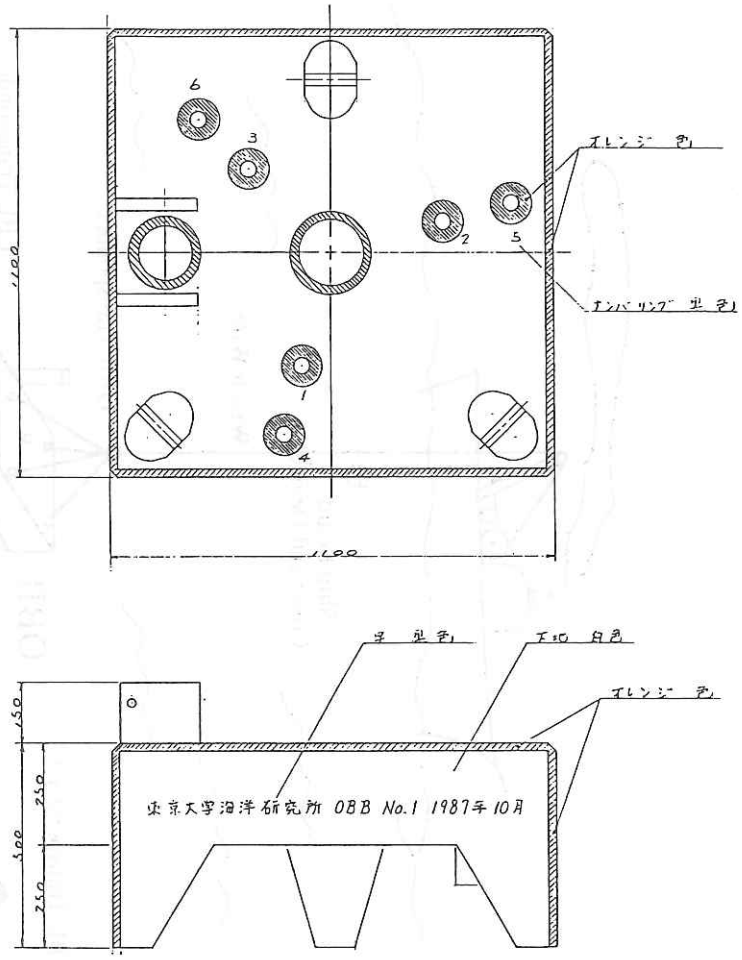

b) A design of OBB.

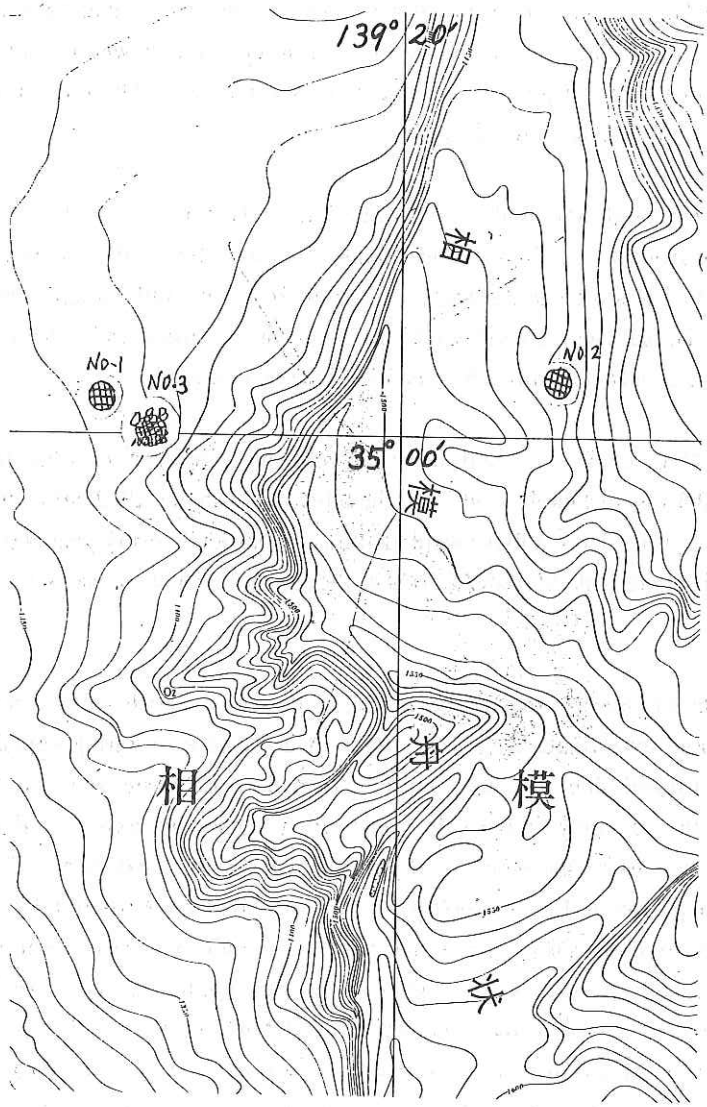

Fig. 3.2.3 Configuration of three OBB's installed at the Sagami Bay.

1. Since the OBB is made of concrete reennforced by carbon fibre and the metal used is exclusively titanium, it is almost non-magnetic. This is an important characteristics for magnetic observation.

2. V-shaped holes are carved on the surface of OBB platform. These holes are configured at vertices of two equilateral triangles, one with the side of 50cm and the other 80cm. On these holes are set observation instruments which require exactly defined positions if a precise measurement is aimed at . The uncertainly of the position setting is ±2mm in this case.

3. There is a through-hole with a radius of 12cm at the center of OBB. This hole is important from the fluid mechanical point of view. Since OBB is dropped to the bottom from a point 2 to 3m high, it is required that the OBB keeps level when it falls. A flat plate with no hole on it is likely to slide in case of fall. With a hole of a proper size it falls vertically while the level is well preserved.

The three OBB's installed in the Sagami Bay have been used for three years. The first OBB was installed in 1987 and the other two were installed with a pace of one installation a year. These OBB's were identified acoustically every year and visited by the manned submersible SHINKAI 2000 of the Japan Marine Science and Technology Center.

In the first year of the OBB experiment the acoustic positioning technique was developed and investigated. The accuracy of acoustic positioning depends on the resolution of travel time of acoustic pulse, information of acoustic velocity structure in water, and the accuracy of the ship's position. In the first experiment of 1987 it became possible to get the accuracy in acoustic positioning to a degree of 2 to 3m. In 1988 an Ocean Bottom Electrometer (OBE) was installed at the site of OBB No.2 with the aid of SHINKAI 2000. This electrometer has two long-span electrodes which align perpendicularly on a horizontal plane. The length of the electrodes are 20m each, which were expanded by using manipulators of SHINKAI 2000, and it was difficult to be realized by a surface ship alone. In 1989 an absolute measurement of magnetic field was made at the site of OBB No.1. A proton magnetometer for the sea floor's use was brought to the site by use of SHINKAI 2000 and the total magnetic force just on the center of the OBB platform was measured. This will be repeated every year from now on.

Although the attempt of ORI to establish the ocean bottom observatory has just started, its usefulness will be demonstrated sooner or later, from the view point of precision and repeatability of observations.

A problem of this, proto-type ocean bottom observatory mentioned above is that it is not equipped with a power charging and a data telemetering device. This mission is essential to a long term and continuous measurement. In order to recharge the battery used in a ocean bottom instrument a plug-in connector for deep-sea use is necessary. A substitute for this is an indirect connector such as the AC coupling connector. To acquire data without retrieving instruments from OBB a short-span laser telemetering may be the best. It is desirable that either a manned or unmanned ROV should be equipped with such devices as provide electric power to or receive data from observation apparata. The submersible available at present however do not have such devices. So, a compromizing idea will be to bring a portable power charger and laser transmitter/receiver to the OBB site by the submersibles to do the same operation.

Figure 3.2.4 is a concept of an observation scheme using an OBB by which supplying electric power and acquiring data can be made remotely without disturbing observations.

3.2.2 Unmanned Submersible (ROV)

It is impossible to maintain the ocean bottom observatory without the aid from either a manned or unmanned submersible. This is like the relationship of a house-to-live with the traffic means on land.

An unmanned submersible or a Remotely Operated Vehicle (ROV) is a robot in water which moves by the command from a surface ship. The ROV was first developed about 20 years ago and has been advancing year by year. Among the ROV's so far developed those for use in shallow water (500m or so) are the most in number. The ROV's for the use in deeper water are not so many. In the United States, GEMINI is famous and used for the sea as deep as 6000m. The ROV named SUPERSCORPIO is a product in Scotland and well known to the world.

There are three ROV's for deep sea use in Japan. One is Marcus 2500 which is owned by KDD company of Japan (Fig. 3.2.5). The other two are owned by the Japan Marine Science and Technology Center, being named Dolphin 3K and Dolphin 10K. Marcus 2500, Dolphin 3K and Dolphin 10K can dive as deep as 2500, 3000

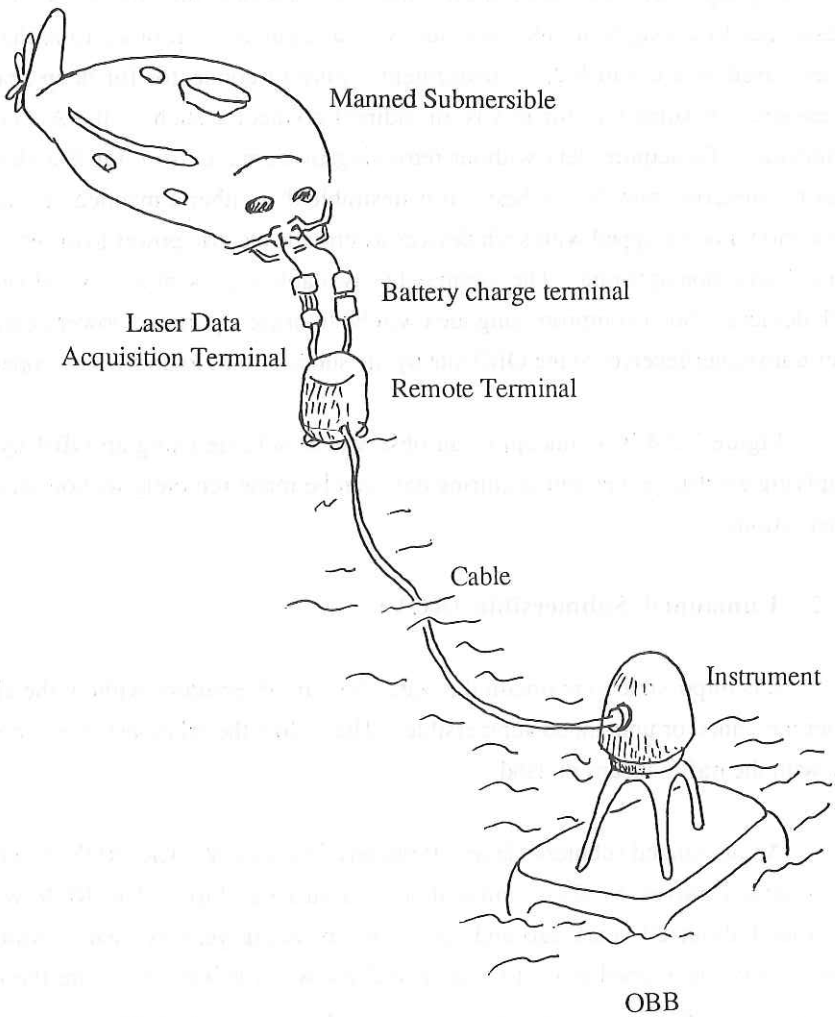

Fig. 3.2.4 An idea of OBB which is equipped with a battery charger and data transmission device.

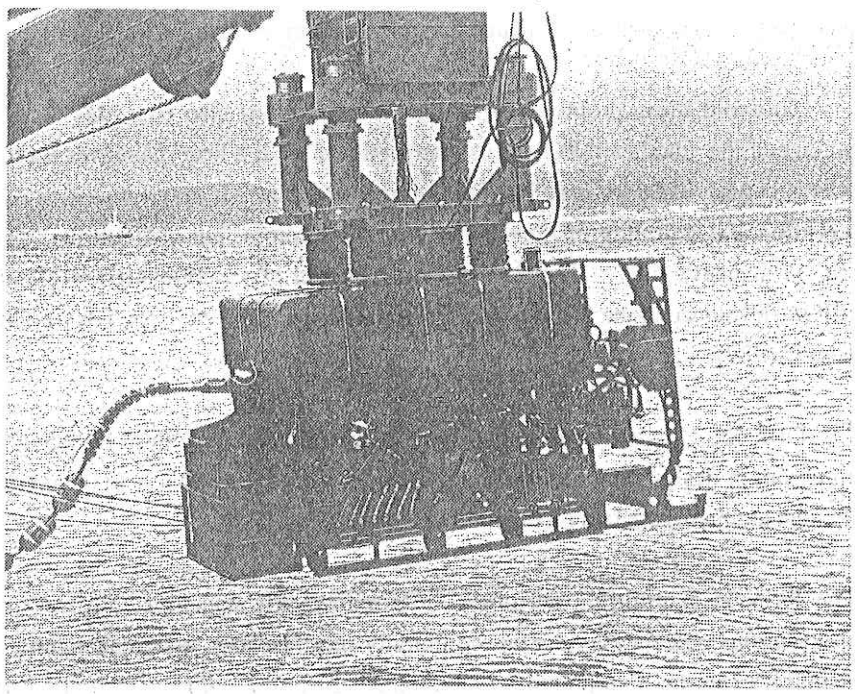

Fig. 3.2.5 ROV Marcus 2500.

and 10000m, respectively. All the ROV's mentioned above are the vehicles tethered from the surface ship by a cable. The tethered ROV can be operated freely from the surface and provides information to the ship in real time via the electric cable. This is a large benefit from the tethered ROV. On the contrary the tethering cable causes a large trouble from the other point of view: An enormous drag acts on the cable, so that the ROV is flown by water current and unable to reach the bottom. The cable winch, on which a cable longer than 8000m or so has to be wound for an ROV of 6000m use, also becomes of the huge size, so huge that a ship might be unable to accommodate.

To avoid these problems an untethered ROV has also been devised. The advantage of the untethered ROV is its compactness, but if a long maneuver is required in water, battery capacity may become a large problem. It may be used for visual observation and sampling of light material on the bottom, but difficult to expect an operation of heavy duty. Fig. 3.2.6 shows a model of an untethered ROV named PTEROA developed at the Institute of Industrial Science, University of Tokyo (Ura and Ootsubo, 1987).

ORI, the University of Tokyo has its own plan to develop a tethered ROV. The maximum design depth to which the ROV can dive is 6000m. In designing the equipment emphases are laid on the following items:

1. The ROV is of multiple purposes. To realize this objective, the sensors for observations, except for several, commonly used sensors, are replaceable. For instance, even the manipulator can be replaced by some other observation tool if necessary.

2. The ROV consists of a launcher and a vehicle. The vehicle is attached to the launcher on board and they are handled together. When the ROV is launched into water and reaches a certain depth the vehicle is detached from the launcher and moves for itself. The vehicle and the launcher is connected by a cable with a length of 200~300m, which is the power and communication line to the vehicle.

3. The launcher itself is equipped with three kinds of sensors which work while being towed behind the ship. In this case the ROV works as a deeep-tow equipment. The sensors include a side-scanning sonar, a subbottom profiler and a proton magnetometer.

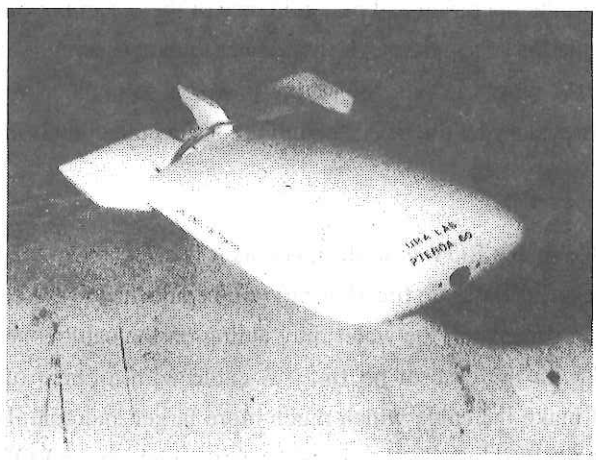

Fig. 3.2.6 Untethered ROV "PTEROA".

4. The vehicle is capable of maintaining its attitude and position automatically. This function is useful when operations are made using manipulators. The position and attitude of a vehicle are forced to change when external forces such as water current or reactive forces are applied to the vehicle. The attitude and position maintaining system senses the external force and drives the thrusters so that the vehicle does not move at all.

5. This ROV does not aim at handling a large and heavy body by the manipulator at the sea floor. Instead, it should handle a comparatively small body by a quick motion. So, the manipulator is designed so that it can behave in a shrewd fashion. It is desirable that the manipulator is as shrewd as it can grasp a moving object.

6. In order to support the operation and maintainance of the ocean bottom observatory the ROV has a function of supplying electric power to the observatory and collecting data obtained at the observatory. Supplying power is so made as to recharge the battery of the observatory by use of AC coupling. Data collection is made by use of laser beam.

7. The tethered cable of the ROV is so designed as it is affected by the least drag by water flow. Streamlined plastic fins (fairing) will be attached to the cable. If these fins have a proper dimension the water drag acting on the cable is reduced to one tenth compared with the case of no fin. A cable with a chain of plastic fins, however, would make the cable winch much more larger and complicated. This problem has to be solved by selecting a proper ship on which the ROV is mounted. Figure 3.2.7 shows an example of the fins attached to the cable and the effectiveness of the fins. Figure 3.2.8 shows a conceptual view of the ROV designed by ORI. It is intended that the ROV should look as nice as possible in addition to its efficiency.

Reference

H.Fujimoto, J. Segawa and T. Furuta : Installation of ocean bottom observation station by means of underwater acoustic positioning, Zishin, 41, 583 ~ 589, 1988.

T. Ura and S. Ootsubo : Design of unmanned untethered submersible for quick swimming, Proc. Japan Ship-building Society, 1987.

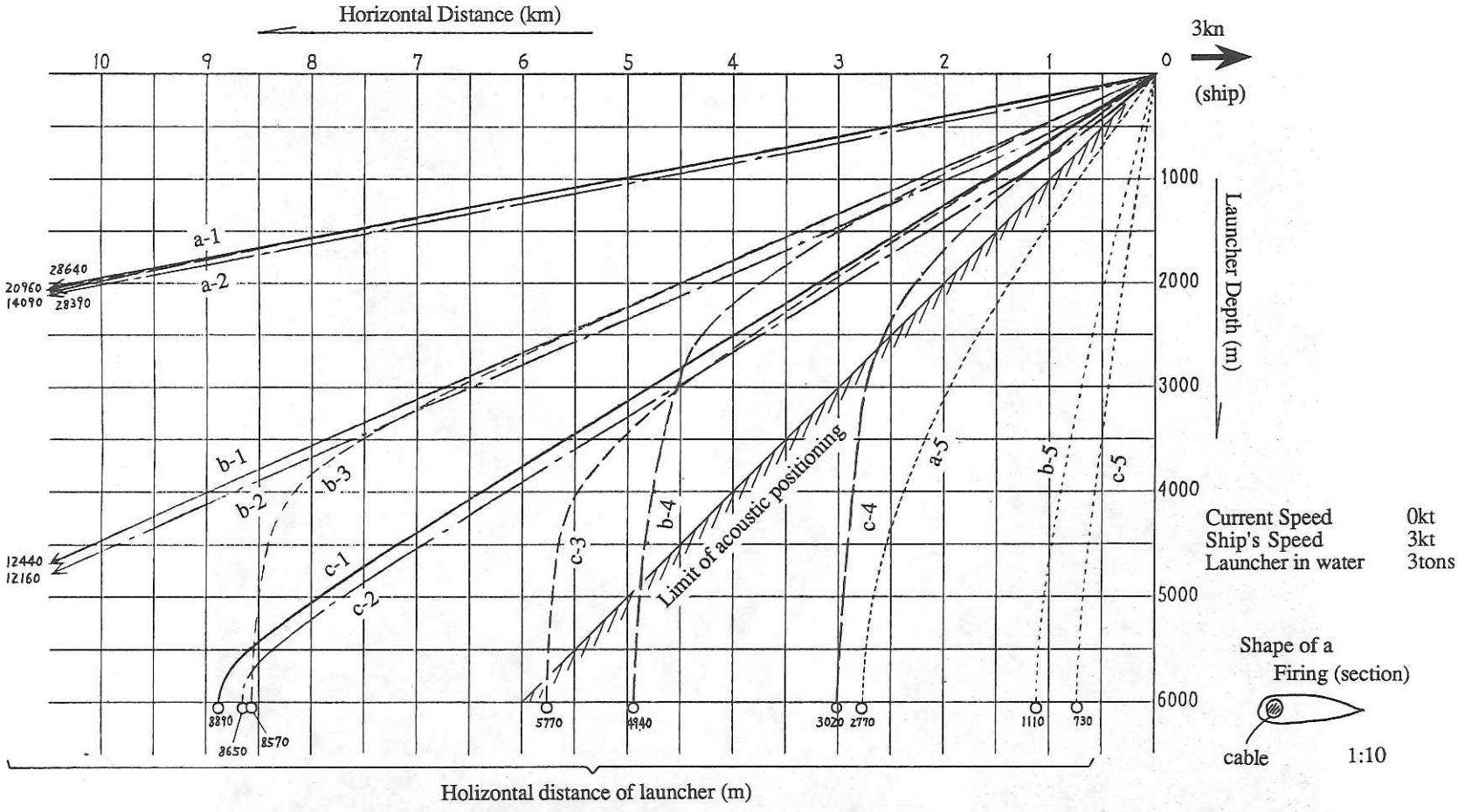

Fig. 3.2.7 Description of streamedlined fins (fairing) attached to the cable and its effect on the drag by water current. Variation of the drag is shown for each combination of the cable (a~c) and fairing (1~5) assuming the case when a launcher 3tons in water is towed at 3 knots at the water depth of 6,000m.

Type of cable : (a) Steel with Zn coating (35mmϕ, ρ= 4.1g/cc), (b) Ti alloy (35mmϕ, ρ=2.7), (c) FRP (45mmϕ, ρ=1.3).

Cable fairing : (1) No fairing, (2) Fairing from surface down to 1,500m, (3) Fairing over 1,500m above launcher, (4) Fairing over 3,000m above launcher, (5) Totally with fairing.

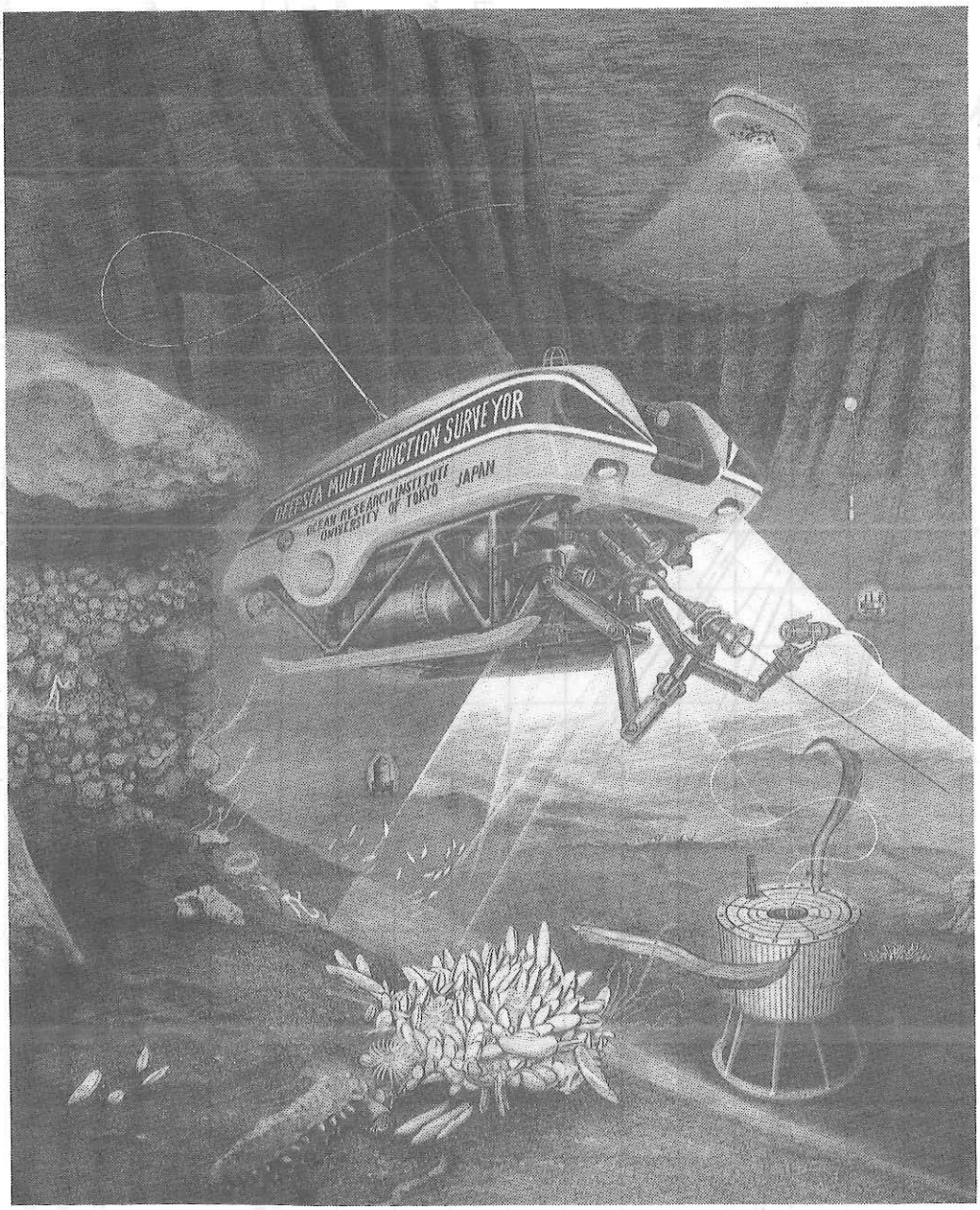

Fig. 3.2.8 A conceptual view of ROV designed by ORI.

3.3 ODP Techniques Involving Wide Applications

H. Kinoshita

Abstract

Development of Ocean Drilling Program (ODP) techniques and its scientific concepts as well as ODP related communities in seagoing geosciences are shortly reviewed. Some important publications and references are also presented here in order to help readers how and where to get materials from these well established scientific organizations and consortiums. It is worthwhile reading carefully these materials for those who are interested in approaching and committing any field of seafaring experiments in the next decade.

3.3.1 Recent geophysical experiments by ODP cruises

Geophysical experiments using DSDP and ODP holes were performed on various problems. Logging which is a technology to obtain informations on the holes physical conditions such as density, elasticity and elctro-magnetic properties of surrounding formations are run in most of ODP holes after drilling. This procedure become one of standard procedures of the ODP program in spite of some kind of logistic difficulties and arguments raised against logging runs. Speciality experiments using ODP holes are ranging from Ocean Subbottom Seismometry, Stress Orientation Measurements, Hydrofracturing, Permeability Test and magnetotelluric Measurements. The results of these experiments run by 1987 are presented briefly in Kinoshita (1988). In the recent years the importance of the geophysical experiments in ODP holes are recognized by many people and many new proposals are written to try new type of experiment in the future.

We proposed also four sets of geophysical experiments in ODP holes around Japan. Ocean Subbottom Seismometry and Oblique Electric Shooting in the central part of Japan sea (refer to ODP cruise report Leg 127 and 128). Another experiment is designed to measure and monitor a change in temperature profile in a deep hole (about 1100 meters) in the accretionary prism of Nankai Trough (Kinoshita et al., 1988). This system is controlled by acoustic linkages as well as stand-alone computerized data acquisition system. Temperature (and pressure) data can be retrieved from a surface vessel by interrogation. Data transmission can be performed beyond 5000 meters of slant range. There is also a program of downhole speciality experiment along a line to the south of

Japanese main island across four plates, Philippine Sea-Eurasian-Northamerican-Pacific (ODP proposal number 159/F; readers are referred to this number in case that one has to request a copy of the proposal) to monitor change in geometrical as well as geophysical conditions within these plates. This program is, however, too expensive to realize and is still in a premature stage of planning. It is hopeful that this kind of large scale experiment is to be conducted offshore in a future using ODP holes which are treasures and wealth of the mankind.

3.3.2 Conferences on scientific ocean drilling (COSOD I and II)

Deep Sea Drilling Project (DSDP)and Ocean Drilling Program (ODP) had long and enthusiastically discussed and argued among many number of scientists from various countries all over the world. The white papers and position papers formed through these conferences were published in a form of a textbook for those who are eager to make any kind of studies in solid earth sciences on an interdisciplinary bases. The reports are well organized on the basis of wide interest and deep and extensive knowledge on the geoscience problems including from extraterrestrial influence through inner core influences on the earths dynamics, environments as well as history. Readers, especially who are interested in continuing seafaring jobs, are suggested to obtain these two reports (COSOD I and II) and associated position papers if possible to familiarize themselves with the global aspects of the future geosciences.

It is possible also for the readers to obtain great number of materials concerning the recent status of technology and future development of the seafaring experimental equipments and systems. Most of the reprints on various problems can also be obtained through JOI (Joint Oceanographic Institutions). It is very helpful for readers to design and to find your own way of enjoying earth sciences by peeking these materials or informations, for instance wire-line reentry system (Langseth and Spiess, 1987) into preserved ODP (or DSDP) holes for your specific experiment using not only traditional research vessels but also newly emerging submersibles. Vertical seismic profiling(Mutter and Balch, 19**), geochemical dry logging, high temperature downhole measurements and other related problems are also very important for the readers to understand and utilize.

3.3.3 RIDGE (Ridge Inter-disciplinary Global Experiment) project

One of the branches of ODP communities which are combined with interests of people who are trying to develop technology on the high temperature measurements tools. The technological difficulties in high temperature drilling, logging as well as downhole experiment have hindered to form a solid community on these problems. Measurement while drilling (MHD), pilot drill hole measurements and high temperature downhole equipments are all long desired but still under developing matter. But this problem cannot be out of our way who live in such a country as active volcanoes and high temperature hydrothermal fluid can be observed everywhere. Some of the techniques developed by this community is still fragile and much more efforts have to be concentrated to pursue this difficult and long-ranged programs. It is clear that the efforts and feasibility studies on this matter have just started in these latest years e.g., RIDGE program, 1989; Sunshine Project, 1975; only partial copy is available, and Miyairi et al., 1986)

Reference

JOIDES, 1981, Conference on Scientific Ocean Drilling (COSOD), proceeding of a conference sponsored by JOIDES (Joint Oceanographic Institutions for Deep Earth Sampling).

JOIDES and NSF, 1987, Report on the Second Conference on Scientific Ocean Drilling (COSOD II), sponsored by both JOIDES (Joint Oceanographic Institutions for Deep-sea Sampling) and ESF (European Science Foundation).

Kinoshita, H., 1988, Present day achievement of downhole measurements and experiment - An example from ODP Hole 504B, Costa Rica Ridge (in Japanese), Earth Monthly, 3, 212-220.

Kinoshita, H., H. fujimoto, M. Ymano, T. Kanazawa and A. Taira, 1988, ODP Nankai Down hole Observatory (ONDO): ODP proposal number 340F, copies aailabel at JOI.

Langseth, M.G. and F.N. Spiess, 1987, Science opportunities created by wireline re-entry of deep-sea boreholes, Proceedings of a Workshop sponsored by JOI (Joint Oceanographic Institutions), copies available at ODP office, USA.

Miyairi, M., J. Yamamoto, K. Tezuka and T. Ohashi, 1986, High temperature geothermal well logging system; (part 1) temperature, pressure and spinner tools, Technical Rept., JAPEX Co., 3, 1-10.

Mutter J. and A. Balch, 19**, Vertical seismic profiling (VSP) and the ocean Drilling Program (ODP), Proceeding of a workshop, copies available at JOI (Joint Oceanographic Institution), USA.

RIDGE, 1989, Initial Science Plan, Copies available at School of Oceanography, WB-10, University oaf Washington, Seattle, WA 98195, USA.

Sunshine Project, 1975, High temperature drilling tools and its applications (in Japanese), Internal Report of the Sunshine Project, 78-93.

4.1 Gravity Measurements and Test of Inertial Navigator

J. Segawa

The Surface Ship Gravimeter NIPR-ORI Model 2 and the Precision Gyrocompass SGC-1 are both new equipments installed at Lab No.9 of the new Hakuho-Maru.

The gravimeter NIPR-ORI was first developed in 1982 by J. Segawa et al (1983) for the purpose of gravity measurement in the southern sea on board Icebreaker Fuji. The second version of this gravimeter is NIPR-ORI model 2 which is equipped with an advanced gyro-stabilized platform. The new version was mostly used on board Icebreaker Shirase. The gravimeter installed on the Hakuho-Maru has been designed similarly with the one on Shirase, except for a minor modification with the data processing unit.

The Precision Gyrocompass SGC-1 is the reference of three dimensional co-ordinates on the Earth, which provides azimuthal, pitching and rolling angles with the accuracies of 0.1 degree and 0.1 minute of arc, respectively. This gyro is also capable of reckoning ship's position in latitude and longitude by a function of inertial navigation, as well as reckoning the heave of the ship relative to mean sea level. SGC-1 is therefore named 'Inertial Navigator'. The accuracy of inertial navigation is formally ±1 nm in 10 hours, but it depends largely on the accuracy of ship's velocity input and position reset input.

4.1.1 Modified NIPR-ORI model 2

Figure 4.1.1 shows the block diagram of the gravimeter. The most characteristic points of the gravimeter is employment of a servo accelerometer as gravity sensor, a Schuler-tuned vertical gyro and a high-grade micro-computer instead of the mini-computer with the previous model.

The gravitmeter of the new Hakuho-Maru is strongly supported by improved environments in the gravimeter room and on-line information networks of the new ship. The largest improvement worth mentioning is the stabilization of the ambient temperature in the gravimeter room. In the present cruise the change of room temperature was, while the gravimeter was on, about ±0.1°C/day and ±0.5°C over a period longer than 10 days. A very sophisticated control scheme adopted for the

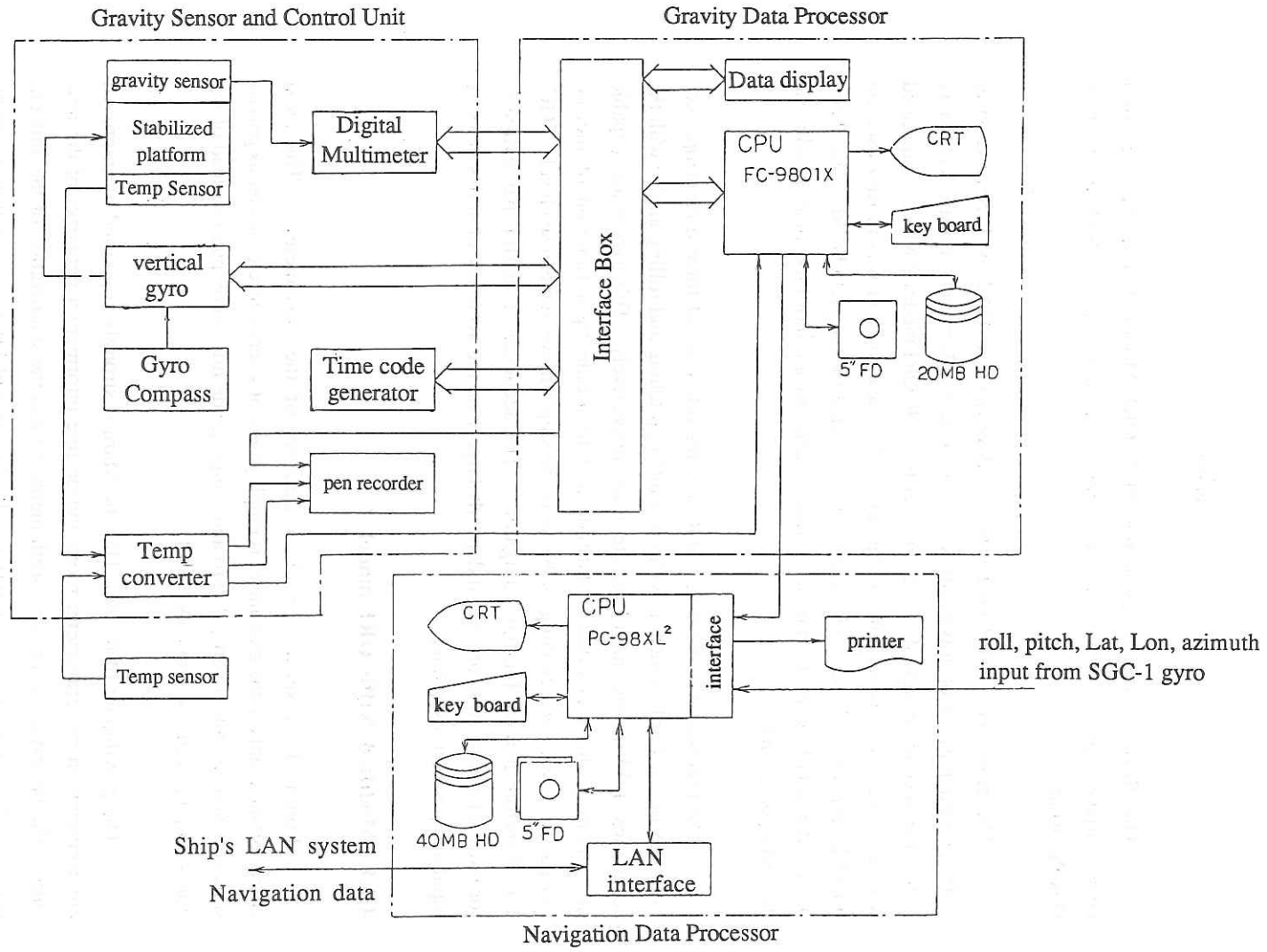

Fig. 4.1.1 Block diagram of NIPR-ORI Model 2 Gravimeter.

temperature regulation of the gravimeter room has made it possible to maintain such a high level stabilization. The information network inside the ship, i.e., LAN system, provides the ship's heading, speed, position and water depth in real time every 1 second or 0.1 second, which are introduced to the gravimeter system for processing gravity data.

4.1.2 Performance of gravimeter

The gravimeter was tested, repaired and adjusted during the first test cruise conducted prior to this cruise, but this process had to be continued until the present cruise because of unexpected failures of the gravimeter. There were three main troubles with the gravimeter. That is:

1. Incorrect inputs of ship's speed disturbed the level of the vertical gyro. This was due to the unproper conversion of the input from the speed log.
2. Data processings were often interfered by some unproper signal from the LAN system, when the gravity calculation terminated. This was because of imperfection of the UNIX program adopted for the processing.
3. There was an unusually large drift in the gravimeter sensor. Unlike the sensors previously used the present sensor showed a drift which did not linearly change with time.

The troubles 1 and 2 were completely solved in the present cruise by modifying electronics and computer programming. The trouble 3 will need more time to clarify the reason and take a necessary step.

Except for the troubles mentioned above the gravimeter worked pretty well. Elimination of the ship's acceleration, resolution of 0.01 mgal and real time Eötvös correction were mostly successful.

4.1.3 Precision Gyrocompass (Inertial Navigator)

The precision gyrocompass installed on the Hakuho-Maru is Model SGC-1 manufactured by Tokyo Keiki Incorporated. The structure of this gyroscope is shown by Figure 4.1.2. The functions of this gyro can be summarized as follows:

1. Indicates ship's heading with the accuracy of 0.1 degree.
2. Measures roll and pitch angles of the ship with the accuracy of 0.1 minute of arc.
3. Provides inertial positions of the ship in latitude and longitude with a resolution of 0.01 nm.

4. Measures the heaving motion of the ship relative to mean sea level with the accuracy of 10 cm.

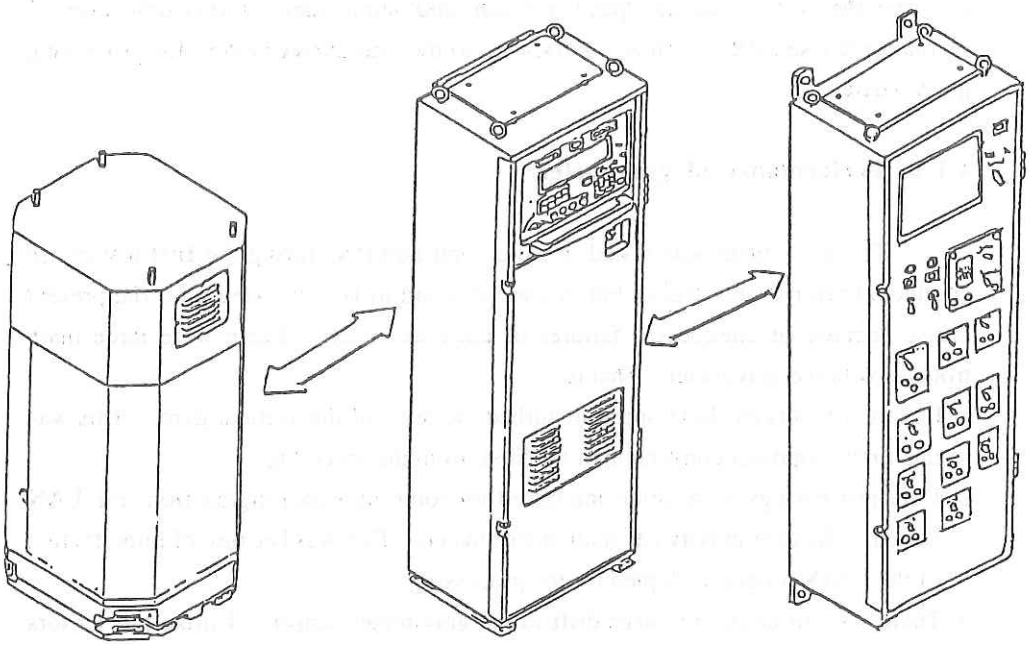

Fig. 4.1.2 Block diagram of the Precision Gyrocompass.

4.1.4 Performance of Inertial Navigator

During the first test cruise conducted before this cruise it was found that the ship's positions estimated by inertial navigation contained larger errors than expected from the capability of SGC-1 and that, in addition, the function measuring the ship's heave did not work. At the beginning of this cruise, therefore, a thorough readjustment was conducted, including reconstruction of the system.

It was found that the erroneous position was caused by wrong log data of the ship. There are two equipments with which the ship's speed is measured. One is the conventional electro-magnetic log and the other is the two-axis acoustic log. Since the electromagnetic log has been more popular than the acoustic one, the present inertial navigator is set to choose the electromagnetic log preferentially when the acoustic log comes into the mode of measuring speed relative to water (This happens when water

depth becomes large). In the case of the new Hakuho-Maru, however, the electromagnetic log did not work well in this leg, while the acoustic log provided reasonable speed data even in the deep sea. So, the logic was changed so that the selection of speed logs could be made manually. As a result the acoustic log data were exclusively used throughout the present cruise.

There was another cause to deteriorate the accuracy of positioning. It is the wrong resetting position. Since the inertial navigation is subject to drift, the inertial position has to be corrected by some reference position from time to time. The reference positions are the positions fixed by NNSS, Loran C or GPS. These reference positions were not correctly input to the inertial navigator at first, so that the position estimation was greatly disturbed. The reason why the ship's heave could not be measured was a miss in electronics cablings. This was repaired soon.

After the repairment and readjustment with respect to the problems mentioned above the inertial navigator SGC-1 worked as was expected. But, in our opinion, its performance is not completely satisfactory. The problems remaining for the future may be as follows:

1) Drift rate of inertial estimation of positions should be further reduced.
2) Too frequent inputs of reference position would make the inertial navigation meaningless. We should investigate the optimal frequency of input to get most reliable positions.
3) It is important to develop the application of the inertial navigator to various geophysical problems.

References

Segawa, J., T. Kasuga and K. Kaminura : Surface Ship Gravity Meter NIPRORI-1. Marine Geodesy, 7, 271 ~291, 1983.

4.2 Bathymetric Mapping Using the Sea Beam System

H. Fujimoto, T. Furuta, A. Oshida, M. Nakanishi, and K. Kobayashi

4.2.1 Sea Beam System on board the Hakuho-maru

A multi-beam echo sounder is a basic system for a research vessel to carry out precise bathymetric survey of the deep seafloor. Two systems were proposed for the Hakuho-maru: "Sea Beam" by General Instrument, USA, and "Hydrosweep" by Krupp Atlas Electronik, West Germany. The latter has larger swath width (90°), narrower beam width (2°) by using higher frequency (15.5 kHz) and higher source level (238 dB at the inclination of 23°) than the former. Specification of Sea Beam for each of these items is 43°, 2.7°, 12 kHz, and 231 dB, respectively. Although Hydrosweep was fully automated and self-calibrating using modern electronics to provide a swath width equivalent to twice water depth, a working group, Dr. K. Tamaki and ourselves, recommended Sea Beam for the Hakuho-maru due to the following reasons. (1) Hydrosweep has no experience of survey of seafloor deeper than 6000 m and we were afraid that the high frequency of 15.5 kHz might have some problems in survey deeper than 8000 m. Because subduction zone in the western Pacific is one of major targets for the Hakuho-maru, mapping of deep-sea topography with enough S/N ratio is highly important. (2) Considering the topographic maps presented as examples of mapping by Hydrosweep, agreement of topography was not so good at crossover points of the ship's track.

Hakuho-maru Sea Beam system was designed by the above-mentioned working group with the following guidelines;

(1)At the ship's speed higher than 17 knots the Sea Beam operation should be fully automatic.
(2)Use of precise gyrocompass as a backup of "Hippy", a standard vertical reference unit of the Sea Beam system.
(3)Capability of digitization of intensity and length of each echo for mapping of reflectivity of the bottom.
(4)Real-time topographic mapping on plotters along the ship's tracks on plotters and displaying 3D graphic images.
(5)Data filing on a hard disk and post-processing of the data by use of shipboard and land-based c omputers linked through an Ethernet work station network.

Block diagram of the signal processing by the Sea Beam system on board the Hakuho-maru is shown in Fig. 4.2.1. Most of the system consists of a standard General Instrument Sea Beam system. Some of the special input/output signals for the Hakuho-maru are managed by the 4-channel serial (RS232-C, 9600 bps) interface ULM/5 inside the mini-computer DG S/140. The signal for each channel is as follows;

Ch. 0	Output:	Initialization of Hippy
	Input:	Roll signal from Hippy or back-up Gyro every 20 msec
Ch. 1	Output:	Output data to Real-time Mapping System every 1 ping
	Input:	Digital speed from Magnavox Series 5000 every 1 sec
Ch. 2	Output:	Output data to ZETA plotter
	Input:	Status input from ZETA plotter
Ch. 3	Output:	Vertical depth to Magnavox every 1 ping
	Input:	Navigation data from Magnavox every 1 sec

Block diagram of the gyro system for the Hakuho-maru Sea Beam is shown in Fig. 4.2.2. The Hakuho-maru is equipped with a precise gyro compass Tokyo Keiki SGC-1, and the gyro is used as a backup of Hippy, a standard vertical reference unit for the Sea Beam system.

Block diagram of the real-time mapping system for the Sea Beam is shown in Fig. 4.2.3. Yokogawa-Hewlett-Packard (YHP) work station 350 SRX with 24 MB memory is used for the processing. Input data from Magnavox Series 5000 and from Sea Beam system are recorded in two files in the 300 MB hard disk: MGD (magnetic anomaly, gravity anomaly, and vertical depth) file and Sea Beam file. The data files are easy to access at any time from any work station by using the optical Ethernet LAN.

Real-time topographic contouring along the ship's track is carried out every Sea Beam ping on an A0-size plotter and on A3-size roll plotters. The system also displays 3D graphic images of topography and plots MGD data on an A3-size roll plotter. Off-line processing of Sea Beam data is carried out by using the mini- computer YHP 835 Turbo SRX with 2 GB hard disk and a color electrostatic plotter in the computer room.

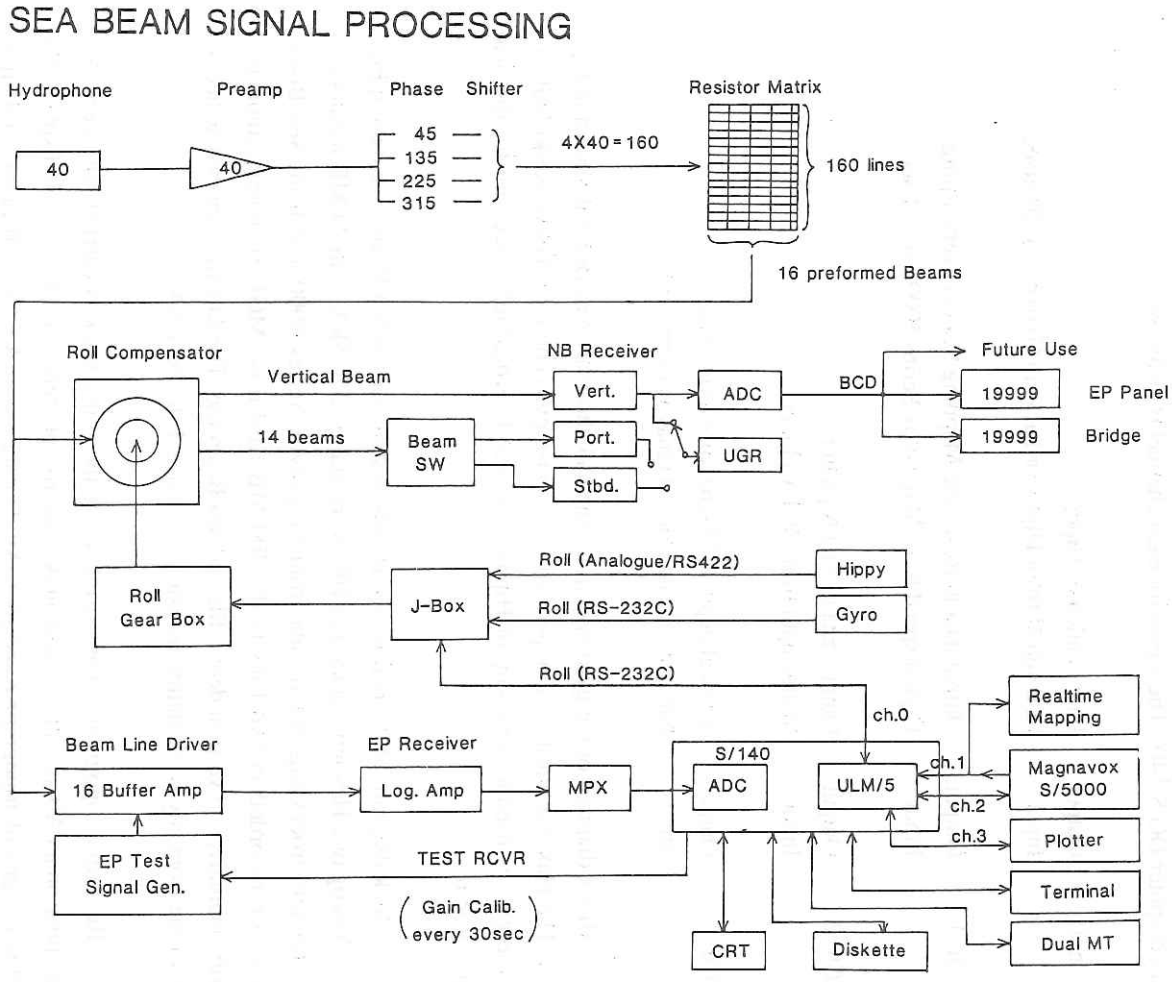

Fig. 4.2.1 Block diagram of the Sea Beam signal processing.

Gyro System for the Hakuho-maru Sea Beam

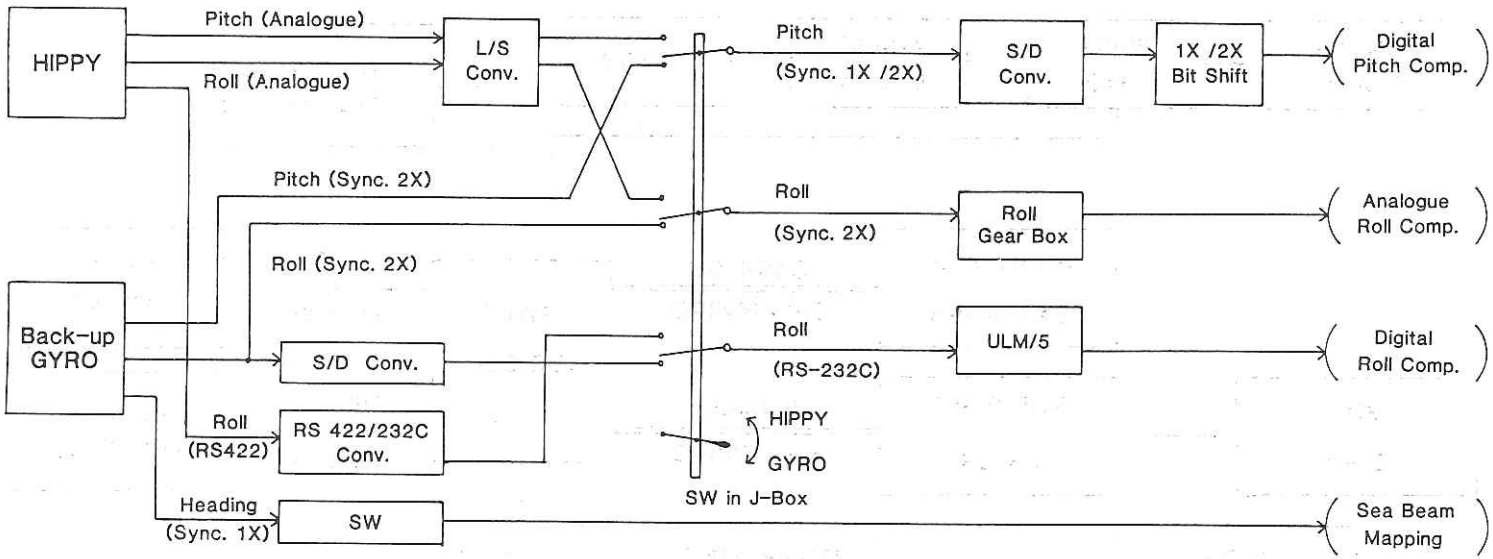

Fig. 4.2.2 Block diagram of the gyro system for the Hakuho-maru Sea Beam system.

Real-time Mapping System

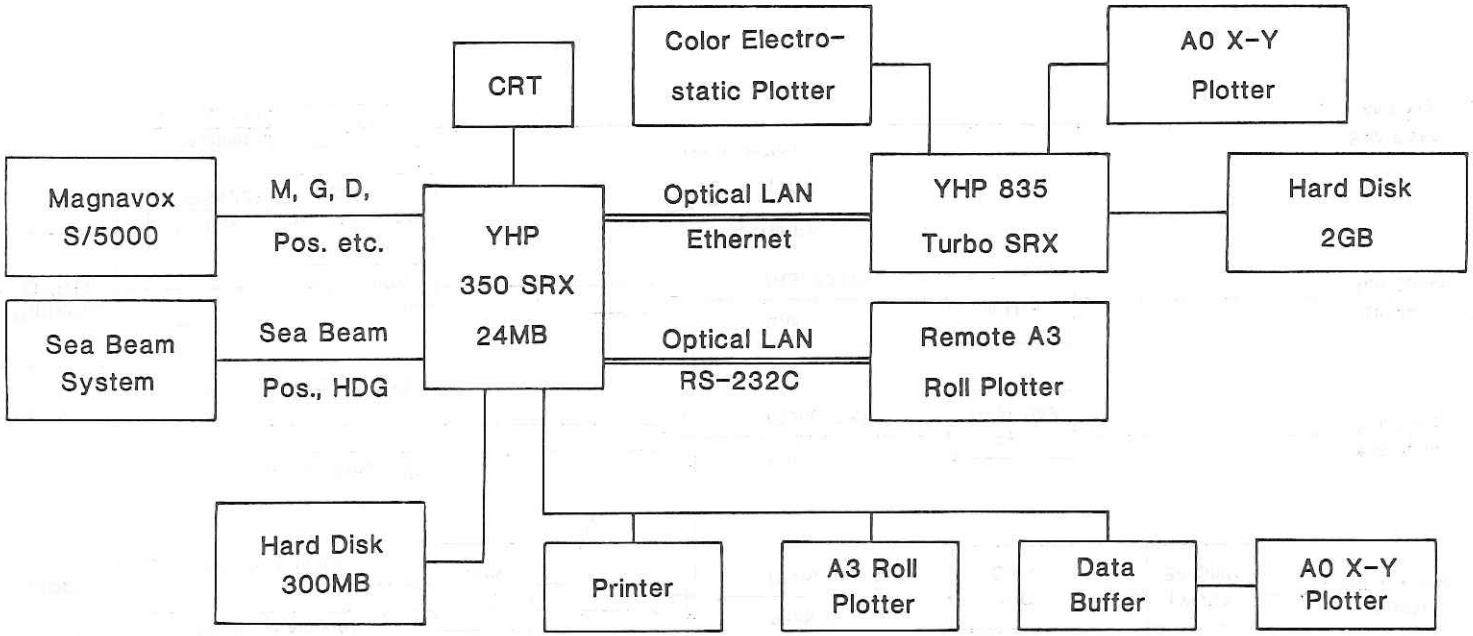

Fig. 4.2.3 Block diagram of the Real-time Mapping System on board the Hakuho-maru.

4.2.2 Off-line processing of Sea Beam data

Off-line processing of Sea beam data are usually carried out by using the data stored in the hard disk of the real-time mapping system in the following HD Format;

Byte	Format	Description for HD Format
001-006	I6	Block length in integer 6 bytes
007-012	I6	Block number (increment every ping)
013-018	I6	Hour in day (0 to 23)
019-024	I6	0.1 sec within 1 hour (0 to 35999)
025-030	I6	Heading (65536 = 360°)
031-036	I6	Average gate depth in meter
037-132	16I6	Sea Beam depth in meter (from Port to Starboard)
133-228	16I6	Cross-track distance in meter
229-324	32I3	Intensity of echo in 0.25 dB and itslength in 3.3 ms
325	A1	Navigation data Header in ASCII 1 character (= A)
326	A1	V (valid data) or I (invalid)
327	A1	N (North) or S (South)
328-329	I2	Degree of latitude
330-334	I5	Minute of latitude in 0.001 min
335	A1	E (East) or W (West)
336-338	I3	Degree of longitude
339-343	I5	Minute of longitude in 0.001 min
344-361	3A6	Terminators (= -00001)
362	A1	Carriage Return

This is the format for data output from the Sea Beam system. There is no data showing date in this format, and date is recorded only in each file name; for example, G062003.dat is created at GMT 03:xx on June 20. Sea Beam data in the hard disk are merged with MGD data and saved on magnetic tapes in the following SPC format, in which top 12 bytes and also 12 bytes in the bottom are changed from HD format;

Byte	Format	Description for SPC Format
001-006	16	Block number (increment every ping)

007-012	3I2	Date in YYMMDD (year, month, day)
013-343		Same as HD Format
344-349	I6	Magnetic Anomaly in 0.1 nT
350-355	I6	Free-air Gravity Anomaly in 0.1 mgal
356-361	A6	Terminator (= -00001)
362	A1	Carriage Return

Sea Beam data are also recorded on one of dual magnetic tapes, which are standard units of General Instrument Sea Beam system. When the MT Recording Switch is turned on, a Header record is written on the magnetic tape, and EOF is recorded when the switch is turned off. Usually several files are recorded on a magnetic tape. The format of the GI-MT Header record and Data record are as follows;

Byte	Format	Description for GI-MT Header Record
001-002	B2	Byte count in binary integer 2bytes (= 76)
003-004	2X	Not used
005-010	A6	MT Volume Name in ASCII 6 characters (ex. SB0123)
011-016	3I2	Date in DDMMYY (day, month, year)
017-020	A4	Mission Number
021-026	6X	Not used
027-076	A50	Comments followed by CR and LF

Byte	Format	Description for GI-MT Data Record
001-002	B2	Byte count in binary integer 2 bytes (= 148)
003-004	B2	Block number (increment every ping)
005-006	B2	Hour in day (0 to 23)
007-008	B2	0.1 sec within 1 hour (0 to 35999)
009-010	B2	Heading (0 to 65535; 65536 = 360°)
011-012	B2	Average gate depth in meter
013-044	16B2	Sea Beam depth in meter (from Port to Starboard)
045-076	16B2	Cross-track distance in meter
077-108	32B1	Intensity of echo in 0.25 dB and its length in 3.3 ms
109-110	1X,A1	Navigation data Header in ASCII 1 character (= A)

111-112	1X,A1	V (valid data) or I (invalid)
113-114	1X,A1	N (North) or S (South)
115-118	2(1X,I1)	Degree of latitude in ASCII 2 digits
119-128	5(1X,I1)	Minute of latitude in 0.001 min
129-130	1X,A1	E (East) or W (West)
131-136	3(1X,I1)	Degree of longitude
137-146	5(1X,I1)	Minute of longitude in 0.001 min
147-148	1X,A1	Carriage Return

The Sea Beam data saved in SPC format from the real-time mapping system and that recorded in GI-MT format are merged during a post-cruise processing into a final KH format shown below;

Byte	Format	Description for KH Format
001-008	A8	Cruise Name in ASCII 8 characters.
009	A1	Geodetic Frame: 8(WGS84), 7(WGS72), L(Loran-C)
010	A1	Normal Gravity: 7(IGSN71), 3(1930), X(?)
011-016	3I2	Date in YYMMDD (year, month, day)
017-018	I2	Hour
019-023	I5	Minute in 0.001 min
024-031	I8	Latitude in 0.00001 deg (Minus for South)
032-040	I9	Longitude in 0.00001 deg (Minus for West)
041-046	I6	Average Gate Depth in 0.1 m
047-052	I6	Magnetic Anomaly in 0.1 nT
053-058	I6	Free-air Gravity Anomaly in 0.1 mgal
059-064	I6	Heading in 0.1 deg
065-160	16I6	Sea Beam depth in meter (from Port to Starboard)
161-256	16I6	Cross-track distance in meter
257-352	32I3	Intensity of echo in 0.25 dB and its length in 3.3 ms

Sea Beam data in KH format then pass the following processings;

(1) Error data check for time and position,

(2) Conversion of geodetic framework, and

(3) Reduction of data volume into one fifth by filtering.

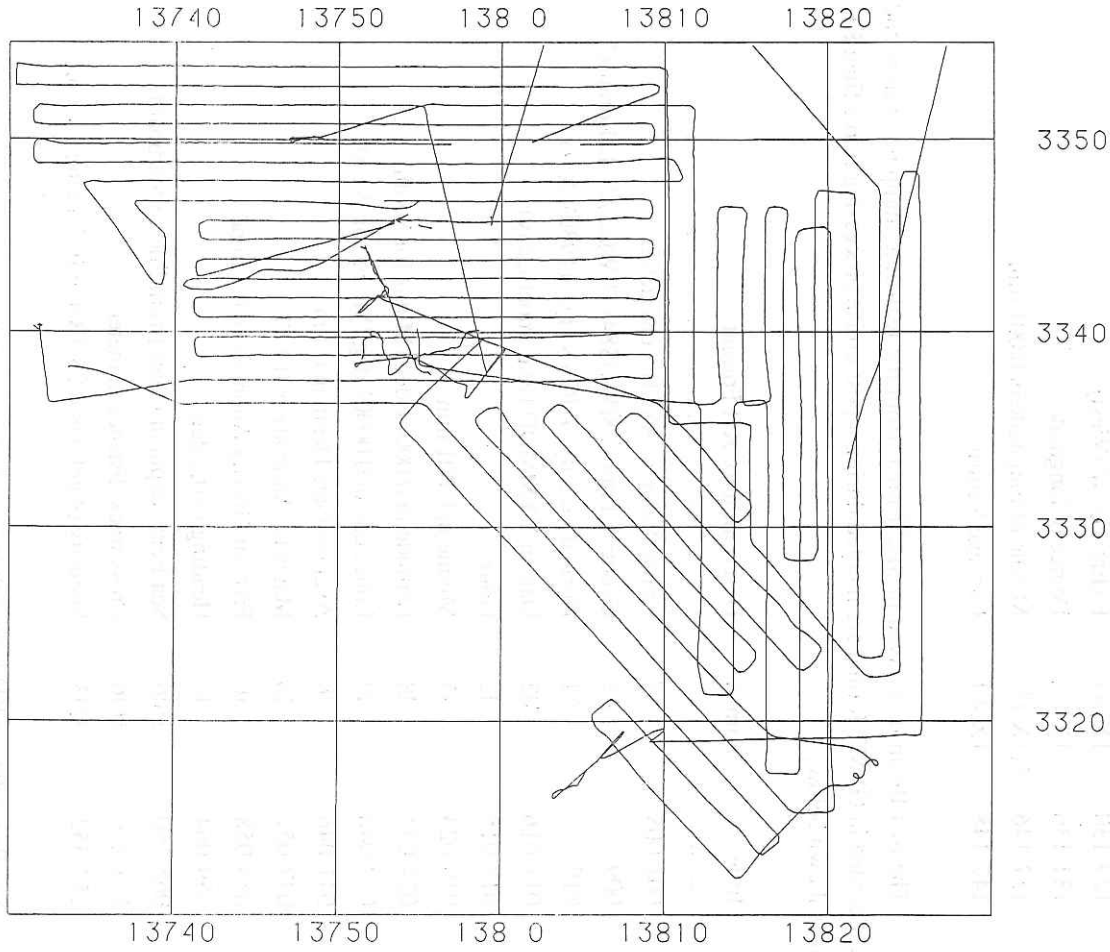

Fig. 4.2.4 Track chart of Sea Beam survey during the KH-89-1 cruise Leg 2.

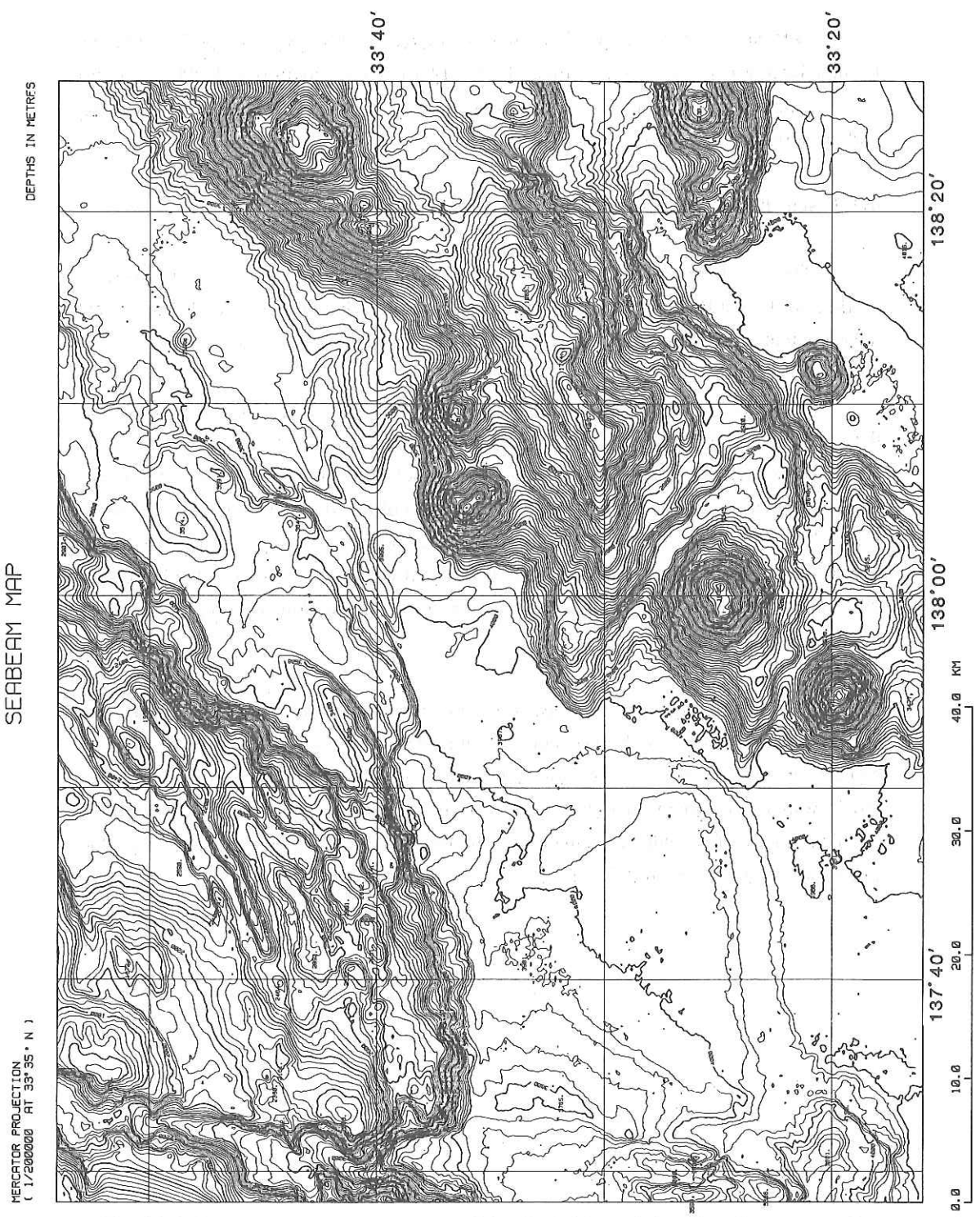

Fig. 4.2.5 Sea Beam map of eastern part of the Nankai Trough based on the surveys of Jean Charcot in 1984 and Hakuho-maru in this cruise (mapping by SPC Co. Ltd.).

Softwares for the mapping of bottom topography were developed during the French-Japanese Cooperative Project Kaiko Phase I carried out in 1984. A color electrostatic plotter can be used also in the computer room of the Ocean Research Institute, and the softwares have been revised.

4.2.3 Sea Beam surveys during KH-89-1 cruise

The Sea Beam system was operated through the entire cruise, and the system worked well. Sea Beam mapping was useful for the site selection for several geophysical measurements at ocean bottom carried out during the first leg of the cruise.

Intensive Sea Beam survey of Nankai Trough area was carried out at night during the second leg as a site survey for the deep-towed camera/sonar surveys and also for the Kaiko-Nankai diving experiments on board the French submersible "Nautile". The deep-towed surveys are reported in Chapter 5. Track chart of the Sea Beam survey is shown in Fig. 4.2.4. The surveyed area covers the gap where Sea Beam survey was not carried out during the Kaiko Project Phase I in 1984. Combined with the Sea Beam data obtained in 1984, a Sea Beam map was compiled in the area of the Suruga-Nankai Trough junction as shown in Fig. 4.2.5.

Real-time topographic mapping was valuable to monitor the ship's track during the deep-towed surveys for the Kaiko-Nankai diving sites. Disappearance of Sea Beam echo signals for several pings was sometimes observed during the deep-towed surveys carried out in rough seas, when air bubbles are probably sucked in under the hull after large pitching motion of the ship and remain near the Sea Beam transducers for certain time due to the slow ship's speed of 0.5 to 1.5 knot.

4.3 The Geomagnetic Total Force Measurement

M. Nakanishi ,T. Furuta, A. Oshida, and K. Sayanagi

The measurement of the geomagnetic total force was carried out by the proton precession magnetometer during the leg 1 of this cruise. The system for measurement is composed of a magnetometer unit, a data processing unit. The block diagram of the system of the geomagnetic total force measurement is shown in Figure 4.3.1. The data processing system was a set of a microcomputer (NEC PC9801VM21) which was made up of a CPU, a color display, and a printer. The navigation data was gotten through the Ethernet network from MAGNABOX SERIES 5000. The magnetometer unit consists of a console and a sensor with a length of 250 m. This sensor has never been towed at more than 12 knot against water. As the new Hakuho-maru can run up at more than 12 knot, the portion which sensor is connected in a cable was reinforced enough not to be broken. We tried to practice measurement at the full speed of the ship. The measurement succeeded and signals were not problematic.

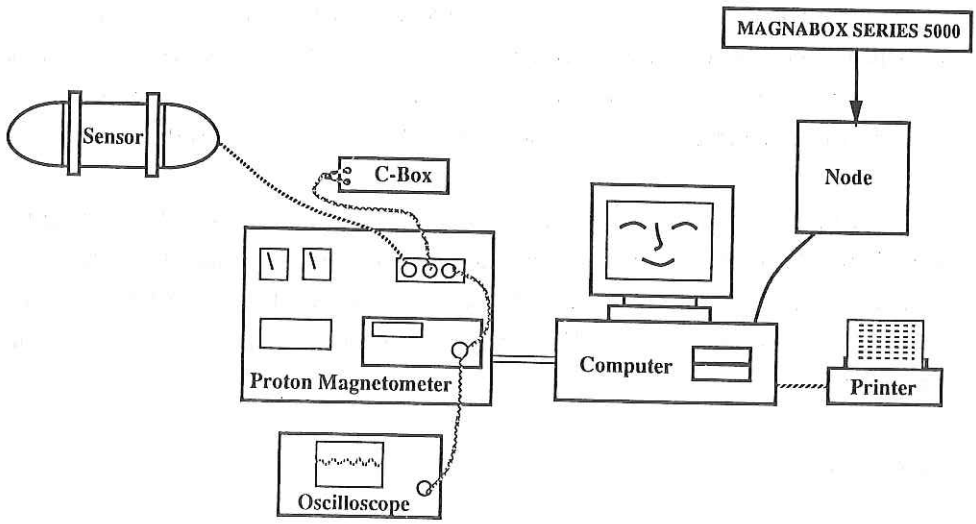

Fig. 4.3.1 Block diagram of the measurement of the geomagnetic total force.

The following is the method of the measurement.

1. The main unit (electronic part) sends an exciting signal to the sensor with 30 seconds interval.
2. In the main unit of the magnetometer the period of proton's precessional motion around the geomagnetic field is converted to frequency.

3. The data of frequency are converted from analog signals to digital signals and then transmitted to the microcomputer.
4. The microcomputer receives the frequency data from the magnetometer with 30 seconds interval and the navigation data of date (day, hour, minute, second), latitude, longitude, ship speed against seafloor, ship direction against seafloor, and depth from the navigation system with one second interval. The data processing system is controlled by this date.
5. The microcomputer calculates the geomagnetic total force from the frequency data.
6. All the data are logged in a floppy disk and printed out with one minute interval.

The tracks of the measurement are shown in Figure 4.3.2. Magnetic anomaly profiles along these tracks are shown in Figure 4.3-3. Magnetic anomalies are calculated with the reference field of IGRF 1985 (IAGA, DIVISION WORKING GROUP 1, 1985).

Magnetic anomalies which wavelength is from several ten kilometers to a few hundred kilometers are observed in all the profiles of Figure 4.3.3. The maximum amplitude is about 400 nT and the average is about 150 nT. Magnetic anomalies east of the Japan Trench, which wavelength is a few hundred kilometers, are due to the seafloor spreading in the Mesozoic (Nakanishi et al., in press) except the vicinity of seamounts. The age of these anomalies is about from 127 to 133 Ma (Nakanishi et al., in press).

The origin of magnetic anomalies west of the Japan Trench, which wavelength is several ten kilometers, is due to irregular topographic highs. Topography in this area is rugged owing to intrusive volcanic bodies (Honza and Tamaki, 1985). Positive anomalies are distinguished. This may implies that intrusive bodies are normally magnetized.

Reference

Honza, E., and K. Tamaki, The Bonin Arc, in The Ocean Basins and Margins, vol. 7A, edited by A. E. M. Nairn, F. G. Stehli, and S. Uyeda, pp. 459-502,Plenum Publishing Corporation, New York, 1985

IAGA, DIVISION WORKING GROUP 1, International Geomagnetic Reference Field 1985, J. Geomag. Geoelectr., 37, 1157-1163, 1985.

Nakanishi, M., K. Tamaki, and K. Kobayashi, Mesozoic magnetic anomaly lineations and seafloor spreading history, J. Geophys. Res., in press.

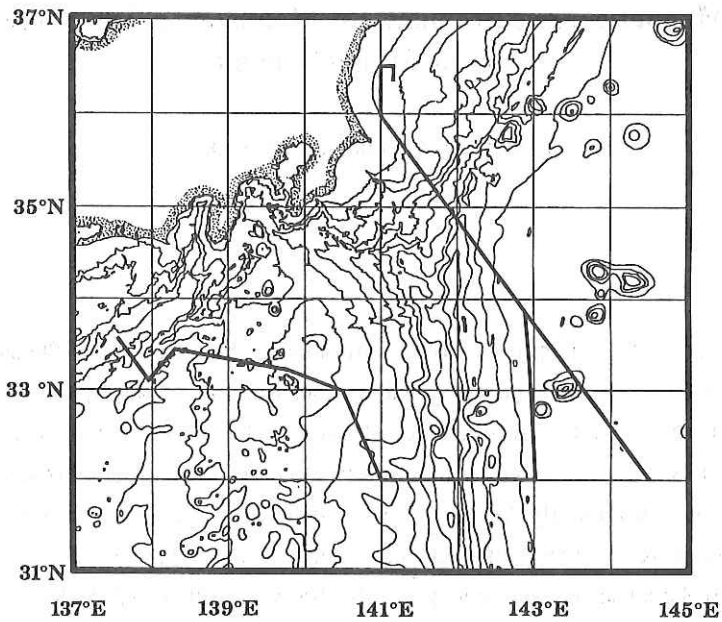

Fig. 4.3.2 Tracks of geomagnetic measurements. Contour interval is 1000 m.

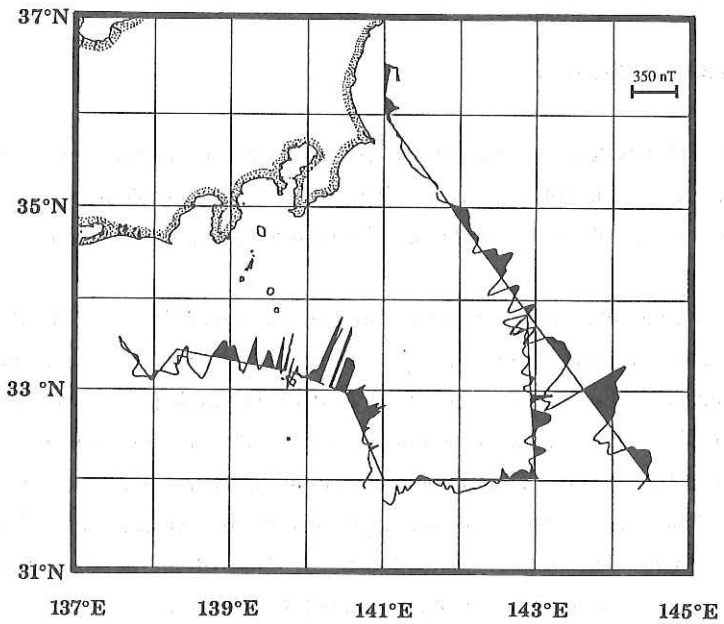

Fig. 4.3.3 The magnetic anomaly profiles along tracks (reference field IGRF 1985).Portions of positive anomalies on the profiles are painted black.

4.4 Magnetic Measurement by Means of a Deep-Towed Proton Magnetometer

K. Sayanagi, A. Oshida, and M. Nakanishi

Abstract

On 25 June 1989 a deep-towed observation using the ORI-DTP I (Ocean Research Institute Deep Tow Proton-magnetometer I) system was carried out by the R/V Hakuho-maru. A measurement of total magnetic intensity at the sea surface also was obtained concurrently with a surface-towed proton magnetometer. Our principal objective was to find a new event in anomaly M9 at the east of the Izu-Ogasawara trench. Magnetic intensity data were collected during this survey along a 17 n.m. long track. The topography in the surveyed area was generally flat with a depth of 5420-5190 m. The maximum value of the pressure case depth was about 2820 m. Peak to trough amplitudes of magnetic intensity obtained from the deep-towed and surface-towed magnetometers were about 380 nT and 170 nT, respectively. These anomalies had a 20 km wavelength. We could not confirm the new event in anomaly M9 from our results.

4.4.1 ORI-DTP I System

The ORI-DTP I system is characterized by installing a proton magnetometer with the internal digital memory in a pressure case. The system is quite simple in operation and low in the production cost. We will describe here the main features of the system.

The system consists of a pressure case and a proton sensor (Fig. 4.4.1). The pressure case contains a Geometrics Model G856 proton magnetometer and a depth meter. The sensor is connected to the pressure case with a 15 m of armored cable. A drogue joined to the sensor is used to reduce sensor yaw, pitch, and roll. The pressure case is towed with a steel wire rope behind a ship. Total magnetic field intensity and depth data are stored on each memory of the magnetometer and the depth meter in the pressure case. The memory size of the magnetometer is about 5700 readings. One of the depth meter is 16000 readings. The system can be used at a maximum depth of 6000 m.

Deep Towed Proton Magnetometer System

ORI-DTP I

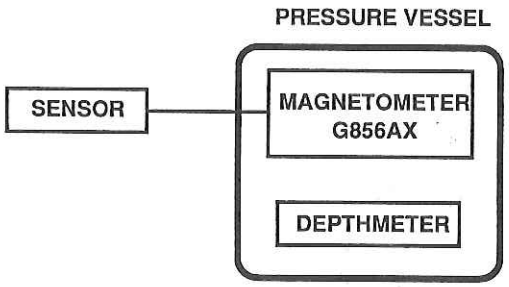

Fig. 4.4.1 Block diagram of the ORI-DTP I (Ocean Research Institute Deep Towed Proton-magnetometer) system.

4.4.2 Method of Measurement

The entire system for this investigation consisted of following three components; (1) ORI-DTP I system, (2) surface-towed proton magnetometer, and (3) acoustic transponder navigation system. Figure 4.4.2 illustrates the towing configuration of three systems. The steel wire rope (9.0 mm diameter) of the No.4 winch was used for towing the ORI-DTP I system and the transponder. The wire rope was connected to the forward end of the pressure case. The transponder was installed at 15 m above the pressure case. The transponder navigation provided relative positions of the deep-towed instrument to a ship by applying the SSBL (Supershort Base Line) method. The sensor of the surface-towed proton magnetometer was towed about 200 m behind the ship. The description of the surface-towed proton magnetometer system has been mentioned in part 4.3 of this report (Nakanishi et al., 1989).

The procedures for data logging of each measurements were as follows:

(1) The total intensity and pressure case depth data were stored on each memory of instruments in the pressure case of the ORI-DTP I system every one minute. These data were transferred to a Macintosh Plus personal computer via an RS-232C serial port on board.

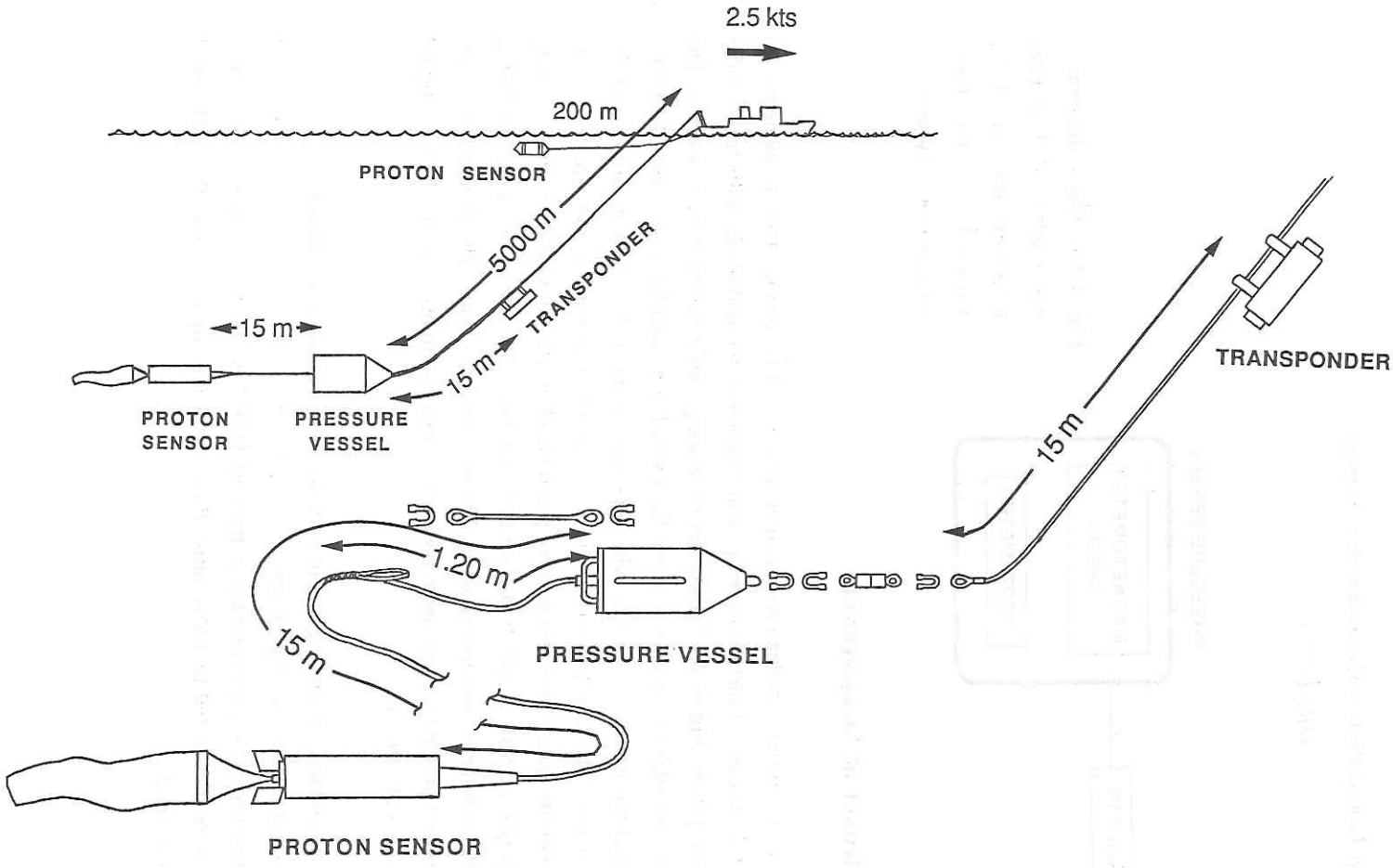

Fig. 4.4.2 Schematic explanation of the entire towing system for this investigaiton.

(2) The total intensity data from the surface-towed proton magnetometer were recorded on a floppy disk every 30 seconds. An PC-9801 VM microcomputer was used for this processing.

(3) The position data of the deep-towed instrument were saved on a floppy disk of an if-800 Model 60 microcomputer. The sampling interval was an average of 40 seconds.

Navigation data were collected by using a Magnavox system. The data contains the following items; (1) ship's position, heading, and speed, (2) water depth, and (3) cable out (length). The water depth data were obtained by the SEABEAM system.

4.4.4 Results

Magnetic intensity data of the deep-towed and surface-towed proton magnetometers were collected along a 17 n.m. track line (Fig. 4.4.3). The track line trending N35° W was perpendicular to the direction of anomaly M9 at the east of the Izu-Ogasawara trench, which was identified by Nakanishi et al. (1989). The ship's and tranponder positions were used to determine the positions of the deep-towed instrument. Unfortunately the depth meter in the ORI-DTP I system did not work correctly on account of broken wires.

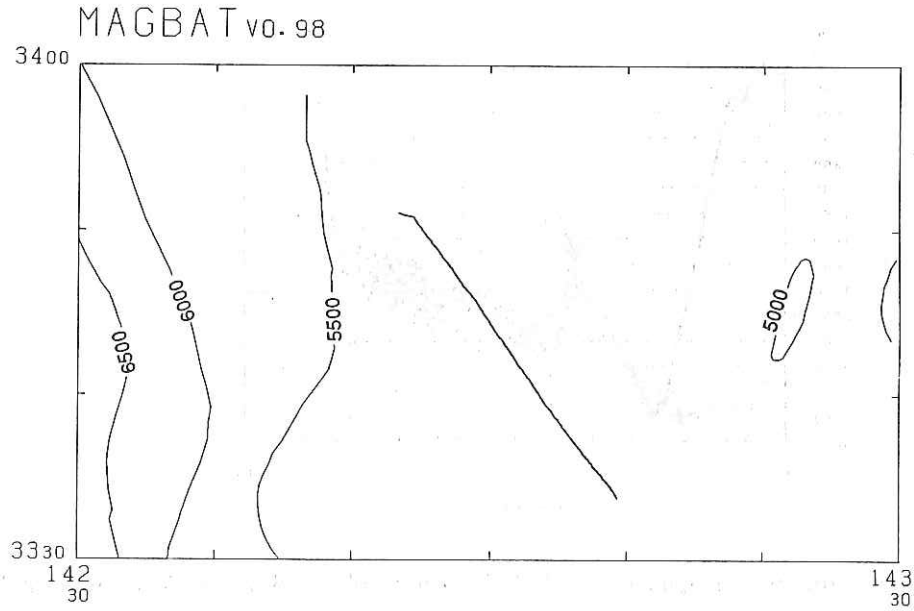

Fig. 4.4.3 Ship's track for the deep-towed proton magnetometer survey. Bathymetry is shown at 500 m intervals.

Figure 4.4.4 (upper) shows the results of magnetic measurements. Positive peaks of two profiles indicate the magnetic anomaly M9. The discrepancy of the peak positions is due to the difference between the relative positions of two sensors to the ship. Peak to trough amplitudes of the deep-towed and surface-towed results were about 380 nT and 170 nT, respectively. These anomalies had a 20 km wavelength.

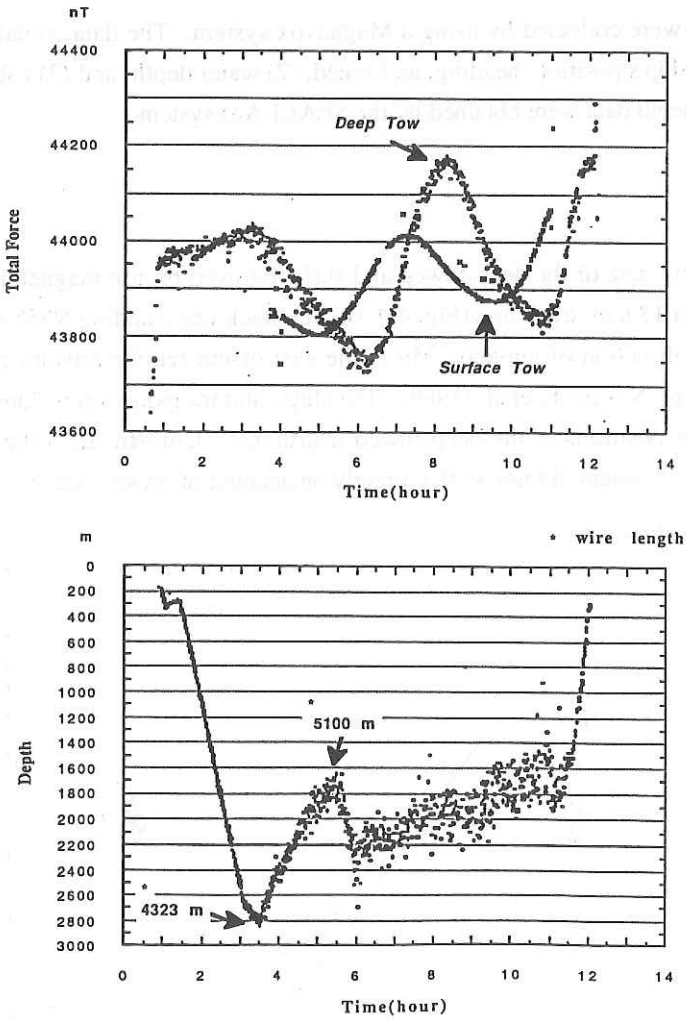

Fig. 4.4.4 Profiles of magnetic total field intensities obtained by the deep-towed and surface-towed proton magnetometers (upper). Transponder depth determined by an acoustic transponder navigation system (lower).

The downward component of the transponder position is presented in Figure 4.4.4 (lower). This indicates the tranponder depth. If the pressure case was at the same depth with the transponder, the maximum value of the case depth was about 2820 m.

The topography in the surveyed area was generally flat. The water depth decreased northward, and was variable between 5420 m to 5190 m.

4.4.5 Discussion

The existence of several additional events in the presently accepted Mesozoic reversal sequence were presented by Tamaki et al. (1989). Anomaly M9 is one of the polarity chrons which are expected to have additional events. Our preliminary results do not support the possibility of an additional event in anomaly M9. The detailed analysis of the obtained magnetic data and further investigation for anomaly M9 in other areas is needed to clarify this discrepancy.

The deep-towed observation in this cruise was the first experiment with geophysical objectives using the ORI-DTP I system. The obtained results show that this simple system can give us useful information for the magnetization of the oceanic crust. To perform more fine investigation, we need to attack the following three tasks; (1) how to tow the DTP more deeply, (2) how to tow the DTP in more stable posture, and (3) how to tow the DTP faster.

References

Nakanishi, M., T. Furuta, A. Oshida, and K. Sayanagi, The geomagnetic total force measurement, in Preliminary Report of the Hakuho Maru Cruise KH89-1, J. Segawa Ed., Ocean Res. Inst., University of Tokyo, 1989.

Nakanishi, M., T. Tamaki, and K. Kobayashi, Mesozoic magnetic anomaly lineations and seafloor spreading history of the northwestern Pacific, J. Geophys. Res., in press.

Tamaki, K., M. Nakanishi, and J. Channel, A revision of Mesozoic magnetic reversal sequence (abstract), 85th SGEPSS Spring Meeting, III-29, 1989.

4.5 Measurement of Three Component Geomagnetic Field by STCM

N. Seama, T. Ichikita and N. Isezaki

Introduction

Improvement of a STCM (Shipboard Three Component Magnetometer; Isezaki, 1986) has been made to provide the high quality data of the geomagnetic field vectors (e.g. Seama et al. 1989). Recently, Seama (1989) and Seama and Isezaki (submitted) pointed out that the accuracy of the STCM largely depends on the accuracy of a gyro compass. The error increases in downward, north and east components of the geomagnetic field in order, which is due to the accuracy of a gyro compass. Especially, the east component is sometimes unstable for about an hour just after a ship changes its course and these data are usually useless. The magnetic data of a detailed geomagnetic survey with many course changes, like a seamount survey, usually have many difficulties.

The main objective of this cruise is to test the performance of a STCM, using the precise gyro compass (SGC-1) equipped with R/V Hakuho-maru Junior. The accuracy of SGC-1 is 0.01 degrees, while accuracy of a gyro compass we have used is about 0.05 degrees.

Outline of STCM system

A micro-computer in Lab.3 controlled sampling all data. Three fluxgate-type sensors in an orthogonal fashion were set on the deck. The ship's heading, rolling and pitching angles were also measured by a precise gyrocompass (SGC-1) in Lab.9 and the data were send to Lab.3 through LAN (Local Area Network) system of Hakuho-maru. Position and depth data were obtained from general informations in the LAN system. Sampling interval was 0.1 second. Data were filtered, averaged and stored in the minifloppy disks every 15 seconds.

Operation

Four troubles occurred during this cruise. The first was wrong sampling of heading data at the micro-computer. Data before June 22 were useless because of this fatal mistake. The second was caused by a elevator in the ship. The sensors were set too close by the elevator which made a magnetic noise. The elevator had been forced to stop by a chief scientist since June 24. The third was that the sensors were moved during the cruise at one time. The data indicated that it happened at June 28. The last was that wrong

sampling of rolling and pitching data at the micro-computer during almost all the cruise. These rolling and pitching data could not be used. However this is not fatal, because rolling and pitching should be deviated symmetrically from those averages if these are observed for a long period.

Seven '8-shape rotations' (the ship run with 8 shape track) were done (Table 4.5.1). These data were used to remove the induced and permanent magnetic field by the ship.

Table 4.5.1. List of '8-shape' rotations

1. June 21 '89, 18h51m-19h11m, 36°12.5'N 141°23.5'E
2. June 25 '89, 07h55m-08h14m, 32°00.3'N 144°29.9'E
3. June 27 '89, 07h23m-07h44m, 32°58.2'N 140°31.0'E
4. June 27 '89, 20h55m-21h15m, 33°33.6'N 137°33.6'E
5. July 5 '89, 20h20m-20h40m, 33°49.8'N 138°09.2'E
6. July 9 '89, 22h50m-23h11m, 33°17.2'N 138°22.0'E
7. July 11 '89, 10h32m-10h52m, 34°04.2'N 138°05.7'E

Data processing

The vectors of the geomagnetic fields were obtained from observed data through the procedure mainly based on the method of Isezaki (1986). 12 constants, relating to the magnetic susceptibility distribution, the permanent magnetization, the position of the sensors and shape of a ship, were determined as Table 4.5.2, using the data sets of '8-shape rotation' (Table 4.5.1). Two sets of 12 constants were determined because the sensors moved during the cruise.

Table 4.5.2. List of '12 constants'

We found new terms which did not mentioned in the basic equation of STCM (equation (4) in Isezaki (1986)) from the data sets of '8-shape rotation'. These are proportional to w*sin(G) for the north component and w*cos(G) for the east component of geomagnetic field, where G is a heading of the ship and w is dG/dt (t is time). Physical meaning of the terms were not known right now. We ignored the terms for the data processing, because w is negligible for almost all the data. And data during the ship changing its course were abandoned.

Table 4.5.2. List of '12 constants'

1. determined by four '8-shape' rotations (1.- 4.) in Table 4.5.1

$$\tilde{A} = \begin{bmatrix} 0.9111 & -0.0882 & 0.0789 \\ 0.1196 & 0.6488 & -0.1832 \\ 0.1034 & -0.0892 & 1.2676 \end{bmatrix}, \quad \vec{H}_p = \begin{bmatrix} 5998 \\ 15698 \\ -2526 \end{bmatrix}$$

2. determined by three '8-shape' rotations (5.- 7.) in Table 4.5.1

$$\tilde{A} = \begin{bmatrix} 0.9062 & -0.0848 & 0.0362 \\ 0.1158 & 0.6504 & -0.0755 \\ 0.1553 & -0.0623 & 1.2531 \end{bmatrix}, \quad \vec{H}_p = \begin{bmatrix} 5453 \\ 10965 \\ -2024 \end{bmatrix}$$

We used a new method for removing errors due to errors of the 12 constants. The 12 constants should have errors even if all the instruments are free from error, because we have two assumptions on determination of the 12 constants: the geomagnetic field where '8-shape rotation' was done was same as IGRF and permanent magnetic moments of ship's body were kept constants during all the cruise. The errors (Xer,Yer,Zer) of the geomagnetic fields due to the errors of the 12 constants are summarized as following equations (See Appendix in detail).

$$Xer = Ax*\sin(G) + Bx*\cos(G) + Cx + Dx*\sin(2*G) + Ex*\cos(2*G)$$
$$Yer = Ay*\sin(G) + By*\cos(G) + Cy + Dy*\sin(2*G) + Ey*\cos(2*G)$$
$$Zer = Az*\sin(G) + Bz*\cos(G) + Cz$$

where Ai, Bi, Ci, Dj and Ej (i=x,y,z; j=x,y) are constants due to the errors. We neglected Dj and Ej this time because they are estimated at smaller than Ai, Bi and Ci. Ai and Bi are able to be obtained using more than two sets of data just before and just after the ship changes its course with an assumption that the geomagnetic field is constant during the period. Ci is only the bias which is able to be removed by subtracting its trend. This method was applied to each data file (An average length of the files is about 12 hours.) and it worked quite well. This method requires an assumption that permanent magnetic moments of ship's body keep constant only for the length of each file.

The residual field of each component was calculated by subtracting the IGRF-85 (IAGA Division I Working Group 1 ,1987) first and then trends from the obtained geomagnetic field data. The short wave length anomalies, which seemed to be noise or a

result of not using rolling and pitching data, were removed using a 5-minute or 9-minute simple moving average method.

Results

The geomagnetic anomaly profiles of the north, east, downward components along the ship tracks in two area are shown in Figs.4.5.1 and 4.5.2.

Measurement of the geomagnetic field vectors by STCM is improved by using the precise gyro compass SGC-1, even if roll and pitch data were not used. Because east component anomalies are stable even when the ship change its course and the noise level of each component of the geomagnetic fields is same as seen in Fig.4.5.2.

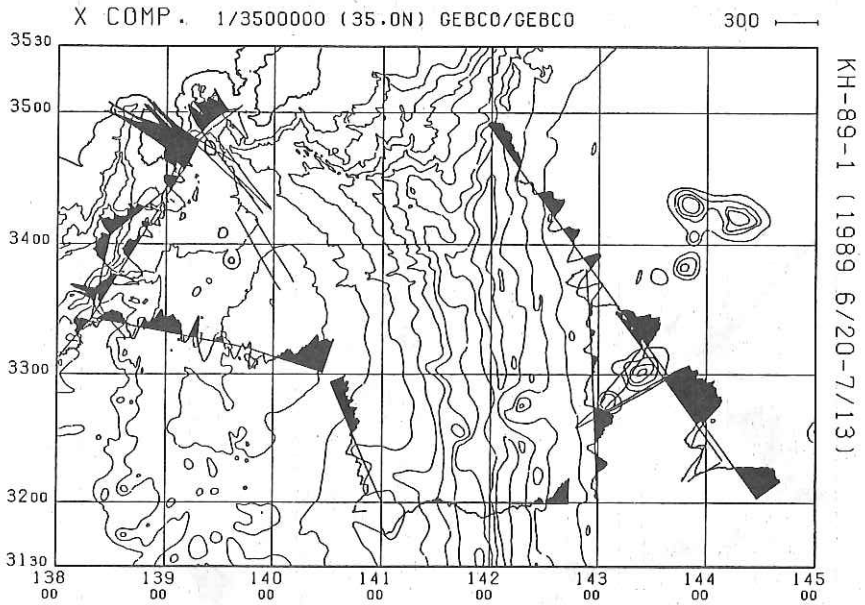

Fig. 4.5.1A

Fig. 4.5.1 Geomagnetic anomaly profiles of (A) the north, (B) the east and (C) downward components along the ship tracks obtained during this cruise except a detailed survey near the Nankai Trough area. Positive anomalies are shaded. Bathymetric features are based on GEBCO(JODC). The contour interval is 1000m.

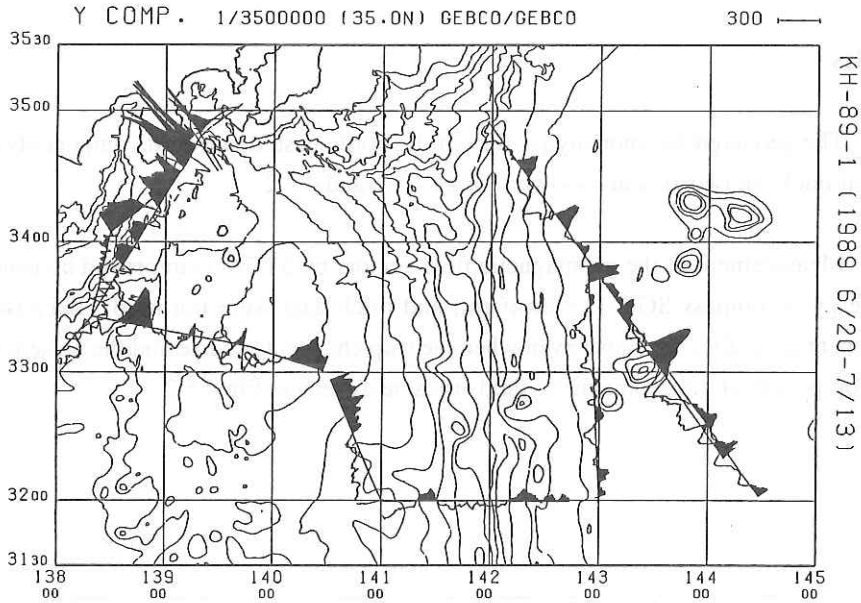

Fig. 4.5.1B

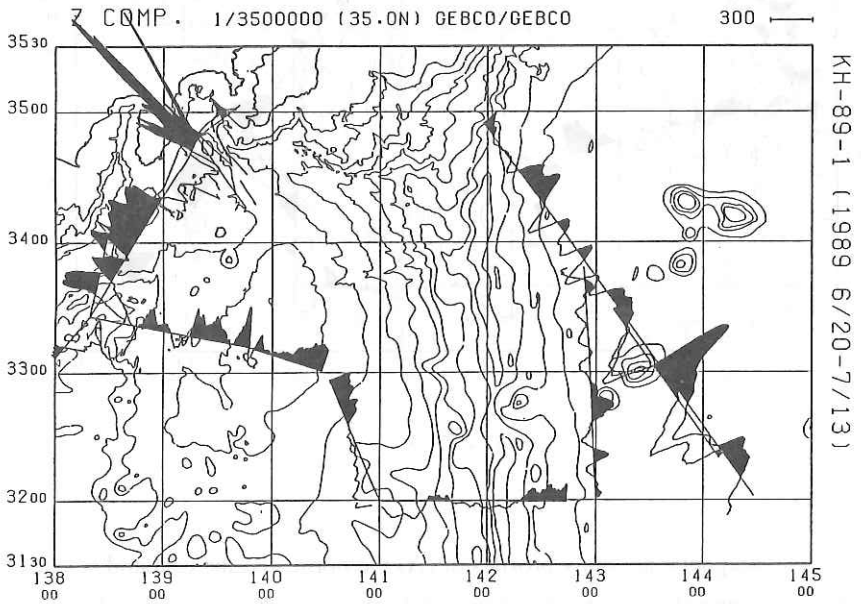

Fig. 4.5.1C

The north of the Nankai Trough is magnetically very quiet, while in the south, there are strong magnetic anomalies, especially in the Zenisu Ridge. The Zenisu Ridge has a normal magnetization if it has an uniform magnetization. It is easily known from a fact that the direction of the anomaly field above the Zenisu Ridge showed the southward direction (Fig.4.5.2A).

In the north of the Oshima Island, there are very strong magnetic anomalies. They are related to recent volcanic activity in this area. It is important to do a detail three component magnetic survey in this area to know recent magmatic activity.

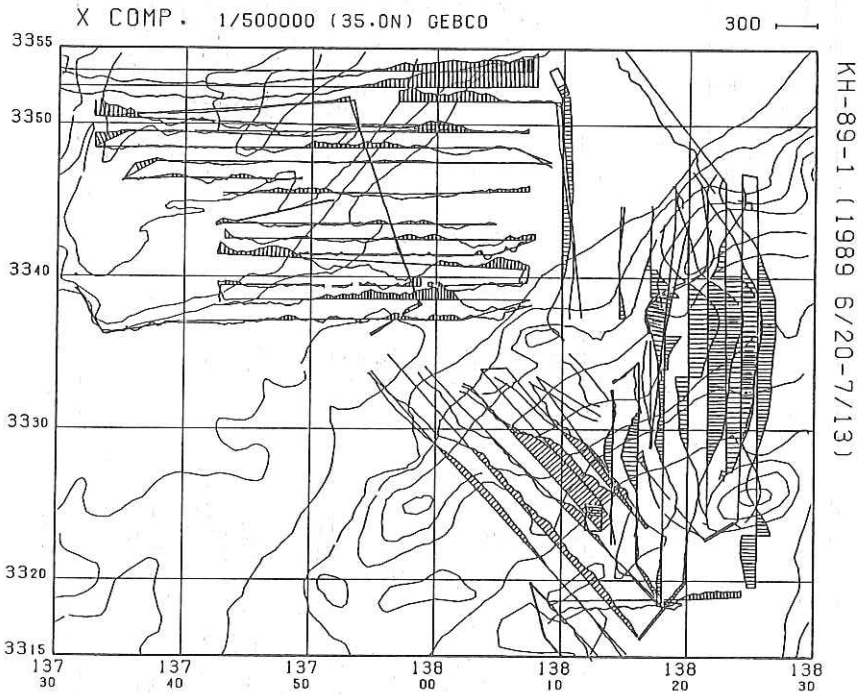

Fig. 4.5.2A

Fig. 4.5.2 Geomagnetic anomaly profiles of (A) the north, (B) the east and (C) downward components along the ship tracks near the Nankai Trough area. Positive anomalies are shaded. Bathymetric features are based on GEBCO(JODC).

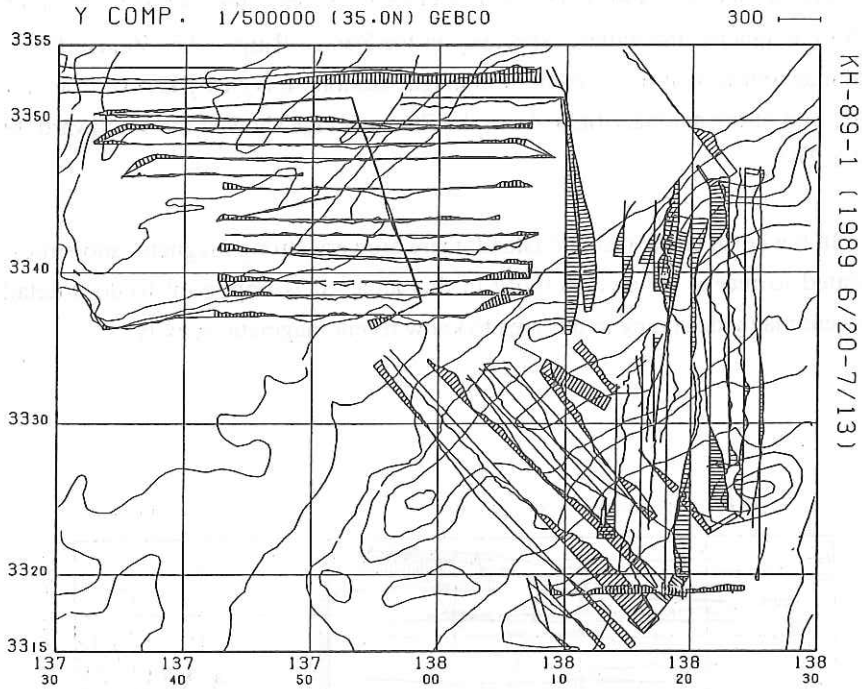

Fig. 4.5.2B

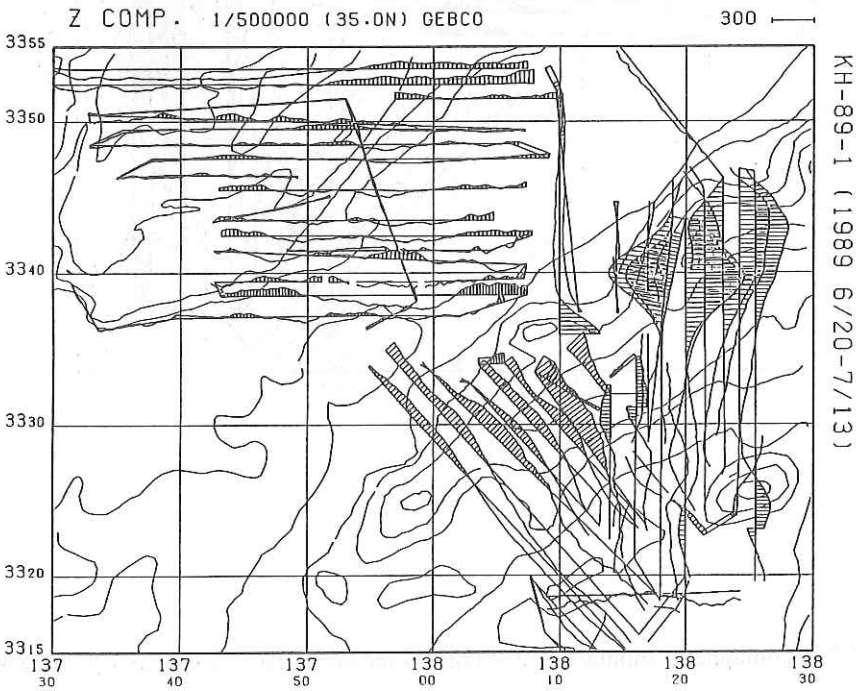

Fig. 4.5.2C

References

IAGA Division I Working Group 1 (Barraclough, D. R., Chairman),1987. International geomagnetic reference field revision 1987.J. Geomag. Geoelectr., 39: 773-799.

Isezaki, N., 1986. A new designed shipboard three-componentmagnetometer. Geophysics, 51: 1992-1998

Seama, N., 1989. The Distribution of Magnetization in theEastern Part of the Japan Basin and Its Tectonic Implications. M.Sc. thesis, Kobe University

Seama, N. and Isezaki, N., (in press) Sea-floor Magnetization in the Eastern Part of the Japan Basin and its Tectonic Implications. Tectonophysics, Special issue on Tectonics of Eastern Asia and Western Pacific Continental Margin.

Seama, N., Sayanagi, K., Nogi, Y. and Isezaki, N., 1990. Vector Anomalies of the Geomagnetic Field measured by STCM. In: J. Segawa (editor), Preliminary Report of The Hakuho Maru Cruise KH-88-3. Ocean Research Institute Univ. of Tokyo.

Appendix

The basic equation for measurement by STCM is

$$\overrightarrow{H_{ob}}=\tilde{A}\tilde{R}\tilde{P}\tilde{Y}\overrightarrow{F}+\overrightarrow{H_p} \quad (1)$$

where $\overrightarrow{H_{ob}}$ and $\vec{F}$ are the observed and the ambient geomagnetic fields, $\tilde{R}$, $\tilde{P}$ and $\tilde{Y}$ are the matrices of rotation due to roll, pitch and yaw of the ship, respectively. Put $\tilde{A}=\tilde{1}+\tilde{A}$ from original equation (4) in Isezaki(1986). $\tilde{A}$ and $\vec{H}_p$ is what we called 12 constants.

The errors of 12 constants, $\tilde{dA}$ and $\overrightarrow{dHp}$ make the errors of geomagnetic field, $\vec{F}_{er}$. Then

$$\overrightarrow{H_{ob}}=(\tilde{A}+\tilde{dA})\tilde{R}\tilde{P}\tilde{Y}(\vec{F}+\overrightarrow{F_{er}})+\overrightarrow{H_p}+\overrightarrow{dH}$$

and using equation (1), we have

$$\vec{F}_{er}=-(\tilde{R}\tilde{P}\tilde{Y})^{-1}(\tilde{A}+\tilde{dA})^{-1}(\tilde{dA}\,\tilde{R}\tilde{P}\tilde{Y}\,\vec{F}+\overrightarrow{dH})$$

Rewriting each component of this equation with an approximation, $(\tilde{R}\tilde{P})=\tilde{1}$, we have

$$Xer = Ax*\sin(G) + Bx*\cos(G) + Cx + Dx*\sin(2*G) + Ex*\cos(2*G)$$
$$Yer = Ay*\sin(G) + By*\cos(G) + Cy + Dy*\sin(2*G) + Ey*\cos(2*G)$$
$$Zer = Az*\sin(G) + Bz*\cos(G) + Cz$$

4.6 Electrical Sounding of the Sea Floor using Controlled Electromagnetic Source Method (MOSES)

J. Oubina, J. Segawa, J. Motta and C. S. Yang

4.6.1 Introduction

Over the past two decades, the electrical conductivity beneath the sea has been estimated by means of magnetotellurics method (MT). The MT methods are a valuable tool for studying the deep earth structure, but unfortunately, they are not applicable for resolving shallow electrical structures because the natural magnetic fields originated above the earth's surface are attenuated (screened) by the conductive ocean and masked by several forms of oceanic background noise (induction from turbulent water motions and surface and internal waves), so that temporal variations in periods shorter than a few minutes can not be observed.

Natural background noises in the sea floor electric field at frequency around 1 Hz, have been obtained at the level approximately 1 pV/m (Cox et al. 1978). Such a low noise level suggests that the weak electromagnetic field propagating through the underlying sediments, crust, and lithosphere from an artificial source installed in water are measurable at significant source - receiver separations. The controlled source electromagnetic techniques are the obvious solution to resolve this problem.

The Controlled Source (CS) method have been proposed by many geophysicists (Banister, 1968; Coggon et al., 1970; Cox, 1980; Edwards et al., 1981 and Cox et al., 1981). Some experiments on this subject were carried out by Young and Cox (1981), Becker et al. (1982), Nobes (1984), Edwards et al. (1985), Wolfgram (1985) and Nobes et al. (1986).

The CS methods consist of four fundamental electromagnetic source types : vertical (VED) and horizontal (HED) electric dipoles which consist of an insulated, current-carrying wire with bared ends; vertical (VMD) and horizontal (HMD) magnetic dipoles which consist of closed loops of insulated, current-carrying wire. According to the type of the sources employed, either transverse electric (TE) or transverse magnetic (TM) mode can be produced. The VED source produces only the TM mode while the HED sources produce both the TE and the TM modes. The VMD and the HMD produce only the TE and the TM modes respectively. For example, according to Chave et al. (1982), in cylindrical coordinates system, a VED source produces only three electromagnetic components: E_r, E_z

(electric) and B_ϕ (magnetic) while an HED source produces all the six electromagnetic field components: E_r, E_ϕ ,E_z(electric), B_r, B_ϕ and B_z (magnetic).

The main objective of this study is to measure the shallow resistivity structure beneath the sea water layer by mean of an off shore controlled source electrical sounding method. To carry out this study, galvanic technique with VED source named magnetometric off shore electrical sounding (MOSES) method was selected. By this method is measured the magnetic field on the sea floor due to the galvanic current flowing from a vertical bipolar transmitter extending from the sea surface to the sea floor. Since this method minimizes the problems that arise due to the presence of the conductive sea water layer, it gives enough sensitivity to sea floor resistivity even when the distance between transmitter and receiver is long. If there exists an intermediate resistive layer or an intermediate conductive layer within the crust, it can be delineated by expanding the transmitter-receiver separations to distances comparable with the length of the bipole, i.e., the depth of the sea (Edwards et al., 1981).

The controlled source electrical sounding by employing the MOSES method was conducted in this cruise at two sites around the off shore Ibaraki Prefecture (Fig. 4.6.1). One site is CS-4 with coordinates 36°14' N in latitude and 141°10' E in longitude where the sea floor depth is about 800 m. The other site is CS-6 with coordinates 36°14' N in latitude and 141°25' E in longitude where the sea floor depth is about 1300 m.

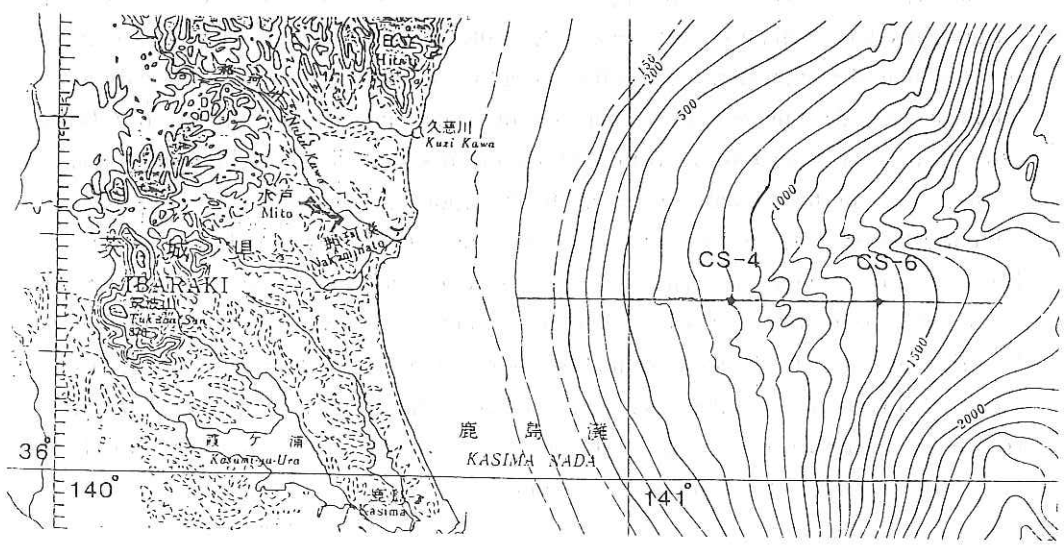

Fig. 4.6.1 Sites CS-4 and CS-6 at off shore Ibaraki Prefecture.

In this report, the principal aspects on the MOSES's theory, experimental equipments, and data processing are presented and preliminary results of this study are described with some details.

4.6.2 Theoretical background

The theory of the MOSES method has been extensively developed by Edwards et al. (1981), Edwards et al. (1984) and Nobes (1984); it is an off shore adaptation of magnetometric resistivity (MMR) method described by Edwards, (1974) and Edwards et al. (1978). The principal bases of the MOSES method are mentioned here. Any CS electrical method requires two fundamental parts: a transmitter of electrical energy and a receiver to detect the presence of the induced electromagnetic field. In the MOSES method, the transmitter consists of a long, vertical, insulated current - carrying wire with bared ends,which extends from the sea surface to the sea floor. The receiver is a magnetometer located on the sea bottom which measures the azimuthal magnetic field (total horizontal components) generated by the bipole.

Following Edwards et al. (1981) the basic principles of the MOSES method are illustrated in Fig. 4.6.2.1.

Consider the sea water as a layer with resistivity ρ_s and thickness d and the crust as a half space with resistivity ρ_c ($\rho_s << \rho_c$) A commuted current flows through a long, vertical, insulated cable to a large electrode at the sea floor. Because the crust is more resistive than the sea water, most of the current returns through sea water directly to an identical electrode at the sea surface, but some of the current penetrates into the crust, flows through the crust and returns to the surface electrode. This configuration is axially symmetric about the vertical axis defined by the bipole and generates only TM mode. In cylindrical coordinates system, the current flows on a vertical plane field, i.e. the current has only r and z components. The azimuthal magnetic field generated from the source and measured at the sea floor is proportional to the current circuit which encloses the field point P. Edwards et al. (1981) demonstrated that this current is proportional to the resistivity contrast between the sea water layer and crustal layer, thus, if the azimuthal magnetic field (magnetic response) for a range of transmitter - receiver separations is measured, an electrical sounding of the crust is to be performed.

Numerical computations indicate that the magnetic field is small for most practical cases, but if the azimuthal field is measured to an accuracy of about 10 percent, the crustal resistivity is obtained with the same degree of accuracy.

Edwards et al. (1981) developed the quasi static electromagnetic (direct current limit) theory of the MOSES method for an isotropic layered crust. They showed that MOSES electrical soundig curves, similar to those for the conventional Schlumberger resistivity sounding method, can be constructed. MOSES curves are valid for alternating current, for ranges small compared with a skin depth in the crust. However, the authors above mentioned estimated that the practical sounding depth is characterized in the order of half range of the transmitter receiver separation. The formulation of the MOSES method is not presented in this report, but the essential formula of the apparent resistivity is

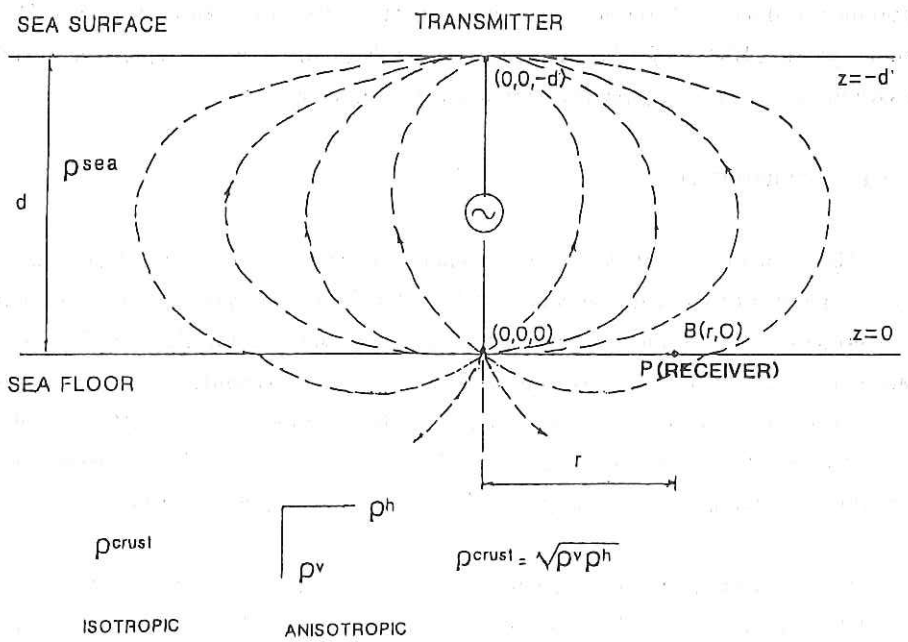

Fig. 4.6.2.1 General scheme of the MOSES method. The electric current flows from the sea surface to sea floor through a cable and returns through sea water. Some current penetrates in the crust and returns to the sea surface. This currents have a vertically symmetric axis and are proportional to the resistivity contrast between the sea water and the crust. The azimuthal magnetic field measured at the sea floor is proportional to the amount of current enclosing the field point P.

essential formula of the apparent resistivity is expressed as the following:

$$\rho_a = (\rho_s \ \mu_o I \, d)/(4\pi \ r^2 B_\phi)$$

where a is apparent resistivity of the sea floor, ρ_s is resistivity of the sea water, μ_o is magnetic permeability of the free space and I is current transmitted through a bipole of length d. Also, r is transmitter - receiver separation and B_ϕ is deconvoluted magnetic field response. This formula is obtained by an asymptotic expansion of the theoretical response

of a uniform crustal layer beneath the sea water layer and is used to transform field data into a domain where they may be compared with typical model.

4.6.3 Equipments employed and procedure

The MOSES method, like any CS method, requires two fundamental parts: a transmitter and a receiver. In addition, the positioning system which determines the distance between transmitter and receiver is included, because this parameter is of relevant importance in the estimation of apparent resistivity of the crust. In this cruise both the Branch system (BRS) and the conventional ship's positioning systems were used to improve the accuracy in estimating the transmitter - receiver distance.

4.6.3.1. Transmitter.

The transmitter provides electrical energy to generate primary electromagnetic field. It consists of two parts; a power supply and a bipole. The power supply, located on the ship, consists of a transformer, a DC power unit and a controller unit. The bipole, located in water, consists of an electrode at the sea floor suspended from the ship by a long, vertical, insulated current - carrying cable. The other identical electrode is situated at the sea surface (near the ship) to compose the electrical circuit. Both electrodes are attached to by a complementary weight of 100 Kg and 20 Kg, respectively.

Three - phase 220 volts alternating current (AC) of the ship is transformed to one - phase 200 volts AC at first. The power unit converts AC to direct current (DC) voltage which is capable of providing a maximum DC voltage of 100 volts and a maximum current of 60 amperes. A controller unit converts a DC voltage into a commutated voltage with a step - like form by means of a relay system. To obtain a valid form of output voltage, it is reversed every 4 sec with an intermediate off - pause of 2 sec duration, so that a series of square wave of 8 sec - period are produced. A switched DC output current generated in this stage is transmitted to the electrodes . To ensure the polarity of the pulse recorded at the receiver, the controller unit has a precise clock which is synchronized with the identical clock in the receiver.

By means of a digital voltmeter and a pen recorder the polarity and the form of the current transmission are registered. This information is used in data processing to carry out deconvolution of the azimuthal magnetic field.

(a)

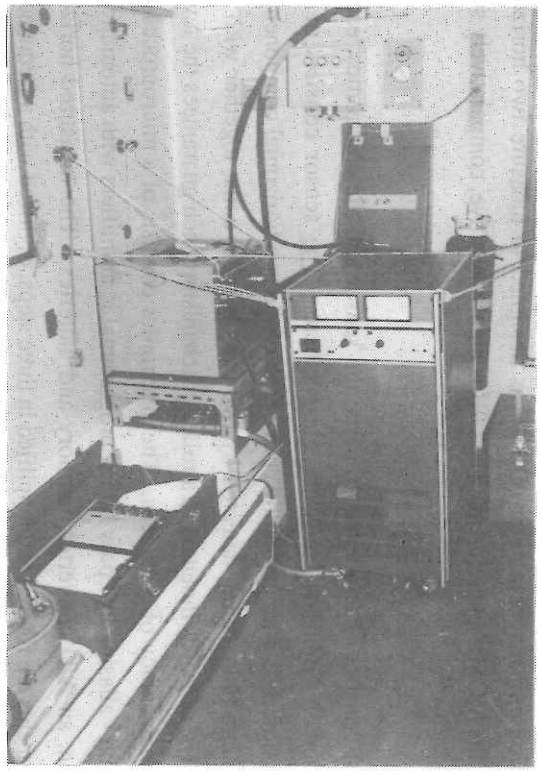

(b)

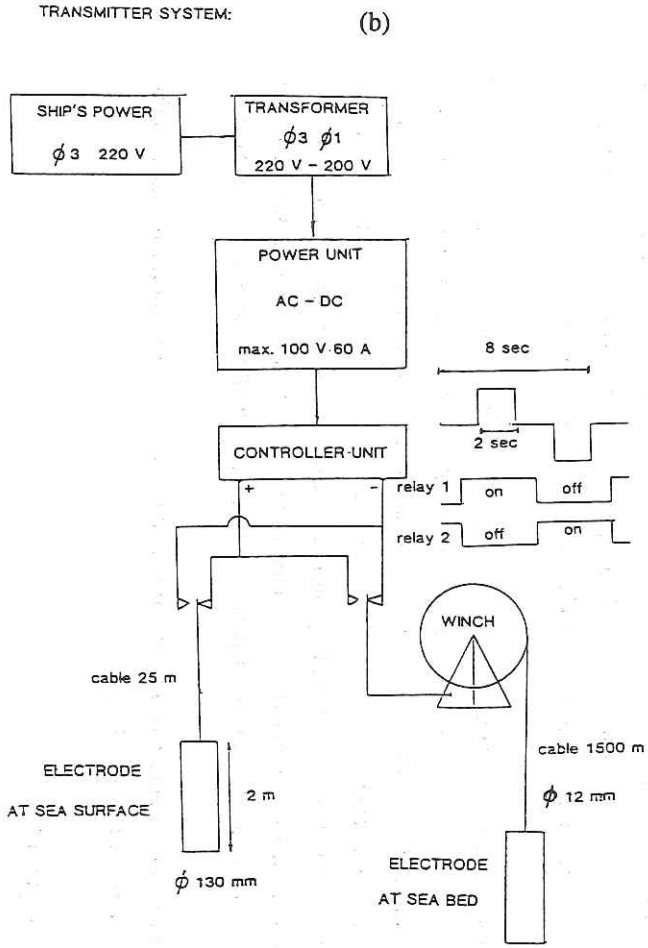

Fig. 4.6.3.1 The transmitter's power supply (a) and its schematic diagram (b). (a) shows the 3 phase-to-1phase transformer, the DC power unit, the controller unit and the pen recorder during the 40 ampere current transmission. (b) represents the diagram to obtain an 8 sec commutated current.

A winch powered by 220 volts, 3- phase AC was used to wind the electrode cable of 12 mm in diameter and 1600 m in maximum length. The coiling speed varies from 8 to 40m/min. The cable used weighs 110 Kg/Km in water and has a resistance of 1.25Ω/Km at 20°C. The electrodes consist of two identical pipes of stainless steel 304 2 m long and 110.6 mm in diameter, to guarantee a good contact with the sea water.

The transmitting current in both sites was 40 amperes with a voltage of about 84 volts. The total resistance of the circuit including the contact resistance of the two electrodes was 2.1Ω. Another effect present was the reactive component of the transmitter system i.e. the inductance, created by the part of the cable remaining spooled on the winch during the current transmission and by mutual coupling between the cable and the sea water; the capacitance, created by the electrode polarization (charge stored in the electrodes). This kind of reactance depends on the frequency of the transmitted current.

A schematic diagram of the transmitter and a view of the equipments used in this study are shown in Fig. 4.6.3.1.

4.6.3.2. Receiver

The function of the receiver is to detect the presence of the electromagnetic field produced by the source. In the MOSES method the source is a VED, by which are generated TM modes only, so that electromagnetic field has the azimuthal magnetic and vertical electric components. In the MOSES method azimuthal magnetic field is measured, thus, an induction coil magnetometer (OBI) was designed to measure two horizontal components for the MOSES experiment. The OBI is highly sensitive, comparatively small, and inexpensive.

The OBI consists of two separate parts: the sensor and the electronics, each of which is encased in "Benthos" pressure glass sphere. The sensor consists of four horizontal induction coils with permalloy cores, each of the two horizontal components (X and Y) of magnetic field being detected by two each parallel coils, together with two preamplifiers. The sensor is mounted in a roller mechanism which guarantees the level of the coils with an accuracy of 3 degrees. The electronics consists of a microprocessor, a precise clock, anti - aliasing low pass filters, programmable amplifiers with automatic gain control function, an A/D converter, memory and batteries. The measured horizontal magnetic components are filtered and amplified in three steps, digitized with a frequency of 128 Hz, stacked (2^n times) and recorded in two static RAM card memories (256

Kbyte/card) under the control of the microprocessor. The 12 volts DC power required is provided by four 3B36 type lithium batteries.

The receiver is synchronized with the transmitter and programmed as to the start time and the total number of hours of the experiment (30 hours), the period of current transmitted (8 sec.), and the number of stacks needed (64 times). With this information, the interval (19 minutes) for one complete record is calculated automatically. This interval is divided in three parts: 1- in the first 5 minutes, optimum amplifiers gain are searched; 2- in the next 9 minutes, data are gated, stacked and saved; 3- in the last 5 minutes, the system remains inactive until the start of the next record interval time. In this form, the memory allotted is completely used. All parameters mentioned above were used in this experiment o compose the scheduled time of current transmission.

The schematic diagram of the OBI and a view of the sensor and electronics are shown in Fig. 4.6.3.2.

4.6.3.3 Branch system

Accuracy of all distances measured between the transmitter and receiver is important in the MOSES experiment, especially for near - field stations. This accuracy is maintained by using the Branch System (BRS).

The BRS consists of two transponders, one is situated at the receiver and the other is attached to at the source cable near the sea floor electrode. The ship's transducer sends and receives the acoustic signals to measure the source-receiver ranges (in meters) which are registered periodically on the ship (Fig 4.6.3.3). Complementarily, the ship's position and sea depth are recorded every 1 minute in a floppy disc for the post processing.

4.6.3.4 Procedure

The MOSES experiment starts with the synchronization between the receiver and transmitter clocks, and time schedule for ON - OFF current transmission is decided. The receiver is encased in the glass spheres and mounted on a 2 m high aluminum frame (Fig. 4.6.3.4). The sensor is located at the uppermost part of the frame which is separated 1 m from the electronics approximately. The OBI is attached to by a 43528 KHz radio beacon, a flasher and an acoustic transducer at the upper part. At the base of the frame are installed an acoustic transponder, a release system and an 80 Kg plumb anchor.

(a)

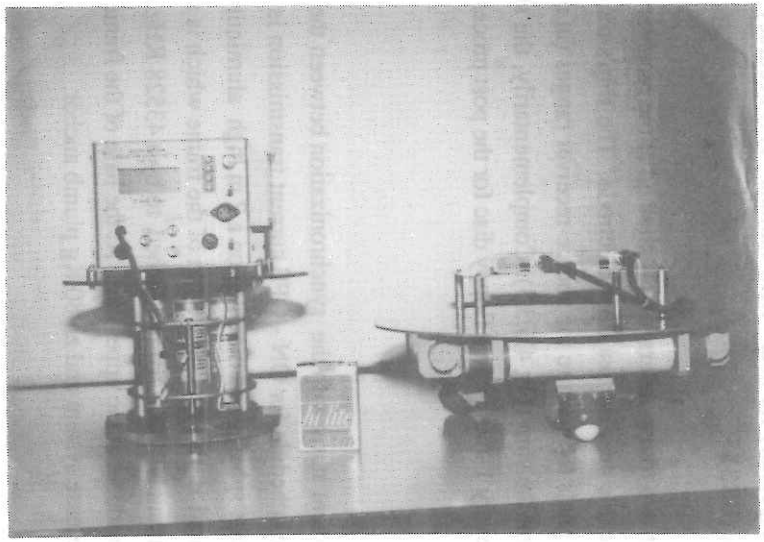

(b)

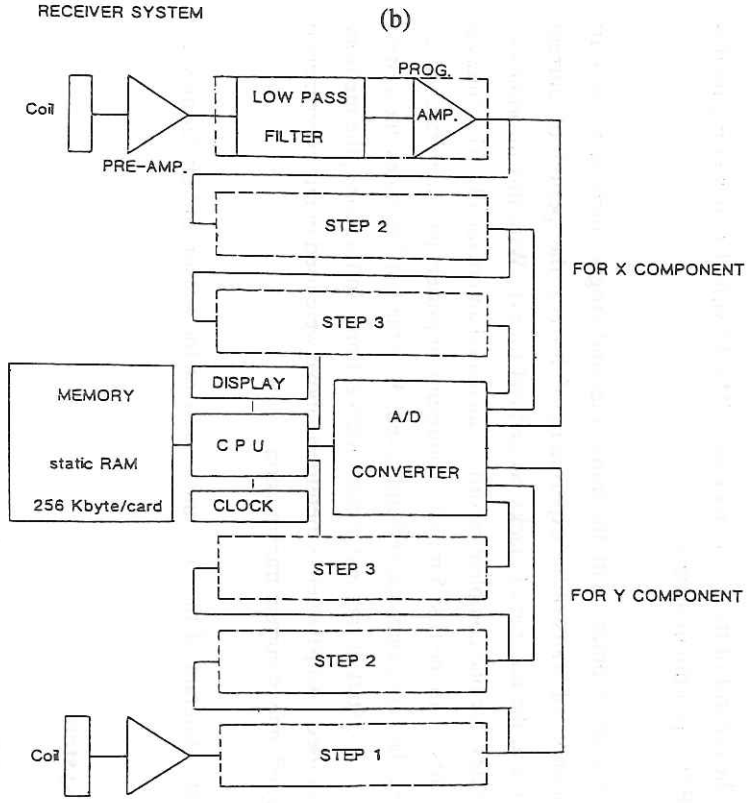

Fig. 4.6.3.2 The sensor and electronics (a) and the diagram of the OBI's signal processing (b). (a) shows the coils and preamplifier mounted in a roller system (right), the electronics and batteries (left). (b) represents the steps in the signal processing for both components from the coils voltage output to saving in the RAM memory. One record consists of 1024 data for each component in the experiment.

The OBI is deployed at a previously determinated point at the sea floor and fixed during the experiment. In the next step, the ship occupies the position of the first station of the transmitter and then extends the bipole. The current transmission is started to obtain two or more complete records.

Periodically, the distance between the source and the receiver is measured. During transmission the ship maintains the same position with an error which depends on the sea conditions (Fig. 4.6.3.3). When the measurement at one station is over the bipole cable isrecoiled and the ship moves to the next station. When all programmed stations are completed the OBI is released by an acoustic command and recovered. The data contained in the memory cards are read and saved in a floppy disc for processing. The OBI position and ship's stations for both sites (CS-4 and CS-6) are illustrated in Fig. 4.6.3.5. The time required for a complete electrical sounding was about 25 hours, when 8 bipole stations were occupied.

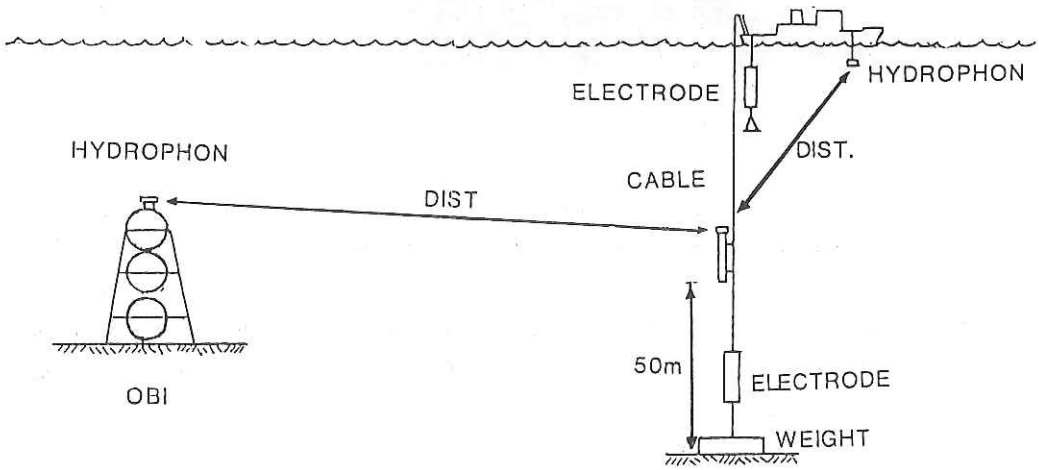

Fig. 4.6.3.3 A view of the MOSES experiment. The transmitter is a vertical insulated current - carrying cable extending from the sea surface to the sea floor. A large electrode and BRS's transponder are attached at the sea floor end of the cable. OBI is deployed at a point of distance r, which has another transponder. The distance r is measured and registered periodically on the ship by means of acoustic signals.

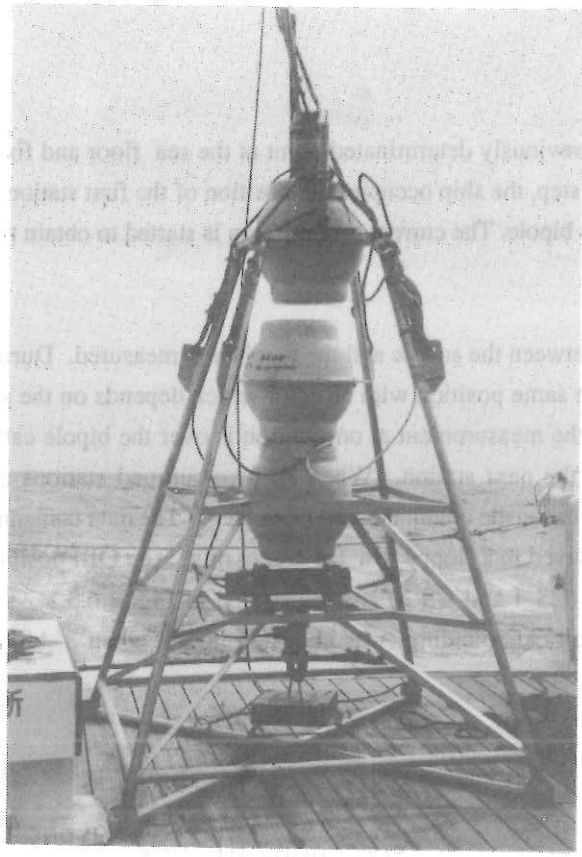

Fig. 4.6.3.4 The receiver (OBI). Three Benthos spheres mounted on the aluminum frame assure the buoyancy. The upper sphere contains the sensor, the lower the electronics. At the top of the frame are attached a flasher, a radio beacon and a transducer and at the base a plumb anchor, a release system and a transponder.

4.6.4. Data processing

The data processing method to obtain the curve of apparent resistivity versus distance between the transmitter and receiver is discussed here. To determine the sea floor magnetic response, which is used in the apparent resistivity formula, we consider the earth and the OBI as two linear systems. The input is the primary field generated by the bipole and the output is the raw data registered at the OBI. The response functions of the OBI and the transfer function of the earth were estimated following the diagram as shown in Fig. 4.6.4.1.

The response function of the OBI was estimated by employing the data measured in the Helmholtz coils at Geomagnetic Observatory, Japan Meteorological Agency (Kakioka). The input for X component was a square wave of 337 nT pp and that for Y component 349 nT pp. The input and output were Fourier transformed by Fast Fourier Transform (FFT). In the frequency domain, the response functions of the OBI for X and Y components and its amplitude and phase spectrum were calculated. The amplitude spectra of OBI's response function for both components are shown in Fig. 4.6.4.2.

The transmitter signal (linear system's input) was recorded, digitized and FFT's transformed. Considering the transmitted signal form (commutated square wave), the

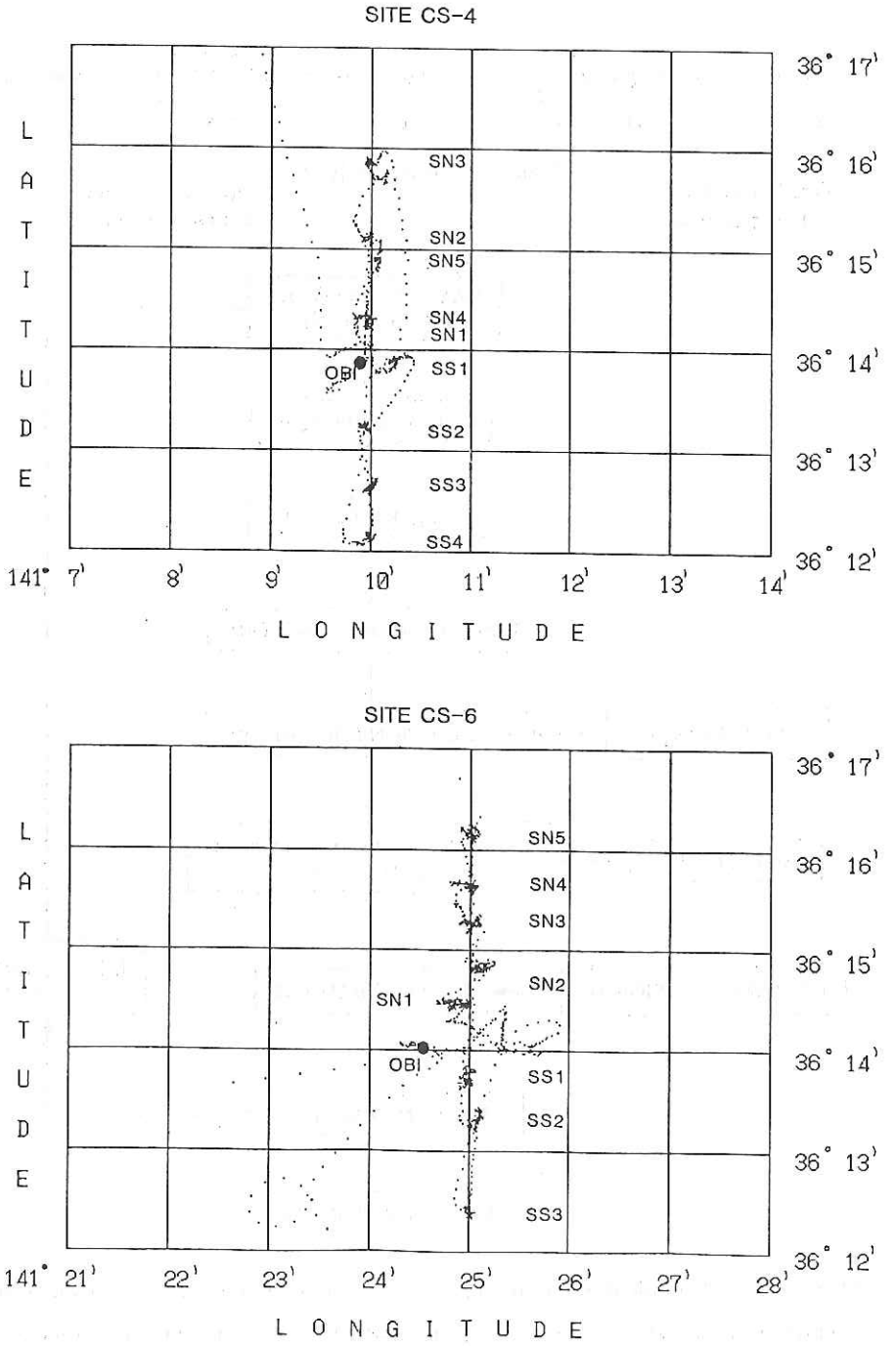

Fig. 4.6.3.5 The locations of OBI and ship's track and stations for both sites CS-4 (top) and CS-6 (bottom). The ship's stations are named SN# (northern part) and SS# (southern part).

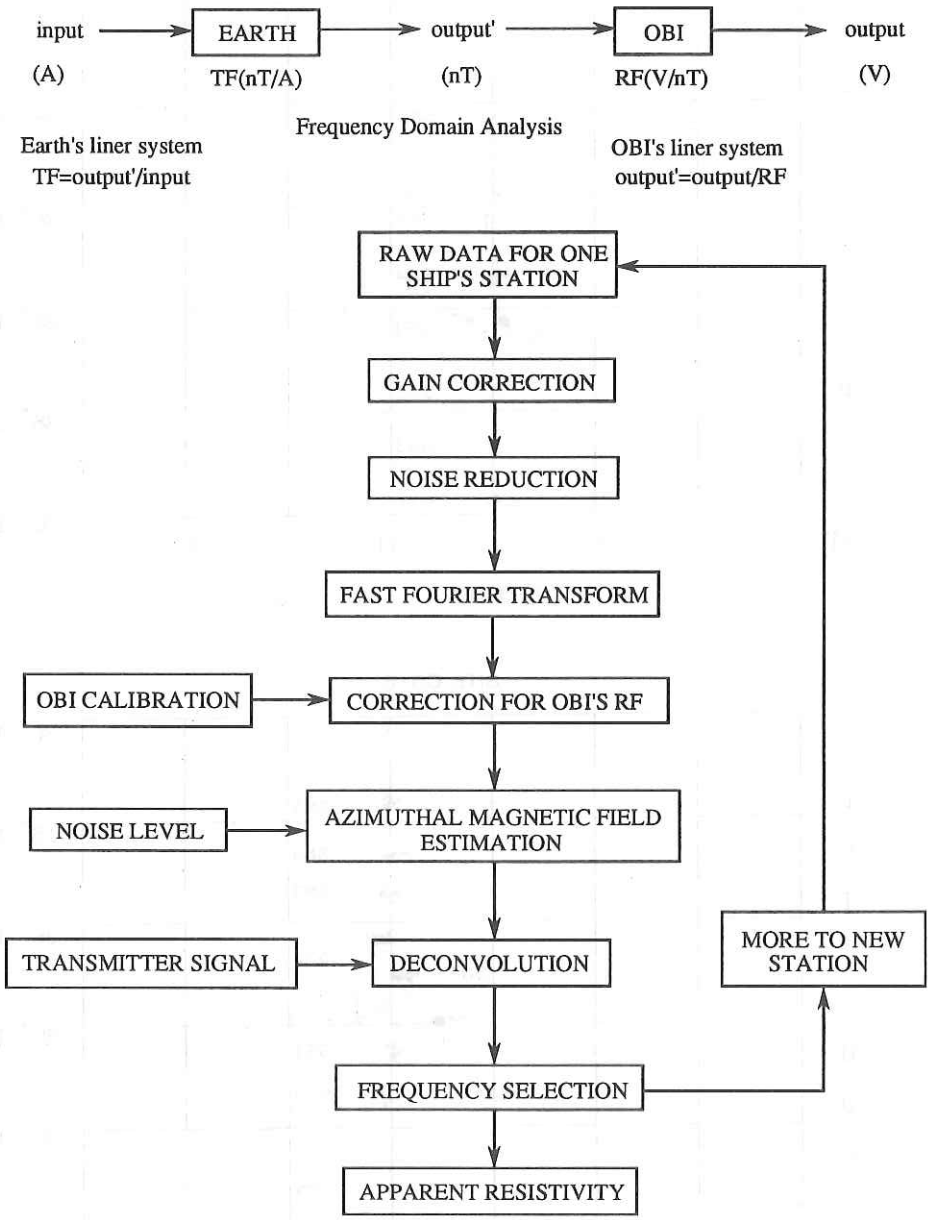

Fig. 4.6.4.1 The schematic diagram to obtain the azimuthal magnetic transfer function of the earth from the two linear systems concatenated. The input at OBI is equal to the earth's output. Also the flow chart of data processing from the output raw data to the apparent resistivity versus source receiver distance for the selected frequency is shown.

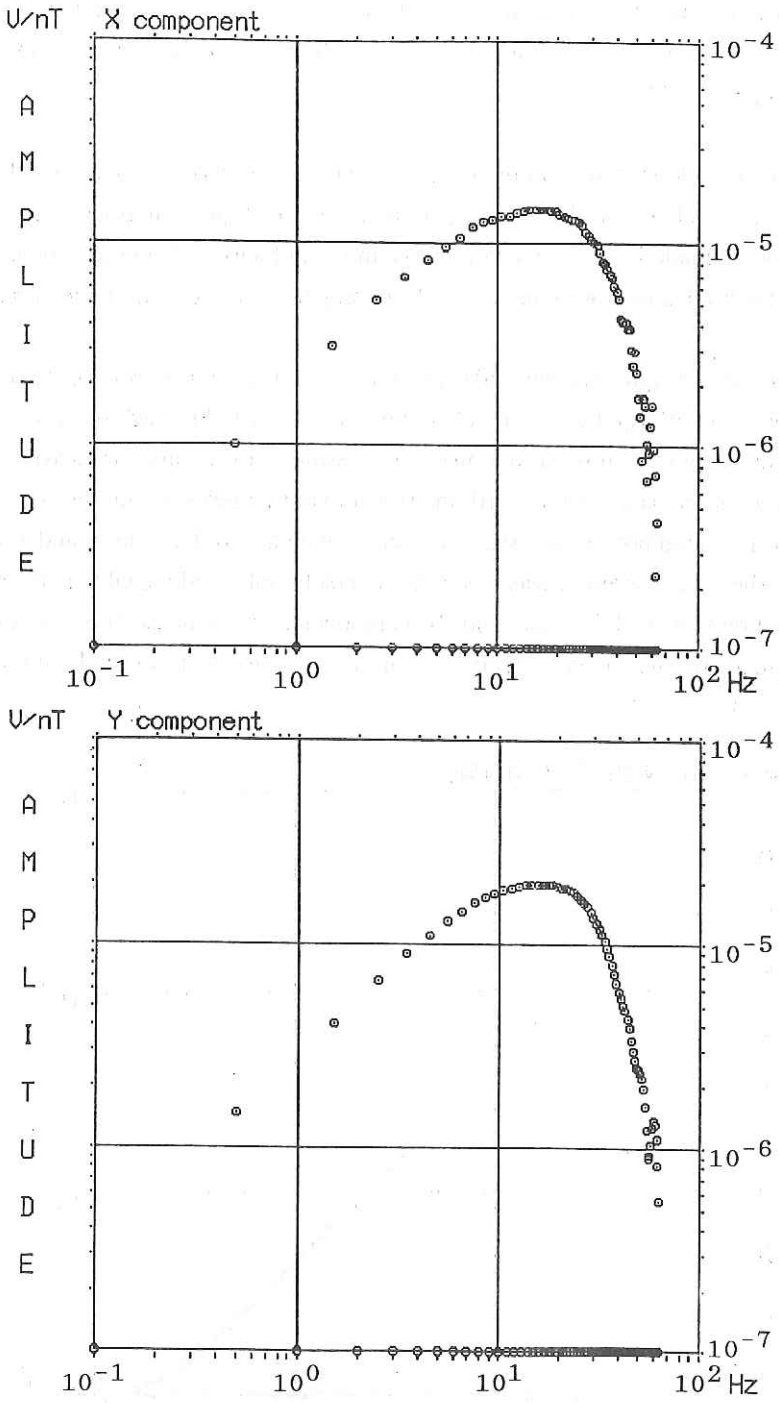

Fig. 4.6.4.2 The Amplitude Spectra of the OBI's Response Function for X and Y components.

amplitude spectra calculated contain only odd harmonics i.e., even harmonics is lacking (Fig. 4.6.4.3). This spectrum was used to estimate the earth's transfer function from the azimuthal magnetic field.

Magnetic field measured at the sea floor contains the two horizontally orthogonal components (X and Y) of the field, generated by the bipole at different stations. Corrections were made by using the corresponding gain factors. Some records in which the source signals are absent were used for determining the noise level of the receiver.

During data acquisition the OBI stacked automatically a 64 sets of 8 sec signal packages consisting of 4 pulses of interchanging polarity. By this stacking were reduced the random noise significantly, so that the signal resolution was much improved. In the post processing of the data from the OBI, the signal to noise ratio was further increased by averaging of the neighboring two signals, each of which was 1 sec long and reversely polarized. When the averaging was made the reversely polarized signal was inverted so that the signal remained while noises and DC components were canceled out. An example of data recorded for one source - receiver separation is illustrated in Fig. 4.6.4.4 (station SN1 for 370 m).

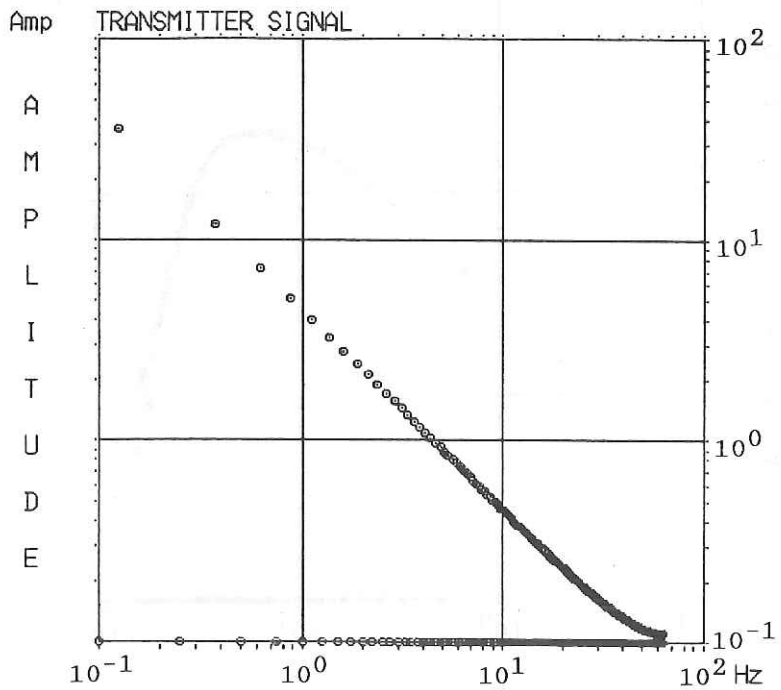

Fig. 4.6.4.3. The amplitude spectra of the transmitter signal. From the 40 Amperes commutated square wave form the FFT's result shows odd harmonics only.

The noise - reduced (output) data were Fourier transformed and the amplitude spectra (Fig. 4.6.4.5) were calculated for both X and Y components. This shows that most of the power is contained in the odd harmonics. The other components shown in the figure include both even and odd harmonics. This is caused by the electronic circuit noises and natural electromagnetic field.

The horizontal magnetic field (X and Y) in the nT unit was obtained from OBI's output data using its transfer function. From the horizontal magnetic field X and Y component s was estimated the azimuthal magnetic field which is related to the earth's transfer function by vector analysis.

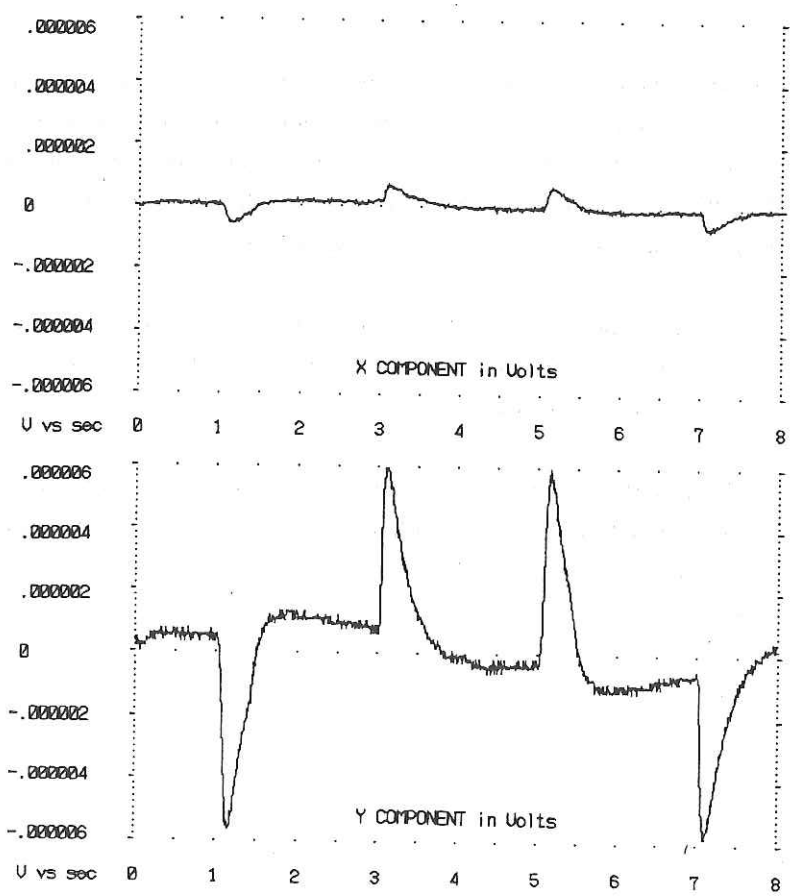

Fig. 4.6.4.4 The stacked time series recorded at OBI (site CS-4) for X and Y components at the station SN1 (370 m between source - receiver).

The amplitude spectra from the records which are void of source signals represent the natural noise level of OBI, which is approximately "white". Its value is about 10^{-8} volts (Fig. 4.6.4.6). From this result the signalsrecorded at the OBI are obviously influenced by this noise level, most likely at far stations.

The earth's transfer function was estimated by deconvolution of the azimuthal magnetic field using the source signal in the frequency domain. This result contains purely the information of the earth's structure i.e. it is proportional to the apparent resistivity of the sea floor.

All records from the receiver, containing source's signal, were processed in the same manner.

The apparent resistivity formula, mentioned above, was used to obtain the resistivity versus frequency curve for all transmitter stations. The amplitude of the transfer function, the mean sea water resistivity (0.31 Ω - m), the current transmitted (40 amperes), sea depth (PDR data every 1 minute) and source - receiver separation (from BRS and ship's positions) were the parameters used in this computation.

most of the power is contained in the odd harmonics. The other components shown in the figure include both even and odd harmonics. This is caused by the electronic circuit noises and natural electromagnetic field.

The horizontal magnetic field (X and Y) in nT unit was obtained from OBI's output data using its transfer function. From the horizontal magnetic field X and Y components was estimated the azimuthal magnetic field which is related to the earth's transfer function by vector analysis.

4.6.5. Preliminary results

For the experiment at site CS-6 it was found that one of the two card memories did not contain data. Some problem related with the back up battery or the writing system must have happened.

Using the estimated earth response function at some frequency for all source - receiver stations (Fig. 4.6.5.1 a) together with other parameters using the formula previously mentioned , the crustal apparent resistivity was calculated. The first harmonic was selected in this experiment (0.5 Hz) since it is close to DC limit. The apparent

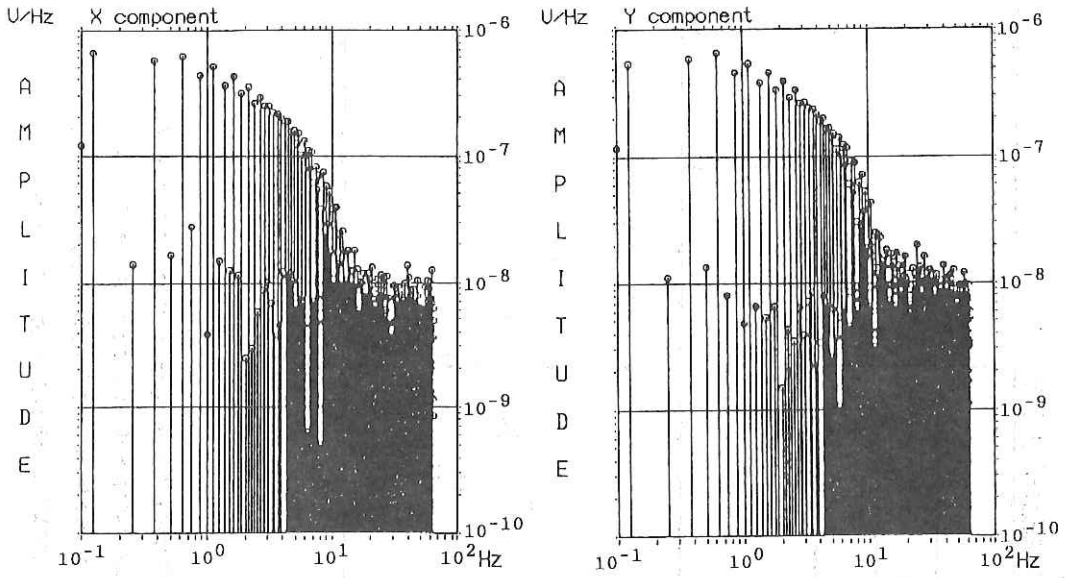

Fig. 4.6.4.5 Amplitude spectra of recorded data for X and Y components. The signal is contained in the odd harmonics.

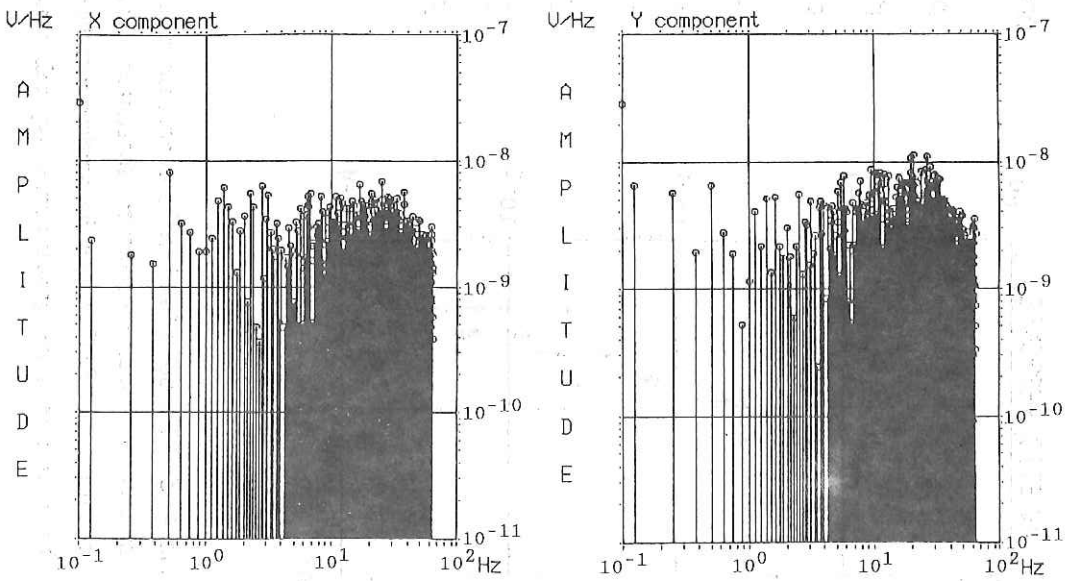

Fig. 4.6.4.6 Amplitude spectra of recorded noise of the OBI at the sea floor. Represents internal electonic "white" noise.

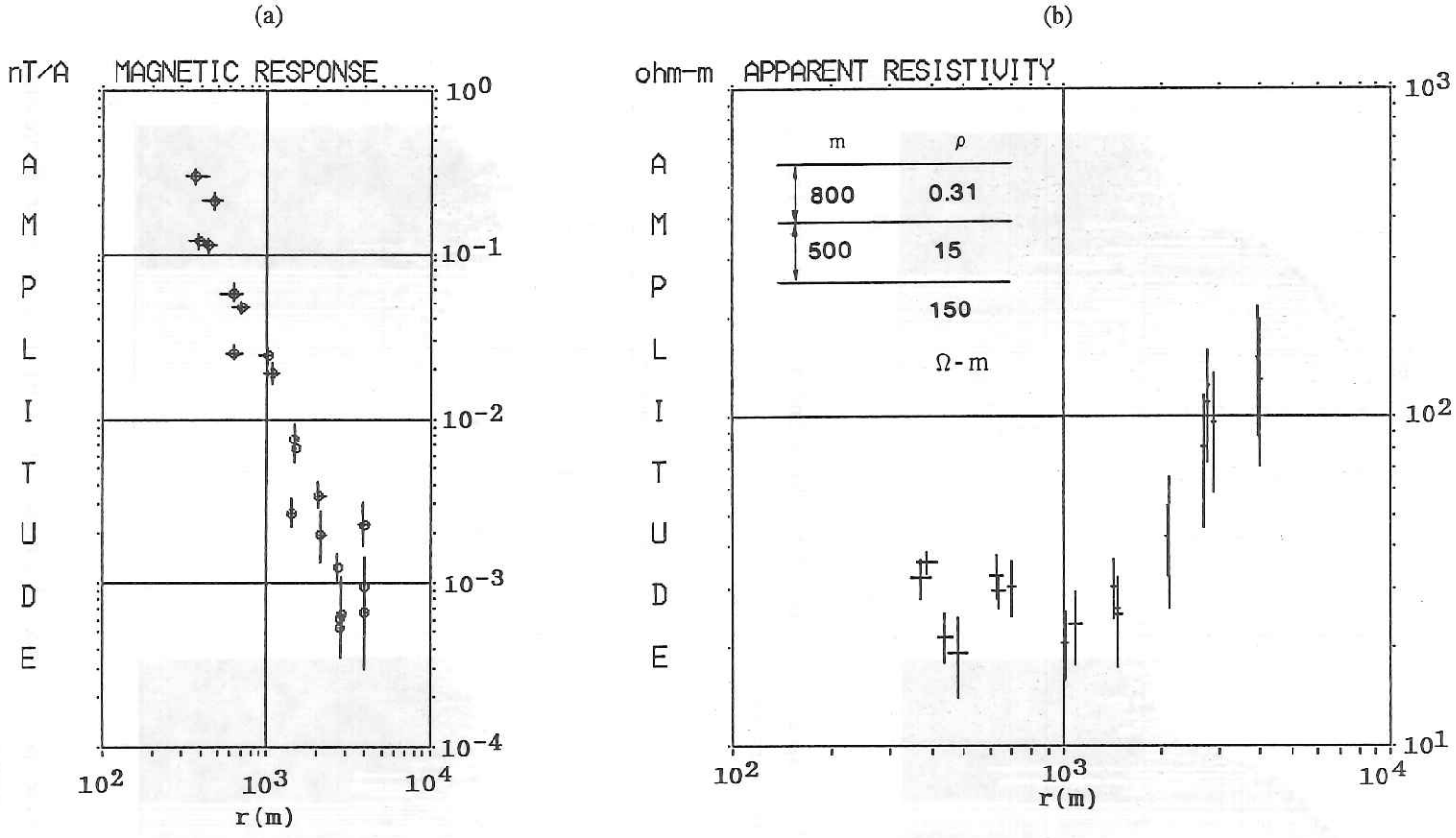

Fig. 4.6.5.1 The normalized earth's transfer function (a) and the apparent resistivity (b) both are expressed as a function of source - receiver separation. The horizontal bars represent the error in the distance measurements (RMS) while the vertical bars the error in magnetic field estimations (maximum noise level). The dots curve is the apparent resistivity calculated from the simple model presented in the right figure.

resistivity defined under quasi static DC limit criterion for all source - receiver distances is presented in Fig. 4.6.5.1 (b). In the results, the error in positioning and in the estimation of magnetic response may be involved. From apparent resistivity curve as a function of source - receiver separations is constructed the sea floor resistivity structure while assuming layers of different hicknesses, by trial and error modeling or inversion, but inversion result is not shown here. Only one apparent resistivity curve of an isotropic two-layer model is presented in Fig. 4.6.5.1 (b) for compaarison. The sea layer with 0.31Ω-m in resistivity and 800 m in thickness overlying a layer of 15Ω-m and 500 m and a homogeneous half space with 150Ω-m is assumed underneath.

References

Banister,P.R., 1968, Determination of the electrical conductivity of the sea bed in shallow waters, Geophysics, 33(6), 995-1003.

Becker,K, VonHerzen,R.P., Francis,T.J.Y., Anderson,R.N., Honnorez,J., Adamson,A.C., Alt,J.C., Emmerman,R., Kempton,P.D., Kinoshita,H., Laverde,C., Mottl,M.J., Newmark,R.L., 1982, In situ electrical resistivity and bulk porosity of the oceanic crust, Costa Rica Rift. Nature, 300, 594-598.

Chave,A.D., Cox,C.S., 1982, Controlled Electromagnetic Sources for Measuring Electrical Conductivity Beneath the Oceans-1: Forward Problem and Model Study, J.Geophys.Res., 87(B7), 5327-5338.

Chave,A.D., 1987, Electromagnetic Exploration Methods. Bell Laboratories, Technical Memorandum 11133-870814-51.

Chave,A.D., Constable,S.C., Edwards,R.N., 1987, Electrical Exploration Methods for the seafloor, in M. Nabighian (ed.), Electrical Explorations Methods, Vol. 2. Tulsa: Society of Exploration Geophysicists.

Coggon,J.H., Morrison,H.F., 1970, Electromagnetic investigations of the sea floor, Geophysics, 35(3), 476-489.

Cox,C.S., Kroll,N., Pistek,P., Watson,K., 1978, Electromagnetic fluctuations induced by wind waves on the deep-sea floor, J. Geophys. Res., 83, 431-442.

Cox,C.S., 1980, Electromagnetic induction in the oceans and inferences on the constitution of the earth, Geophys. Surv., 4, 137-156.

Cox,C.S., Deaton,T.K., Pistek,P., 1981, An active source EM method for the sea floor, Radio Sci.

Edwards,R.N., 1974, The magnetometric resistivity (MMR) method and its applications to the mapping of a fault, Can. J. Earth Sci., 11, 1136-1156.

Edwards,R.N., Howell,E.C., 1976, A field test of the magnetometric resistivity (MMR) method, Geophysics, 41(6A), 1170-1183.

Edwards,R.N., Lee,H., Nabighian,M.N., 1978, On the theory magnetometric resistivity (MMR) method, Geophysics, 43, 1176-1203.

Edwards,R.N., Bailey,R.C., Garland,G.D., 1981, Conductivity anomalies : lower crust or asthenosphere ?, Phys. Earth Planet.Int., 25, 263-272.

Edwards,R.N., Law,L.K., deLaurier,J.M., 1981, On Measuring the Electrical Conductivity of the Oceanic Crust by a Modified Magnetometric Resistivity Method, J.Geophys.Res., 86(B12), 11609-11615.

Edwards,R.N., Nobes,D.C., Gomez-Trevino,E., 1984, Offshore electrical exploration of sedimentary basins: The effects of anisotropy in horizontally isotropic, layered media: Geophysics, 49(5), 566-576.

Edwards,R.N., Law,L.K., Wolfgram,P.A., Nobes,D.C., Bone,M.N., Trigg,D.F., deLaurier,J.M., 1985, First results of the MOSES experiment: Sea sediment conductivity and thickness determination, Bute Inlet, British Columbia, by Magnetometric Off-Shore Electrical Sounding: Geophysics, 50(1), 153-161.

Nobes,D.C., 1984, The Magnetometric Off-Shore Electrical Sounding (MOSES) method and its applications in a survey of Upper Jervis Inlet, British Columbia, PhD thesis, Department of Physics, University of Toronto.

Nobes,D.C., Law,L.K., Edwards,R.N., 1986, The determination of resistivity and porosity of the sediment and fractured basalt layers near the Juan de Fuca Ridge: Geophys.J.R.astr.Soc., 86, 289-317.

Wolfgram,P.A., 1985, Development and Applications of a Short-Baseline Electromagnetic Exploration Technique for the Ocean Floor, PhD thesis, Department of Physics,University of Toronto.

Wolfgram,P.A., Edwards,R.N., Law,L.K., Bone, M. N., 1986, Polymetallic sulfide exploration on the deep sea floor: The feasibility of the MINI-MOSES experiment: Geophysics, 51(9), 1808-1818.

Young,P.D., Cox,C.S., 1981, Electromagnetic active source sounding near the East Pacific Rise. Geophys. Res. Lett., 8(10), 1043-1046.

4.7 Magnetotelluric Study of the Sea Floor

H. Toh, J. Segawa, V. Bapat, Y. Nagaya and T. Ichikita

4.7.1 Introduction

Since 1986, we have operated sea floor geomagnetic and geoelectric observations around the Izu Bonin ridge. The aim of those observations is to construct a model of an electrical conductivity structure beneath the ridge, which will lead to the whole understanding of the origin, the evolution and the present structure of a typical island arc system when it is interpreted together with other geophysical investigations. Some features have been revealed by those observations so far, and we qualitatively summarize them by mapping of induction vectors. Figure 4.7.1 shows the map of the induction vectors. Although the induction vectors of the southmost observation line show an almost two-dimensional structure of the Izu Bonin ridge, those of the northmost observation line seem to be definitely affected by the Japan arc. It implies that the conductivity anomaly around this region consists of one originated from the Izu Bonin ridge itself and one from the Japan arc. We think it is meaningful to estimate a two-dimensional conductivity structure of the Izu Bonin ridge first as a initial model in order to construct a final three-dimensional conductivity model around this region.

A two-dimensional modelling of a conductivity structure requires boundary conditions at both infinities. For this purpose, a magnetotelluric method is more preferable than a geomagnetic deep sounding method because oceanic basins are, to first approximation, considered to have stratified structures. Utada (1987) estimated the depth of the upper mantle conductor beneath the Shikoku basin as about 30 km through the sea floor magnetotelluric observations around the Philippine sea, but there is no data available on the Pacific plate side except for only one site off Tohoku District (Yukutake et al., 1983). This is the main reason why we make this magnetotelluric observation at the sea floor across the trench.

4.7.2 Instruments

Total five instruments were installed in four observation sites. They consisted of three fluxgate type three-component ocean bottom magnetometers (OBM's), one ocean bottom two- component electrometer (OBE) and one ocean bottom electromagnetometer

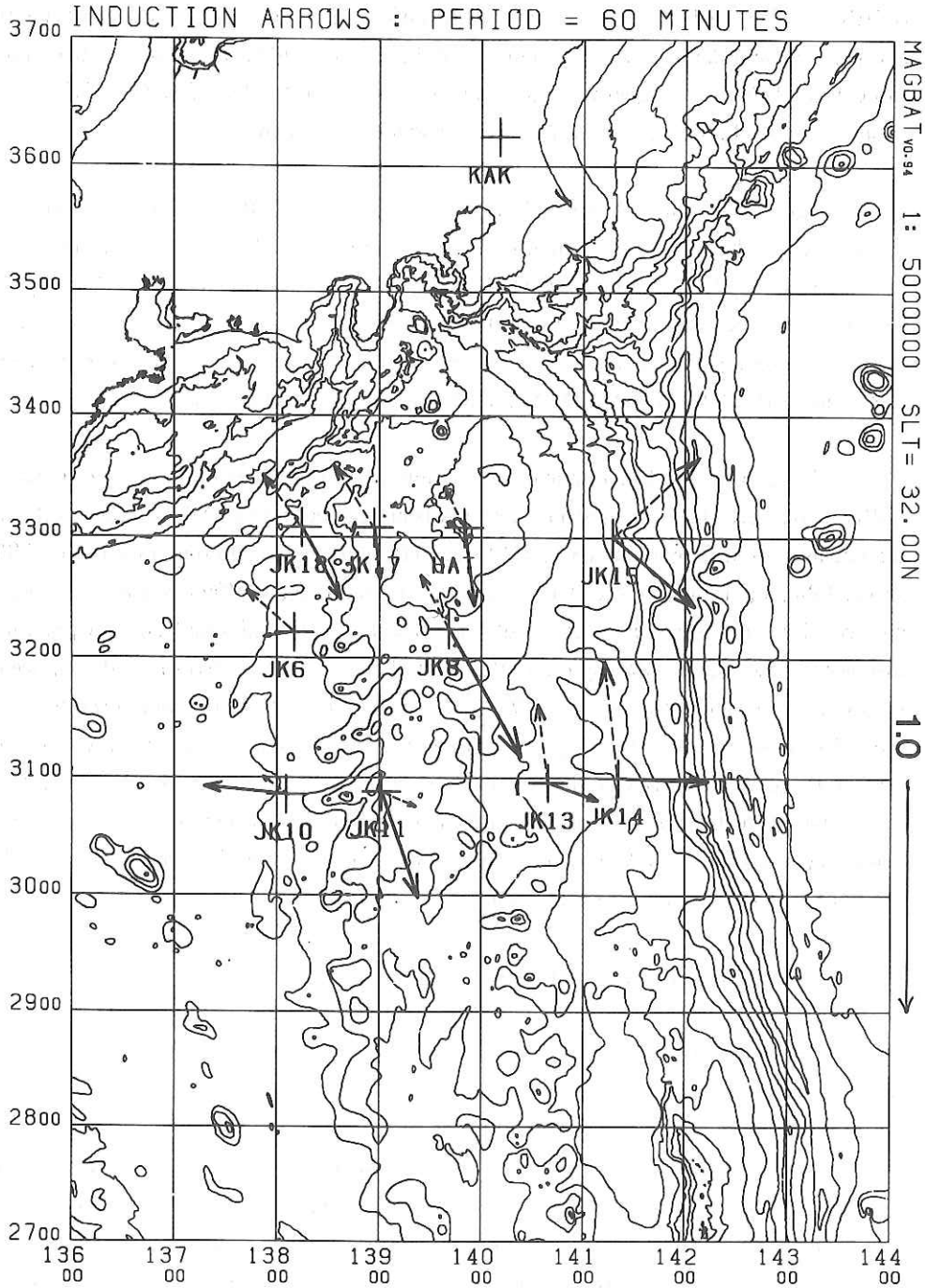

Fig 4.7.1 Mapping of the induction vectors around the Izu Bonin ridge for the period of 60 minutes. The induction vectors were calculated from the data obtained during the previous three cruises; KT86-12, KH87-3 and KT88-10. Solid arrows indicate the real parts of the calculated transfer functions, while dashed arrows denote imaginary ones.

(OBEM). The OBEM can measure two electric components and three geomagnetic components simultaneously. OBE and one of the OBM's (OBM-S4) were installed at the same site (JK20) for magnetotelluric measurement. Each OBM, OBE and OBEM was equipped with a beacon, a flasher and an acoustic release system.

Figure 4.7.2 through 4.7.4 show the outer view of OBEM, OBE and OBM-S4, respectively. These three instruments were deployed in the observation sites across the trench whose depths were much deeper than 5000 m. The lack of data on the Pacific plate side is mostly because it is too deep for the usual pressure tight vessels we use. Therefore, the pressure tight glass spheres for these three instruments were replaced by either stainless steel spheres (for OBEM and OBM-S4) or a titanium cylinder (for OBE).

Here, we would like to make some comments on the ocean bottom electrometers (OBEM and OBE) because they have recently been applied to practical use compared with the ocean bottom magnetometers used here. Hamano (personal communication, 1985) showed that a pair of sintered silver-silverchloride electrodes is effective for the sea floor electric field measurement because of its small drift rate and small contact potential difference in seawater. Making use of this kind of electrodes, we also succeeded in ocean bottom electric field observation in 1987. This time, these electrodes were used for both OBEM and OBE as well. Long span electrodes are preferable in terms of the low signal to noise ratio of electric fields at the sea floor, however, it is impossible to extend the span more than 10 m for the sake of on board operation of the instruments. A 5 m span is usually adopted and considered to be enough for practical electric field measurement at the sea floor as is the case of this observation.

4.7.3 Installation of the Instruments

The installation of instruments was mainly made on the east- west transverse section of the Izu Bonin Ridge at 32°N. It took about three days to complete all the installations. Figure 4.7.5 shows the location of the installation points on a bathymetric chart together with the other previous observation points. The key stations of this experiment lie on either side of the trench. OBEM, OBE and OBM-S4 were installed in the east of the trench for the magnetotelluric sounding of the Pacific plate whose implications have already discussed before. The other two OBM's were distributed on the fore arc in order to make a sharp contrast to the geomagnetic measurement on the Pacific plate. The previous observations also revealed that the induction vectors on the fore arc of the Izu

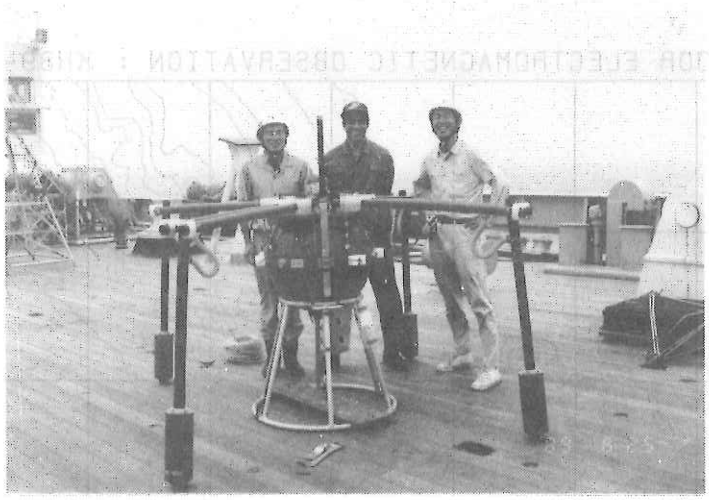

Fig 4.7.2 A photograph of OBEM just before launch on board.

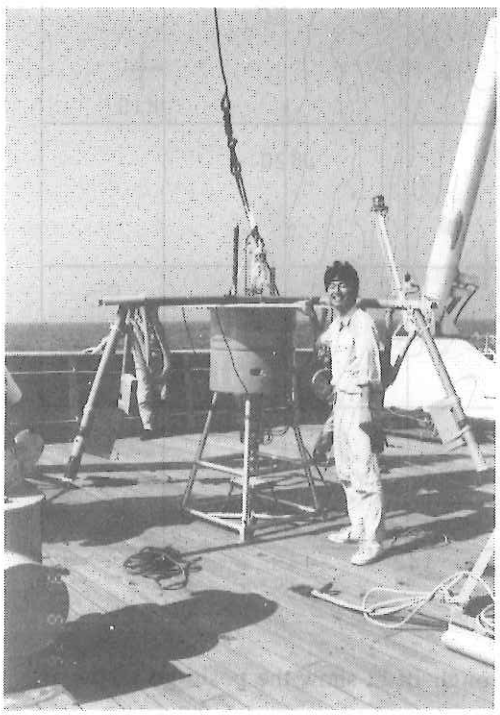

Fig 4.7.3 A photograph of OBE just before launch on board.

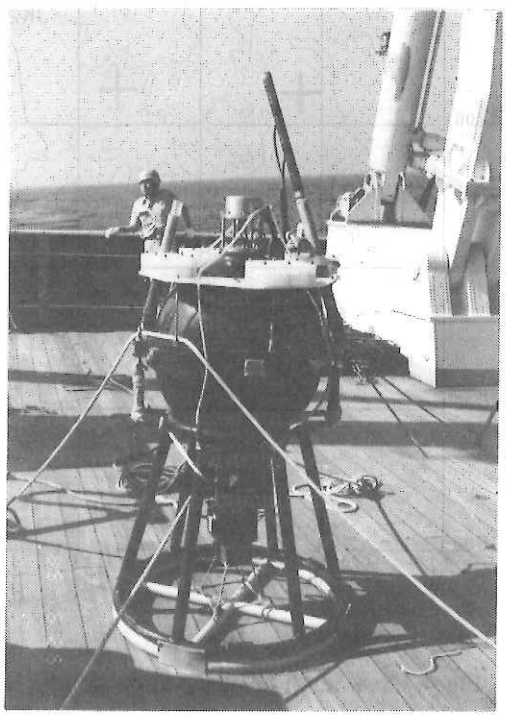

Fig 4.7.4 A photograph of OBM-S4 just before launch on board.

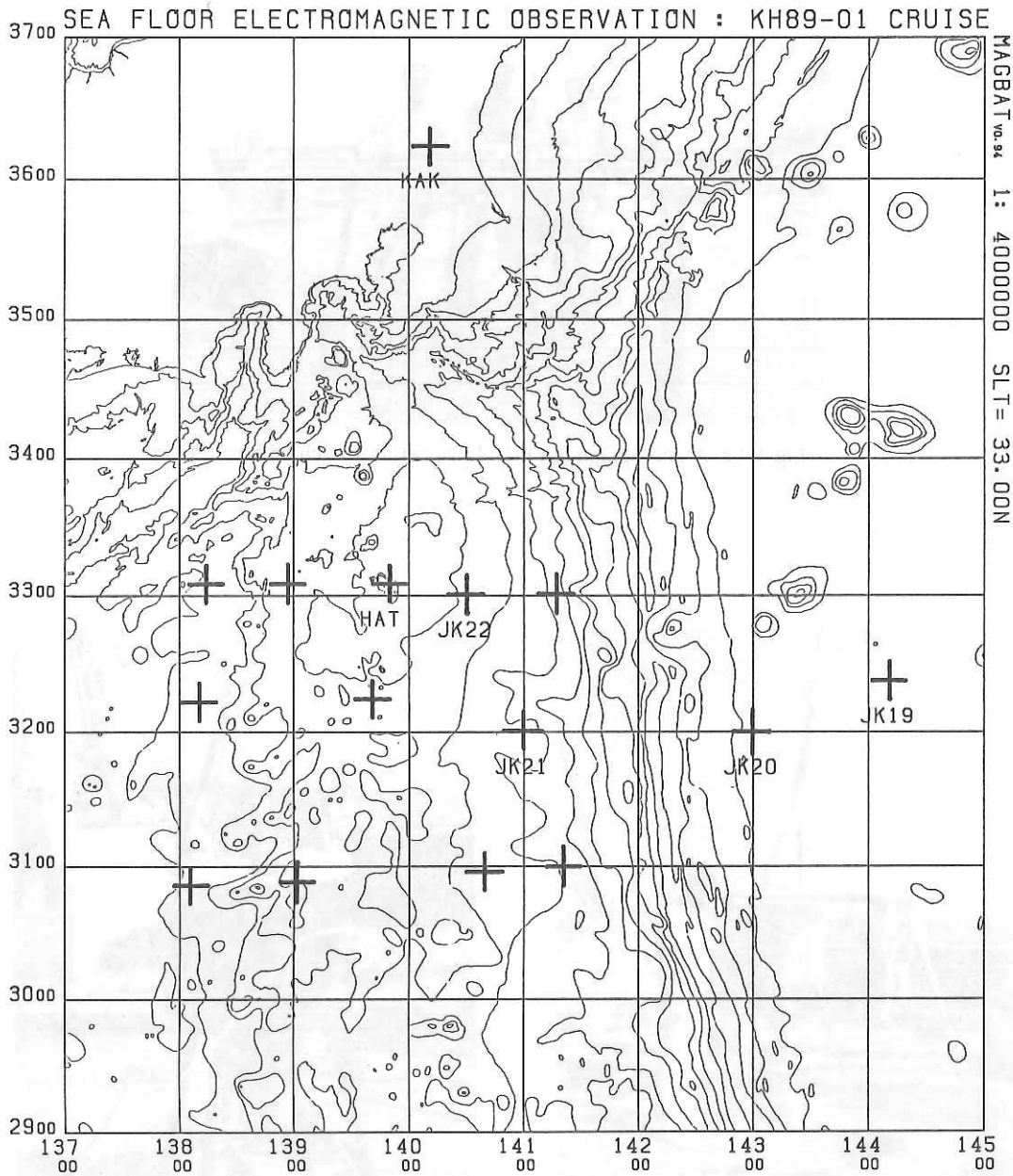

Fig 4.7.5 A map of observation points. JK19 through JK22 show the positions of the present observation points. Cross marks without site names represent the previous observation points in this area. The locations of Kakioka (KAK) and Hachijo-jima (HAT) are also shown in this figure.

Bonin ridge would show rather small amplitudes compared with the corresponding vectors of Tohoku District (Ogawa et al., 1986), which is possibly speculated as the net conductance of back arc side is relatively larger than that of northeast Japan. Whether or not it is attributed to the Philippine sea as an open sea and/or the shallow upper mantle conductor beneath the the Philippine sea plate, it would be added to the purposes of this experiment to ensure the small amplitudes of the induction vectors on the fore arc of the Izu Bonin ridge.

As for more detailed informations of the installation sites, refer to Table 4.7.1.

Table 4.7.1 Observation Log of KH89-1 Cruise

Apparatus	Site	Position	Depth	Duration	Sampling Rate
OBEM	JK19	32°22.1'N 144°11.0'E	5431m	-	1 min.
OBE	JK20	31°59.8'N 143° 0.1'E	5685m	83 days	1 min.
OBM-S4	JK20	31°59.6'N 140°59.9'E	5696m	83 days	2 min.
OBM-S5	JK21	32° 0.0'N 140°59.9'E	2703m	82 days	2 min.
OBM-C3	JK22	33° 0.1'N 140°30.1'E	1218m	81.5 days	2 min.

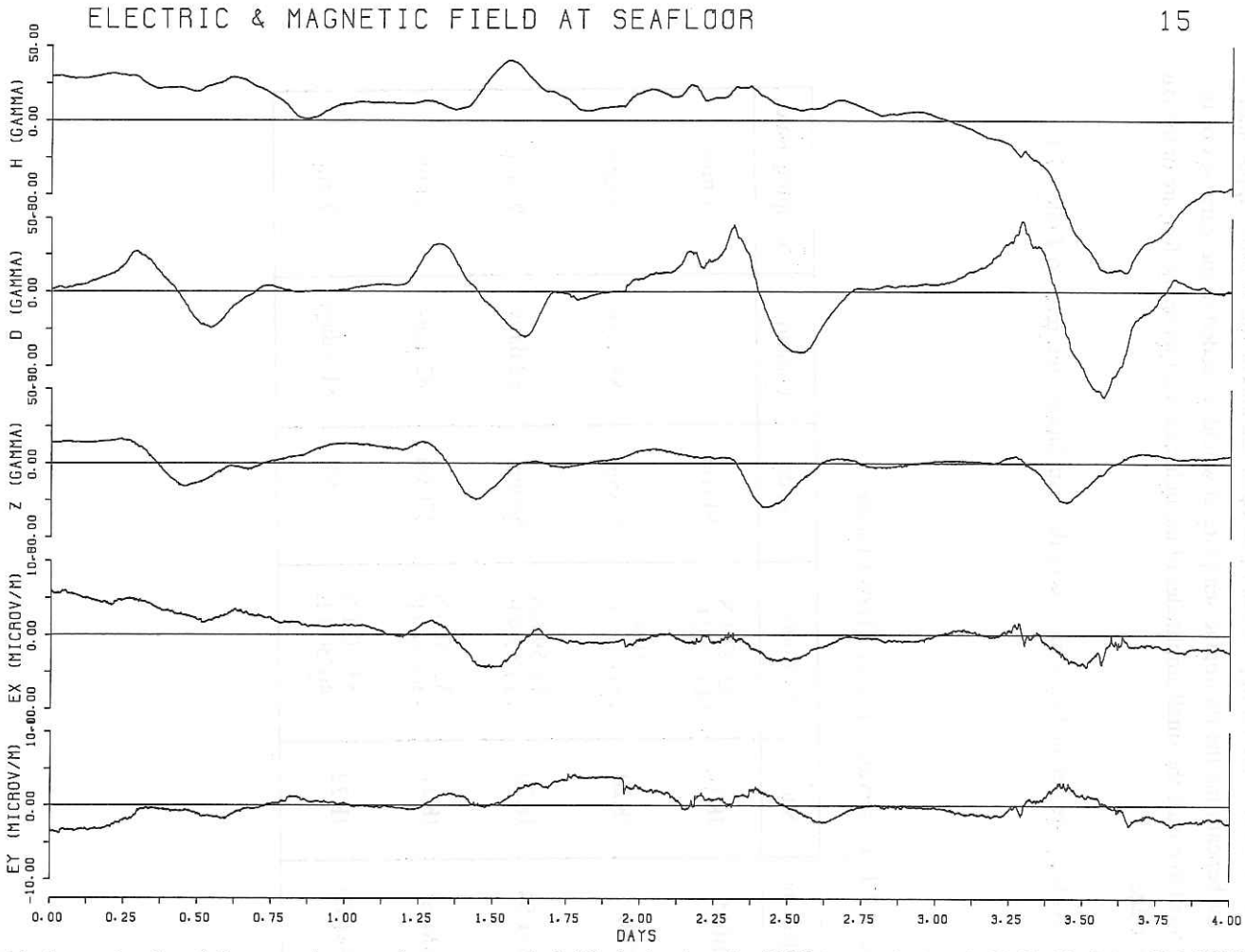

Fig 4.7.6 A sample plot of the ocean bottom electromagnetic field obtained at site JK20 from 26th/AUG/'89 00:00 JST to 29th/AUG/'89 23:59 JST. Upper three solid lines are geomagnetic three components and lower two are electric field components. One division of the vertical axes is 20 nT for geomagnetic components and 5 microV/m for electric field components. The coordinates are taken as geomagnetic north (H and Ex), geomagnetic east (D and Ey) and downward (Z).

4.7.4 Data

The recovery of all the instruments was successfully finished by Umitaka-maru, Tokyo University of Fisheries, from 16th/SEP/'89 to 19th/SEP/'89. Unfortunately, OBEM failed to work well, but the rest of the instruments gave enough amount and enough quality of geomagnetic and geoelectric variational data at the sea floor. Figure 4.7.6 shows a sample plot of ocean bottom electromagnetic five components obtained at site JK20 from the instruments, OBE and OBM-S4. As for the data analysis and the interpretation, we shall wait and see our future work.

Acknowledgments

We are grateful to all the crews on Hakuho-maru. We also wish to express our sincere thanks to every crew of Umitaka-maru, Tokyo University of Fisheries.

References

Ogawa, Y., T. Yukutake and H. Utada, Two-dimensional modelling of resistivity structure beneath the Tohoku District, northern Honshu of Japan, by a finite element method, J. Geomag. Geoelectr., 38, 45-79, 1986

Utada, H., A direct inversion method for two-dimensional modeling in the geomagnetic induction problem, Ph. D. Thesis, Univ. of Tokyo, 1987

Yukutake, T., J. H. Filloux, J. Segawa, Y. Hamano and H. Utada, Preliminary report on a magnetotelluric array study in the northwest Pacific, J. Geomag. Geoelectr., 35, 575-587, 1983

4.8 Heat Flow Measurements Around the Zenisu Ridge

M. Kinoshita, H. Kinoshita, T. Koizumi,
H. Nanbu, and T. Nakakuki

4.8.1 Introduction

The Nankai Trough is situated on the northern margin of the Shikoku Basin. It is generally believed that the Nankai Trough is the convergent boundary between the Philippine Sea Plate and the Eurasian Plate. The heat flow profiles around the western part of the trough differs from those of other trench systems in a way that the heat flow has the highest value (130 to 150mW/m^2) at around the trough axis and lower values landward (Yamano et al., 1984; Kinoshita and Kasumi, 1988). The heat flow survey further in the eastern part of Nankai Trough, which is tectonically interesting area, have been poorly performed so far. Recent studies on the seismicity in this area have revealed that the seismic activity in the main Nankai Trough (off Enshunada) is very low while in the Zenisu Ridge much larger number of earthquake occurrences have been observed (Ukawa et al., 1985). Shimamura (1988) noted this point and the topographic similarity between the Nankai Trough and the basin to the south of the Zenisu Ridge, and suggested that the intraplate deformation zone migrated seaward recently. Also, the calyptogena communities were found in the Tenryu Canyon and the southern foot of the Zenisu Ridge (Le Pichon et al., 1987) accompanied by anomalously high heat flow. It is attributed to the interstitial water seepage along the thrust (Henry et al., 1989).

During the first leg of the KH89-1 cruise, we have conducted heat flow measurements around the Zenisu Ridge in order to fill the blank of data and to clarify thermal features around.

4.8.2 Method of Measurements

A heat flow value in marine areas is determined as the product of geothermal gradient and thermal conductivity. Only thermal gradients are measured in some stations and nearby values of thermal conductivity are substituted, on an assumption that the variation of thermal conductivity is significantly small in general.

Geothermal gradients are measured using the Ewing type probe (long, short) and the Bullard type probe. The Ewing type (long, 'EL' in Table 4.8.1) is 4.5m long and weighs 500kg, whereas the short version ('ES' in Table 4.8.1) is 3m long and weighs

Table.4.8.1 Results of heat flow measurement

Station		Latitude	Longitude	D m	PR	PEN m	N	G mK/m	K W/m K	Q mW/m^2
KH891	HF 4	33°33.69'N	137°32.94'E	3828	B	2.5	7	61	0.98*	60
	HF 5	33°35.69'N	137°32.61'E	3869	B	1	3	(111)	0.98*	(109)
	HF 2A	33°22.62'N	137°44.29'E	4057	EL	1	6	(>86)	0.98*	(>84)
	HF 2B	33°22.70'N	137°44.28'E	4062	EL	3	4	81	0.98*	79
	HF 2C	33°22.80'N	137°44.28'E	4065	EL	2.5	5	69	0.98*	68
	HF 2D	33°22.86'N	137°44.26'E	4077	EL	2	4	81	0.98*	79
	HF10A	32°56.26'N	137°11.30'E	4183	ES	1	4	(>99)	0.80*	(>79)
	HF10B	32°56.32'N	137°11.33'E	4189	ES	1	4	(>87)	0.80*	(>70)
	HF10C	32°56.38'N	137°11.40'E	4188	ES	1	3	96	0.80*	77
	HF 1A	33°07.72'N	137°57.37'E	4113	EL	fell				
	HF 1B	33°07.85'N	137°57.35'E	4112	EL	fell				
	HF 1C	33°07.83'N	137°57.43'E	4113	EL	fell				
	HF 1GC	33°07.76'N	137°56.80'E	4115	GC	fell				
	HF 7A	33°17.98'N	138°09.80'E	4035	EL	1	3	70	0.86	60
	HF 7B	33°18.00'N	138°09.80'E	4039	EL	0.5	4	(>67)	0.86	(>58)
	HF 7C	33°18.11'N	138°09.73'E	4039	EL	1	3	67	0.86	58
	HF 7GC	33°17.96'N	138°07.89'E	4039	GC	0.6	10		0.86±0.02	
	HF 8A	33°23.78'N	138°16.05'E	4007	ES	2.5	3	25	0.86*	22
	HF 8B	33°23.76'N	138°16.09'E	4007	ES	2	4	22	0.86*	19
	HF 8C	33°23.78'N	138°16.11'E	4007	ES	2.5	3	23	0.86*	20
	HF 8D	33°23.68'N	138°16.19'E	4007	ES	2.5	4	19	0.86*	15

[Notes]

D : Water depth (in meters) by the SEABEAM.

PR : Probe type; B is the Bullard type, EL the Ewing type (4.5mlong), es the Ewing type (3m) and GC is the gravity corer.

PEN : The length of probe or corer below the seabottom. 'fell' meansunsuccessful penetration.

N : Number of sensors used for estimation of temperature gradient, or number of measuring points of thermal conductivity (GC).

G : Estimated temperature gradient. Values with parenthes are less reliable ones. '>' means that the probe was tilted by more than 40 degrees.

K : Thermal conduictivity used for heat flow estimation. '*' means nearby value.

Q : Heat flow estimated by products of G and K.

150kg. The probe is made of steel rod, along which 6 to 7 thermistors (covered with stainless steel tube of 3.5mm in diameter) are outriggered. They allow multiple penetrations which improves the efficiency of data collection and enables to make closely-spaced measurements. On the other hand it is rather difficult to penetrate them into coarse sediments due to the large diameter of the lance. The temperature recording system was developed by the Woods Hole Oceanographic Institution. The resistance of each thermistor and instrument tilt are recorded every 30 seconds in an IC memory (RAM). They are also telemetered with 12kHz acoustic pulses to the ship for real-time monitoring, so that we can save time by abandoning unsuccessful stations.

The Bullard type probe ('B' in Table 4.8.1) was developed by Applied Microsystems Ltd. The lance (made of stainless) is 3m long and 16mm in diameter in which seven thermistors are installed every 45cm and entire equipment weighs about 100kg. Because the lance is thin and easy to bend, it is suitable to penetrate the coarse sediment, although it does not allow multiple penetrations. The resistance are recorded every 6 seconds.

Because a probe is heated by friction on penetration into sediments, we extrapolate the obtained temperature data as a function of time to the equilibrium temperature, using the function derived by Bullard (1954). It is necessary to keep the probe in the sediment without moving for 10 to 15 minutes, depending on its diameter.

The estimated in situ temperature at each depth is used for calculating geothermal gradient, using a least square method.
This best-fit value is then corrected for the instrument tilt angle.

Thermal conductivity values are measured on gravity core samples using the needle probe method (von Herzen and Maxwell, 1959) on board. The recovered sample is kept vertically, taking care not to lose the interstitial water, for a few hours to equilibrate to the room temperature. The obtained results are corrected for the temperature and pressure conditions at the sea floor following Ratcliffe (1960).

4.8.3 Results

We tried measurements at seven stations for thermal gradients, and two for gravity coring, listed in Table 4.8.1. Before the measurement we made a site survey along the line A-A' in Fig. 4.8.1, using 3.5kHz subbottom profiler (Fig. 4.8.2). Stations HF-1, 2, 4 and 5 were aligned perpendicular to the trough axis across the

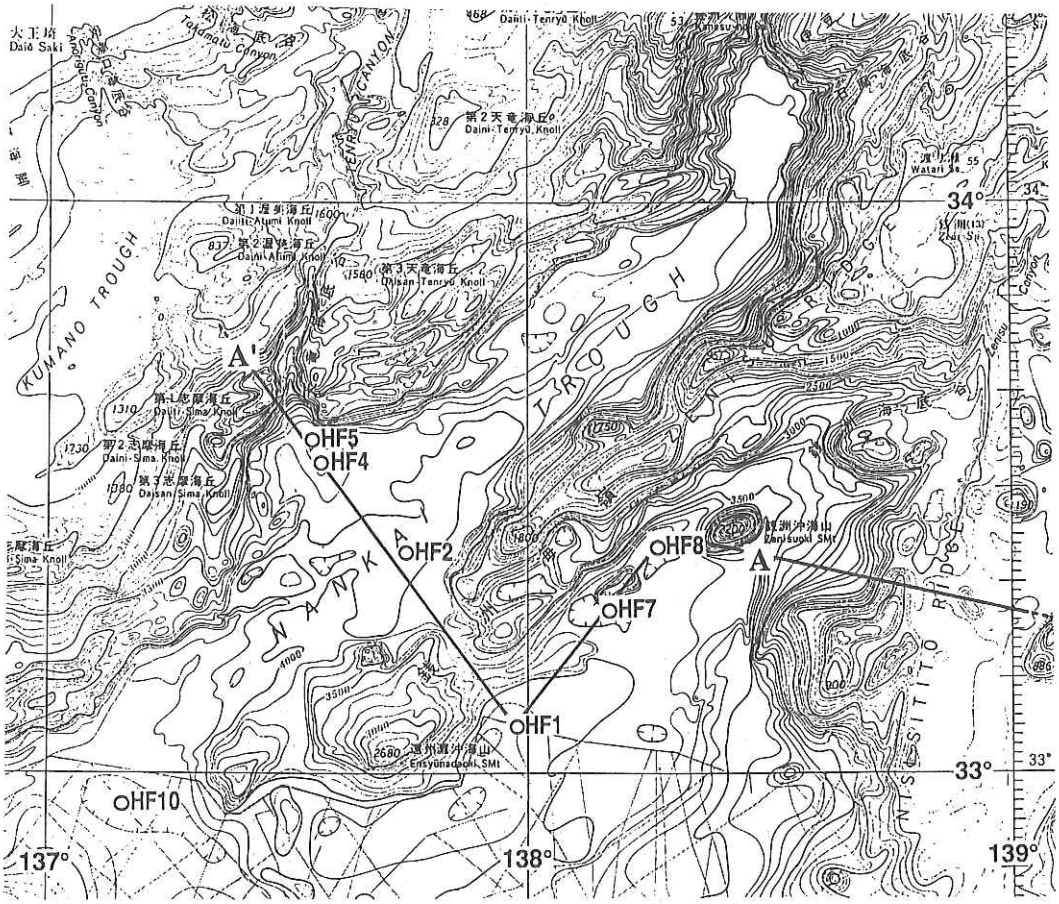

Fig.4.8.1 Position of heat flow station plotted on a bathymetry map. Line A-A' indicates track line, and 3.5kHz subbottom profile along this line is shown in Fig. 4.8.2.

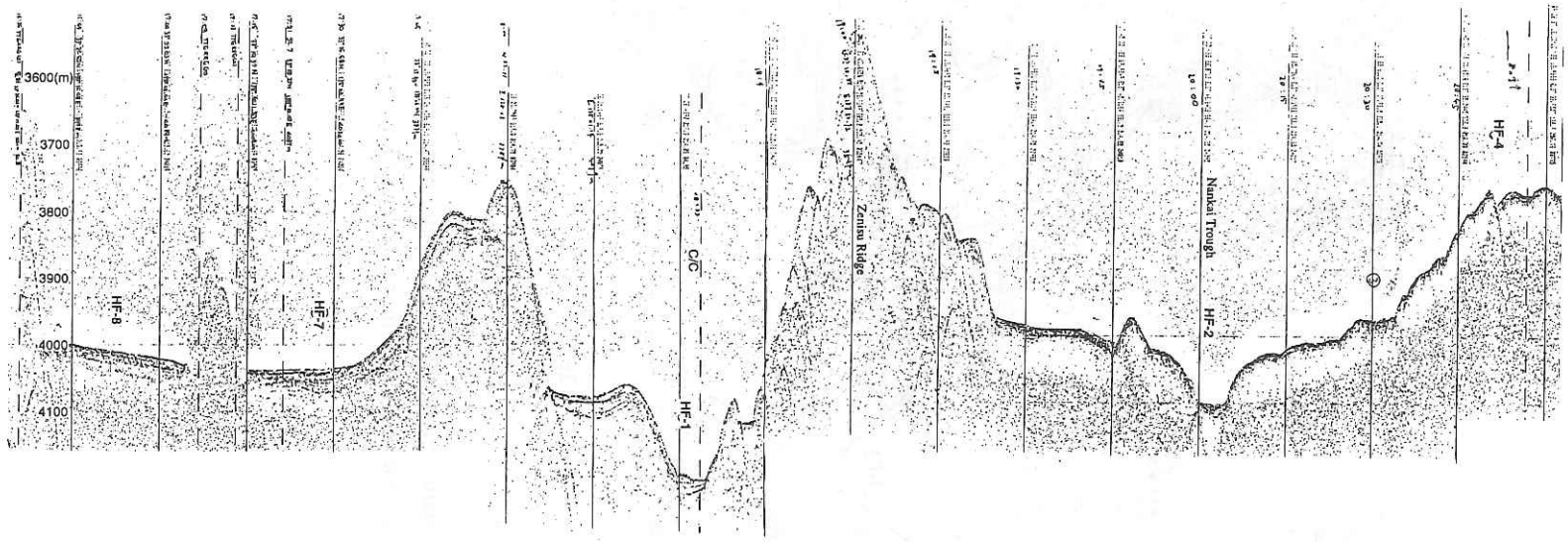

Fig.4.8.2 A 3.5kHz subbottom profile along the line A-A' in Fig. 4.8.1. On the left side is shown the water depth; C/C is the couse change point.

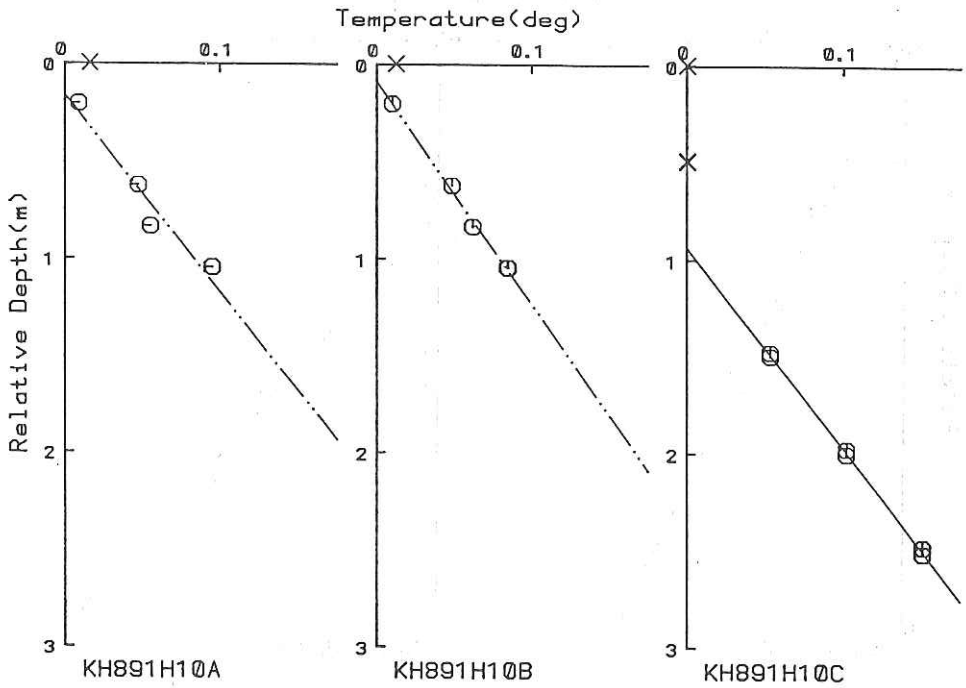
Temperature(deg)
0
0.1
Relative Depth(m)
0
1
2
3
KH891H10A
KH891H10B
KH891H10C

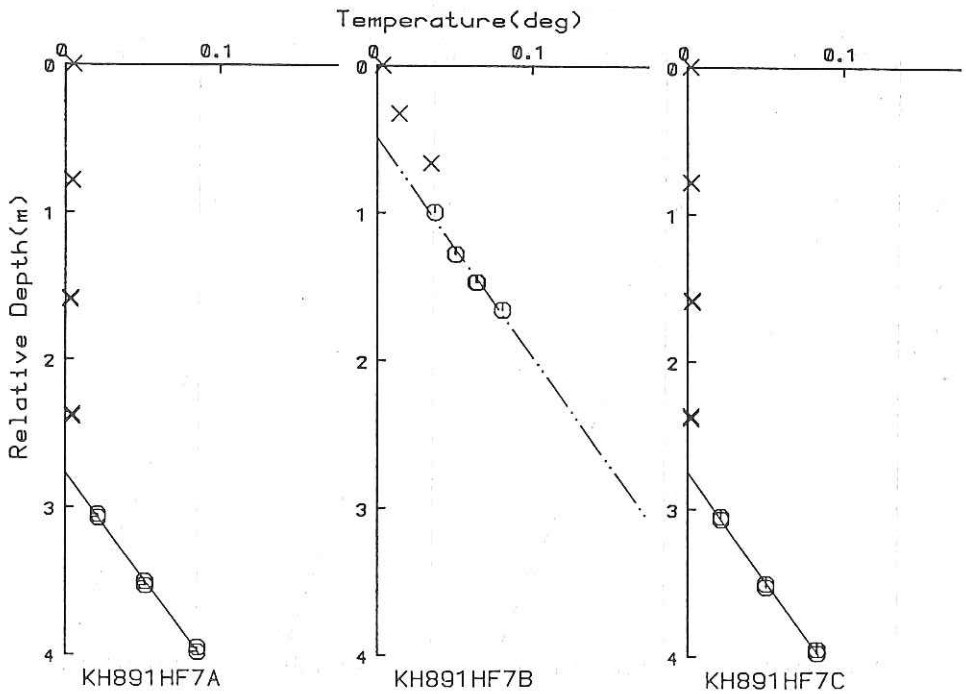
Temperature(deg)
0
0.1
Relative Depth(m)
0
1
2
3
4
KH891HF7A
KH891HF7B
KH891HF7C

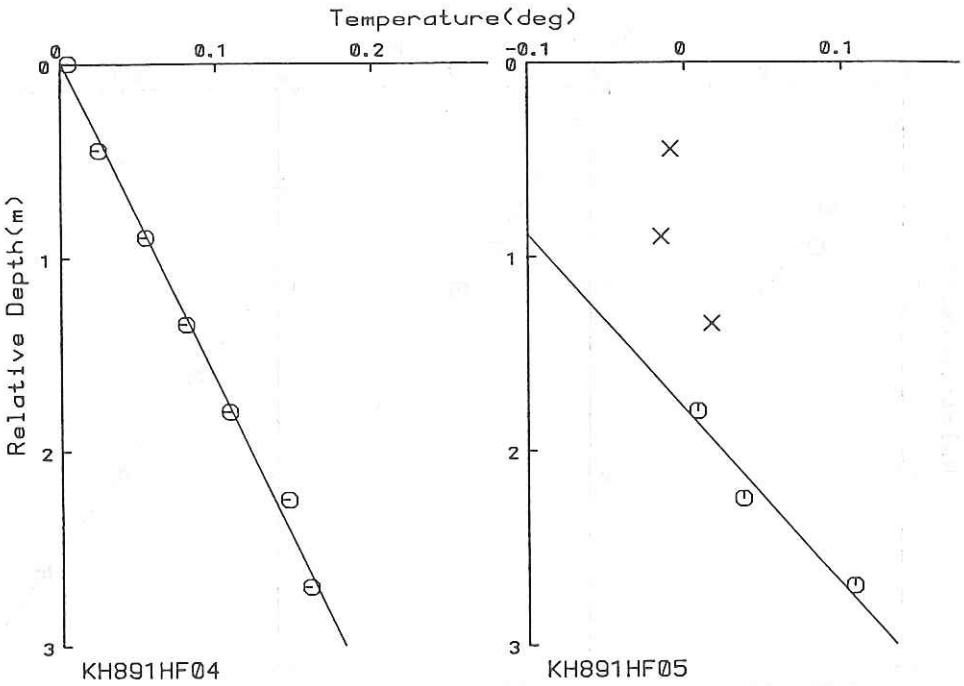
Temperature(deg)
Relative Depth(m)
KH891HF04
KH891HF05

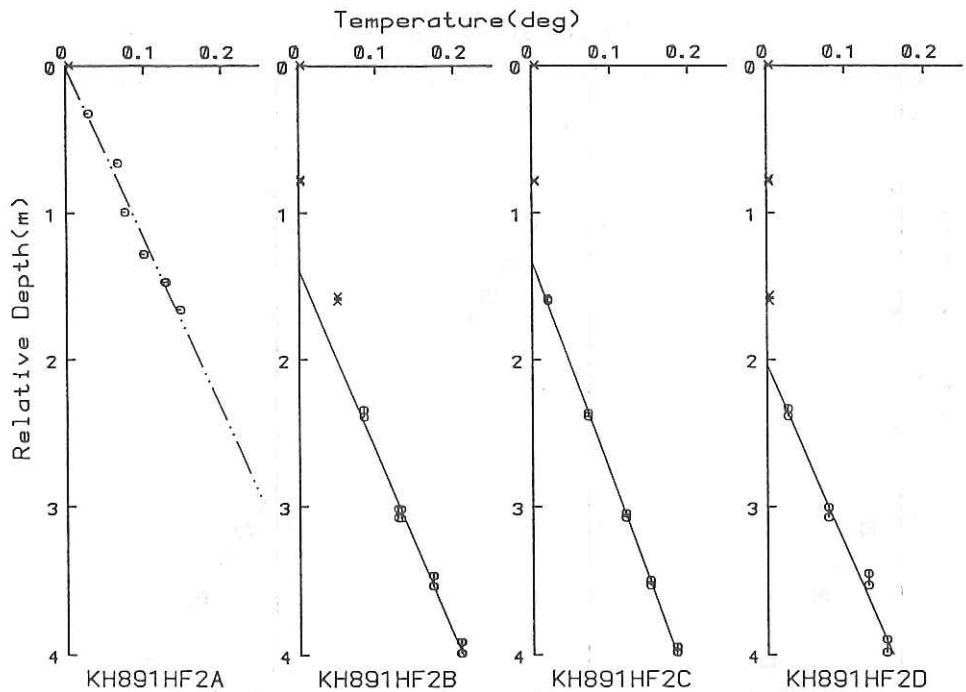
Temperature(deg)
Relative Depth(m)
KH891HF2A
KH891HF2B
KH891HF2C
KH891HF2D

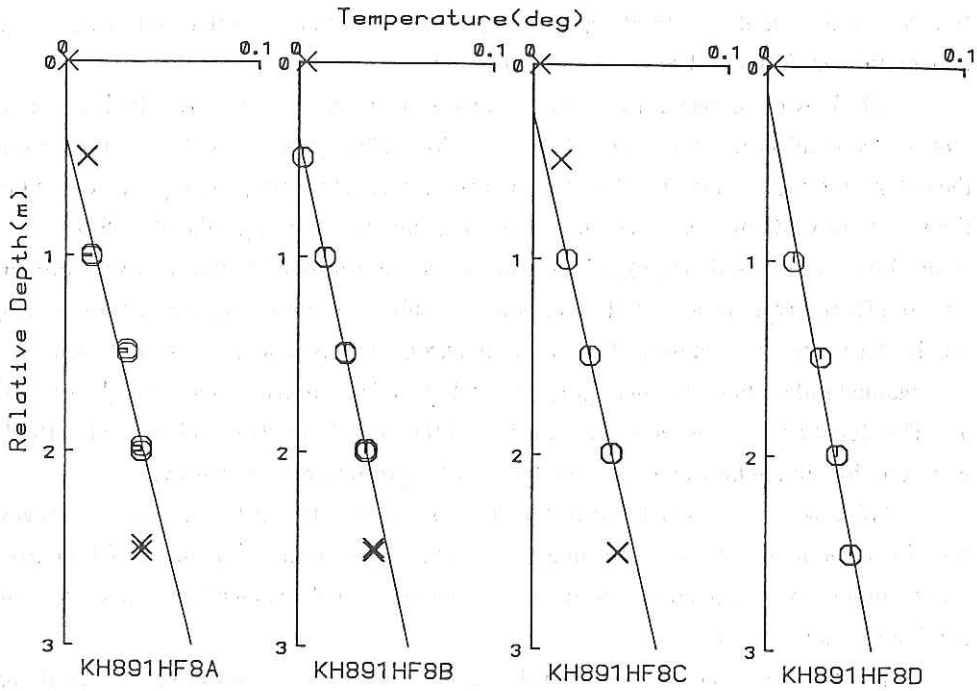

Fig.4.8.3 Temperature versus depth profiles. A straight line is the best fit line for data except for cross-mark (x) ones, which mean that they did not penetrate, or the record was unstable. Depth values are corrected for the instrument tilt.

Zenisu Ridge, while HF-1, 7,and 8 were situated on the southern foot of the Zenisu Ridge. Gravity corings were tried at stations HF-10 and HF-7. Obtained thermal gradients and thermal conductivities are plotted on Figs. 4.8.3 and 4.8.4, respectively.

HF-4 was located on the Tenryu Canyon, a few miles seaward of the clam site (HF-5). We used the Bullard type probe, and it resulted in full penetrations. The temperature vs. depth profile was linear (61mK/m).

HF-5 was aimed at the Tenryu Canyon deep sea colony (Le Pichon et al., 1987). As mentioned, anomalously high heat flow (2200-4500mW/m2) was obtained in the colony by the submersible 'Nautile' investigations. However, the depth extent at that time was only 10cm. We tried heat flow measurement during the KH86-5 cruise (Kinoshita and Kasumi, 1988), which was not successful due to the coarse sediment, with the Ewing type probe. Following these results, we tried again the same site using the Bullard type probe in turn. As a result, the probe did not penetrate so well (1m), but we obtained rather high thermal gradient of 111mK/m, almost twice as high as at HF-4. The location was within one miles from the clam fields (Le Pichon et al., 1987), therefore this station may be influenced by upwelling of water at the colony.

HF-2 was on the axial part of the Nankai trough. Hereafter we used the Ewing type instrument so that we could make multiple penetrations. At three of four trials (penetrations) the probe stood vertically, and obtained results showed similar values one another (around 80mK/m).

HF-10 was located at the tip of the Zenisu Ridge. We tried three penetrations, and only one (HF-10C) of then were successful. However, it was sure that other two (HF10A and B) were not fell but stood, although tilted by about 40 degrees, because temperature vs. depth profile were linear and corrected thermal gradient showed similar values as HF-10C.

At HF-1, gravity coring was also tried. The bottom seemed coarse because both (probe for thermal gradient and corer) did not penetrate the sediment at all.

HF-7 was located near the southern foot of the ridge, as HF-1. The probe penetrated by 1m, and the gravity coring resulted in taking 60m core sample.

HF-8 was located northeast of HF-7. All trials were successful (more than 2m penetration), and obtained data showed uniquely low values around 20mK/m.

4.8.4 Preliminary Interpretation

Heat flow values including previous ones are shown in Fig. 4.8.4. We can see characteristics about heat flow distribution, some of which is discussed here.

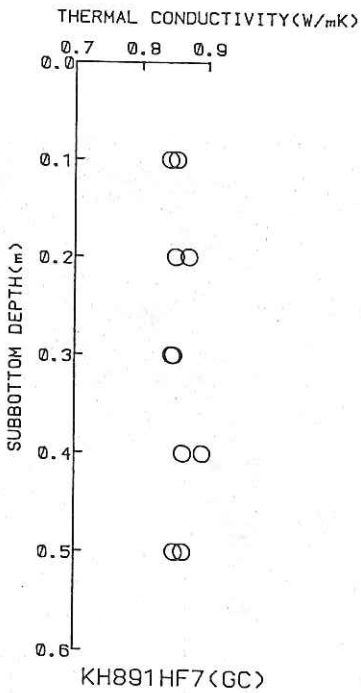

Fig.4.8.4 A thermal conductivity versus depth profile at HF-7.

First, as already mentioned, heat flow at the Tenryu Canyon differs between HF-4 and 5, although they are rather closely spaced. Also, these values are much lower than observed in the colony itself. This anomaly may be due to the fluid vent around the colony in a very local scale.

On the Nankai Trough axis, heat flow values seem to be compatible to the basement age of the Shikoku Basin, i.e. around 70mW/m^2. In the western part heat flow is rather high on the trough axis, which may be attributable to the seepage of pore water. The lower heat flow in eastern part of the trough axis may indicate a lower tectonic activity associated with subduction.

The heat flow in the southern part of the Zenisu Ridge is low, and especially at HF-8 heat flow is quite low. This result does not necessarily rule out the idea of the migration of the location of the subduction front from the main Nankai Trough toward south, because lower heat flow values at HF-7 and HF-8 could be influenced by a rapid sedimentation which reduces surface heat flow (von Herzen and Uyeda, 1963). If

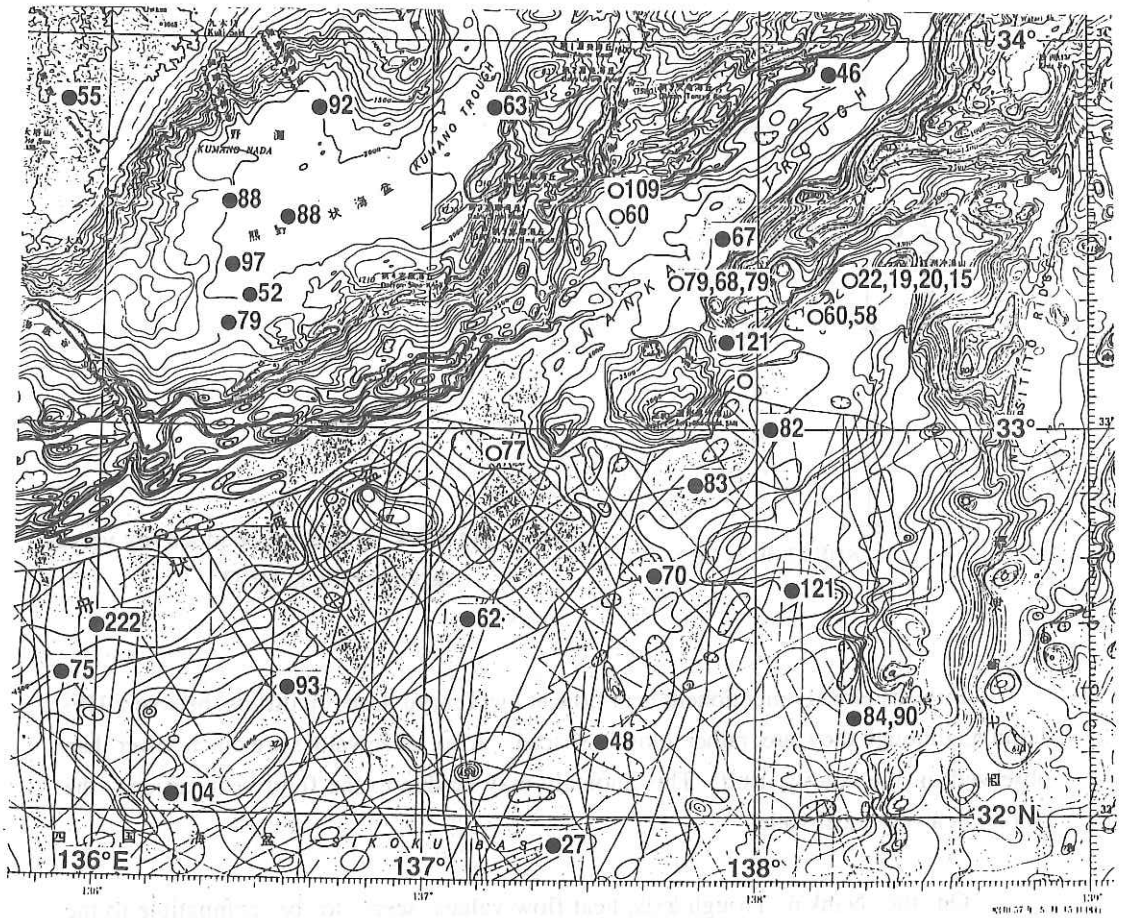

Fig.4.8.5 Heat flow distribution around the surveyed area (unit: mW/m^2). Open circles are obtained by this study; closed circles are previous results.

it is the case, the heat flow from below should increase. We need to survey more in detail anyway.

References

Bullard,E.C., 1954, The flow of heat through the floor of the Atlantic Ocean, Proc. R. Soc. London, Ser. A., 222, 408-429.

Henry,P., Lallemant,S.J., Le Pichon,X. and Lallemand,S.E., 1989, Fluid venting along Japanese trenches: tectonic context and thermal modeling, Tectonophys., 160, 277-291.

Kinoshita,M. and Kasumi,Y, 1988, Preliminary Report of The Hakuho Maru Cruise KH86-5, 190-206.

Le Pichon,X., Iiyama,T., Boulegue,J., Charvet,J., Faure,M., Kano,K., Lallemant,S., Okada,H., Rangin,C., Taira,A., Urabe,T. and Uyeda,S., 1987, Nankai Trough and Zenisu Ridge: a deep-sea submersible survey, Earth Planet. Sci. Lett., 83, 285-299.

Ratcliffe,E.H., 1960, The thermal conductivities of ocean sedi-ments, J. Geophys. Res., 65, 1535-1541.

Shimamura,K., 1988, Sedimentation and Tectonics of Zenisu Ridge, Eastern Nankai Trough and Suruga Trough Regions, Tohoku Univ. Sci. Rep., 2nd Ser. (Geol.), v.58, No.2, 107-167.

Ukawa,M., Eguchi,T. and Fujinawa,Y., 1985, Microseismicity in and around Suruga Bay Revealed by an Array Observation of Ocean Bottom Seismometers, J. Seismol. Soc. Japan, v.38, No.2, 381-397.

von Herzen,R.P. and Maxwell,A.E., 1959, The measurement of ther-mal conductivity of deep-sea sediment by a needle-probe method, J. Geophys. Res., 64, 1557-1563.

von Herzen,R.P. and Uyeda,S., 1963, Heat Flow through the Eastern Pacific Ocean Floor, J. Geophys. Res., v.68, No.14, 4219-4250.

Yamano,M., Honda,S. and Uyeda,S., 1984, Nankai Trough: A Hot trench? Marine Geophys. Res., 6, 187-203.

4.9 Heat Flow Measurement with Acoustic Digital Data Telemetry

T. Furuta, M. Nakanishi and H. Fujimoto

Acoustic digital data telemetry makes it possible to arbitrarily retrieve the observed data during long term underwater measurements. During KH89-1 cruise, ocean bottom heat flow measurement with acoustic data telemetry system was carried out to prove the feasibility and reliability of telemetry of measured heat flow data on real time by means of acoustic pulses. More than 90% of retrieved data by the acoustic data telemetry is in good agreement with the memorized ones in the bottom equipment which is newly developed for long term ocean bottom heat flow measurement. Bit length of each acoustic pulse of the data telemetry system can be selected from 100 msec to 10 msec in accordance with the ambient acoustic noise level. Figure 4.9.1 shows a result of heat flow measurement at 33°45.25'N, 137°59.05'E, water depth of 3,770m, in the Nankai Trough. At this trial, heat flow was measured by telemetry 0 commands fed from the Hakuho-Maru at sea-surface. From the gradient of temperature measured by three temperature sensors, the heat flow value at this point is estimated approximately to be 80mW/m^2 assuming the heat conductivity of the uppermost sediment as 2.0 mcal/cmsec°C.

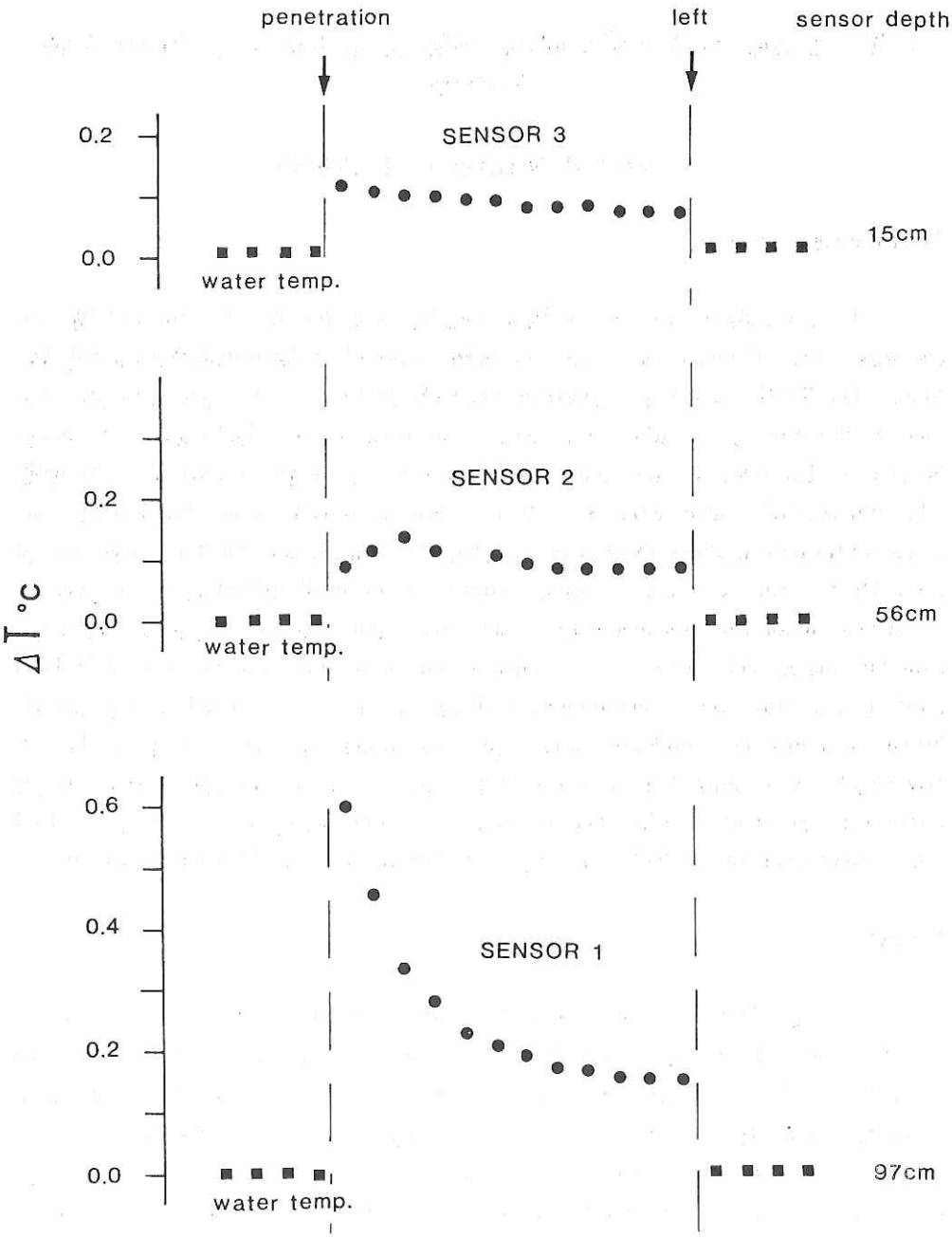

Fig. 4.9.1 Temperature variation of each heat sensor before and after penetration into sediment. The ordinate shows variation of temperatures (ΔT°C) of each sensore, and abscissa shows measuring time (full scale approximately 15 minutes); interval of each data telemetry is about 30 to 45 seconds.

4.10 A Super-Short-Baseline (SSBL) Tansponder Navigation System

T. Furuta, M. Nakanishi and H. Fujimoto

Transponder system

A super-short-baseline (SSBL) acoustic transponder system capable of navigation and subnavigation as deep as 6500 meters has been installed on Hakuho-Maru. The SSBL system is utilized in the following two modes; one is to carry out precise ship's navigation when more than one acoustic target is deployed on the ocean bottom, another mode is to determine the underwater target position three dimensionally when one acoustic transponder is installed on the deep-towed system. The former mode is useful for precise ship's navigation in a relatively limited region such as hydrothermal area. The latter one, on the other hand, is useful for the position fixing of towing system or wired senor for long distances. These two modes can be, of course, operated simultaneously. The SSBL system consists mainly of three segments (Fig. 4.10.1); i) onboard electronic circuits including track display and remote one which is in navigation bridge, ii) transducer and hydrophone array installed under the hull, which can be put down by 2m from ship's bottom, iii) at least one transponder in water. The onboard circuit is transportable and installed in the No.3 or container laboratory. Figure 4.10.2 shows an example of installation onto the JAMSTEC deep-towed TV Camera system.

Result

During KH89-1 cruise, several trials of the SSBL navigation are done to determine the underwater positions of such kinds of sensors as deep-towed proton, deep sea TV and side scan soner etc. Figures 4.10.3 and 4.10.4 show the results of ship's and deep-towed system's positions. The accuracy of position determination using the SSBL is approximately better than 2% of the slant ranges when it is estimated by the simple filtered calculation, about 55 to 60 % of all return signals are fallen into these accuracies. The bad data may be caused by i) high ambient acoustic noise level around both hydrophone array and underwater transponder, ii) effect of multipasses, iii)mis-adjustment of AGC (TVG) circuit in the transponder.

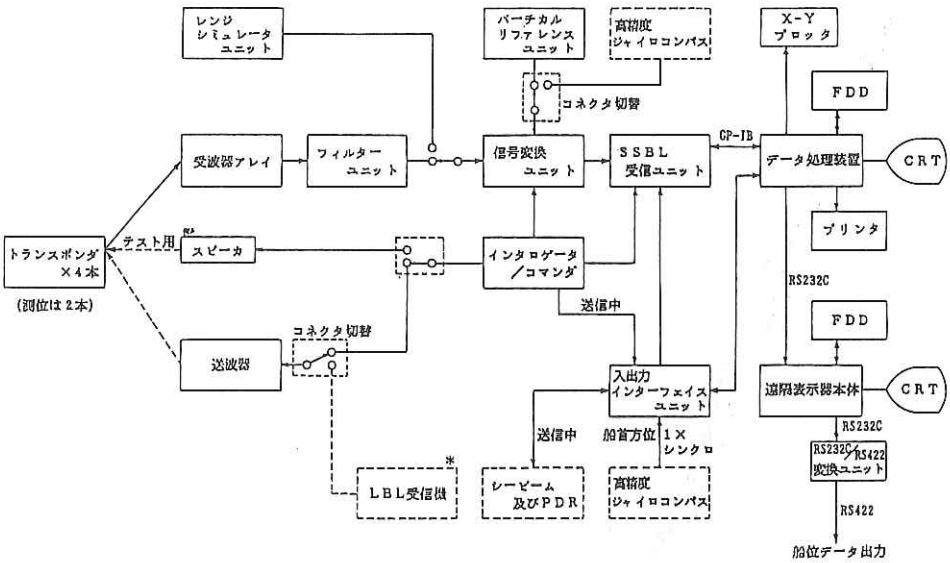

Fig. 4.10.1 Block diagram of the SSBL trasnsponder system.

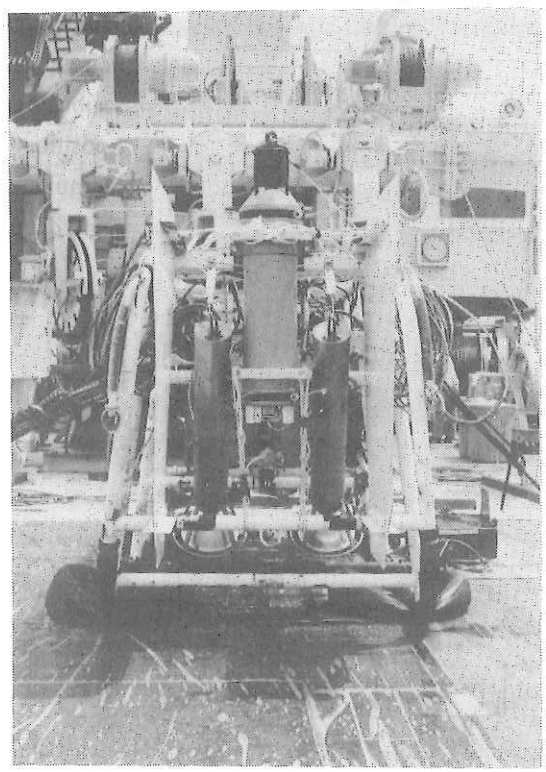

Fig. 4.10.2 Subnavigation transponder installed on the deep-towed TV system.

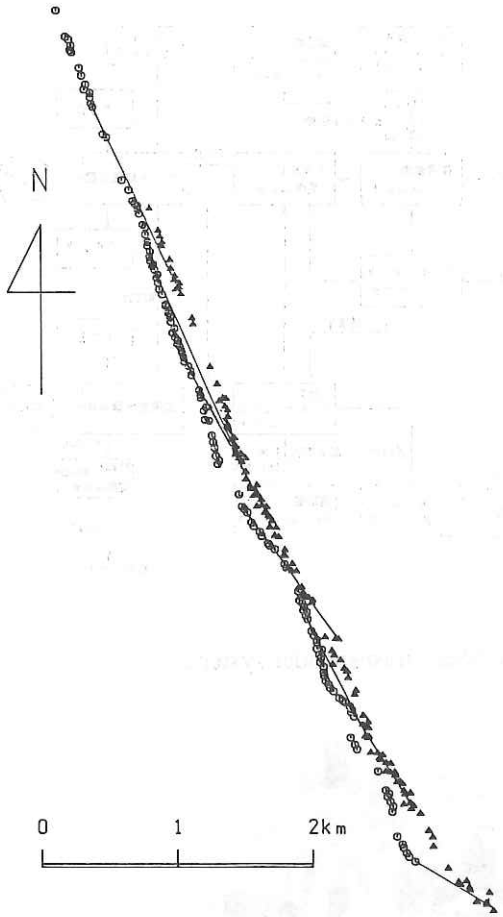

Fig. 4.10.3 Tracks of the ship and subnavigation transponder. circle: ship position, triangle: subnavigation transponder position. Tie line shows the simultaneous positions of ship and deep tow.

Fig. 4.10.4 Vertical section of positions (depth) of the sub-navigation transponder.

4.11 Report on ODP Nankai Downhole Observatory (ONDO) Tested on KH89-1 Cruise of Hakuho-Maru

H.Kinoshita, M. Yamano[1], T.Kanazawa, H.Ishizaki[2], H. Matsuoka[3], H. Murakami[4], H. Fujimoto, T. Furuta and A. Taira[5]

(1)Earthquake Research Institute, University of Tokyo, Tokyo 113
(2)Ocean Cable Company, Tokyo 150
(3)Japan Drilling Company, Tokyo 105
(4)Kaiyo Denshi Company, Saitama 350
(5)Ocean Research Institute, University of Tokyo, Tokyo 164

Abstract

ODP (Ocean Drilling Program) is going to drill a 900 meter deep hole in Nankai Trough area early in 1990 dedicated to a long-term temperature monitoring experiment. A set of thermistor sensors with lead cable attached to a data logger and acoustic transmission devices will be deployed into one of the holes which will penetrate ca. 50 meters into oceanic (basaltic) basement layer of the subducting oceanic lithosphere (northern tip of the Philippine Sea plate) underneath Nankai area. Thermistor cable carries 19 sets of sensors with entire length of about 800 meters. Temperature and pressure gauges of high precision quartz crystal sensors are also attached to top and bottom of the thermistor cable. Temperature and pressure data will be measured once a day and stored in a downhole data logger. A part of the data can be retrieved by use of an acoustic linkage system from a surface or a submersible vessel. Electronics system was tested twice in a temperature controlled onshore laboratory, mechanical parts were tested on Leg 124E (Philippine Sea cruise) of ODP and whole system was tested lately on KH89-1 cruise of Hakuho-Maru and other cruises at water depth about 5000 meters off coast of Japanese main island in June, 1989. As a result of these pre-deployment experiments it was made sure that the ONDO system is well conditioned and can be used for a long-term temperature monitoring in Nankai Trough.

Introduction

The importance of the role of interstitial pore fluids in the friction regime of subduction associated with accretion processes has long been recognized. Seepages of water from accreted materials are observed in a zone between deformation front and accretionary prism

uplifted by thrusts along the trough and trench areas (e.g., Mascle and Moore et al., 1988) Some direct and indirect evidences of the seepage are obtained by observations in conjunction with the appearances of calyptogena colonies or mud volcanoes in the accretinary toes of trench slope front areas. Most of these occurrences are observed by submersible diving and, in some cases, by a detailed monitoring of subseafloor temperature variation (e.g., Kinoshita and Kasumi, 1988; Ohta and Laubier, 1987). We have little knowledge, however, of the manner and origin of seepages of subbottom interstitial fluids.

Nankai Trough (Fig. 4.11.1) is an ideal place to study behaviors of deformation processes in the accretionary prism for several reasons. This is probably acceptable on the fact that several detailed geological and seismic structures and heat flow distribution along Nankai Trough has been investigated by seismic profiling (e.g., LePichon et al, 1987), seismic refraction study (e.g., Kinoshita and Matsuda, 1989), drilling and logging conducted by DSDP Legs (e.g., Kagami and Karig et al., 1986) and heat flow measurements (e.g., Kinoshita and Yamano, 1986). Some of these results are briefly reviewed later in this article.

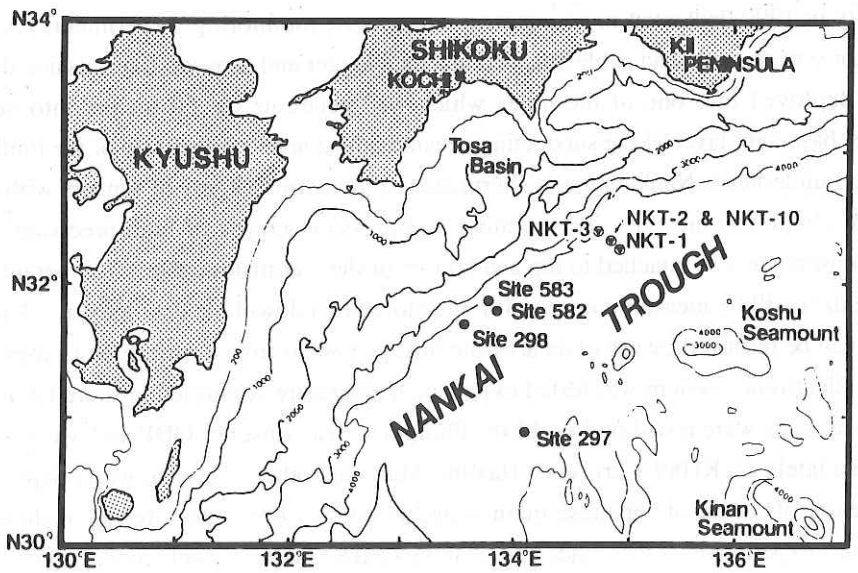

Fig. 4.11.1: Schematic sketch of location of Nankai Trough and its surrounding area where the northern tip of Philippine Sea plate and Japanese landmass collide to form a subduction zone. Previous DSDP sites (297-583) and proposed ODP sites (NKT's) are plotted. ONDO will be deployed into Hole NKT-2.

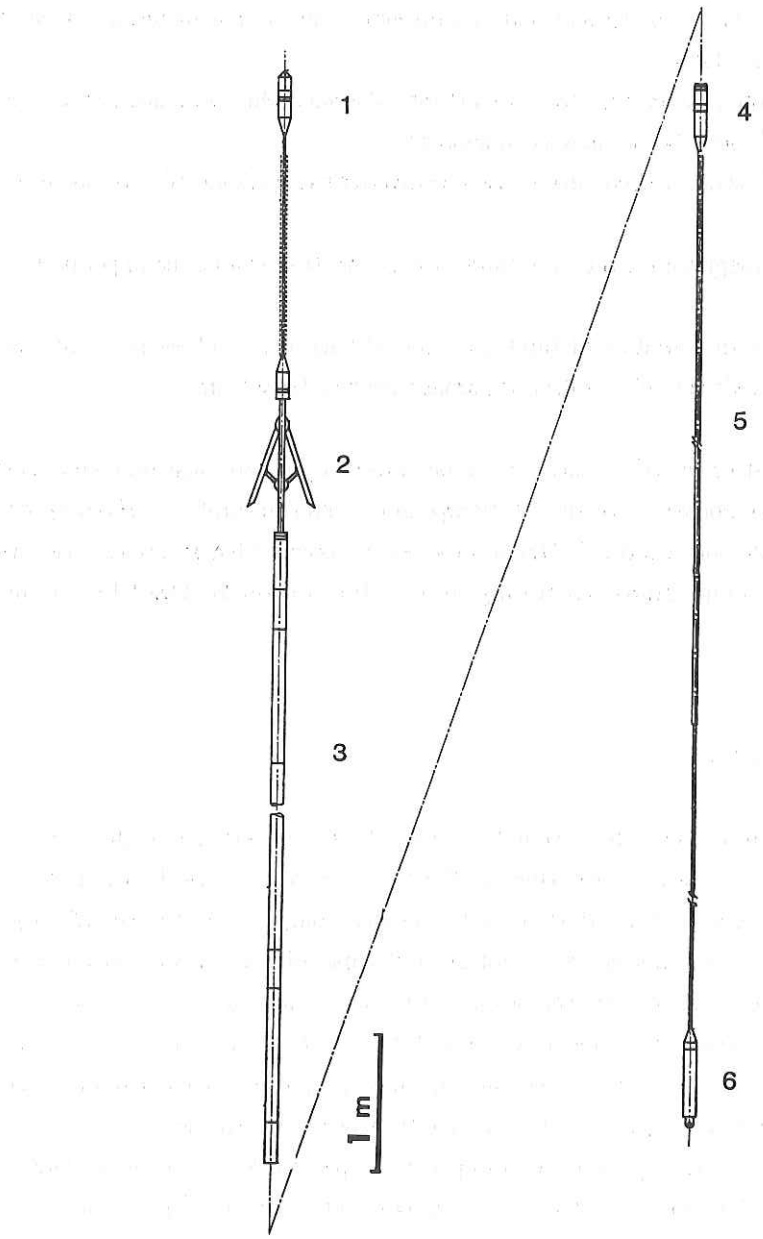

Fig. 4.11.2: Schematic illustration of ONDO. From top left (1) through bottom right (6) are; (1) Acoustic element, (2) Landing pad, (3) Pressure housing with power supply, data processor and data logger, (4) Connector of thermistor cable with data processor, (5) Thermistor cable (800 meters) with 19 sets of ceramic thermistor, and (6) Pressure gauge and a dead weight below it. Approximate scale of dimension is given in bottom left in unit of meters.

Following problems are addressed as the objectives of the Nankai ONDO experiments.

1) Study on the geological and geophysical conditions of the trench turbidite fill and underlying hemipelagic layer.
2) Observation of the pore fluid pressure and calculation of permeability at the toe and across the accretion, from deformation front to decollement.
3) Estimation of fluid flow rate and possible hydrothermal circulation through the decollement zone.
4) Determination of the depth of the origin of fluid seepage probably within the upper part of oceanic basement.
5) Correlation of long-term variation of fluid flow rate, change in downhole pressure and temperature with seismic activities in the crust around Nankai Trough area.

Some of these objectives (i.e., 2 and 3) can be studied by in situ measurements and long-term downhole monitoring of pressure and temperature, and their profiles. The purpose of the present experiment on board R/V Hakuho-maru is to assess a feasibility of a newly developed downhole temperature monitoring system for the future ODP long-term experiment.

Previous Observations

A distribution of heat flow values around a restricted area of Nankai Trough has been obtained in detail (e.g.,Yamano and Uyeda, 1988). The heat flow distribution is characterized by an existence of high heat flow values nearly along the Trough axis although there does not seem to be an active rifting or volcanism (**Appendix 1**). This high heat flow can be partly explained by (1) an existence of lines of hidden seamounts still hot enough to warm up the whole section of the sedimentary cover of the area, (2) thermal reactivation due to large scale faulting of lithospheric plate subducting underneath the Shikoku, (3) reheating of the topmost part of the lithosphere by choking the fluid circulation through sedimentary cover thickening rapidly while the part of the lithosphere is approaching the bottom of Nankai Trough or (4) seepage of warm subseafloor fluid into sediment cover for some reasons such as dewatering processes by compaction of sedimentary materials.

Structural as well as simulation studies on these hypothetical causes of high heat flow pattern show that the cases (1) and (2) are scarcely possible and (3) does not explain well the

present maximum of heat flow values and, as a result, (4) (seepage of fluid) is the most plausible candidate of explanation on high heat flow values.

Previous measurements of the sub-bottom temperature in DSDP holes of Leg 87 (Kagami and Karig et al., 1986) showed an erratic change with depths and this has been explained by one of the present authors as caused by (1) mechanical failure of the measuring system, (2) thermal disturbances by drilling operation or (3) some subseafloor circulation of fluid at depths. Some of the unpublished data from this experiment (DSDP, Leg 87) are given in **Appendix 2.**

After accumulation of knowledges on the possibilities of seepage and resultant mud diapirism in the accretionary prism as observed in the Barbados (Mascle and Moore et al. from ODP Leg 110, 1988), the authors suspect that the erratic variation of the bottom hole temperature of Hole 583, 583A, B, C, D and F of DSSP Leg 87 (Kagami and Karig et al., 1986) in Nankai Trough may possibly be attributable to a subseafloor fluid motion through fault lines. If this is the case, the two branches of temperature variation (called as normal and low temperature zone by the author; Fig.4.11.A-3 in Appendix 2) obtained by Leg 87 seem to show that there are systematic sucking of water within restricted interval of depths from underneath the decollement. The seepage or sucking of water might be observed as a drastic jump of the temperature profile in the holes of Leg 87.

The sucking and some counterbalancing fluid transportation will pump thermal energy toward the ocean floor as a whole and the temperature gradient near the sea floor becomes high and reveals an apparent high heat flow values. The rate of heat transfer from deeper part of the crust to seafloor surface can be simulated with a two dimensional simple model as shown in **Appendix 3.** Repeated seepage of the subseafloor fluid from the crustal material can be driven by tectonic forces which causes an rupturing (seismicity) of crustal formations. By applying appropriate rate of repetition of seismic rebound (e.g. caused by a large earthquake of magnitude 7-8 every 100 years) and other thermal parameters of the crust, we can explain reasonably the supply of heat energy from below in this area.

Downhole Temperature Monitoring System

Lateral cross section of entire length of the long-term downhole temperature monitoring system (ONDO) is illustrated in Fig. 4. 11. 2. The recording package (part number 3 of Fig. 4.11.2) consists of data logger, batteries, one pressure gauge, and a connector (part 4)

between thermistor cable (part 5) and the recording device. The acoustic transmitter element (part 1) is mounted above the top of the recording package lifted by an elastic bar possibly 1 meter above the top edge of the re-entry cone. The landing pads (part 2) hang on a specially designed niche (landing sub in Fig. 4.11.3 in detail) inside the collar connecting casing and a re-entry cone and support the whole downhole system. The sensor cable carries 19 thermistors for temperature measurements between 0 and 800 meter sub-bottom depths. A couple of crystal pressure and temperature gauges are also attached to its top and bottom. Entire thermistor cable will be shipped to J/R rolled in a winch spool before deployment.

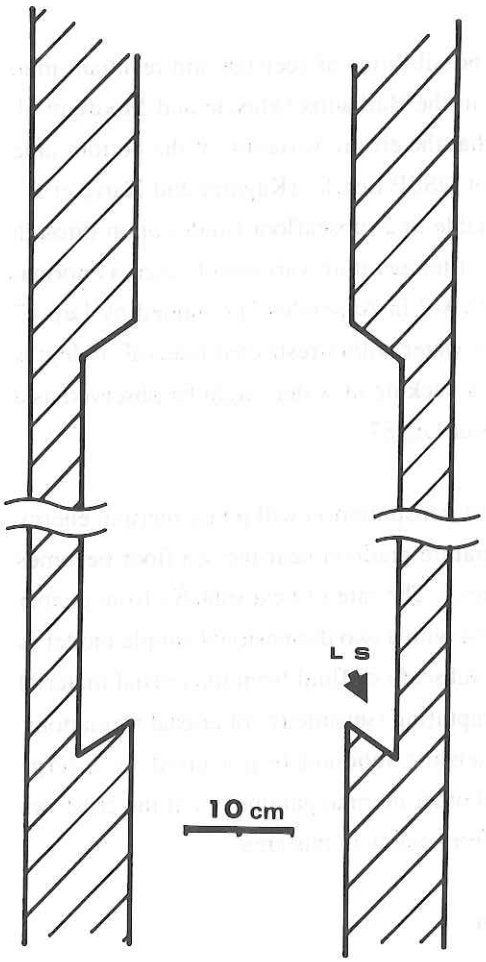

Fig. 4.11.3: Cross-section of a landing sub (LS with a thick arrow) carved on a wall of casing in a shape of a niche. Approximate scale is given in bottom center in unit of cm.

The maximum diameter of the system with the landing pads retracted is 98 mm so that it can pass through the drill pipe. The thermistor cable is 38 mm in diameter and 800 m long. If penetration of the hole is shorter than 800 m, the length of the cable will be adjusted on board Joides Resolution before deployment. The estimated total weight of the system is about 900 kg in water and about 1500 kg in air. Temperature and pressure are measured once a day and the digitized data are stored in IC memories. Resolution of temperature and pressure is 0.001°C at 0°C and 0.01°C at 80°C and 10 millimeters of water column, respectively. The large capacities of memory and battery allow measurements for up to five years. Other specifications of the ONDO system are given in Table 4.11.1.

The stored data are retrieved with acoustic telemetry between the system and the surface ship at any time (Fig. 4.11.4). A pop-up type acoustic data retriever will be set on the seafloor near the re-entry cone after ONDO deployment and the data will be transmitted to the data retriever from ONDO with minimum consumption of battery powers during the monitoring operation. The surface ship can locate the instruments (retriever and ONDO) through transponder navigation. Both of the instruments can send the data of a certain time span requested by the acoustic commands from the surface ship. Retrieval of the data from the downhole system to a surface ship is planned to be done once or twice a year. Thus we can monitor time dependent temperature versus depth profile and pressures at the top and bottom of hole.

Test of Landing Scheme by ODP Cruise

Most difficult phase of the deployment of the ONDO system is expected at the time of opening landing pads and of settlement on the niche carved inside the casing pipe. Landing latch mechanism is checked and tested at ODP Leg 124E by ODP engineers and resulted in a good response. No conceivable failure or malfunctioning was pointed out by engineers who designed or tested this system.

It is desirable to drill a brand-new hole cased for this experiment as collapse of the wall long time after drilling of virgin hole may obstacle the entry of the thermistor cable. No sampling or logging are to be made in this hole, but it is necessary to install a re-entry cone with an acoustic transponder attached on its top and casing with a landing sub (Fig. 4.11.3) as described below. The casing must be perforated with small holes probably punched every 1 meter.

Table 4.11.1 Instrumental specification of the ONDO monitoring system

1. Temperature Measurement
   (1) Sensor: 19 thermistors
   (2) Temperature range: 0 - 80°C
   (3) Data bit and sampling rate: 16 bits per data and 23 data every 24 hours (additional two pairs of pressure and temperature data included)
   (4) Resolution :+/-0.001°C at 0°C and +/-0.01°C at 80°C

Temperature dependence of thermistor resistance

T°C	0	10	20	30	40	50	60	70	80
R kOhm	29.57	19.17	12.74	8.66	6.01	4.26	3.07	2.26	1.69
DR kOhm/°C	1.040	.643	.408	.265	.175	.118	.082	.057	
S °C/1mV	.008	.013	.020	.031	.048	.070	.101	.146	

T: temperature, R: resistance, DR: variation of resistance per degree C, D denotes a deviation, S: electronics output sensitivity.

(5) Temperature dependence of resistance of 800 meter lead cable (round trip).

0°C	60.65	Ohm
10	63.15	
20	65.74	(Average gradient = 0.265 Ohm/°C)
30	68.34	

100	87.19	

Temperature dependence of total impedance of 800 meter long lead cable is linearly fit to: R(2*800m)=60.64+0.2647*(T-273), where T in Kelvins and R in Ohms.

(6) Drift of thermistor resistance: (temperature converted) 0.01 °C/year, provided every temperature value is measured in reference to a pair of standard resistors of which the change by aging is less than 0.05 %/year.

2. Pressure measurement
   (1) Sensor: two sets of Digiquartz gauges with temperature monitor.

(2) Pressure range: 0 - 10,000 PSI (equivalent to water depth 0 - 7,000 meters).

(3) Data sampling: 16 bit, applicable also to temperature monitor

(4) Resolution: pressure 1 cm water column, temperature 0.002° C

(5) Accuracy: pressure 70 cm water column, temperature 1°C.

3. Memory capacity

(1) 48bytes /day

Date: 2 bytes, Temperature: 38 bytes, Pressure: 4 bytes,

Temperature monitor of pressure gauge: 4 bytes.

(2) 87,600 bytes for 5 year operation.

4. Acoustic data retrieval

(1) Modulation by three frequency bands

Send data command: , 13.889, 14.706 and 15.625 kHz.

Receive data acknowledg: 13.889 and 14.706 kHz.

(2) Pulse width for data transmission through sea water 10, 20, 50 and 100 msec are selected by a command.

(3) Command from surface

(a) Send power supply (battery) condition.

(b) Measure and send present temperature data.

(c) Send data for a full day of a required date.

(d) Send ten-day data from a certain date.

(4) Distance between ship and repeater is obtainable on request command.

5. Power requirement for five-year operation

Total capacity is 36 AH for lower tension supply (9 volts) including maintaining active electronics timing circuit, measurement, data processing and data storage, and 45 AH (30 volts) for telemetry system.

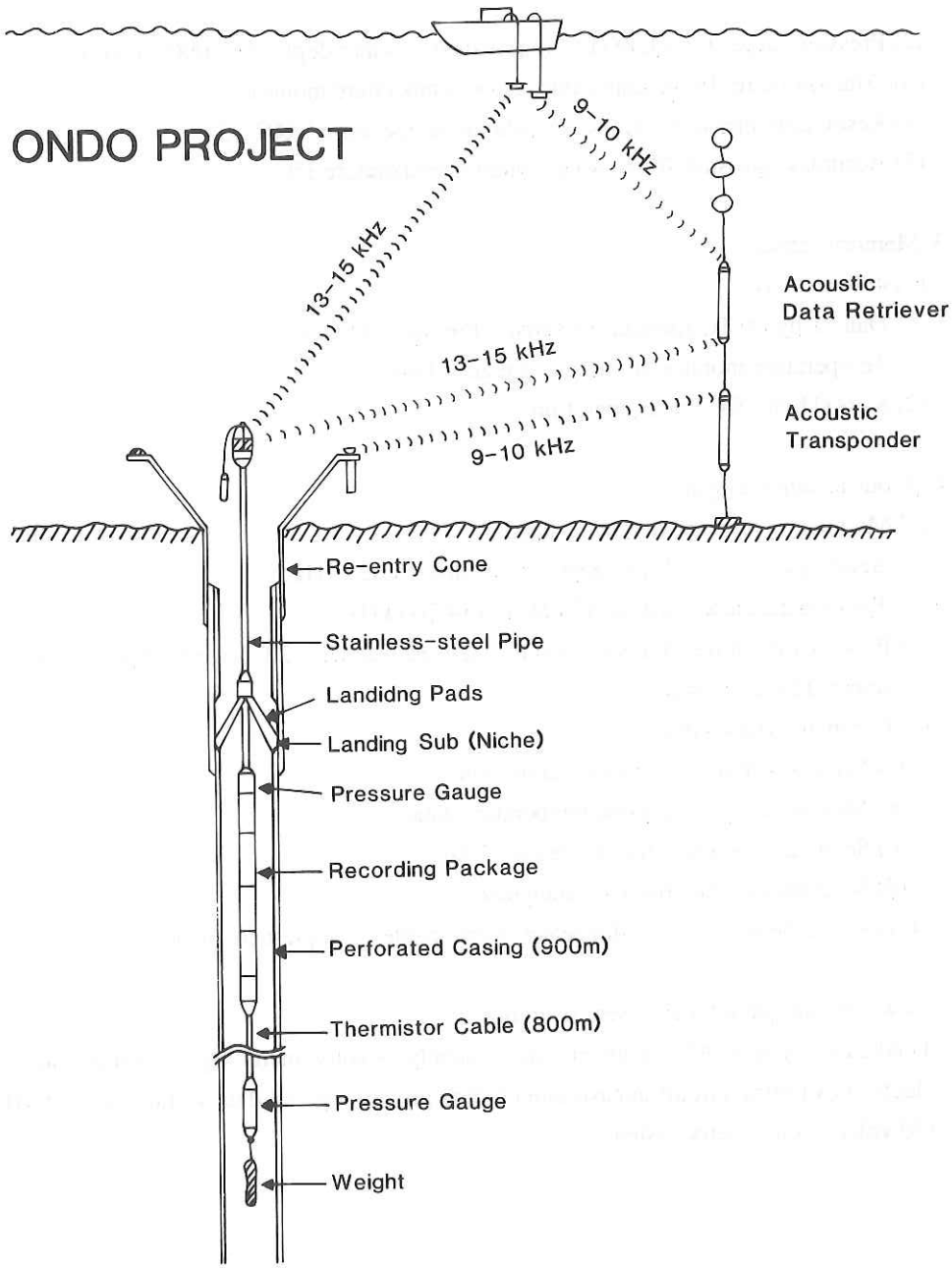

Fig.4.11.4: The temperature monitoring system after the deployment and data retrieval with surface vessel. A transponder is used also for range measurement to the re-entry cone. Acoustic data retriever (right) sitting on the sea floor receives data on carrier frequency of 13-15kHz transmitted from the downhole system (ONDO) according to "Send Data" command (9-10kHz) from the surface ship. It surfaces after retrieval of the ONDO data by use of a releaser of the acoustic transponder.

Table 4.11.2 Test on Acoustic Data Retrieval from ONDO Tool during KH-89-1

Slant Range (m)	Pulse Width (ms)	Temperature		Pressure	
		micro sec	deg C	micro sec	mH2O
1027	50	5.774364	12.183	29.3385	1018.08
2037	50	5.776479	3.611	28.9328	2085.30
2037	50	5.776531	3.398	28.9329	2085.13
2037	50	5.776478	3.205	28.9325	2086.29
2035	20	5.776647	2.992	28.9322	2087.23
3036	50	5.776863	2.034	28.5518	3129.01
3037	20	5.774873	1.993	28.5515	3129.87
3036	20	5.774879	1.968	28.5520	3128.48
3037	10	5.776884	1.948	28.5520	3128.49
4028	20	5.774959	1.639	28.1864	4171.55
4027	50	5.776960	1.635	28.1862	4172.13
4028	20	5.776963	1.622	28.1868	4170.39
5007	20	5.776982	1.544	27.8372	5208.39
5003	20	5.776980	1.552	27.8372	5208.38
5003	50	5.776974	1.577	27.8374	5207.76
5034	100	5.776972	1.585	27.8375	5207.45
5004	50	5.776979	1.556	27.8409	5197.18
5003	20	5.776978	1.561	27.8418	5194.45

Time necessary for deployment after establishment of experimental hole is estimated by ODP engineers as to be about 42 hours including additional time for confirmation that the system is operating properly. It does not include time of drilling a dedicated hole and mounting re-entry system with casing pipes.

Test of Data Aquistion and Retrieval Sytem

The data logger and data transmissions were tested in the cruise of KH89-1 on board R/V Hakuho-maru at water depths about 5000 meters. Water tightness and mechanical strength of the recording package seem to be good for a handling of deployment. Mounting and readjustement of the equipment could be performed within a reasonable limit of time (a few hours) on board. Acoustic transmission and receiving data between surface and at depths every 1000 meters down to 5000 meters were run without loss of data bits. Bottom temperature and pressure data were displayed at each transmission trials without noticeable error (Table 4.11.2).

The acoustic data retriever was also tested by two of the present authors in combination with ONDO main section on KT89-19 cruise of Tansei-Maru, Ocean Research Institute, University of Tokyo, in November, 1989 in Nankai Trough area. ONDO main section was hang with steel wire from the surface ship and lowered as deep as 4000 meters. The acoustic retriever was lowered from the ship by 20 meters, and acoustic link between the retriever and the ONDO main section was tested. It was confirmed that whole system worked properly as initially designed (private communication, Fujimoto and Kanazawa, 1989). Therefore, we conclude that the ONDO system works well if its deployment into an ODP hole is successful. Temperature data from downhole thermistor set are obtained in a form of resistance values including resistance of full extent of lead cable. The derivation of the downhole temperature from these data is described in **Appendix 4**. Also shown in **appendix 5** is the methods of derivation of the pressure and temperature values from a set of high precision sensors made of quarts crystals.

References

Carslaw, H.S. and J.C.Jaeger, 1959, Conductiion of heat in solid, 2nd ed., Oxford Sci. Press, p97.

Kagami, H., D. Karig, D.E. Coulbourn and Shipboard Scientific Party, 1986, Site, 583, Initial Report of the Deep Sea Drilling Project, 87, 123-256.

Kinoshita, H. and M. Yamano, 1986, The heat flow anomaly in the Nankai Trough, Initital Report, Deep Sea Drilling Project, 87, 727-743.

Kinoshita, H. and N. Matsuda, 1989, Seismic structure and Geomagnetic Anomaly in the Nankai Trough Related to Subduction of the Philippine Sea Plate, J. Geomag. Geoelectr., 41, 161-173.

Kinoshita, M. and Y. Kasumi, 1988, Heat flow measurements in the Nankai Trough area, Prel. Rept. Hakuho Maru cruise KH86-5, Ocean Res. Inst., Univ. Tokyo, 190-195.

LePichon, X., T. Iiyama, H. Chamley, M. Faure, H. Fujimoto, T. Furuta, Y. Ida, H. Kagami, S. Lallemant, J. Legget, A. Murata, H. Okada, C. Ragin, V. Renard, A. Taira and H. Tokuyama, 1987, Nankai Trough and the fossil Shikoku Ridge: results of Box 6 Kaiko Survey, Earth Planet. Sci. Lettr., 83, 186-198.

Mascle, A., J. C. Moore, E. Taylor and Shipboard Scientific Party, 1988, Site 676 and Summary, Proceeding of the Ocean Drilling Program, Initial Report, 110, 509-602.

Nagihara, S., H. Kinoshita and M. Yamano, 1989, On the high heat flow in the Nankai Trough area -a simulation study on a heat rebound process, Tectonophys., 161, 33-41.

Ohta, S. and L. Laubier, 1987, Geochemical and biological observations on the biological communities associated with fluid venting in Nankai Trough, Earth Planet. Sci. Lettr., 83, 329-342.

Yamano M., S. Uyeda, M. Joshima, M. Kinoshita, S. Nagihara, R. Bo and H. Fujisawa, 1987, Report on DELP 1985 Cruises in the Japan Sea, part 5: Heat flow measurements, Bull. Earthquake Res. Inst., Univ. Tokyo, 62, 417-432.

Yamano, M. and S. Uyeda, 1988, Heat flow, in "The Ocean Basins and Margins, 7B, edit. Nairn, E.M. et al.", 523-557.

Appendex 1; On the High Heat Flow in Nankai Trough Area

- Simulation of Heat Rebound Process -

A concentration of high heat flow (as high as 120-160 mW/m^2)has been observed in the Nankai Trough, off southwest Japan where the Philippine Sea plate (Shikoku Basin) is subducting underneath Japanese landmass (Fig. 4.11.A-1). We interpret this high heat flow in the subduction zone as caused by the recovery of conductive heat flow to the theoretically expected value for young Shikoku Basin lithosphere after cessation of hydrothermal heat exchange through sediment (Nagihara et al., 1989). The thickening sedimentary cover suppresses the free and rapid heat exchange between basement and sea water whereas the topmost part of the basement allows a hydrothermal circulation within it to pump heat up from the hot plate to the sediment cover. We proposed to call this process as "heat rebound". Numerical simulation shows that significant heat flow recovery can occur and it is largely influenced by the sedimentation rate. We consider that the high heat flow in Nankai Trough is basically caused by the heat rebound. However, rapid sedimentation in the trough also indicates that the heat flow recovery expected by the simulation is not large enough to explain the trough high heat flow only by the heat rebound. Some additional mechanism, such as dewatering from compaction in hemipelagic sediments may play a role to some extent. This problem will be discussed in other appendix and does not interfere with the present model simulation study.

Figure 4.11.A-2 is showing calculated heat flow value versus time in the case where water circulation through sediment layers is sealed when sediment thickness reaches 300 m (indicated by an arrow). Thermal conductivity of thickened sediment is 2.5 W/°C/m. Apparent thermal conductivity within the hydrothermally activated layer (top 2 km of basement layer) is assumed to be twice as high (10 W/°C/m) as ordinary thermal conductivity of the lithospheric solid materials (5 W/°C/m). Curve R is the heat rebound model calculated on the above assumption. N is heat flow recovered without hydrothermal activity within basement layer and T is equivalent to the heat flow vs. age relation of cooling model of oceanic lithosphere. Sedimentation history was determined mainly based upon DSDP (Leg 87) sedimentological data with some constraint from seismological parameters observed around this area. At 1 and 2 Ma the sedimentation rate fluctuated according to DSDP data which is reflected in the heat flow growth curves.

Appendix 2; Bottomhole Temperature Profile Observed by Leg 87, DSDP, Nankai Trough Area

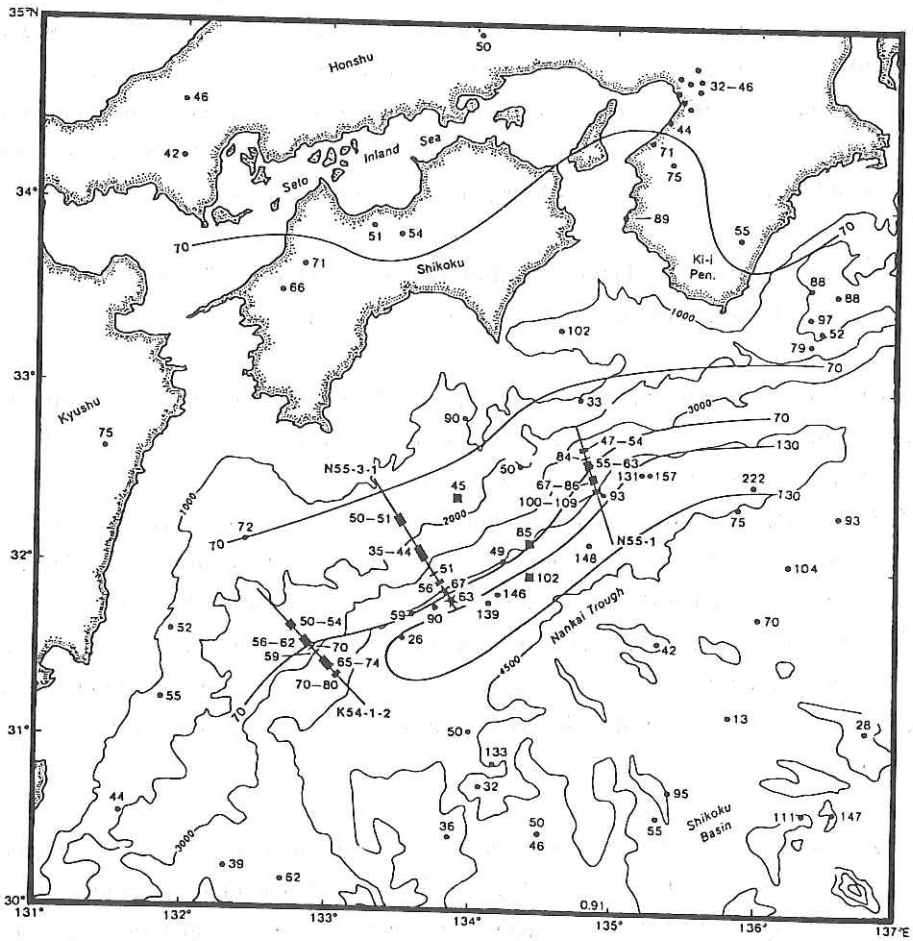

Fig. 4.11.A-1: Heat Flow distribution around Nankai area (Yamano and Uyeda, 1987; Kinoshta and Yamano, 1986). Values are given in mW/m2.

Methods of measurements are described in detail in Kinoshita and Yamano (1986). We observed a highly variable temperature profile by DSDP (Leg 87) operation (Fig. 4.11.A-3) and we guessed that this is probably caused by difference in position of holes drilled close to each other. Recently we obtained an idea that we see some kind of underground fluid motion in the toe of accretionary prism. Also in the ILP-DELP CRUISE OF 1985 (Yamano et al., 1987), we found a vague acoustic reflection imagery which may indicate discharge of some bouyant material from sea floor in the vicinity of a presumable thrust belt along the western edge of the Northeast Japan. These observations shall be tested through detailed experiment below sea floor such as ONDO program proposed here.

Appendix 3; Heating of Trough Sediment by Seepage of Fluid From Deeper Part of Basement - A Simplified Modelling -

Suppose some episodic dewatering from subducting plate (including sedimentary cover) occurs and a part of seepage fluid from deeper part is mixed with sedimentary materials of trough fill. Geometrical model on the top left of Fig. 4.11.A-4 (NANKAI SECTION) is replaced by a simple model of right (HEATING BY MIXING) with different thermal parameters. B is representing the sea floor sediment with temperature To (= 0 ° C) and A represents seepage fluid with initial temperature T (ca 80 °C). Volume of seepage fluid, heat capacity of materials and density of materials are given in the base of figures. Then we can approximately estimate the effect of seepage fluid on the heat flow scheme on the sea floor. It is assumed that the volume of A + B remains unchanged from volume B after mixing.

Episodic seepage and mixing of A and B on the right figure gives an sudden increase of the average temperature of part B ca 0.8 °C. After homogenization of temperature of part B by mixing, change in temperature of sediment slab with surface temperature T_0 = 0 deg. C can be estimated (Carslaw and Jaeger, 1959; page 97). Using thermal conductivity of solid rocks (3 W/°C/m), heat flow through sea floor can be as high as 300 mW/m^2 at 1 year after fluid mixing and becomes to 30 at 100 years later. Thus dispersed and repeated seepage of deep seated water leaves its significant thermal effect even after 100 years. If this kind of episode occurs every 100 years in average in a restricted region such as Nankai area, the superficial heat flow value can be maintained considerably higher than those of surrounding areas as observed by our field measurements in the past.

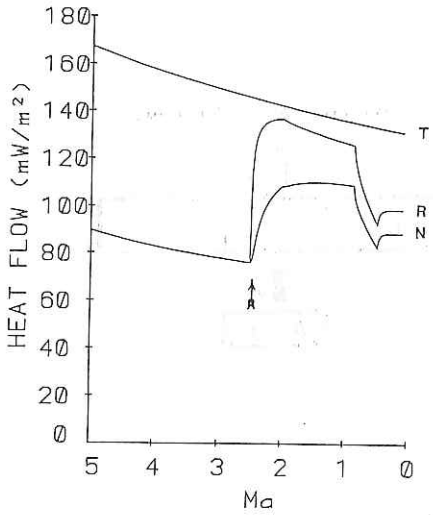

Fig. 4.11.A-2: Heat flow rebound after enough accumulation of sediment cover to choke hydrothermal circulation. R and N represent cases of (R) convective heat transfer in subseafloor basement layer, and (N) pure conductive transter. T is empirical plate cooling curve. Further details are referred to in Nagihara et al. (1989).

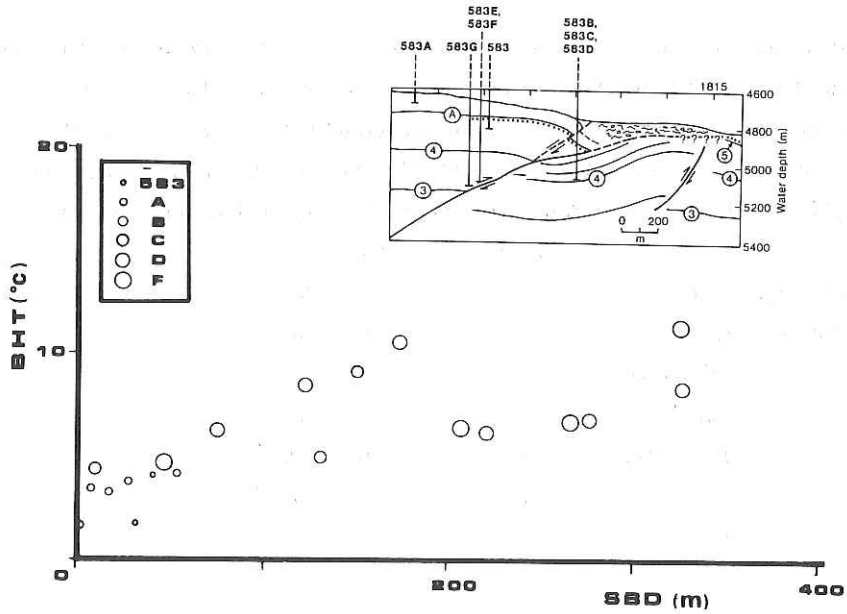

Fig. 4.11.A-3: Bottomhole temperatures (BHT) versus subbottom depths (SBD) measured in Leg 87, DSDP (Kagami and Karig et al., 1986). Top insert shows relative positions and depths of each holes measured. Hole assignments are given as legend in a frame on left side.

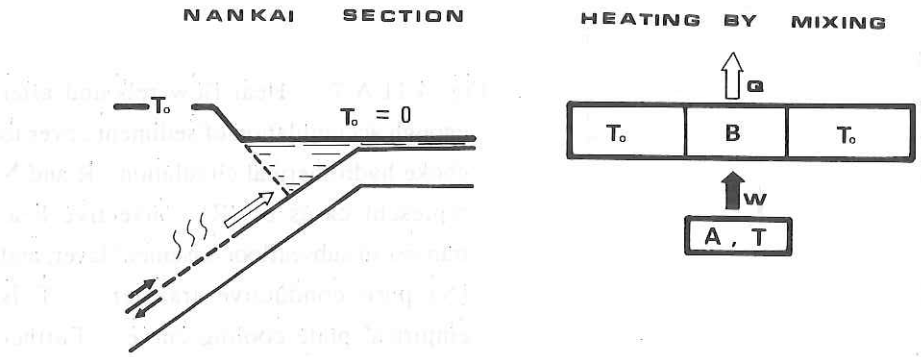

Fig. 4.11.A-4: Schematic cross-section of Nankai Trough (left). Subducting plate squeezes some fluids upward while rupture occurs deep in the subseafloor faults. Seafloor temperature is kept approximately constant and equal to 0 degree C. Two dimensional model is assumed. Mixing of warm fluid (right) with top sediment cover produces heat flow (Q) higher than that of surrounding area. Parameters used for this model are:

		Part A	Part B	
Initial Temperature		80	0	deg. C
Geometry:	depth	2	0	km
	thickness	0.1	1.0	km
	length	1	10	km
	Heat capacity	1	0.5	cal/g
Density		2	1	g/cm^2

Appendix 4; Derivation of Downhole Temperature

The total impedance (pure resistance) values measured on both ends of the leading wire is a combination of resistance of leading cable and that of thermistor. Following factors have to be taken into account to derive apparent resistance of the downhole thermistor sensors.

1) Temperature dependence of thermistor resistance.
2) Temperature dependence of cable resistance.
3) Cable length along which downhole temperature varies.
4) Pressure dependence of these values are small and are consequently neglected.

The method presented here is a simple one to obtain recursively approximate values of the downhole temperature from thermistor resistance. The method we present here is basically dependent upon an assumption that the downhole temperature can be linearly interpolated with subbottom depths. In actual case, the downhole temperature profile may not be a linear one which hinders a simple approximation. However, the variation of resistance of thermistor with temperature (> 265 ohm/deg, see Table 4.11.1) is larger by more than 3 orders than that of the lead cable (0.265 ohm/deg) and we can utilize a simple method. Laboratory-tested temperature dependence of the thermistor sensor is given in table 4.11.A-1. B-value of each thermistor which characterizes the temperature dependence of the resistance value is also given.

The derivation of the temperature value, for instance of the k-th thermistor from the top, is given by the following five step recursive algorism. 1) Get total impedance of the k-th thermistor including lead cable (round trip). 2) Estimate approximate lead cable resistance of a round trip assuming linear temperature gradient. 3) Calculate a corrected impedance of the k-th thermistor by subtracting 2) from 1). 4) Calculate pseudo temperature value of the thermistor from the temperature versus resistance table 4.11.A-1. 5) Get back to process 2). After a few rounds of recursive calculations we obtain correct temperature value of the k-th thermistor.

When the temperature value of the k-th themistor is calculated, temperature distribution of the lead cable is already obtained except the lower end, and the lead cable resistance is fairly well estimated by using the temperature coefficient shown in table 4.11.1. Because the temperature coefficient is much smaller than that of the thermistor, the recursive calculation quickly converges. The obtained temperature value of the thermistor is used for

Table 4.11.A-1 Characteristics of thermistor chips used for ONDO

Chip No.	B-value	R_{273}	Standard Devisation for fit to curve *1
0 *2	3469.684	30.09	9.54×10^{-3}
1	3464.777	29.78	9.53
2	3477.345	30.16	9.51
3	3462.712	29.79	9.52
4	3450.077	29.55	9.53
5	3446.236	29.37	9.53
6	3460.853	29.83	9.49
7	3448.338	29.49	9.54
8	3468.386	29.87	9.47
9	3467.974	30.07	9.49
10	3463.439	29.94	9.51
11	3464.151	29.93	9.52
12	3471.211	30.14	9.51
13	3466.947	30.04	9.51
14	3462.676	30.72	9.48
15	3453.387	30.32	9.55
16	3459.195	30.70	9.52
17	3457.484	30.50	9.53
18	3461.264	30.59	9.50
19	3467.875	30.67	9.53

*1 $\ln(R/R_{273}) = B(1/T-1/273)$, T in Kelvin.

*2 This chip is set in the data logger section ob Fig. 4.11.2.

the calculation of temperature of the next thermistor. Downhole temperature is derived from the top to the bottom in this way.

Appendix 5; Derivation of Pressure and Termperature Values from High Precision Quartz Crystal Sensors and Their Calibration

Two sets of pressure and temperature sensors are attached to top and bottom of the thermistor cable. The derivations of these values are given by following sets of formulae for pressure (P) and temperature (T) based on measured period length of pressure sensor (T_p) and temperature sensor (T_t). Specifications of the coefficients of these sensors are given here.

$$T = A \cdot U + B \cdot U^2 + C \cdot U^3$$

$$U = T_t - U_0$$

where T_t is observed period (in microseconds) of the temperature sensor oscillation.

also

$$P = D \cdot (1 - T_0^2/T_p^2) \cdot \{1 - E \cdot (1 - T_0^2/Tp^2)\}$$

$$D = D_1 + D_2 \cdot U + D_3 \cdot U^2$$

$$E = E_1 + E_2 \cdot U$$

$$T_0 = T_1 + T_2 \cdot U + T_3 \cdot U^2$$

where T_p is observed period (in microseconds) of the pressure sensor oscillation.

Sensor No.	25603 (Top)	24670 (Bottom)	
U_0 =	5.792629	5.777356	microsec
A =	-4085.748	-4136.841	Deg.C/(microsec)1
B =	-16807.04	-22417.56	Deg.C/(microsec)2
C =	-113925.5	-227985.1	Deg.C/(microsec)3
D_1 =	-53360.34	-51977.61	PSI
D_2 =	-1298.306	-3650.036	PSI/miocrosec
D_3 =	121600.6	155527.8	PSI/(microsec)2
E_1 =	0.0388229	0.0355242	dimensionless
E_2 =	0	0	
T_1 =	27.68209	29.74519	microsec
T_2 =	0.6059785	0.7739375	dimensionless
T_3 =	36.61023	52.44179	1/microsec

Accuracy: 0.01 % of fullscale 7000 PSI (Pounds/Inch^2)
(1 PSI = 70.3g/cm^2 = 6.895kPa)

The pressure test of these sensors were achieved onland at the stream line experiment laboratoty of Institute of Industrial Science, the University of Tokyo. Results of measurements are shown in Fig.4.11.A-5(1) and (2) where (1) shows the output frequency of temperature sensor versus pressure at room temperature (15-16 degree C), and (2) gives output frequency of pressure sensor versus pressure at 15-16 degree C. We found that the accuracy and repeatability of pressure controller of the test machine seems to be much lower than that of the sensors based upon its specifications released by its producer.

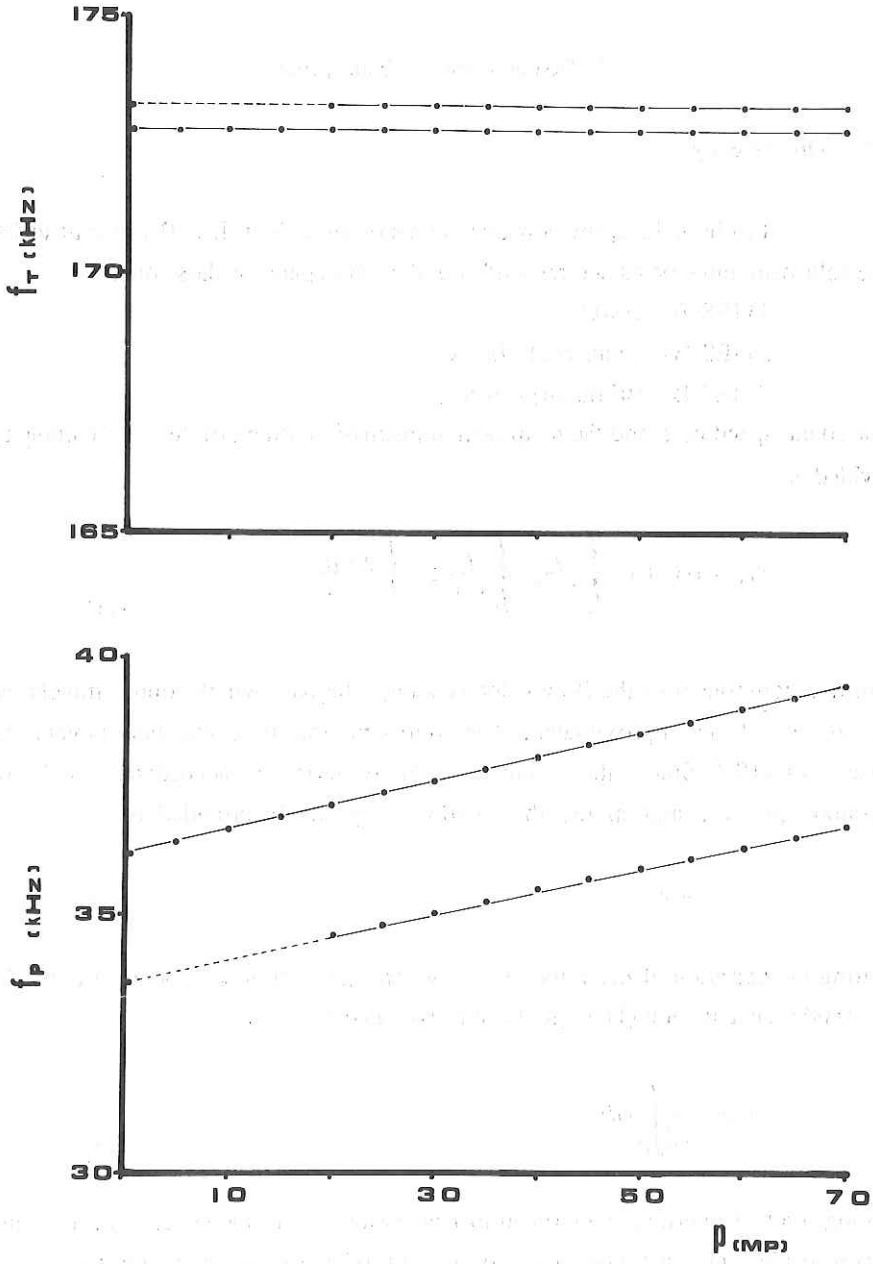

Fig. 4.11.A-5(1) and (2): Frequency change with hydrostatic pressure of high resolution quartz temperature sensor (1). Same for pressure sensor (2). Measurements were run at room temperature (15-16 deg. C). Frequency is in kHz, and pressure is in MPa.

4.12 Measurement of Oceanic Current by Means of the IES (Inverted Echo Sounder)

T. Takeuchi and M. Nakayama

4.12.1 The theory

In Fig. 4.12.1, the acoustic waves emitted from IES-B transmit to IES-C via the following three paths and respond via the same paths as those ones.

1) IES-B - IES-C

2) IES-B - A(surface) - IES-C

3) IES-B - B(bottom) - IES-C

Let the sound speed be c, and the reciprocal transmission time differences Δt along a path is provided as

$$\Delta t_{12} = t_{12} - t_{21} = \int_{\Gamma} \frac{ds}{c+v} - \int_{\Gamma} \frac{ds}{c-v} \cong - \int_{\Gamma} \frac{2v}{c} \frac{ds}{c} \tag{1}$$

by setting a component of the flow velocity along the path which sound travels as v, where $v/c << 1$ as approximated. The approximation involved here is very good, because $v/c<10^{-3}$. Since the acoustic velocity varies in accordance with water temperature, pressure and salinity, the sound velocity can be provided as

$$c = c_o + \delta c \tag{2}$$

by setting the variation of the velocity as c, where c_o is the mean sound velocity. Since $\delta c/c_o < 0.003$, the equation (1) might be approximated as

$$\Delta t_{12} \cong - \frac{2}{c_o^2} \int_{\Gamma} v ds \tag{3}$$

Assuming that the vertical component of flow velocity in the ocean can be ignored and considering just the horizontal component of the velocity, we put the horizontal component in question as u(z).

In Fig. 4.12.1, if each time when the sound emitted from IES-B has traveled along the path of 2) and the path of 3) above mentioned is respectively represented as t_2 or t_3 they are provided as

$$t_2 = M_- + N_- - L_-$$
$$t_3 = M_+ + N_+ - L_+ \qquad (4)$$

L, M, and N are respectively time for sound to travel along each side of the vertical triangle, whereas + and - denote the opposite directions. From these equations, reciprocal travel time differences Δt are provided as the following equation.

$$\Delta t = t_3 - t_2 = (M_+ - M_-) + (N_+ - N_-) - (L_+ - L_-) \qquad (5)$$

If the acoustic ray paths are almost straight lines, the following equations are valid.

$$M_+ - M_- = -\frac{2}{c_o^2}\int_{-D-\Delta D}^{0} u(z)\cot\theta dz \qquad (6.a)$$

$$N_+ - N_- = -\frac{2}{c_o^2}\int_{-D}^{0} u(z)\cot\theta dz \qquad (6.b)$$

$$L_+ - L_- = -\frac{2}{c_o^2}\int_{\Delta D}^{0} u(z)\cot\varphi dz \qquad (6.c)$$

Therefore,

$$\Delta t = -\frac{L'}{c_o^2}\frac{1}{D}\int_{-D}^{0} u(z)dz - \frac{L'+2\Delta L'}{c_o^2}\frac{1}{D+\Delta D}\int_{-D-\Delta D}^{0} u(z)dz + \frac{2(L'+\Delta L')}{c_o^2}\frac{1}{\Delta D}\int_{\Delta D}^{0} u(z)dz \qquad (7)$$

is obtained. By putting mean currents U and Ub, the equation (8) is obtained from the equation (7).

$$U - U_b = -\frac{c_o^2}{2L\cos\varphi}\Delta t \qquad (8)$$

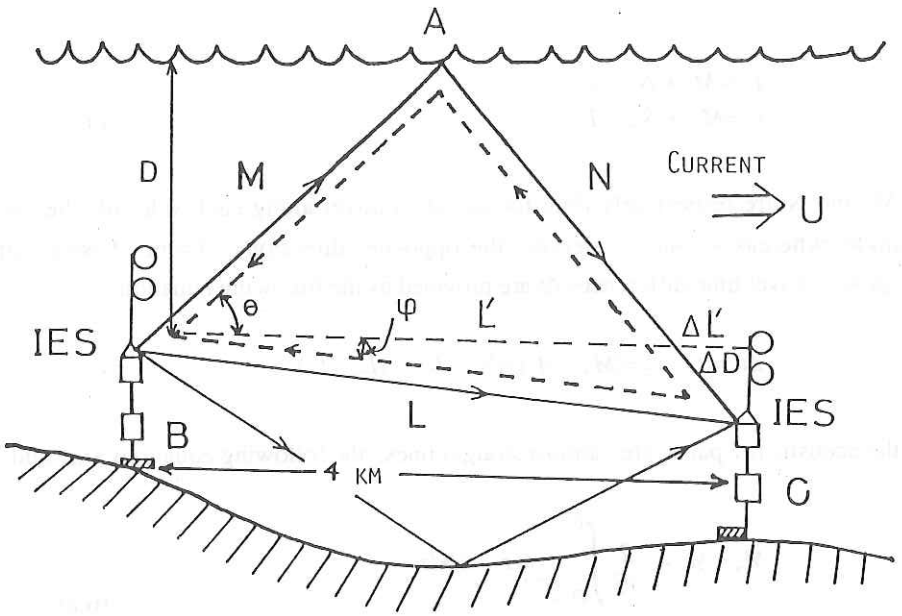

Fig.4.12.1 Schematic diagram for measuring mean currents in the ocean by using IES's.

Thsu, it is known that the horizontal average currents can be measured, from the equation (8), with the bottom mean flows as a reference. In the equation (8), L can be obtained from the travel time via the path 1), where φ might be calculated by using L and the difference of depths between IES-Band IES-C.

4.12.2 Measurement results

The acoustic waves emitted from IES-B moored rising up 800m at the bottom of the depth of 2430 m in the water arrive at sea surface and reflect off, or directly and reach IES-C which were moored at the bottom of about 4000 m distant from the IES-B. They were respectively moored at 34°03.47N, 138°06.11E and 34°04.98N, 138°07.85E.

Fig.4.12.2 shows the acoustic ray paths calculated from the profile of the water temperature measured with XBT. It takes 2800 msec for the acoustic wave to propagate directly from IES-B to IES-C under no current. When the sound arrives at surface, reflects off and reaches IES-C, it takes 3597.8 msec. Fig. 4.12.3 shows sound waveforms propagated between IES-B and IES-C. Table 4.12.1 shows propagation time between them. From this table, L can be calculated as L=4167 m using mean sound velocity 1488 m/s. The difference time between IES-B and IES-C is 0.93 msec (see Table 4.12.1). Therefore, the mean currents directed toward IES-B from IES-C will be about 25 cm/sec using the equation (8), assuming that flows between IES-B and IES-C is 0.

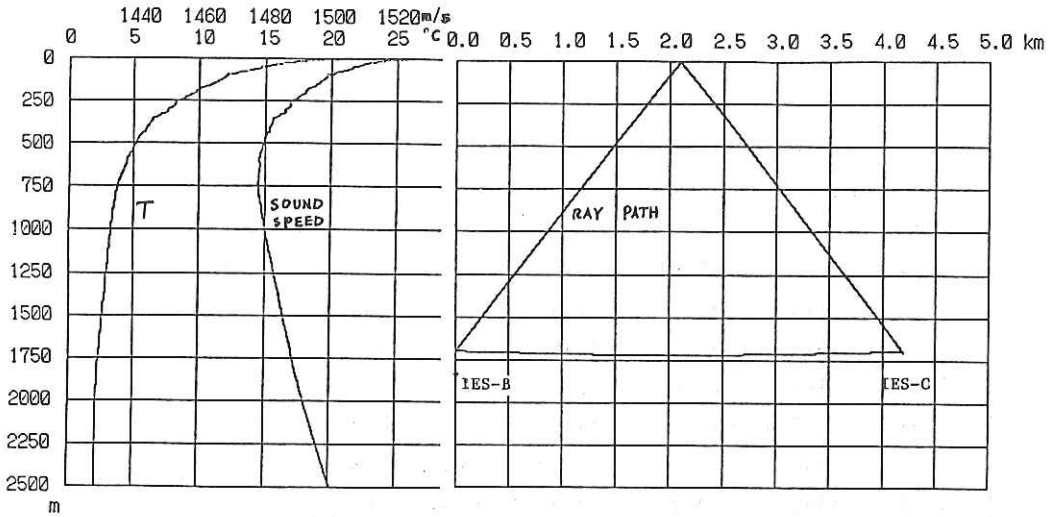

Fig.4.12.2 Ray paths from IES-B to IES-C

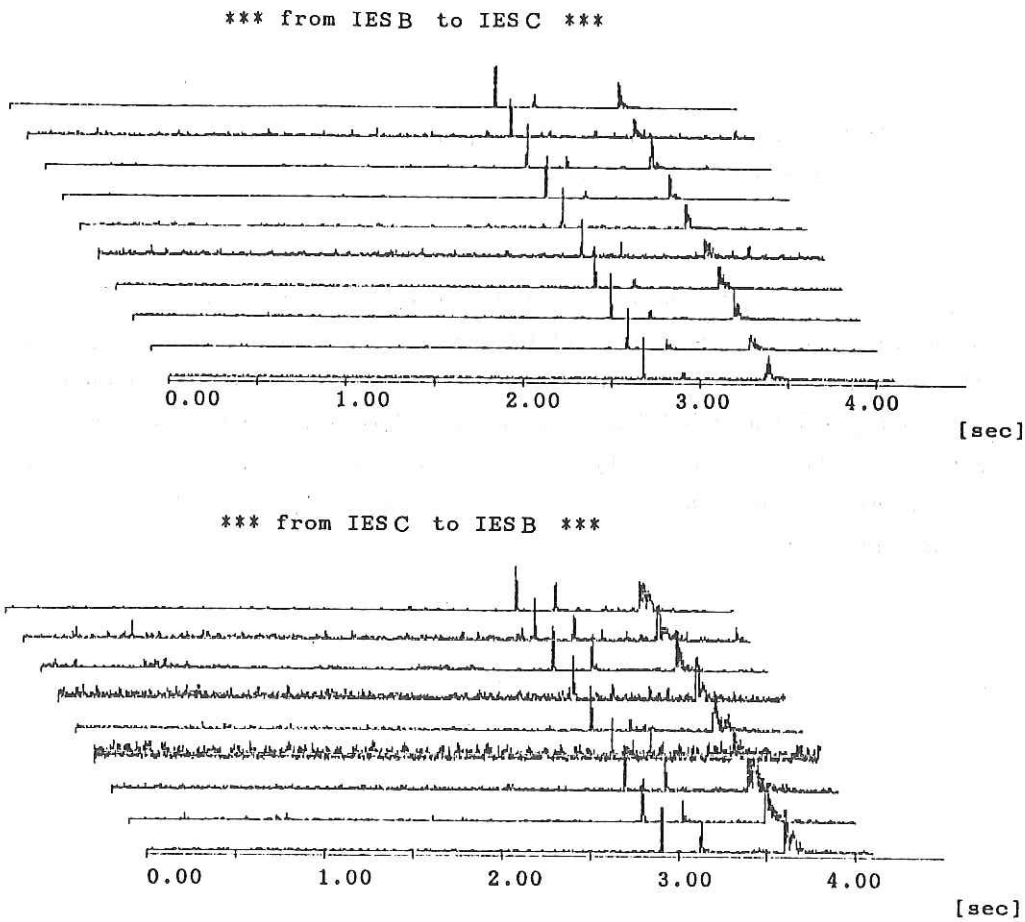

Fig.4.12.3 Soundwave forms propagated between IES-B and IES-C

B→C(msec)		δ t1	C→B(msec)		δ t2	δ t1-δ t2
2731.0	3429.0	698.0	2869.5	3567.0	697.5	0.5
2714.5	3413.0	698.5	2880.0	3576.5	696.5	2.0
2715.0	3413.5	698.5	2897.0	3594.0	697.0	1.5
2724.5	3422.5	698.0	2915.5	3611.5	696.0	2.0
2697.5	3397.0	699.5	2893.5	3592.5	699.0	0.5
2687.5	3386.5	699.0	2892.5	3592.5	700.0	-1.0
2684.0	3383.5	699.5	2900.5	3599.0	698.5	1.0
					mean value	0.93

Table 4.12.1 Sound propagation time and reciprocal time difference between IES-B and IES-C.

Fig. 4.12.4 shows currents measured by Aanderaa current meters which are moored at the same position as IES-B(top) and IES-C(bottom). Currents vary as the time proceeds. The magnitude of them are between -10 and +10 cm/sec. The mean value of currents at IES-B is larger than at IES-C. The direction of it is almost right to the line connected from IES-B to IES-C. The mean value of the current in the direction along IES-B to IES-C is 0 cm/sec. This shows that the average current of the layer between surface and depth of 1700 m is 25 cm/sec.

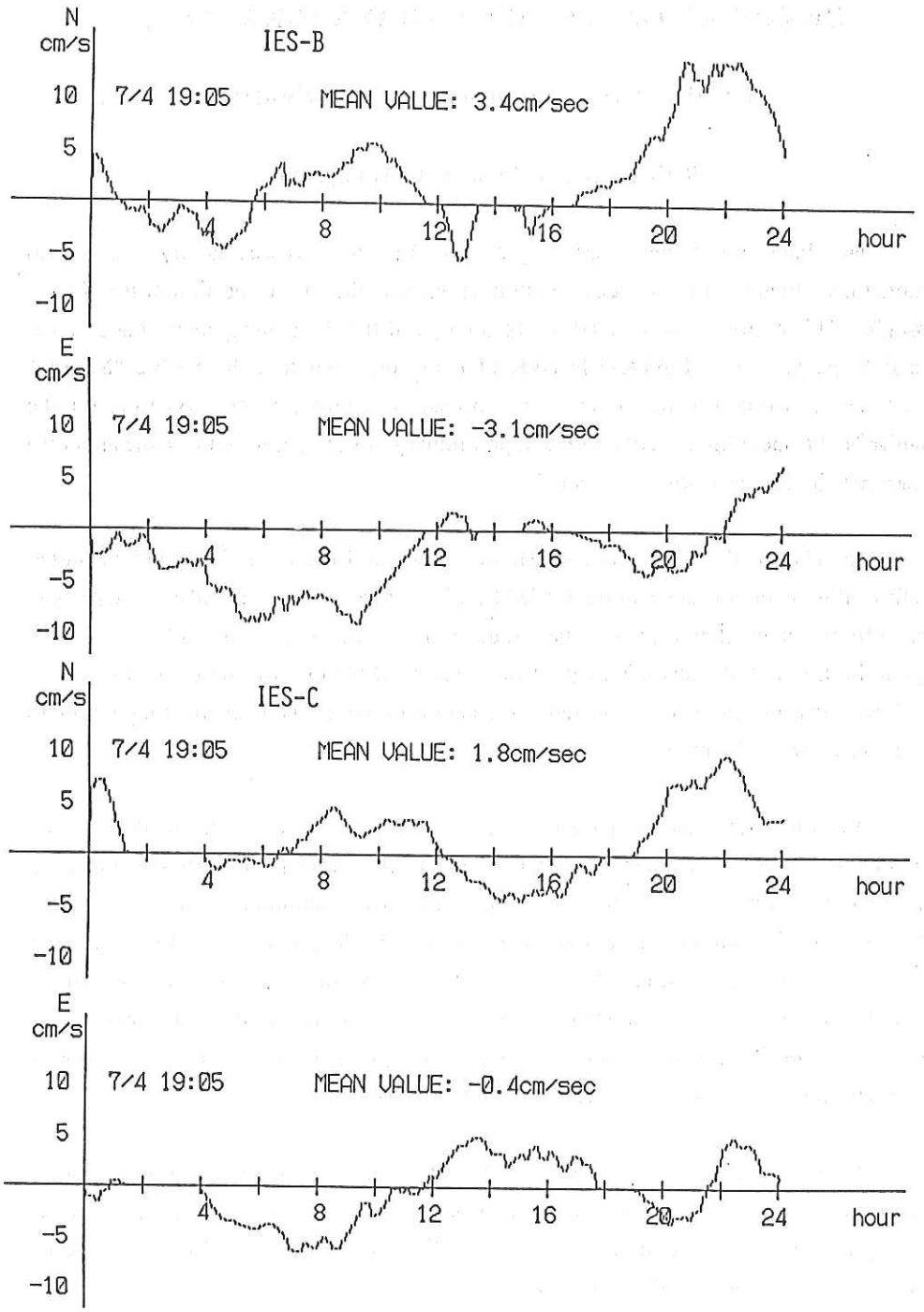

Fig.4.12.4 Currents measured by Aanderaa current meters at the depth of 1700 m.

5. DEEP-TOWED TV AND SIDE-SCANNING SONAR OBSERVATION AT THE KAIKO-NANKAI SITES

5.1 Principal purposes of investigation

K.Kobayashi, Y. Monma and H.Fujimoto

The later half of this cruise (Leg 2: July 4 to July 13) was mostly devoted to detailed investigation of the ocean bottom features in the eastern portion of the Nankai Trough. This region is nominated to be a target of the French-Japanese cooperative research project, the **KAIKO-NANKAI** using the French submersible "Nautile" which was scheduled to be executed in August-September, 1989. As time for the Nautile/Nadir operation is very restricted, preliminary investigation of the same area by a Japanese ship has been strongly desired.

The Nankai Trough was already surveyed by Jean Charcot in 1984 and by Nautile/ Nadir in 1985 under the aegis of the KAIKO Project. A set of precise Seabeam maps were drawn by the Jean Charcot, while the Nautile had 8 dives in Tenryu Canyon-Zenisu region in the central Nankai Trough. Communities of bottom dwelling animals such as bivalves *Calyptogena* were discovered at the landward toe of the Nankai Trough close to the Tenryu Canyon junction.

As cold deep-water seepage in the accretionary prism which feeds the bivalves was decided to be the principal subject of the forthcoming Nautile dives, the most important task of our pre-site survey is to locate fair-sized communities of animals in the target region. The bottom transponder network used for the previous KAIKO dives was retrieved so that relocation of the same bivalve communities was supposed to be difficult. Furthermore, the KAIKO Steering Committee recommended to investigate sites east of the Tenryu junction from viewpoint of apparently more intense accretion in the eastern portion which was not surveyed by the Jean Charcot.

A Seabeam map of the target area with 1/50,000 scale prepared by their Survey Ship Takuyo was offered for our use by the Hydrographic Department, Maritime Safety Agency of Japan. We combined it with the KAIKO maps and pointed out several candidate sites in a wide region between 137°30'E and 138°10'E.

More than 15 multichannel seismic reflection profiles in this region were obtained by this time by the R.V.Tansei Maru and a chartered ship Kaiko Maru V of Tokai

Offshore Corporation. Data was processed by Kuramoto and others to reveal tectonic features of the subduction and accretion. Several high-angle faults seen in the profiles indicate possible occurrence of deep-water seepage to the bottom surface on the accretionary prism. However, pin-pointing of the seafloor oasis needs more detailed survey.

Joint effort has been proposed by the Japan Marine Science and Technology Center (JAMSTEC) and the Ocean Research Institute (ORI), University of Tokyo to precisely investigate this region using a deep-towed TV and side-scanning sonar owned by JAMSTEC and facilities of the newly built R. V. Hakuho Maru of ORI.

A cable winch and two removable container laboratories with deep-towed TV and sonar sensors were loaded onboard the R. V. Hakuho Maru on the 30th of June, 1989 at the new pier of Yokosuka wharf. Steel bases were specially prepared to fit their winch and containers on the aft deck of Hakuho Maru. High-pressure oil power and electricity were supplied from Hakuho Maru. The cable was cast into the sea through a flexible reel equipped on the swing-type stern gantry. Set and retrieval of the instruments were easily operated by the gantry.

An SSBL transponder was attached to the deep-towed instrument to fix its positions relative to the ship while it was slowly towed. The ship's transducer array was set 2 m down from the bottom hull to transmit and receive the signals. The ship's positions were fixed by Loran C, as the Loran C network in this region is sufficiently good to continuously locate ship's positions whereas the GPS was only received for about three hours per day. The same Loran C receiver was installed with the Nadir during the KAIKO-NANKAI dives to reproduce positions in the same coordinates.

The color TV images taken by the deep-towed camera were simultaneously reproduced in No. 3 laboratory on the upper deck and also in the chart room of the Hakuho Maru in addition to direct observation and operation in a container to facilitate observation by a number of scientists onboard. Three French scientists participating in this Leg of the cruise were also attending observation and description.

The deep-towing operation was made in daytime and the ship surveyed the same area by Seabeam at night. The region covered by the Hydrographic Department map was completely reproduced to confirm ability of our new instrument and further extend our survey to the surrounding areas. In particular the original HD map is drawn in

coordinates of the Tokyo Datum, whereas the Nadir/Nautile cruise is based upon WGS on which our survey on the Hakuho Maru was also relied.

The ship's high maneuverability helped to tow the TV camera and sonar along the lines we planned. The speed of the ship was controlled carefully to suit the best observation of the bottom with high efficiency. While the ocean current was strong, the ship's heading was far different from the observation direction desired and actually taken. Continues monitoring of the positions of the ship and towed device provided sufficient control of the lines of observation.

The winch was operated by the ship's crew under the initial instruction of the JAMSTEC specialists. We are grateful to great cooperation of the ship's officers and crew for both maneuvering the ship and the winch operation.

5.2. Brief description of instruments

5.2.1 JAMSTEC / Deep Tow Camera

Y. Monma

The JAMSTEC / Deep Tow system comprises (1) towed sled equipped with underwater instrument such as camera and sonar, (2) onboard units of underwater equipments in container vans, (3) launch / recovery and on board gears such as A-frame, Gimbal Sheave, winch, hydraulic unit and tow cable, (4) acoustic navigation system for precise underwater positioning , and (5) a support ship which is equipped with basic scientific instruments such as echo sounder or Sea Beam. The maximum depth capability of the system is 6,000 or 4,000 meters depending on the cable length. In the KH-89-1 cruise, 4,500-meter cable and winch system were equipped on board "Hakuho Maru".

The JAMSTEC / Deep Tow camera allows both real time observations, measurements and sampling in the deep sea environment. The camera is towed at speeds of 0.5 to 1 knots and 3 to 4 meters above the sea floor. Specifications of the equipments on the deep Tow camera are listed in Table 5.2.1.

5.2.2 JAMSTEC / Deep Tow Sonar

The JAMSTEC / Deep Tow sonar comprises a 70 kHz side scan sonar, a 4.8 kHz sub-bottom profiler and a depth sensor. The underwater units are equipped in an open frame, 1.2 m ^{W} x 3.0 ^{L} x 1.4 ^{H} m in size and weighs 1.0t in air and 0.8t in water. The sonar data are displayed on a graphic recorder and stored in an anolog data recorder for post processing. Maximum swath width of the side scan sonar is 1,000 m per side, and maximum penetration of the sub-bottom profiler is 50 meters below the sea floor depending on the sea bed characteristics. Nominal towing speeds are 1.5 to 2 knots and towed between 100 and 120 meters above the sea floor. Specifications of the sonar components are listed in table 5.2.2.

Table 5.2.1 Specifications of JAMSTEC / Deep Tow Camera

Components	Specifications	Notes
Color TV	Panasonic WV-F50AH (3-1"CCD video camera) Horizontal resolution:620 lines Minimum luminous intensity : 21 lux Lens focus : 6.5mm Illumination : 250W hallogen lamp x 3(or4) Maximum depth : 7,000m(camera) 6,000m(light)	
Black and White TV	SONY XC-77 (Single 2/3"CCD video camera) Horizontal resolution:600 lines Minimum luminous intensity :0.5 lux Lens focus :16mm Illumination :250W hallogen lamp x 1 Maximum depth : 4,000m(camera) : 6,000m(light)	B/W and color TV are switched alternatively.
Still Camera	Benthos model 372A standard camera x 2 Benthos model 382 flash x 2 Number of exposures : 800 with 100 ft film Illumination : 100W x 2 Maximum depth : 10,000m	Shutters are remotely actuated by command signal from on board unit via coaxial tow cable.
CTD	Tsurumi Seiki (TSK) Model TS-CTD-M1 C(Conductivity): resolution 0.01 mmho/cm accuracy ±0.05 mmho/cm T(Temperature): resolution 0.01°C accuracy ±0.025°C D(Depth) : resolution 0.1%FS accuracy ±0.25% Maximum depth : 6,300m	CTD data are displayed on TV monitors and stored in 5" floppy disk.
Altitude Sonar	Frequency : 120 kHz Range : 0.3~30m Resolution : 2.5cm Accuracy : ± 5cm	Altitude data are displayed on TV monitors and stored in 3.5" floppy disk.
Precision Memory Thermometer	Rigosha Model RMT-DS Range : 0~20°C or 0~10°C Resolution : 0.002°C or 0.001°C Accuracy : ±0.005°C~±0.0025°C Sampling interval : 6 sec Maximum data storage: 16,000 Maximum depth : 6,000m	
Box Dredge	Size : 360^{W} x 140^{H} x 500^{L} mm	Dropped by remotely actuated release, or put underneath TV camera.

Table 5.2.2 Specification of JAMSTEC / Deep Tow Sonar

Components	Specifications	Notes
Side Scan Sonar	NEC Model NE-157 Side Scan Sonar Frequency : 70kHz Pulse width : 0.3~1.0 ms Transmit level : 122dBrms(0dB=1 μbar at 1m) Directivity : 1° (horizontal) Maximum range : 1000m for each side	Data display : • 162mm x 2ch(SSS) • 117mm x 1ch (SBP) Data storage : • 7ch analog data recorder with extra audio input. • 1/2" open reel tape
Sub Bottom Profiler	NEC Model NE-157 Sub Bottom Profiler Frequency : 4.8kHz Pulse width : 0.2~1.0 ms Transmit level : 103dBrms(0dB=1 μbar at 1m) Directivity : 45° conical Maximum penetration : 50m(depends on sea floor characteristics)	
Pressure Sensor	Teledyne Taber Model 2403 Maximum range : 3500 kg/cm^2 Resolution : 0.1%FS Accuracy : ±0.25%	

5.2.3 Deck Arrangement of the Apparatus

M. Watanabe

This section presents the deck arrangement of the on board components of the deep towed TV camera and side scan sonar system.

The on board configuration consists of two containers, a cable winch, a control valve unit, two attachment bases, and two attachment plates (Fig. 5.2.3.1 ~ 6). These apparatuses were installed on the rear deck of the R/V Hakuho-Maru so that the operation of the deep towed system could be conducted easily. Fig. 5.2.3.7 shows the deck arrangement of the system.

The attachment bases and plates were used to mount the containers, the cable winch, and control valve unit on the deck.

The bases and plates were attached on deck-holes using M20-bolt. The containers were fixed on the respective bases with the attachment junctions. The cable winch and the control valve unit were fixed on the plates by welding. This system is shown in Fig. 5.2.3.8. The attachment bases and plates were made by TOKAI FRUEHARF Co. Ltd.

High pressure oil hose for connect with the oil pressure supply was renewed by TSURUMI Co. Ltd., because the type of the couplers were changed from one of R/ V KAIYO, and length of the hoses were not enough to connect between the oil supply and the control valve unit.

Electric power supply, AC100V and AC220V, into the containers were installed from the electric box in front of exit of No.7 laboratory on deck.

Signal lines, data of LAN and trucking data for transponder navigation, were installed from the signal box in No.3 laboratory.

Interphone and speaker were installed to communicate with each laboratory or container.

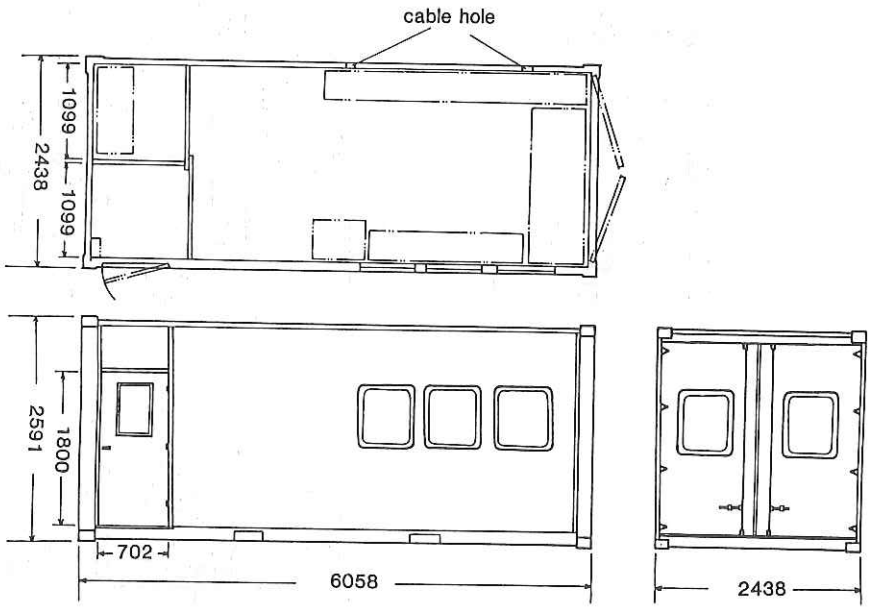

Fig. 5.2.3.1 Plan of container for operating TV camera system.

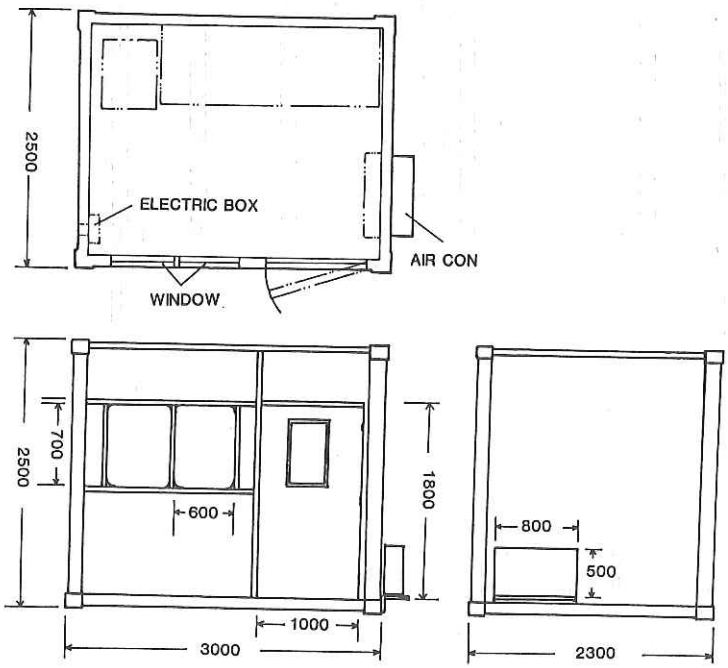

Fig. 5.2.3.2 Plan of container for operating side scan sonar system.

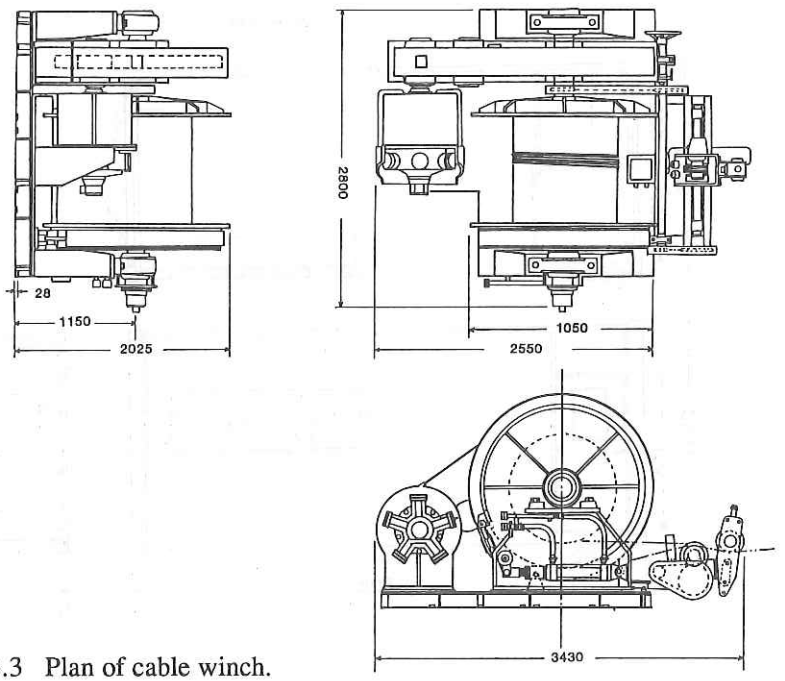

Fig. 5.2.3.3 Plan of cable winch.

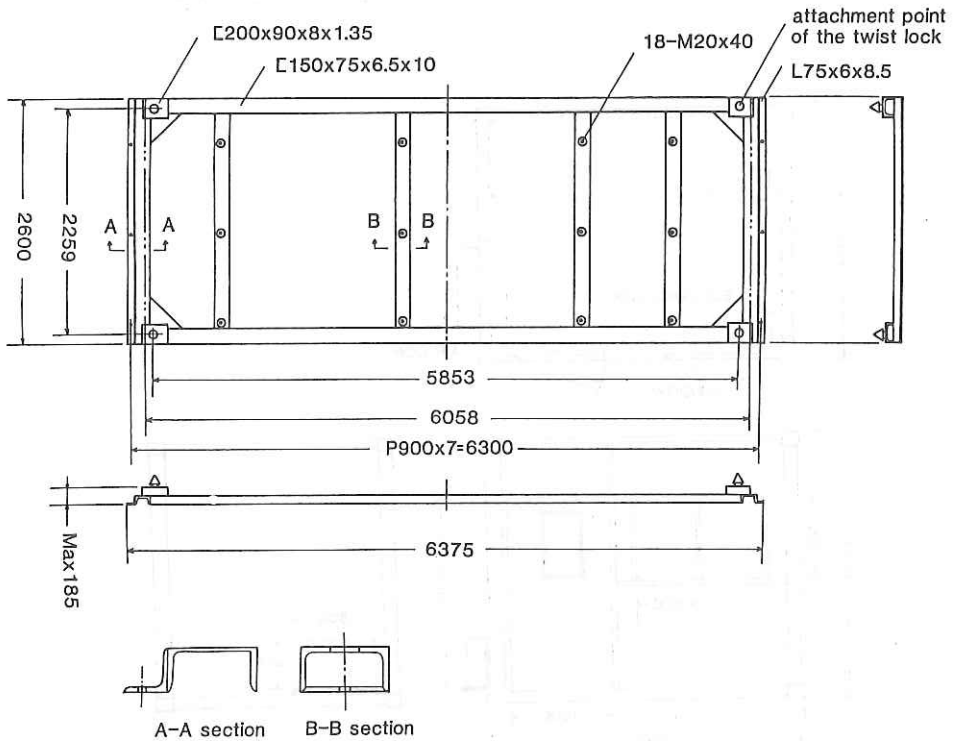

Fig. 5.2.3.4 Plan of attachment base for the container to operate TV camera system.

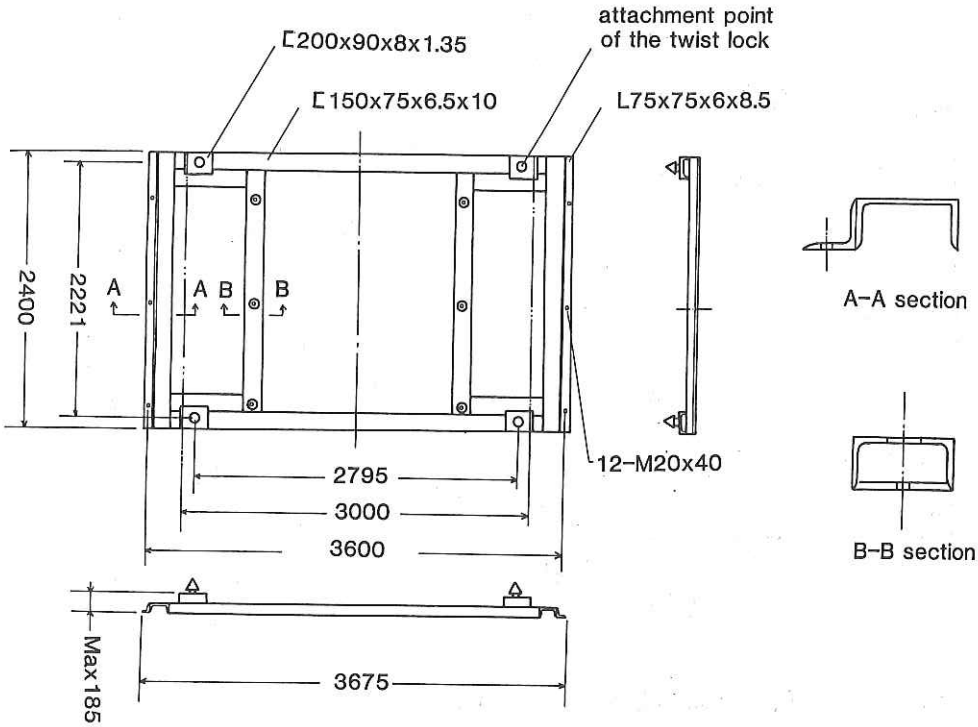

Fig. 5.2.3.5 Plan of attachment base for the container to operate side scan sonar system.

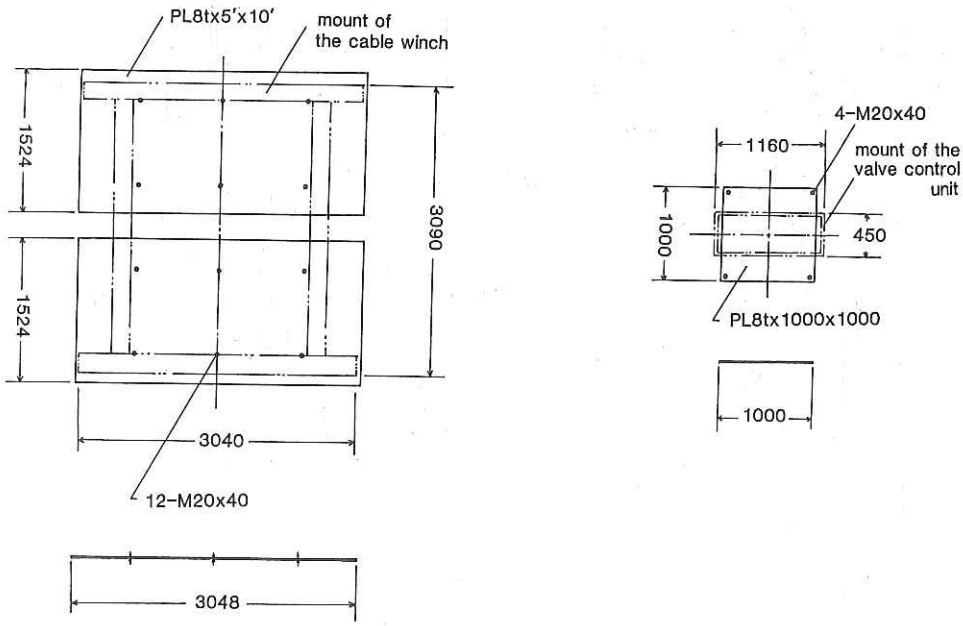

Fig. 5.2.3.6 Plan of attachment plate for cable winch (left) and control valve unit (right).

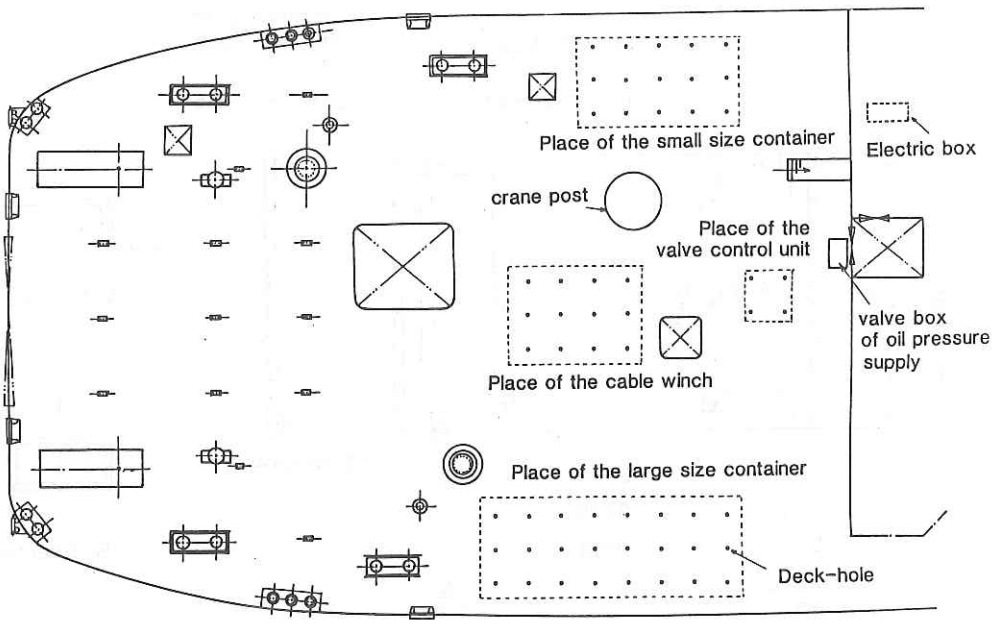

Fig. 5.2.3.7 Rear deck of R/V Hakuho-Maru.

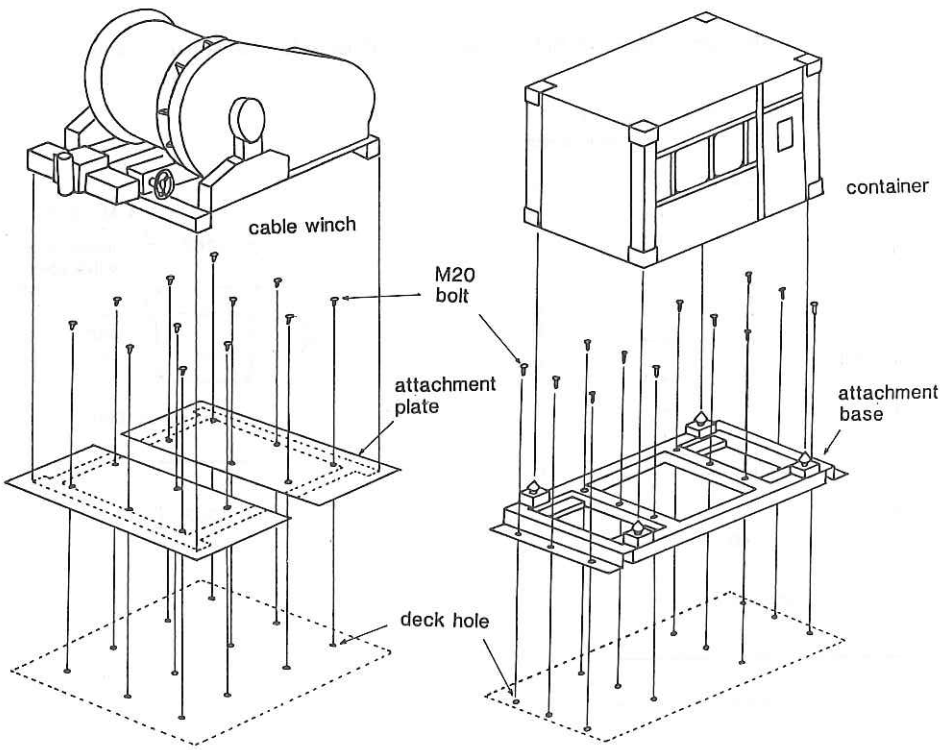

Fig. 5.2.3.8 Block-diagram of setting the cable winch (left) and the container (right).

5.2.4 Position fixing for deep-towed survey

T. Furuta, M. Nakanishi, H. Toh, A. Oshida and H. Fujimoto

Deep-towed surveys in the Kaiko-Nankai sites were carried out based on navigation by Loran-C of WDS-84. Navigation and data logging system of the Hakuho Maru, Magnavox Series 5000, gave "system position" every 1 second by the Kalman filtering of several navigation data given by GPS, NNSS, Loran-C, gyrocompass, Doppler log, electro-magnetic log, etc. Repeatability in real time positioning is most important for navigation during deep-towed surveys and site surveys, Loran-C was selected to be the main navigation data; GPS was received several hours a day and was not reliable. Following the deep-towed surveys Kaiko-Nankai diving surveys were carried out on board a French submersible "Nautile" based on the same Loran-C navigation.

Underwater positioning of the deep-towed system was carried out by use of a super-short baseline (SSBL) acoustic transponder system of the Hakuho Maru. As is illustrated in section 4.10, a transponder was installed onto the JAMSTEC deep-towed system, and its position relative to the ship was determined by the SSBL system with no transponder on the sea floor. When the SSBL system is operated, positioning data of the ship and the deep-towed vehicle obtained at each interrogation sequence are displayed in both the chart room and No. 3 laboratory. During the deep-towed survey in this cruise, the data were also displayed in the container laboratory for the deep-towed camera system in order to control the deep-towed cable winch. Sea Beam system and 3.5 kHz sub-bottom profiler were operated simultaneously with the SSBL system; the mutual interference was not serious.

5.3 Brief Description of Observation

5.3.1 Tracks of Observation and Brief Description of Each Line

Location of the surveyed area is shown in Fig. 5.3.1, and tracks of deep-towed observation are shown in Figs. 5.3.2 ~ 5.3.4. Brief description of each line is given below by the respective scientists who described the time log.

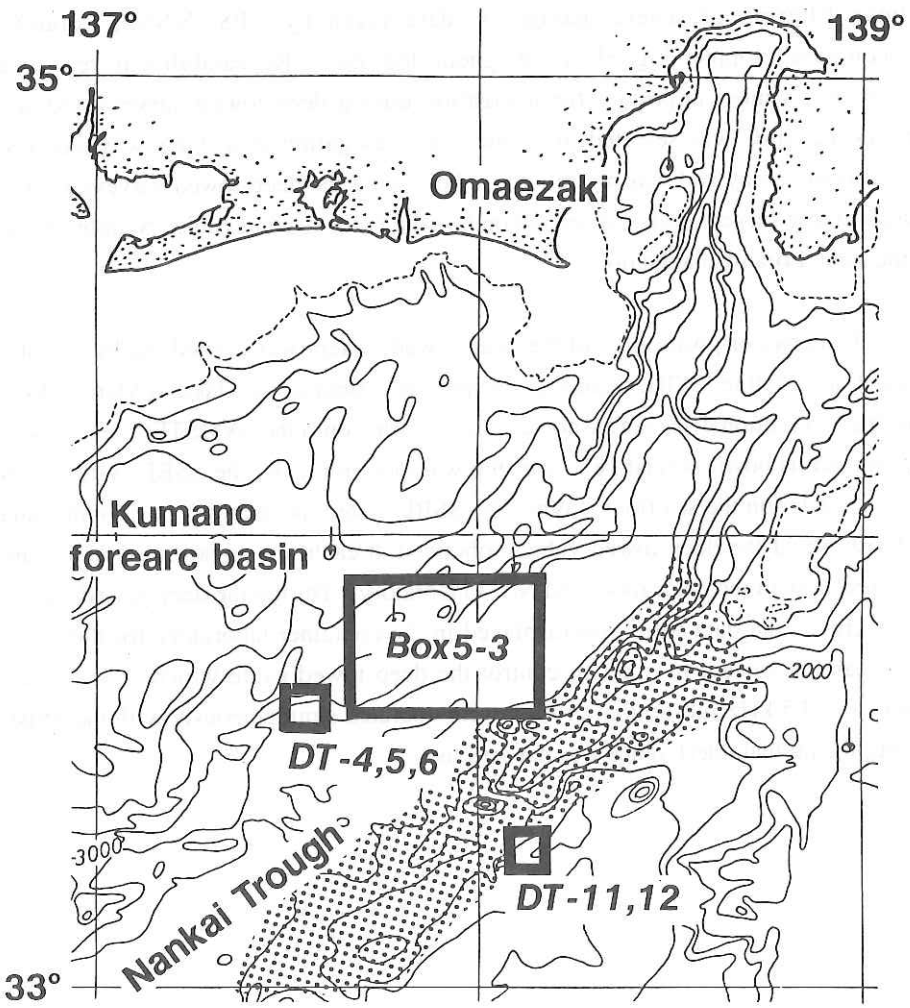

Figure 5.3.1 General location map of deep-tow survey. Dotted area is Zenisu Ridge. Box5-3 is sited on the front of accretionary prism, and DT-4,5,6 is located on the mouth of the Tenryu Canyon. DT-11,12 run across the mud volcano.

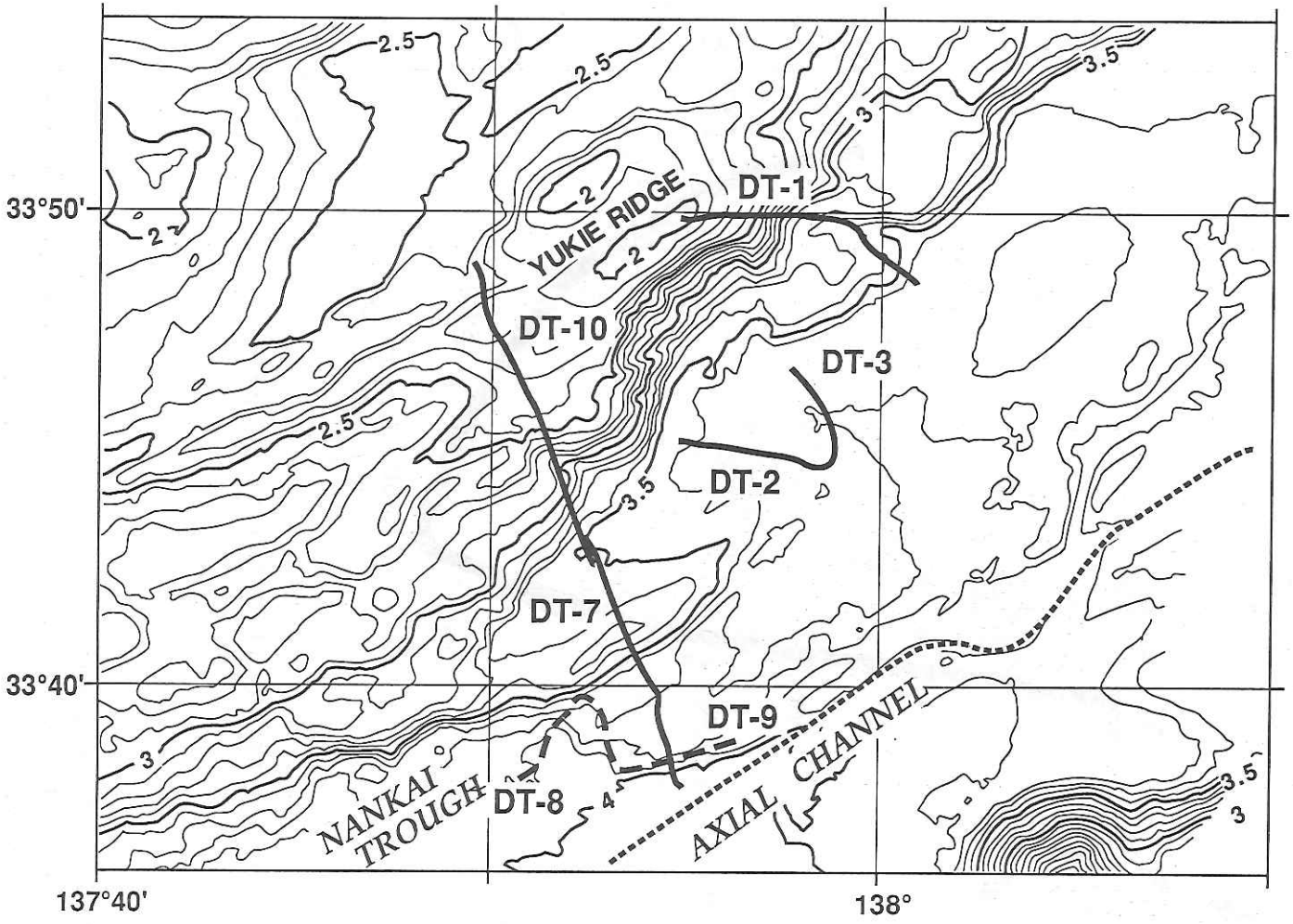

Figure 5.3.2 Bathymetry and location of DT-1, DT-2, DT-3, DT-7, DT-8, DT-9 and DT-10.

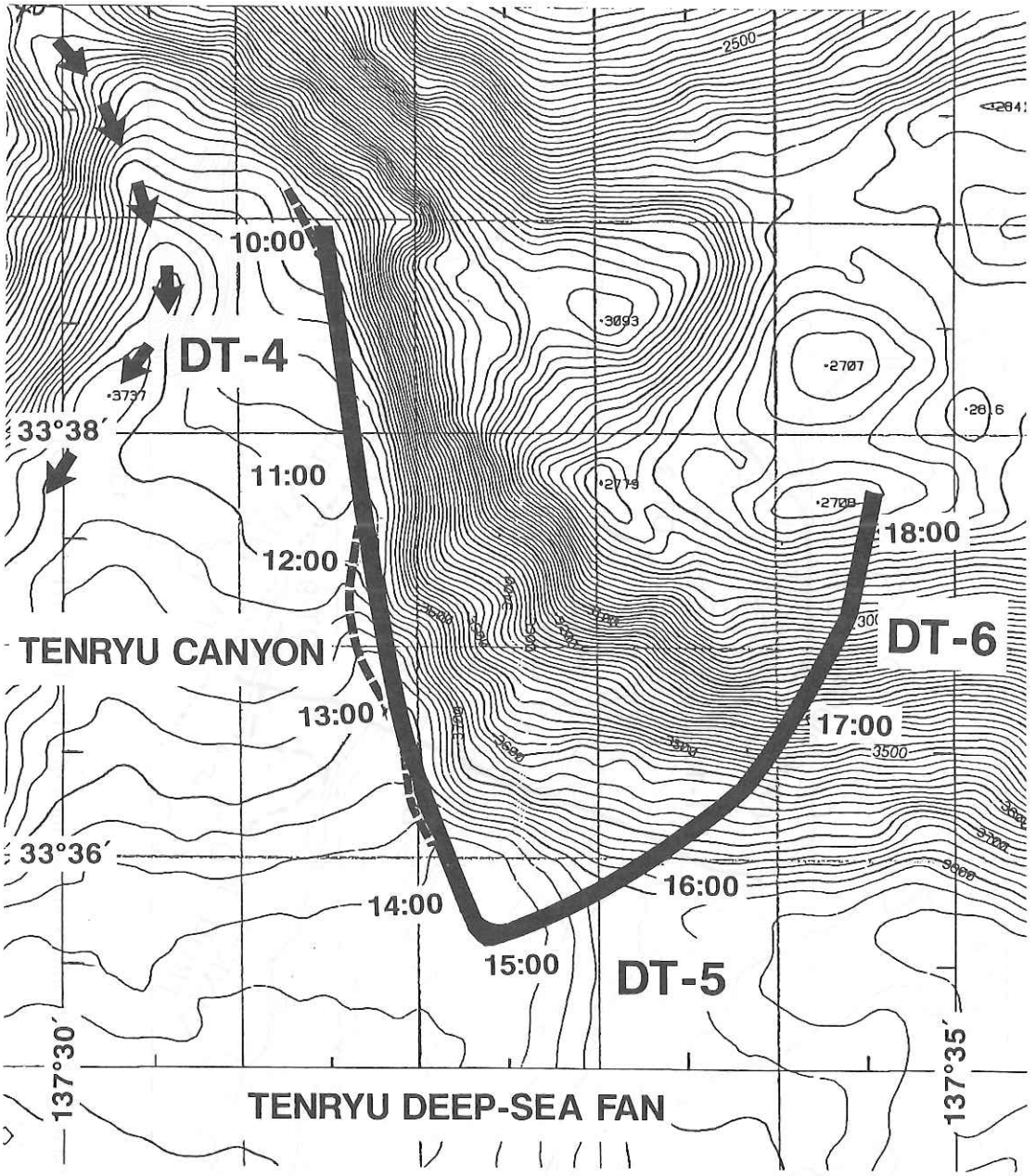

Figure 5.3.3 Bathymetry and locations of DT-4, DT-5 and DT-6. The active, erosional (?) channel in the Tenryu Canyon is indicated by the arrow stream. Broken line shows the inactive channel in the Tenryu Canyon. The Calyptogena colony have been discovered in the inactive channel (DT-4).

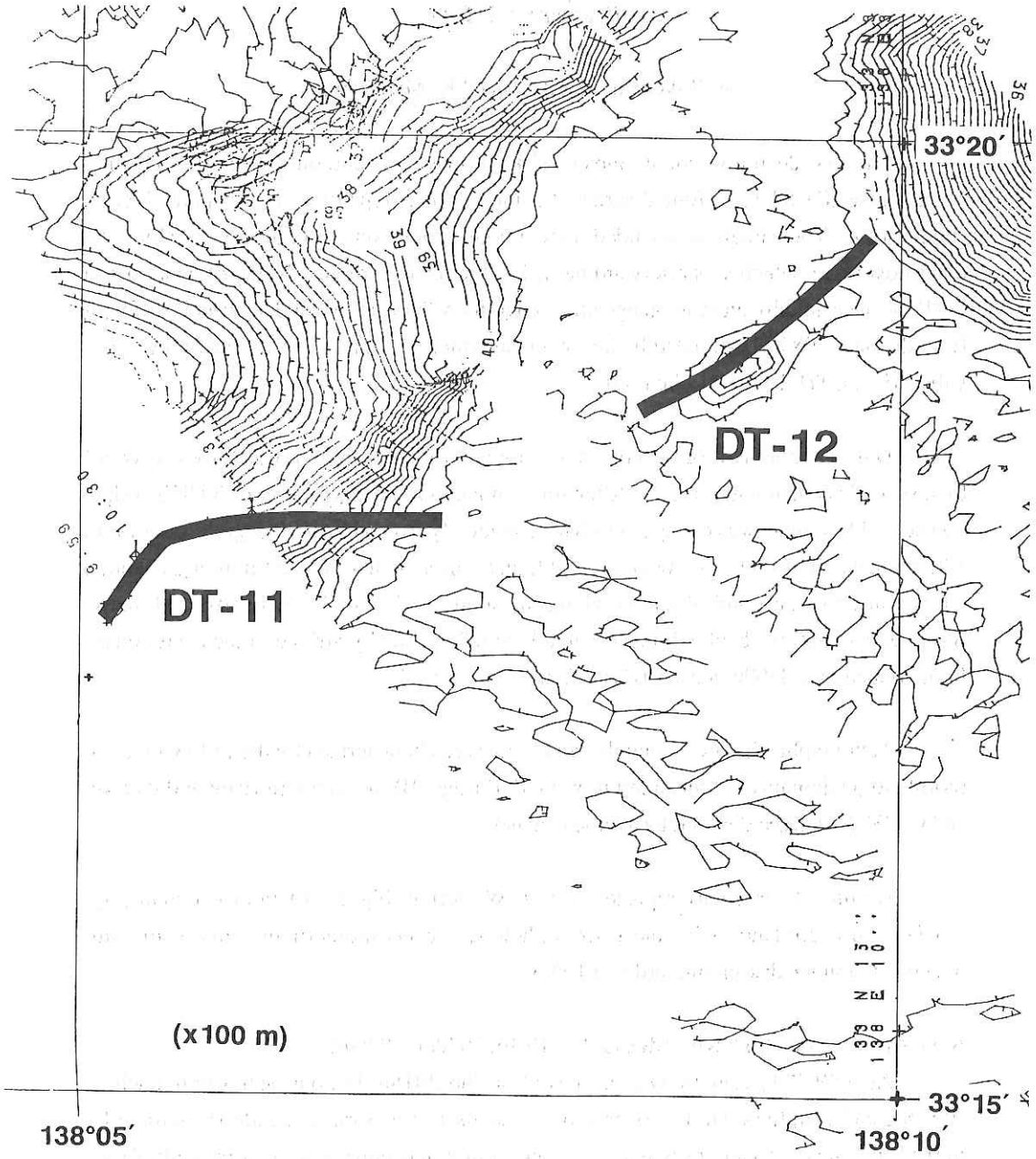

Figure 5.3.4 Bathymetry and locations of DT-11 and DT-12.

Line 1 : South of Omaezaki (July 5)
(Camera : DT-1)

A. Takeuchi, M. Okada and K. Mitsuzawa

The first deep tow line by means of TV Camera system, during the R/V Hakuho Maru cruise KH-89-1, perfomed across the inner trench slope of eastern Nankai Trough (Fig. 5.3.5). The camera was landed upon a point around one of highest peak along the outermost ridge, which was afterward named as the YUKIE ridge. Value of water depth (2018m) measured by pressure gauge attached to the vehicle at the landed point is different from the one (1980m) estimated by Seabeam bathymetry. Herein, the former bathymetric values (i.e., CTD depth) will be used.

During earlier half of the course of survey, the camera system was towed eastward by a speed less than half a knot. After surveying down the steep flank of YUKIE ridge, course of TV vehicle was changed clockwise gradually from almost 90 degrees of north to 130 degrees. Then the camera crossed obliquely through an east-west trending channel, which cut down an uplifted terrace along the southern foot of YUKIE ridge. Finally, traversed its southern bank with a very gentle relief and finally arrived in the accretionary basin topped by a 3500m terrace (Enshu Deep-sea Terrace).

Topographic features along the survey line are characterized by the following three morphologic domains; A) the summit of YUKIE ridge, B) the southern flank and its foot, and C) 3300m terrace disected by a large channel.

Results of survey are represented in E-W section (Fig. 5.3.6) and route map (Fig. 5.3.7). In accordance with the geomorphology, observations of the survey line are documented in the descending order as follows.

A-1) Apex region of YUKIE ridge (9:49~ 10:16, 2020m~2078m)

At 9:49 JST, camera system arrived on the 2018m bottom near summit where siltstone and conglomerate layers crop out. Landscape was rather gentle in gradient by rugged in a sclae of camera window. Pockets or small tunnels were commonly found even on the flat surface of outcrop. Metric blocks and smaller rubble were also common. Within follows on the floor and gaps among larger blocks, dead shells of *calyptogena* were often observed.

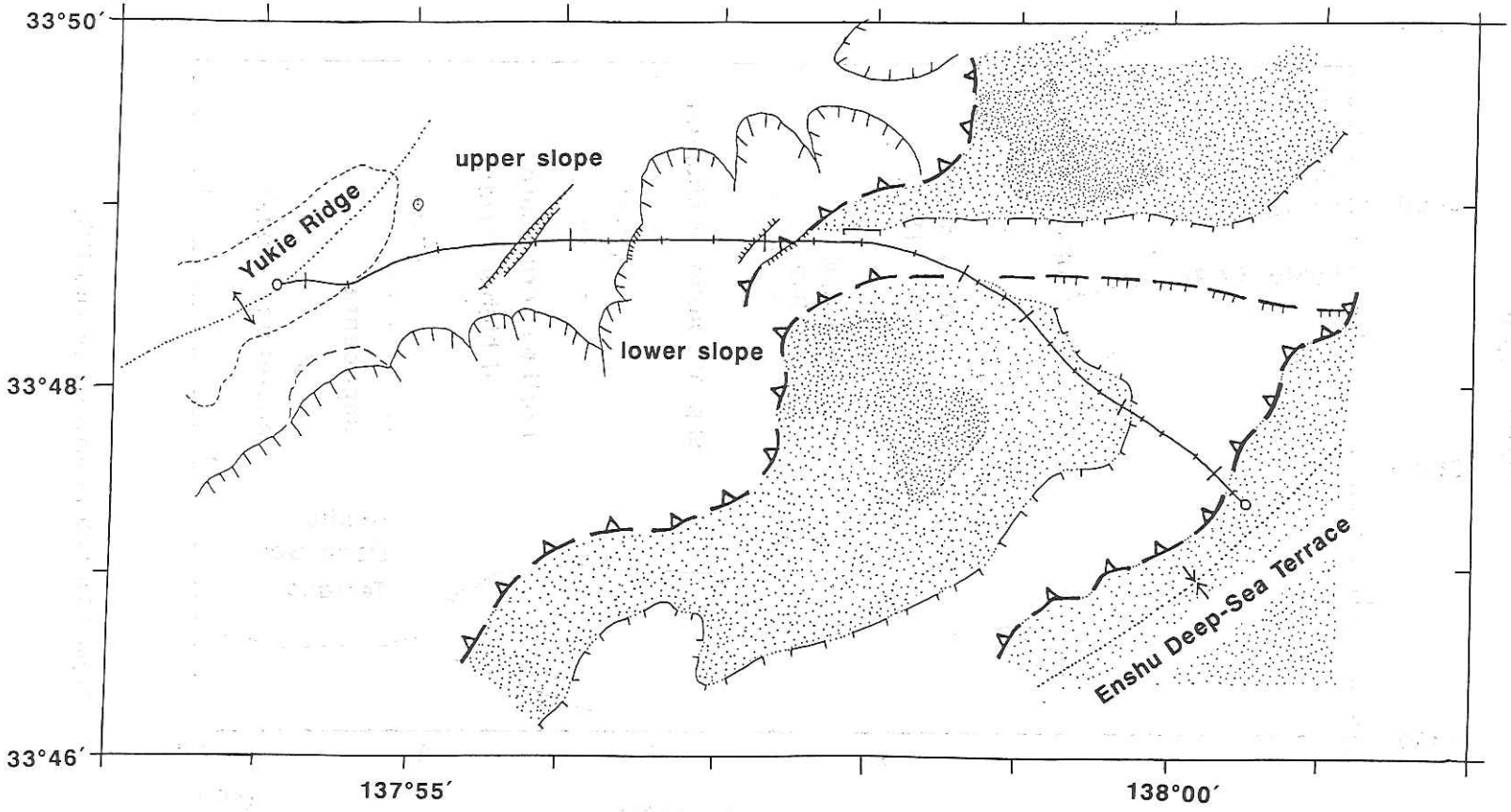

Figure 5.3.5 Structural Map.

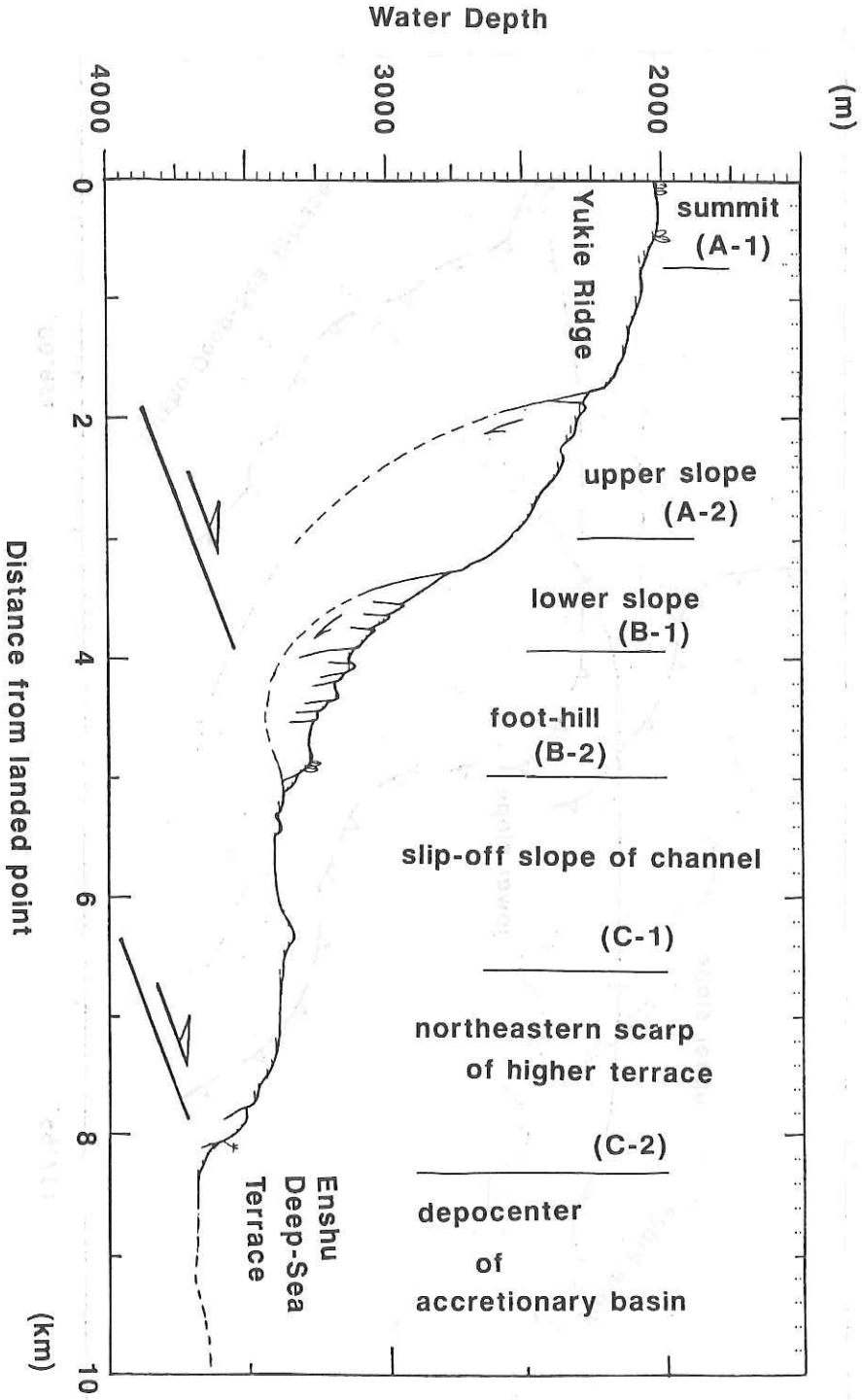

Figure 5.3.6 E-W section of surveyed line DT-1.

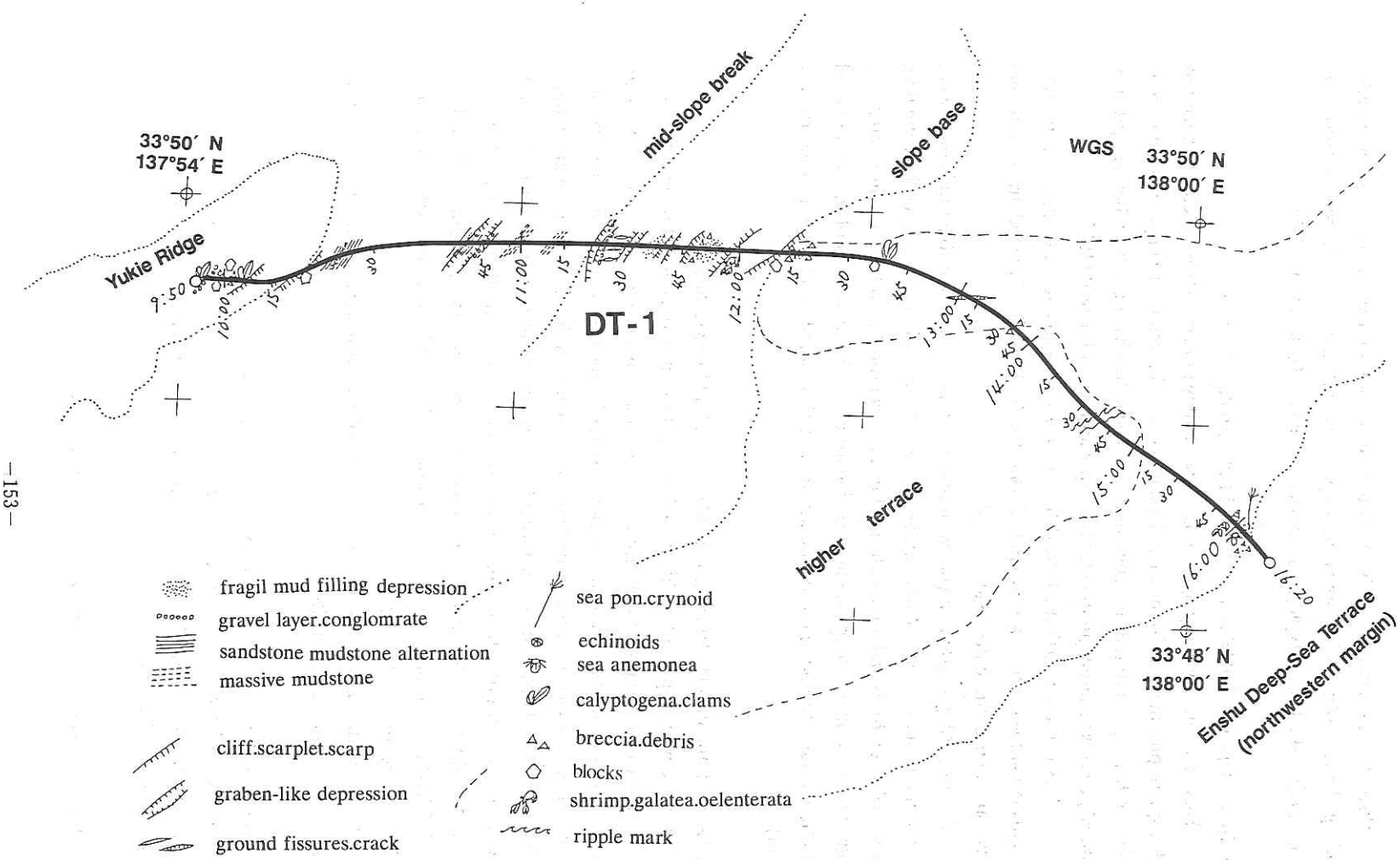

Figure 5.3.7 Plane view of DT-1.

Pockets and tunnels can be attributed to dissolution of concretions or nodules including shells. With going down the slope, steep cliff and debris were observed more oftern. Living shells of calyptogena was discovered at 2050m (10:07'40").

A-2) Upper slope of YUKIE ridge (10:16~11:20, 2078m~2542m)

This domain, especially uppermost slope shallower than 2150m, is characterized by rough topography marked by blocks of metric sized, irregular in shape, with the same dissolution features as in the sub-domain A-2. These blocks could be called as "pseudo-chimnies", because a slight jump in CTD temperature was observed (10"22').

A fresh graben striking NNE-SSW with steep walls several meters high was distinguished at the central part (around 2280m, 10:40'~10:48"). Layered gravel and mud alternation cropped out in the southern wall.

As for geology, gravel layers with pale grey matrix and massive mudstones were often observed in the area. Although attitude of strata could not easily be investigated, existence of steep folds and other deformed features is probable in the uppermost area. In the other area, no more steep dipping was identified. The sequences of gravel and mud alternation would be underlain apparently by a dark colored layer of mudstone (below 2335m).

B-1) Lower flank of YUKIE ridge (11"20'~11:55', 2542m~3129m)

Gradient of slope within this domain is the largest in the entire line **DT-1**. Steep cliffs with eastward dipping are more common than in the upper domains, although geologic observation of outcrops was rather difficult for the downgoing camera because of large steepness. As a few cases, gravel layers are visible in the crests of high angle faults (11:27'~11:29'). Those cliffs are possibly gravitational in origin because they were followed by smaller cliffs facing backward (or landward). Another remarkable graden with muddy floor was located at the knick point between the domains B-1 and B-2 (11:51'~12:00'). Ground fissures or tension gashes with an E-W strike were often identified (typically at 11:24'~11:26').

Most small cliffs in the lower part were observed to face landward and bottom geology became muddy gradually.

B-2) Foot-hill of outermost ridge (11:55'~12:39', 3129m~3382m)

Many *coelenterata* were found at the foot of landward facing scarp of small ridge. Then camera met muddy flat hill, at whose edge a cluster of dead shells of *calyptogena* and other clams were observed.

C-1) Channel cutting the 3300m terrace (12:39'~15:30', 3382m~3487m)

The survey course is divided into two parts at 15:00' point: a canyon and its southern wall (ie. slip-off slope) and terrace scarp proper (ie. fault scarp) facing southeastward.

At the axis of disecting channel, a crack with an E-W trend 5-10 cm in width was found (13:15). This crack could be related to a probable fault along the canyon, which had displaced the both sides of terraces.

Surveyed bottom was quite smooth and ripple marks were common on it, but no living shell nor outcrop was observed.

C-2) Northern margin of accretionary basin (15:30'~16:34', 3487m~3689m)

Towards the terrace scarp of 300m high relatively, living activity such as burrows became more and more evident. After 15:49' as black colored (Mn-coated) gravels and blocks came into view, living things on the lower scarp increased in number. The 3300m terrace mentioned above had been uplifted and tilted by thrusting along the northwestern margin of accretionary basin topped by ENSHU Deep-sea Basin.

Finally at 16:34, the camera work was ended at the 3678m bottom, where flat, muddy floor of landward margin of the accretionary basin.

On the basis of outlined geomorphology and brief description of camera observation, the following points are summarized:

The morphologic features of landscape here are classified into three domains:

A) Summit region of the outermost ridge, YUKIE ridge, or continental slope break: Outcrops and blocks of sandstone, mudstone and conglomerate are abundant.. Cemented material with irregularly shaped pockets and tunnels due to dissolution are often observed. Animal communities composed of tube warms and calyptogenas were found in gashes and gullies among rugged relieves.

B) Inner trench slope along Nankai Trough (south folank of YUKIE ridge): Slightly less abundant blocks but more outcrops than on the summit were visible. Because of the convex outline with fresh landslides, thrust faulting beneath the Ridge is possible along base line of the slope.

C) Landward margin of accretionary basin(ENSHU Deep-sea Terrace): Underthrusting along the northwestern margin of accretionary basin, SHIMIZU Thrust, may result in relative deepening of basin and could explain;

1) uplifting and disecting of higher terrace on the hanging wall,
2) downcutting channel along an oblique fault which cuts the hanging wall,
3) landward tilting of ENSHU Deep-sea Terrace, and
4) landward shifting of depo-centers on accretionary basin.

Line 2 : Across mud mound in the Nankai Trough (July 6) (Camera : DT-2 and DT-3)

J. Ashi ,T. Koizumi and J. Naka

Two mud mounds could be recognized in the Izanagi side looking sonar image during the site survey of the KAIKO-NANKAI Project. They occur within the accretionary prism between the steep slope which continues westward to the mouth of Tenryu canyon, and the deformation front. The side looking image shows that the landward mound is conical in shape and the seaward one appears to be a chain of three mounds. The reflectance of side-scan suggests that muddy sediments cover both mounds. The purpose of this deep-towed TV survey is to know whether these mounds are active mud volcanos.

DT-2 : East of the steep slope thick hemipelagic mud deposits everywhere and no talus deposit can be seen in spite of the foot of the slope. The tops of the landward and seaward mounds bounded by the steep criffs are very smooth and flat. Hemipelagic cover is not so thin and appears to be harder than fills of the foot. No calm colony can be found. Mudstones in the steep cliffs crop out and are intensely fractured. Hemipelagic cover is very thin in the outcrops. Moreover, the sharpness of fracture surfaces suggests that the formation of outcrop is relatively new.

We could not find out the evidence that the mounds were active mud volcanos by the deep-towed TV survey. Deformations of mounds, however, are still active and may be related to tectonic force.

DT-3 : This line cut across the deep-sea channel north of the seaward mud mound. Owing to the thick hemipelagic sediments, it is difficult to know the channel axis, although this channel is easily recognized in the seabeam map and the side looking image. The deep-towed TV survey shows that this channel is inactive now.

Line 3 : Tenryu Canyon and Canyon Wall (July 7)
(Camera : DT-4, DT-5 and DT-6)

S. Wonn, J. Ashi, M. Murayama, H. Monma, K. Otsuka and J. Naka

DT-4 was sited along the eastern axial channel of the Tenryu deep-water canyon, ranging from 3324 m to 3876 m in contour depth. The observation of the deep-tow-camera starts at the point of Lat. 33° 38.77'N, Long. 137° 31.30'E (time 09h 41m) toward south. The end of the **DT-4** is sited on the point of Lat. 33° 35.23'N, Long. 137° 32.46'E (time 14:23). As shown in the bathymetric sea beam map, there are two deep-water channels in the lower reach of the Tenryu Canyon : the western active and eastern inactive channels, and **DT-4** run along the thalweg of the eastern inactive channel. From the the screen of the deep-tow-camera, the cover sediment on the channel floor is mostly unconsolidated clayey silt to silty sand, yellowish gray in color. The debris and gravels, ranging from several to tens cm in diameter, are scattered on the channel surface. In the case of sandy surface, wave ripples are commonly recognized, and the crests of the ripples are normal to the channel course, suggesting the currents along the thalweg. The channel floor was not smooth, some steps were found (e.g. screen at 12h 46m.). The thickness of the cover is likely not to be same, that it would thin in the probable uplifted area caused by faulting. A *Calyptogena* community had been previously found by the *Nautile* submersible in the eastern inactive channel, probably along the blind continuation of the deformation front (main Nankai thrust). Our camera survey confirms that this community is still active 4 years after the first observations of the *Nautile* (cf. the scene at 13h 47m.). The colony is distributed into patches, ranging from 0.2 m to 5 m in diameter, on the muddy bottom floor. We did not find any clam colony further north in the Tenryu Canyon, at least along the eastern edge of the canyon.

DT-5 is the line that climbed up the escarpment to east of the Tenryu Canyon. The observation of the deep-tow-camera started at the point of Lat. 33° 35.23'N, Long. 137° 32.46'E, 3876 m deep (time 14:23), and the end of **DT-5** was sited on the point of Lat. 33° 36.63'N; Long. 137° 34.35'E, 3146 m deep (time 16h 20m.). In the deep-tow-camera, steps of several to tens meters in relief, and narrow terraces are repeated again and again. These topographic steps were extended in different directions, thus, they are likely to be formed by faulting or slumping. Thin muddy sediments cover these terraces. A number of*Calyptogena* colonies were discovered on the terraces of **DT-5** (e.g. scene at 16h 03m.), and were densely distributed.

DT-6 started from the point (Lat. 33° 36.63'N; Long. 137°34.35'E) of 3146 m water depth (time 16h 20m.) to the point (Lat. 33° 37.61'N, Long.137°34.44'E) of 2754 m water

depth (time 18h 10m.). The topographic condition of **DT-6** is very similar to that of **DT-5**, which was made of steps and terrace. *Calyptogena* colonies were also found on the narrow terraces. Thin muddy sediments covered the surface of the terraces.

The *Calyptogena* colony was composed chiefly of clams, sea slugs, sea cucumber and shrimps, together with many trails and biogenetic mounds on the bottom surface. These animals were almost linearly distributed, but the precise trend of the distribution is unclear from the deep-tow-camera screen. The most clams in the colony is likely not to be alive. The trials are several cm to tens cm in wide, which are produced mainly by sea slugs and bivalves, and they are good makers for the present-day biological activity. The biogenetic (?) mounds that are conical in shape, approximately 10 cm in diameter, were commonly found around the colony. Noteworthy is that the sediment around the colony is black in color, suggesting that the sediment is most likely to be an anoxic in condition, where some kind of bacteria seems to live by taking hydrocarbons and sulfur from the pore water that is welled up from the deeper horizon, as their food.

Line 4 : First deformation front (July 10)
(Camera : DT-7)

Y. Ogawa, T. Yamagata and K. Mitsuzawa

Line 4 was deliniated at the first deformation front of the Nankai accretionary prism, east of the mouth of the Tenryu deep sea fan on July 8, 1989. The dive of the deep-towed camera began at 33°37.88'N, 137°54.62'E (4027 mbsl) and ended at 33°43.68'N, 133°51.68'E (3194 mbsl). According to the SeaBeam map, the line is just from the deformation front of the accretionary prism. The general topography is that there is one small step from the Nankai trough floor which seems to be occupied by an axial channel from east to west . The trough floor is about 4030 m deep, and the first step, 300 m high, whose foot corresponds to the very deformation front of the prism makes a convex curve towards SSE. The slope dip calculated from the SeaBeam map is about 12.5 degrees to SSE.

Then generally a gentle slope of 4km wide develops. Within there three sets of anticline and cyncline are seen probably due to active folding of NE trend. This flat surface constitutes the lowest terraces in this area of about 3600 to 3700 m deep, called the Enshu deep-sea terrace. Steep slope begins again at the next foot, which is just the eastern continuation from the Omaezaki deformation front. This makes one ridge, called the Haibara ridge, forming oblate shape trending NE of 380 m high. The summit of this ridge is about 3280 m deep. This ridge is asymmtrical, the SE slope is about 16 degrees while the NW slope is about 10 degrees.

Then rather gentle slope dipping NW begins until the end of the line. The line continues to Line 6.

As described in Fig.5.3.8, the floor of the flat surface on this line is covered by mud, but it seems not thick but just to the cover mudstone or sandstone sediments, because the chain from the deep-tow camera did not penetrate the floor. There are sporadic exposures of mudstone beds with fractures. The fractures trend nearly N-S, but exact is not well known from the camera. The most prominent observation is colonies of *Calyptogena*. They are seen abundantly on the first step of the slope, just NW of the deformation front. They are not common on the foot or the lower parts of the slope but on the upslope of the slope. The colonies are composed of several tens to a hundred of individuals of relatively small and rarely big species. Sea anemonea are often associated

with the colonies. Many trails of *Calyptogena* and gastropods are also associated with these colonies.

On the other hand the flat surfaces of the Enshu deep-sea terrace has no *Calyptogena*, instead biogenic mounds, suggesting hemipelagic animal activity, are abundant.

On the foot of the Haibara ridge several colonies of *Calyptogena* were seen, but one of them just on the foot of the first scar of the ridge (seen at 13:46:54) might be a vent of fluids. The Haibara ridge, 360 m high, exposes alternated beds of mudstone with N-S fractures. *Calyptogena* colonies are commonly seen in the middle of the slope; there are several scattered colonies of *Calyptogena* around 16:36. One more steep cliff was on the end of the slope, cropping out alternated beds of mudstone. Sporadic gastropods were seen on the cliff.

The gentle downslope north of the ridge has just mud floor, then before reaching the next step, where is around the end of the line, several small *Calyptogena* colonies were seen.

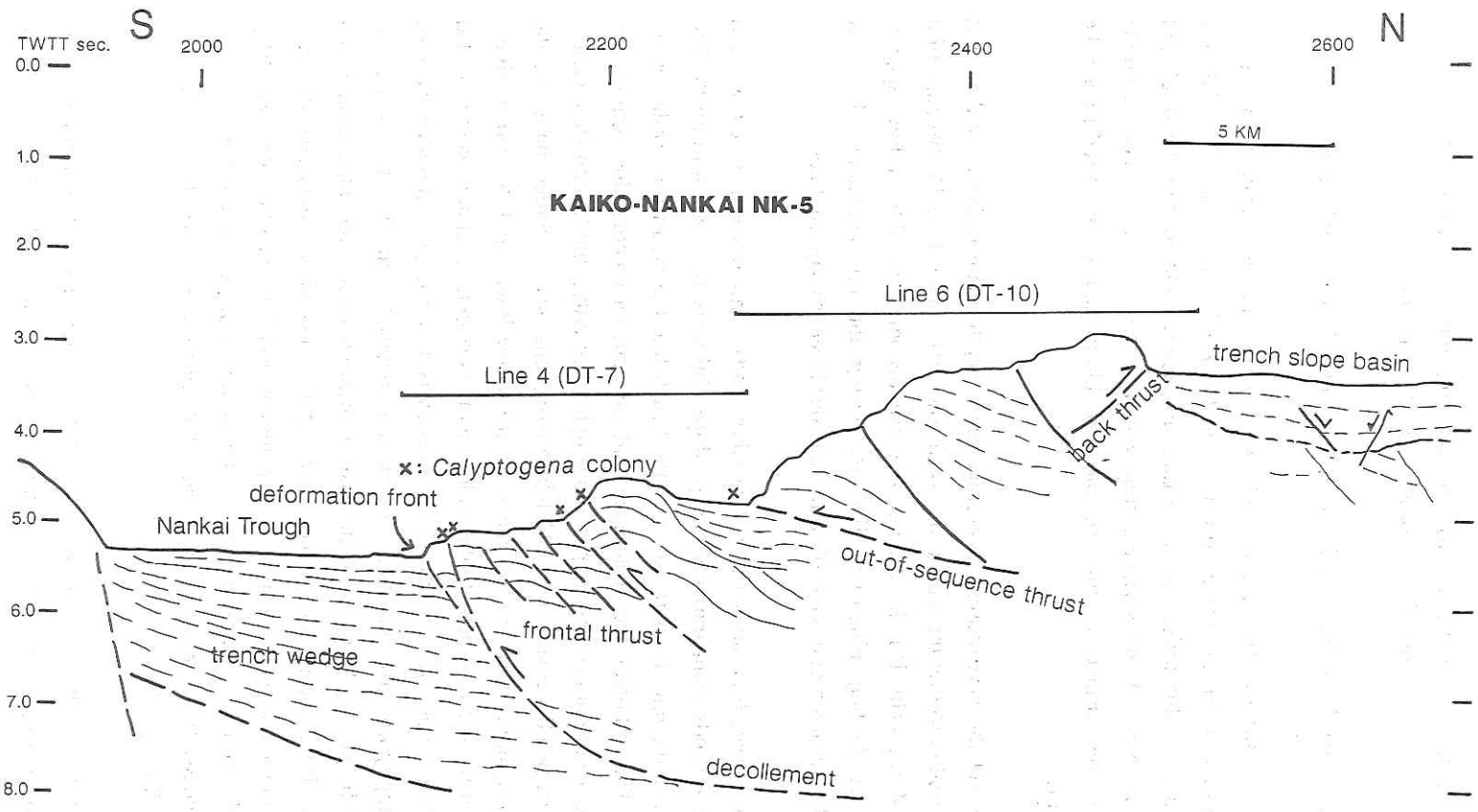

Figure 5.3.8 Interpretation of seismic profile NK-5 by Y. Ogawa taken at KAIKO MARU KN88 Cruise processed by Mr. Kuramoto, showing DT-7 (Line 4), DT-10 (Line 6) and location of *Calyptogena* colony. "Trench wedge" might be combination of part of older accretionary prism and the present trench floor sediments.

Line 5 : Along-contour on deformation front (July 9) (Side Scan Sonar : DT-8 and DT-9)

H. Monma, K. Mitsuzawa, J. Naka, K. Otsuka, J. Ashi and T. Koizumi

During the KH89-1 criuse Leg 2, we carried out a side scan sonar survey around the foot of the continental slope of the Nankai Trough, about 30km SSE off the Omaezaki. In this cruise, only one side sonograph was obtained by the trouble of the side scan sonar. As the surface current was from west to east, we conducted the survey along the surface current, and the port side transducer was used to see the upward slope.

Around the survey area, the average water depth attained about 3500m, so, it was not possible to tow the side scan sonar tow fish faster than 1kt because of a limitation of the cable length. As the tow fish becomes unstable at low speeds, especially at the beginning of the line and during the course change, the sonar record of the linear structures are distorted and displayed as zig-zag lines.

The survey line can be divided into three parts. The first one is the western part which ascends comparatively steep slope obliquely from south to north. The second one is the middle part and run the bench-like flat area from northwest to southeast. The last one is the western part and run along the contour line from west to east. The record of the western part show high reflectivity, and few hundred meters long some striped linear structures which look like steps were recorded on it. In the middle part, the reflectivity of the sea bed become lower, and the same linear structures were also recorded. In the middle part, horizontal stratums were recorded on the subbottom profile. So that weak reflectivity seems to present not only on the flat topography but also on the soft bottom material. In the last part, the reflectivity became high again, and the striped linear structures were also observed on the record. From the middle of the western part, very high reflectivity area was appeared, and the boundary between very high and high reflectivity area was very sharp. This boundary corresponds to the intersection of steep and moderate slopes on the Sea Beam map, and in the latter half of the western part tow fish faced to steep slope(Fig. 5.3.9).

Prior to the sonar survey, we observed the sea bottom of the central part of the middle part by deep tow camera. The area was widely covered with fine mud. In some places, step-like cliffs where semiconsolidated mudstone croped out on them

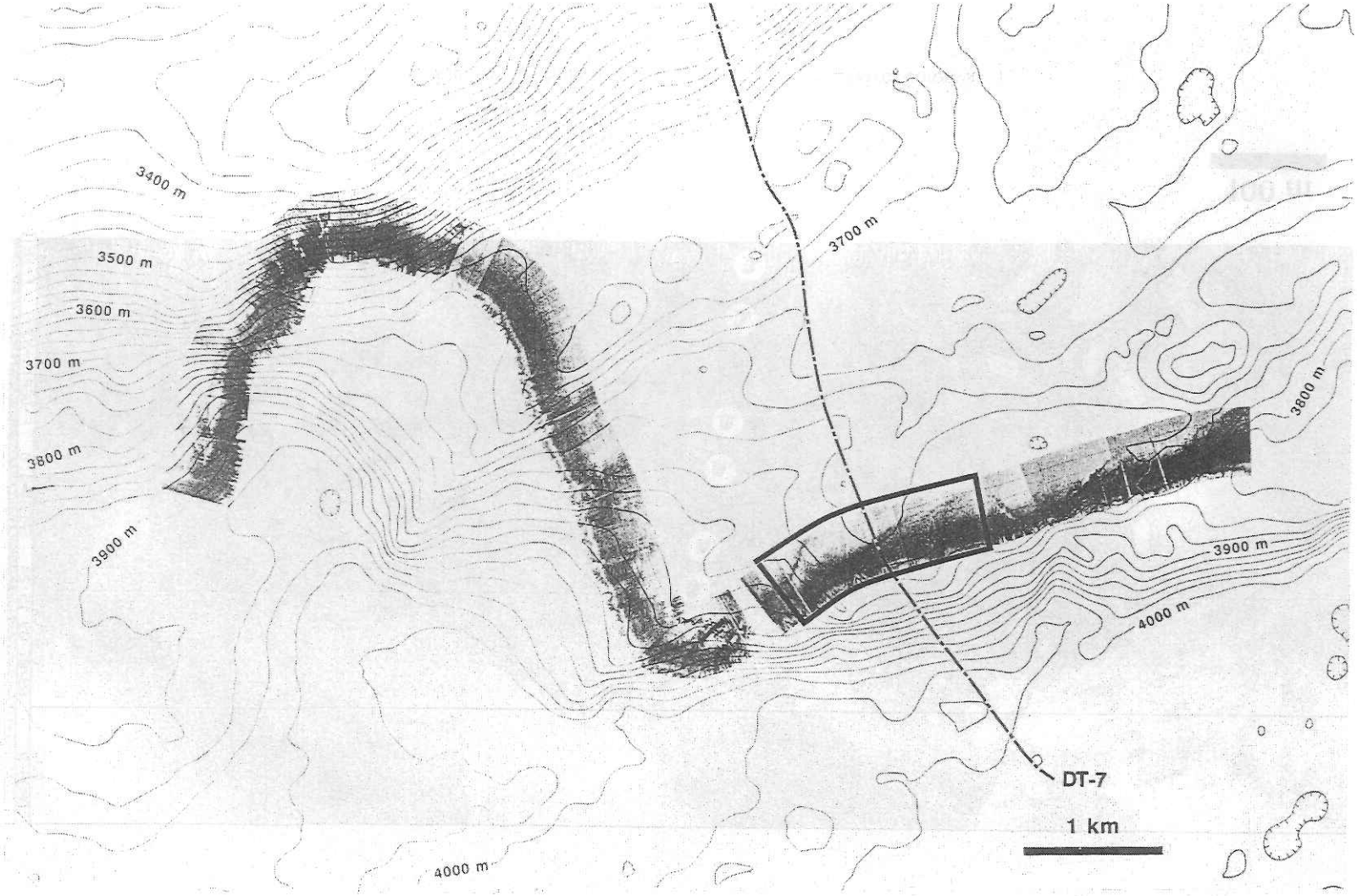

Fig. 5.3.9 Side scan sonograph of the DT-7.

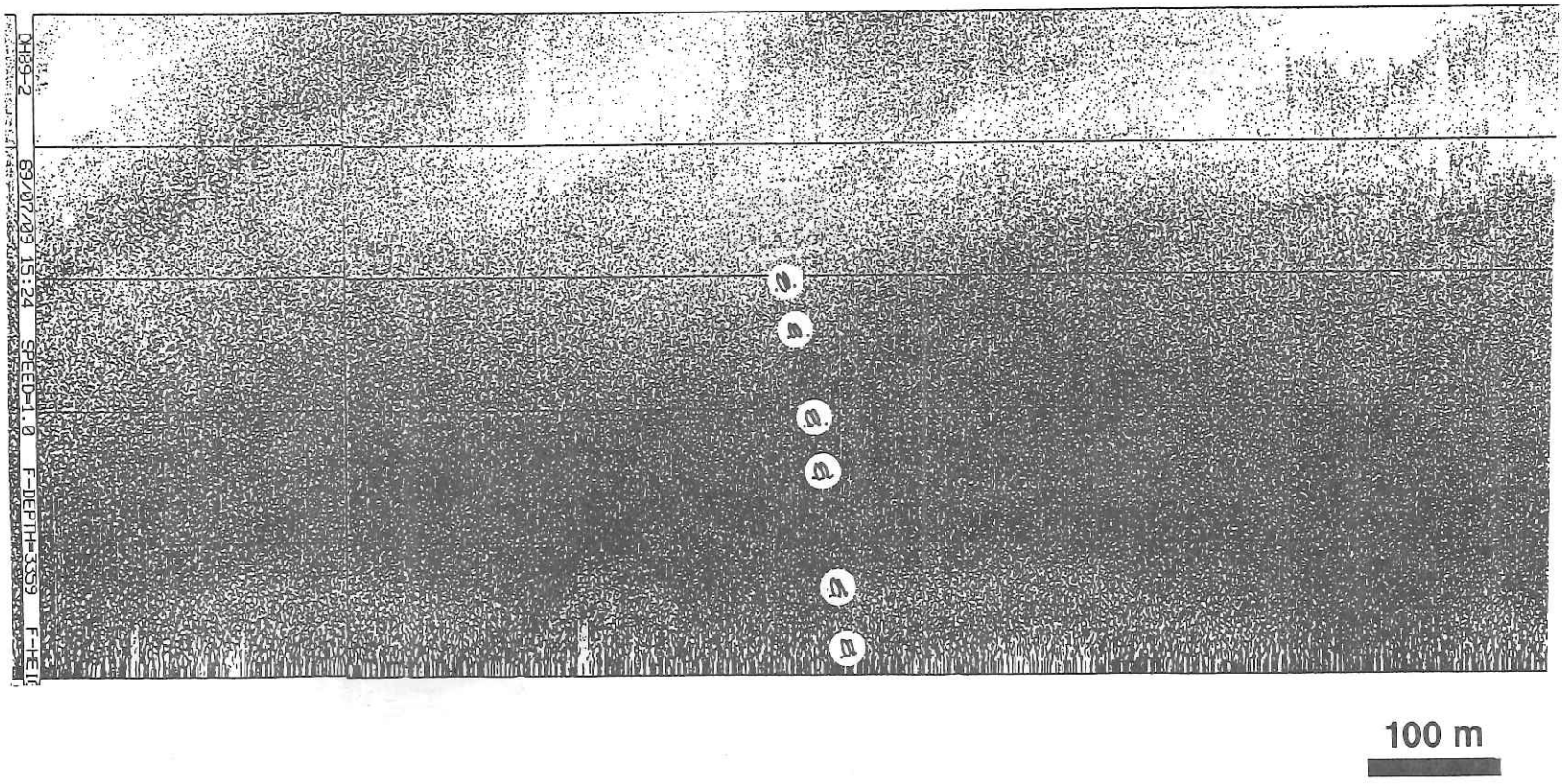

Fig. 5.3.10 Side scan sonograph around the divalves colonys.

were observed. It seems these cliffs correspond to the striped linear structure on the sonograph. According to the camera observation, colonies of bivalves, the size of which were few tens meter, were observed in several place. However, no distinct record which corresponds to the colony was not observed on the sonograph(Fig. 5.3.10).

Line 6 : Upper Nankai prism (July 10)
(Camera : DT-10)

Y. Ogawa, T. Yamagata and K. Mitsuzawa

Line 6 (**DT-10**) was delineated from the flat surface at the foot of the second step of the Nankai acretionary prism wast of the Tenryu deep-sea fan to tne top of the ridge(later called Yukie ridge) on July 10, 1989. The dive began at 33°42.61 N, 137°52.14 W (3512 mbsl), and ended at 33°49.61 N, 137°49.14 E. This slope is on the SE face of the first steep and big ridge of the Nankai accretionary prism, and constitutes almost a continuous steep slope of 1500 m high with two gentle terraces.

At the biginning the line followed the last part of the Line 4. Only a few *Calyptogena* colonies were seen on a mud floor at the foot of the cliff. The first scar, corresponding to a sharp thrust which continues from west to east, is the most striking deformation feature in this prism. This first slope dips to SE at about 15 degrees. All the way of the slope no more colonies of *Calyptogena* were seem but some gastropod colonies were observed. The slope exposes mudstone outcrops with fractures or lineation of NS trend. In some places, particularly on the gentle terrace of 2950 m deep, coarse sediments, sandstone and/or conglomerate, were seen.

Next steep scar, 500 m high, is occupied by alternated beds of mudstone and sandstone outcrops. The slope averagely dips to S at about 22 degrees, but there are many small steeper steps repeatedly developed. After the steep slope, agentler slope continues with some undulation until the summit of the Yukie-Yasumi ridge. Many small colonies of gastropds were observed and abundant red seapens were seen. Floor seems to be rough and paved by coarse sediments. In some places mudstone outcrops were exposed on cliffs.

After the ridge a steep downslope to N exposed mudstone layers which were commonly covered by black materials probably Manganese oxide. Pebbles were scattered on the floor. On the gentle floor after the slope sands or pebbles cover the muddy sediments.

Line 7 : East Zenisu thrust and mud volcano (July 12)
(Camera : DT-11 and DT-12)

H. Cambray, N. Chamot-Rooke, T. Iiyama and J. Naka

The purpose of this deep-towed TV camera dive was to cut across a thrust fault immediately south of East Zenisu Ridge, and to study a 80 meters high mud volcano a few kilometers south of the thrust. The thrust structure south of Zenisu and the existence of the mud volcano were discovered during the KAIKO project phase I (1984-1985). The compressive origin of Zenisu is now beyond dispute. The mud volcano was interpreted as further evidences for compressive tectonics and related fluid circulation.

Going down slope towards Zenisu upper thrust, the sedimentary sequence is made of manganese coated mudstones, outcroping in places but generally covered by a thin hemipelagic mud cover. Stratification was clearly recognized along the slope, including various tilting from sub-horizontal to sub-vertical dips. Mudstones are locally fractured, but no clear faulting pattern was observed. This overall structure suggests strong compressive deformation affecting layered consolidated rocks. Weither this thrust is nowadays still tectonically active is questionable, as faulting was scarcelly observed and no clam community was found. However, the hemipelagic cover is very thin in many places (less than a few centimeters), despite fast sedimentation rates, thus suggesting recent tectonic movements. No definite conclusion should thus be drawn from the camera observations regarding todays tectonic activity of the area.

We left the bottom after crossing Zenisu thrust, as the cable was too short (and drift was fast) for the flat muddy plain. The bottom was reached again just before the base of the mud volcano. It is built as a serial of sediment piles, probably semi- to unconsolidated mudstones. The same sedimentary facies was observed across the volcano. Steep scarps alternate with flat areas. The genesis of this feature issued from a mud diapir, which is formed by the uplifting of partly indurated mud in an over pressured system, owning to a compressional field. No life community was observed linked to this mud volcano. This fact probably means no connection of overpressured sediment with a methane bearing layer. Regarding the pelagic mud covering several centimeters of the flatest areas, this feature, although young, seems to be not recent. Its age may be thousand to ten thousand years.

5.3.2 Cross-section with time table, and table of positions

Cross-section with Time Table

W. Soh and J. Ashi

Cross-section and time table for the survey lines 1 to 7 are shown in Figs. 5.3.11 ~5.3.16. Cross-sections were automatically made by the CTD system of JAMSTEC in the deep tow camera (Vertical exaggeration: approximately three times). Some symbols were added on the cross-sections in order to give an outline of the result of the observation for the surface morphology and the position of clam colony, etc.

Table of Positions

A. Takeuchi, H. Toh and M. Nakanishi

Table of positions was compiled as a reference table for the time log. We can know the seafloor position and the condition of the deep-towed survey for each observation described in the time log. As is described in section 5.2.4, position in the table are obtained by Loran-C with the geodetic framework of WGS-84. We owed much to the on-board scientists who helped us complete the table.

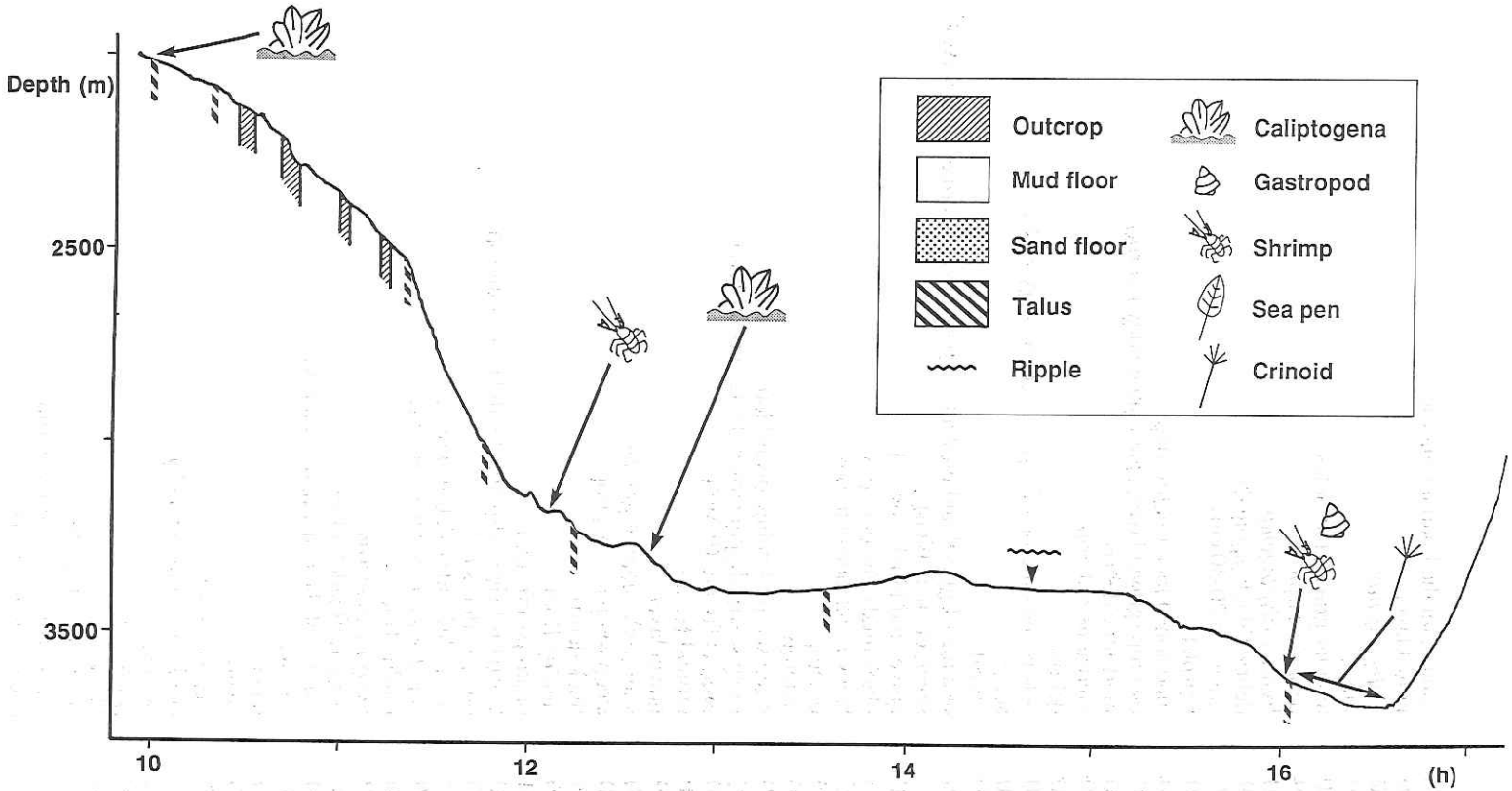

Figure 5.3.11 Bathymetric position vs time of tow fish of DT-1.

DT-1

09:49:00	camera on the bottom (outcrop)
50:00	gravel layer
51:00	*Calyptogenas*
53:20	blocks
10:03:30	angular gravel, bio-holes
06:39	debris, scarplet
07:40	living *Calyptogenas*
16:49	debris (black, spotted)
17:20	gravel (ø 20-30 cm)
19:00	scarplet
22:00	mudstone block (metric size)
26:00	outcrop (gravel layer, pale gray muddy matrix)
29:40	mudstone debris
33:00	mudstone outcrop
38:40	debris
40:10	debris and outcrop of layered sedimentary rocks
42:00	scarp
44:00	gravel
46:30	outcrop of gravel and mud alternation, graven (strike NNE-SSW?, several meters high)
10:50	gravel and block, spotted
10:56	black mudstone outcrops
11:11:03	black mudstone outcrops
07:40	outcrop
08:20	outcrop
20:00	steep scarp (dipping toward left)
22:40	steep scarp (dipping toward left), gravel layer
24:20	ground fissure (E-W?)
26:00	ground fissure
27:39	gravel layer
29:00	wall (right side) of graven
30:30	steep scarp and outcrop
34:45	thick debris
36:40	muddy floor
37:04	outcrop (left side)
41:50	scarp (left side), dipping south layers, outcrop
45:00	outcrop (left side)
47:00	scarp (left side), debris, breccia
48:30	angular white rocks (5-10 cm)
51:50	muddy floor
59:10	*many Coelenterata*?
12:12:00	scarp (left side), block
18:30	bottom of the canyon, muddy floor
19:40	breccia
37:40	block
38:40	clams
39:30	*Calyptogenas*
13:09:11	crack (5-10 cm in width)
47:10	breccia
14:38:30	ripple mark
15:49:00	block
59:00	shell and echnoids
16:05:00	gravel (block), crynoid, shrimp
34:00	end of camera-work

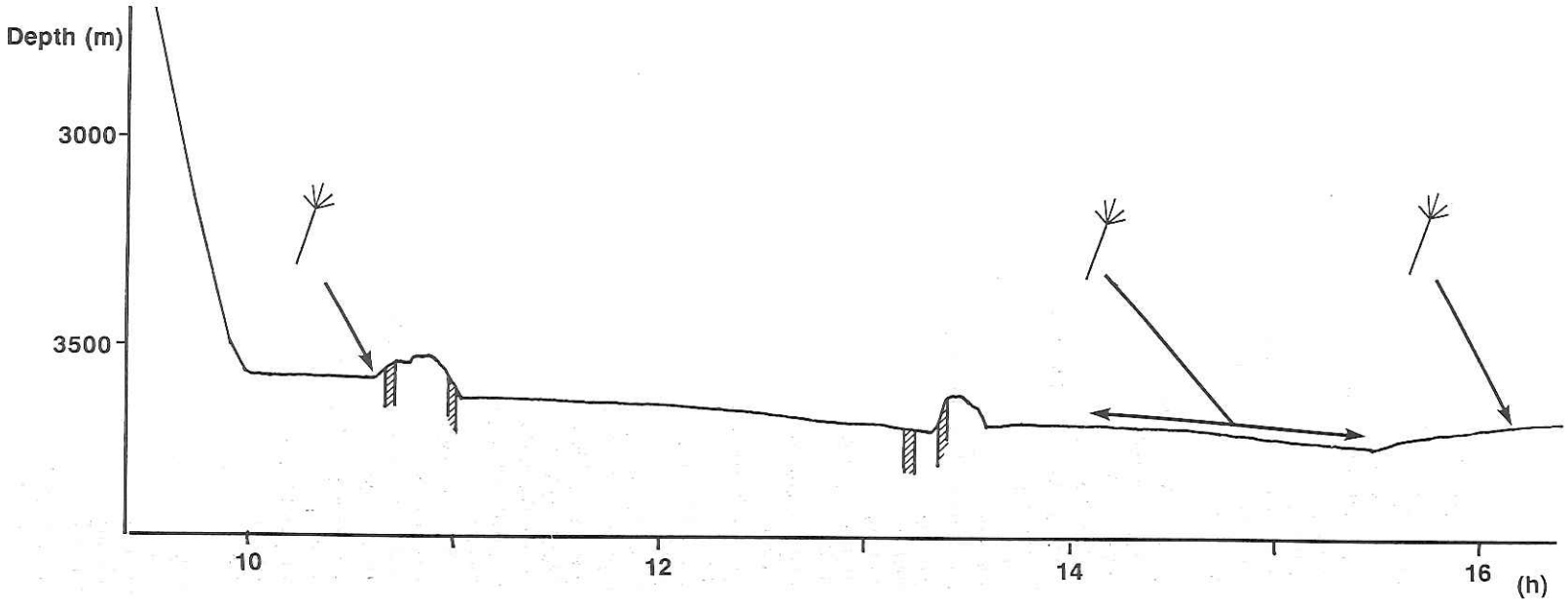

Figure 5.3.12 Bathymetric position vs time of tow fish of DT-2 and DT-3.See Figure 5.3.11 for legend.

DT-2

08:15:00	camera in the sea
10:01:16	camera on the bottom, mud, no pebble, no rock
14:13	trace of benthos
23:39	shell fragments
24:50	silici-sponge
25:08	two shell fragments
29:49	crinoid
33:59	echinoid, mud
37:59	steep slope, right-side down
40:43	slope, continuous slope
43:29	outcrop
43:50	steep scarp
44:53	steep scarp, fracture
46:55	block of mudstone
47:00	steep scarp
54:30	shell?, down slope
56:59	steep scarp, right-side down
58:19	down slope
59:05	steep scarp
59:40	left-side down
11:00:30	escarpment, left-side down
01:11	outcrop
04:00	shell?
27:47	crinoid
35:05	slightly up slope
49:46	shell?
50:14	lateral lineation
54:14	shell?
56:32	block of mudstone
12:02:08	shell?
04:16	trace of benthos
07:07	shell?
10:00	lateral lineation
18:20	fragments of shell?
22:18	trace of benthos
23:33	fragments of shell?
31:32	fragments of shell?
40:05	fragments of shell?
13:00:14	outcrop
04:32	fragments of shell?
19:55	steep scarp
20:39	steep scarp, outcrop, fracture
29:20	down slope
34:27	outcrop left-side down
41:14	lineation
51:20	trace of benthos
55:05	crinoid
58:20	end of DT-2
14:10:10	start of DT-3
58:30	crinoid
15:02:40	crinoid
11:40	crinoid
19:20	crinoid
35:00	many crinoid
49:00	depression?

52:27	fragments of white matter
53:04	fragments of white matter
57:57	fragments of shell
59:18	crinoid
16:03:32	fragments of shell?
07:05	fragments of shell?
14:25	crinoid
17:15	crinoid
18:55	trace of benthos
29:01	trace of benthos
31:55	breccia
37:19	breccia
40:00	end of DT-3

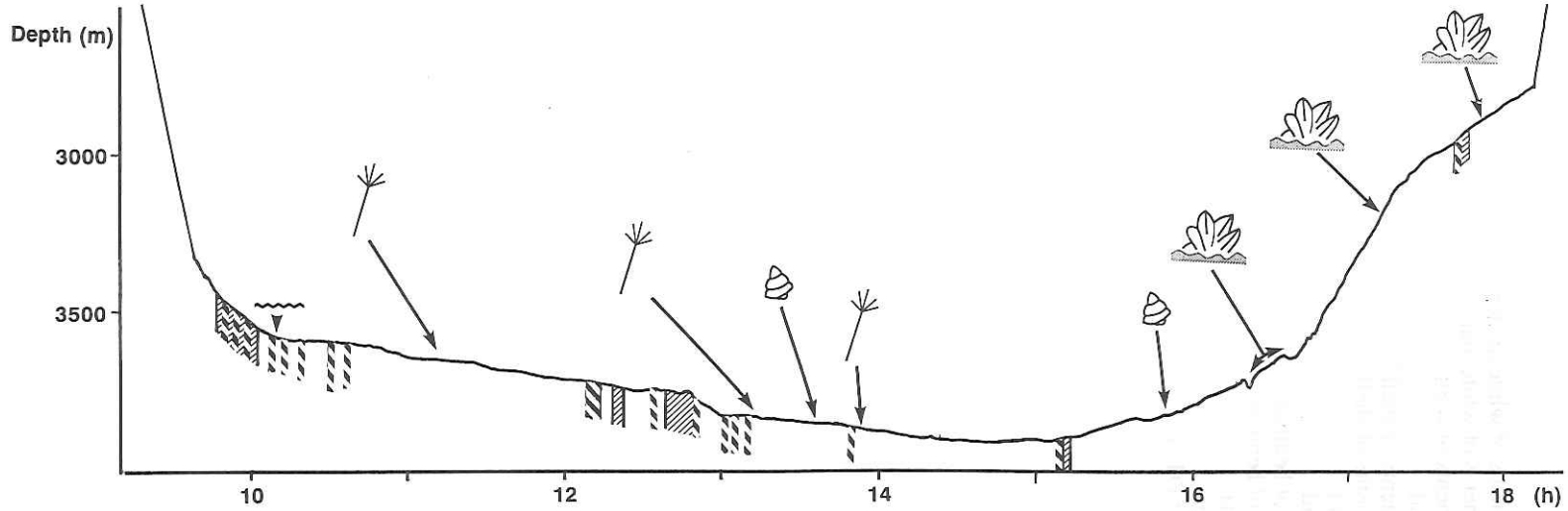

Figure 5.3.13 Bathymetric position vs time of tow fish of DT-4, DT-5, DT-6. See Figure 5.3.11 for legend.

DT-4, 5 and 6

09:41	camera on the bottom
:47	outcrop, wall (left side about 3 m high) with angular talus blocks
:48	small scarp facing SW
:50	wall of talus (left side)
:51:20	steps
:55:18	step (left side)
:57:20	scarplet, block, and outcrop
10:00	sea anemoena is densely gathered
:01	debris (20 cm)
:02:45	debris (5-10 cm) on a flat muddy floor
:07	small talus on muddy floor
:08:17	blue fish (60 cm)
:10	soft muddy cover of c. 10 cm thick
:12	ripple marks (c. 1 m wave length interval, 2-3 cm high crest ridge)
:16	current ripple from S to N (?)
:22	current ripple (1-0.5 m wave length interval)
:31	debris, fish
:34	debris with mud covers
:36	debris
11:00	debris with sea anemone
:11:38	sea anemonea is densely gathered
:13	sea anemonea
:15	sea anemonea
:54:19	sea cucumber
12:05	step and escarpment
:12	debris with thin mud cover
:22	rock outcrop and step dipping backward
:24:50	block with sea anemonea on the top
:34	rock outcrop and step
:39	step upward and outcrop
:40:30	blocks on the flat muddy floor
:42:37	blocks
:45:40	cliff (front side, c. 10 m high)
:47	escarpment
:49:20	escarpment (left side)
:52:40	outcrop (right side) with a bedding surface
13:03:30	many debris
:05	large number of debris
:09	blocks with sea anemonea on the muddy floor
:35:40	trails on the floor
:38:36	*Calyptogena* colony (maybe dead) and many trails
:43:02	trails on the floor
:43:40	step (right side)
:44	trails on the floor
:46-48	living *Calyptogena* (small patches) and trails on the floor
:53	block with sea anemonea
:56	block with sea anemonea
14:23	End of DT-4
14:24	start of DT-5
:44	block on the muddy floor

:49	fish
15:11	block
:14	debris scattered on the muddy floor
:20	step forward (several meter separation)
:22	step forward (several meter separation)
:24:40	trails on the floor
:38	mound (burrow ?)
:49	trails on the floor
:52:19	*Calyptogena* (dead ?)
:53:23	*Calyptogena* colony (dead) and trails
:54	steep scarplet (dipping backward)
:57:10	small trails
:58	slope (tilting forward)
16:02:58	*Calyptogena* colony (dead)
:03:09	*Calyptogena* colony
:03:38	*Calyptogena* colony
:08	trails and Calyptogena
:10:12~19	*Calyptogena* colony
:11:50	black (anoxic) mud recognized in dredge sampler
:14:06	*Calyptogena* colony
:15:40	fluid venting area (?) Many *Calyptogena* colony
:15	End of DT-5
16:16	start of DT-6
:17	dipping right backward
:22	steep scarp upward (thrust)
:23:19	living *Calyptogena* colony with black mud
:30:40	trail and *Calyptogena* colony with black mud
:31:17	*Calyptogena* colony
:31:46	*Calyptogena* colony
:38:01	*Calyptogena* colonys
:38:15	*Calyptogena*
:38:31	*Calyptogena*
	slope upward
:43	steep scarp upward
:47	*Calyptogenas* on steep scarp
:57	steep scarp outcrop overhanging wall
17:07	Sea cucumbers
:08	cliff (right side) and ground fissure (N30°E)
:12:18	*Calyptogena* colony and trail
:12:23	*Calyptogena* (scattered distribution)
:13:20	same pieces of *Calyptogena*
:16	steep scarp upward
:34	*Calyptogena* colony
:35	small patch of *Calyptogena*
:44	mudstone (small cliff)
:45	angular debris (10~20cm)
:52	angular blocks
:58:10	small patch of *Calyptogena*
18:00	continuous outcrop
:10	end of bottom observations

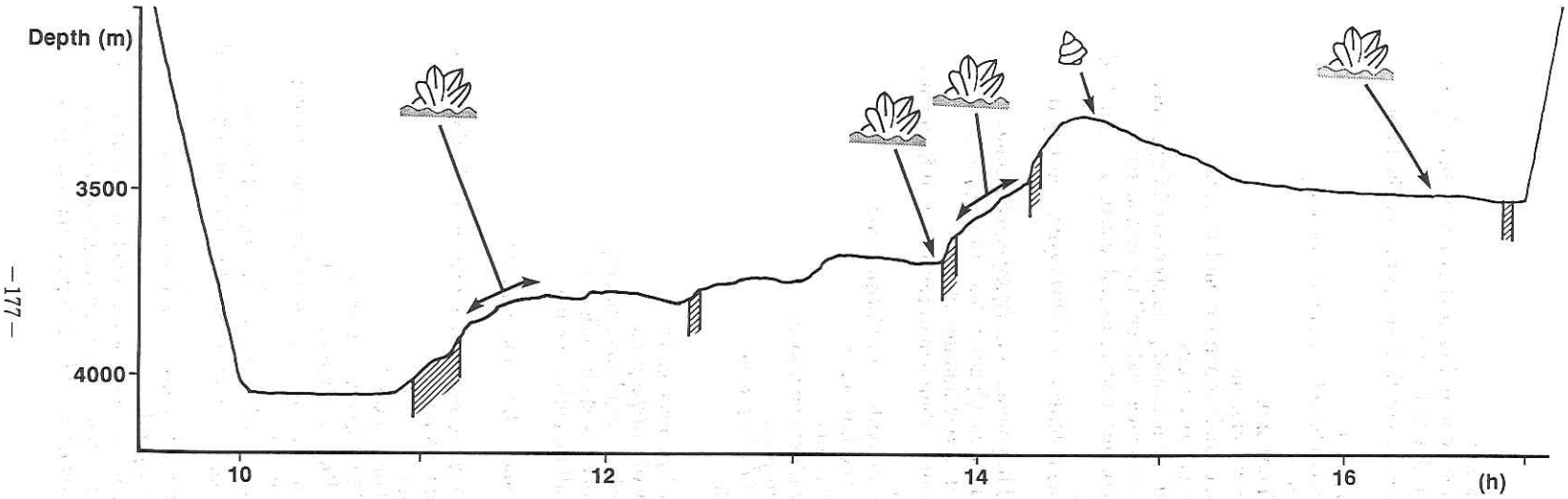

Figure 5.3.14 Bathymetric position vs time of tow fish of DT-7. See Figure 5.3.11 for legend.

DT-7

H. M. S.

08:14:00 camera in the sea
10:04:39 camera on the bottom(4037m deep), very flat plane of white soft mud with brown spots
10:10:48 worms moving, chain does not penetrate the floor
30 echinoid
52 climbing up a cliff
11:04 steep cliff, small boulder, fractured outcrop
06:40 sea cucumber
12: walls of cliff continue
20:54 sea cucumbers abundant
21:46 *Calyptogena* colonies continue until 11:22:27
24:59 steep cliff, mudstone blocks
27:20 *Calyptogena* colonies and gastropod shell fragments
28:32 *Calyptogena* colonies and shell traces abundant
29:22 big colonies of meter size (several tens or one hundred individuals)
30:30 ten to twenty colonies of *Calyptogena* during five minutes
32:14 colonies and fragments of *Calyptogena* continue
35:56 colonies and traces, gigantic clams of *Calyptogena* huge colonies of one hundred clams
37:05 flood of colonies, abundant traces and shell fragments
40:10 small colony
40:51 colony of 40 individuals of *Calyptogena*
41:40 big colonies and fragments
43:49 colony of 30 clams
45:50 big colony with sea anemonea
46:30 trails of gastropods
48:17 big colony of *Calyptogena*
50:42 dense colonies
52:27 big colony
54:41 colony of *Calyptogena* ends
12:07:00 small colony of *Calyptogena*
28:20 climbing upslope, mudstone outcrop
34:00 many trails but few shells; crinoid
45:45 biogenic small mounds abundant
54:03 echinoid
13:08:29 star fish, echinoid, biogenic mounds
42:03 cliff
46:54 colony of *Calyptogena,* black circle due to fluid venting and redux condition
50:20 mudstone cliff
54:10 many trails but few shells
57:58 colonies of *Calyptogena* scattered
14:00 steep slope, 300m high, until 14:30
02:10 shell fragments of *Calyptogena* and biogenic mounds
04:50 mudstone outcrop
07:40 very steep cliff, vertical fracture of about N-S trend
16:10 colony of *Calyptogena*, very steep wall of alternated beds of mudstone
18:36 mudstone outcrop, many "Yagis" (Gorgonians)
30:43 slope becomes gentle.
34:37 until 16:34:00, monotonous mud slope and flat with sporadic shell frgments and echinoid, sea cucumber, shrimp, star fish, trace of gastropod, many biogenic

	mounds
1 6:35:32	colony of ten clams of *Calyptogena*
36:52	colony of *Calyptogena*
39:50	small colony
43:40	many biogenic mounds
55:21	rectangle blocks of mudstone
56:10	mudstone outcrop covered by dusty mud
58:05	dense marine snow
17:00:30	wire up, end of line
18:10	camera onboard

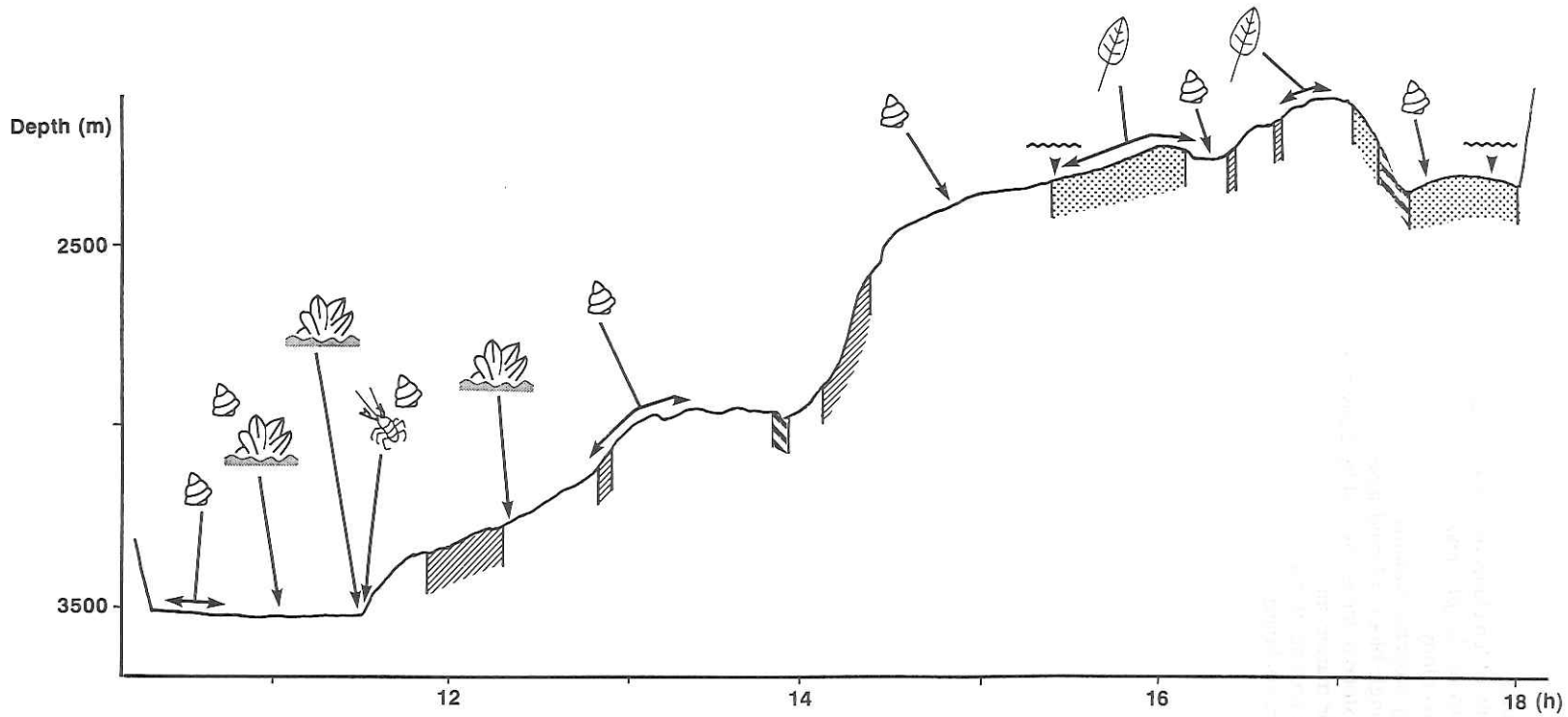

Figure 5.3.15 Bathymetric position vs time of tow fish of DT-10. See Figure 5.3.11 for legend.

DT-10

08:38	camera in the sea
10:19:28	camera on the bottom; flat surface of dusty mud with no sedimentary structure
24:10	gastropods
29:15	biogenic mounds abundant
33:00	sporadic gastropods, sea anemonea
51:40	gastoropods
53:12	until 11:04:14 sporadic sea cucumbers, star fishes, shrimps, gastropods
11:04:39	a few *Calyptogena*
09:06	gastropods, echinoids, shrimps, biogenic mounds, star fishes, sea anemonea, until 11:25:20
30:27	several shells of *Calyptogena*(not alive), floor depth becomes shallow
31:20	cliff of soft mudstone of 100m high until 11:41:10, sporadic gastropods, red shrimps
41:10	slope becomes gentle, sea cucumber
53:22	steep cliff
12:00:29	shell fragments, rod-like material
05:04	ripples
07:13	until 12:19:32 sporadic shell fragments
21:24	rough bottom surface, outcrop
22:45	two valves of *Calyptogena*
30:00	biogenic mounds abundant but no trail; until 12:48:00 gentle upslope with "Yagis"(Gorgonians), star fishes, crabs, gastropods, fishes, sea cucumbers
44:25	colony of gastropods
48:00	ibid
51:20	cliff right-side down
51:37	mudstone outcrop, lineation of N-S trend right-side down
53:20	gastropods abundant
13:01:20	colony of gastropods
10:00	sporadic gastropods, corpse of fish
14:30	colony of gastropods
17:43	until 14:08:50 sporadic crinoids, star fishes, "Yagi", sea cucumbers, gastropods, fishes, shrimps
29:20	bottom sediment coarse
50:14	continuous steps
51:45	blocks of mudstone
52:00	steep slope
53:20	gash on the bottom in these minutes
14:05:50	small blocks of mudstone
09:00	steep cliff(320m high) of bedded mudstone begins until 14:25:30
14:00	bedding right-side down
22:50	many steps made of alternated beds of sandstone and mudstone
25:30	bottom sediments coarse
27:56	orange sea pens begins to appear all the way
31:31	gray coarse bottom, many orange sea pens until 14:49:28
52:07	until 14:54:09 shell fragments
55:21	many shells of gastropods
58:07	until 15:08:47 many orange sea pens
15:13:19	rough bottom surface (probably sandy or pebbly)
16:13	current ripples by west-east flow
22:38	small colony of gastropods

25:50	many gastropods
26:49	until 15:39:49 ripple marks, coarse bottom surface
27:44	until 16:59:36 many orange sea pens
34:17	steep cliff
36:05	many small gastropods
44:35	scarp, lineation of N-S
47:55	colony of small gastropods
16:03:27	bottom lithology sandy
12:51	small gastropods
13:15	"Yagi", very flat until 16:22:10
15:00	bottom surface covered by mud, trails of gastropods(?)
16:20	several blocks of mudstone
18:50	scattered colony of gastropods
22:38	small outcrop of mudstone
23:50	acute outcrop of hard lithology with gastropds
38:25	outcrop, steps of mudstone
39:37	cliff, blocks of mudstone
46:25	big colony of orange sea pens and "Yagi" a while
17:01:40	downslope begins
06:45	cliff and ramp
08:02	ramp, mudstone blocks, many down-steps
10:36	coarse sediments, black maganese oxide crust
16:19	fractured outcrop covered by black materials
19:00	slope down left
21:30	steep cliff, rough floor of pebble-sized clasts covered by black materials
22:30	outcrop covered by fine sandstone
25:20	white spots of gastropods and Mn-coated pebbles
30:15	gastropds, rough floor of sand sediments containing many sand-pebbles, steps covered by mud?
35:10	smooth floor of sand covered by mud, many gastropods, a few "Yagis"
39:39	coarse floor made of mud containing sand and pebble
18:00:00	end of line, DT-10

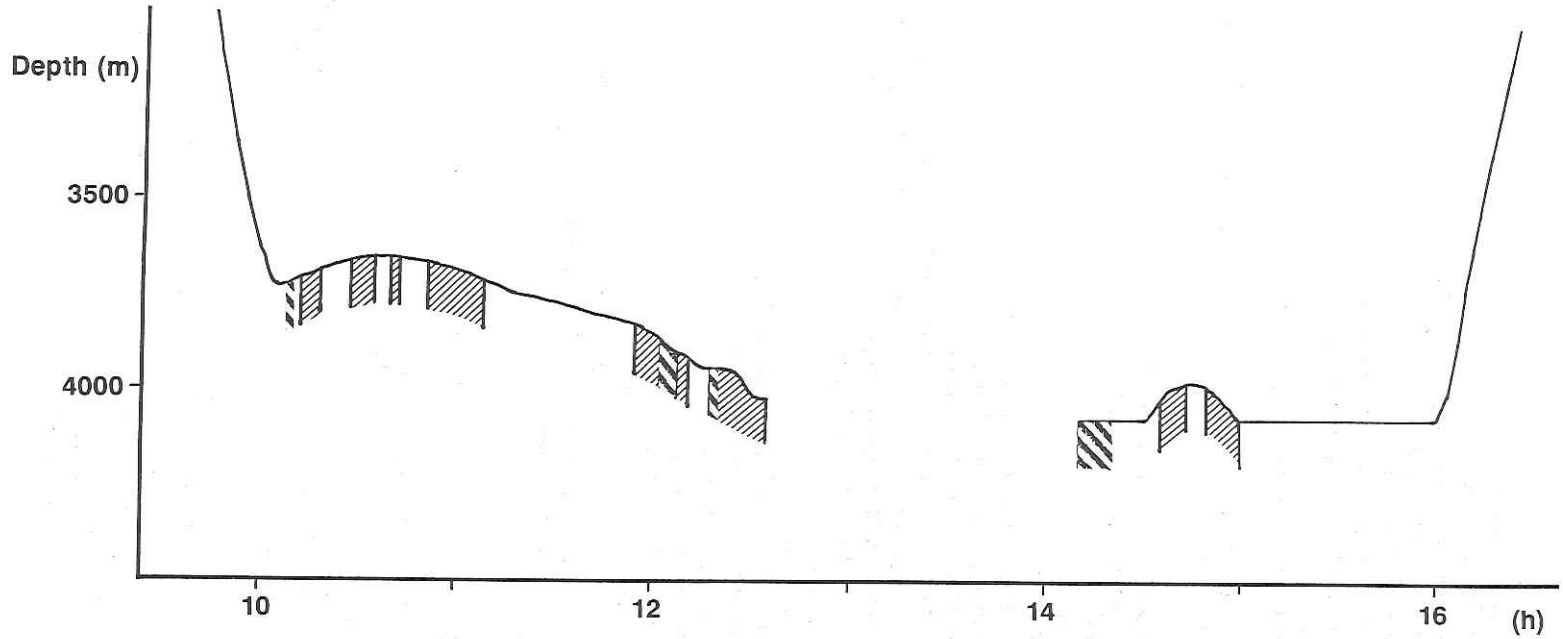

Figure 5.3.16 Bathymetric position vs time of tow fish of DT-11, DT-12. See Figure 5.3.11 for legend.

DT-11, 12

08 :15: 00	camera at sea
10 :05: 45	camera at the bottom
10 :05: 50	white yellowish mud
06: 00	muddy floor with small pebbles (2 to 5 cm)
10: 49	dark debris covered with mud
11: 29	dark debris (10 to 50 cm)
13: 58	coated mudstones partly covered with mud
16: 00	small mudstone outcrop, fractured
16: 58	bier can
19: 44	dark outcropping sediments, probably
	mudstone coated with manganese. Partly covered with a 2-3 cm thick mud small similar outcrops prevail until 10 : 29 : 00
29: 00	sedimentary beds visible, slightly tilted ?
31: 23	small outcrop, partly covered
32: 10	small outcrop
33: 01	small outcrop
33: 28	small outcrop
33: 46	small outcrop, made of sed. beds, tilted
34: 44	small outcrop, made of sed. beds
34: 44	small outcrop, made of sed. beds
35: 53	sedimentary beds, sub-vertical, slightly oblique to the direction of the camera (right) forming a distinctive ridges and troughs topography on the sea floor small similar outcrops prevail until 10 : 41 : 10
41: 10	fractured mudstone (vertical fault?)
43: 00	small outcrop
44: 05	small size debris
45: 16	sub-horizontal stratification, thin mud layer
46: 55	quantity of debris increases (Gomi also...)
53: 00	small mudstone outcrop
53: 22	small mudstone outcrop
54: 42	going down, thickness of mud increases
56: 20	muddy floor, no more outcrop
58: 24	small size white particules (debris or most probably serpulid worms)
59: 12	outcropping layered sediments with clear beds dipping towards the slope
11 :00: 00	many white particules and bioholes
02: 26	outcrop
03: 09	outcrop
05: 30	smal size dark debris, again outcropping dark mudstones covered with thin mud
09: 30	some outcrops, no visible stratification
10: 22	some outcrops, no visible stratification
11: 09	dark debris
12: 00	dark brownish coated mudstones partly or almost entirely covered with mud, probably tilted beds. Prevails until 11 : 36 : 00 (nice example at 11 : 18 : 38 and 11 : 25 : 40)
41: 00	muddy floor
43: 58	muddy with sporatic pebbles
55: 04	small outcrops of non-stratified rocks prevails until 11: 59 : 40
59: 40	horizontal bedding, fractured ?
12 :01: 00	small dark outcrops (coated mudstones) possibly down-faulted (also at 11 : 02 : 39,11 : 02 : 46, 11 : 03 : 33, 11 : 04 : 40)
05: 45	nice outcrop of brownish to dark mudstones
08: 00	muddy floor, with dark pebbles
09: 57	outcrop of angular dark rocks

10: 10	outcrop partially covered with mud
11: 36	outcrop with thin mud (2-3 cm)
18: 39	debris
19: 49	outcrop with dissolution traces, pebbles
20: 10	rough outcrop, dredging ?
21: 10	layered sediments, possibly tilted
22: 20	layered sediments, possibly tilted
23: 40	nice beddings, tilted towards the slope
24: 55	layered sediments
27: 49	down-faulted mudstones
29: 53	tilted layered sediments
12 :36: 00	end of line
	Cable length out has reached its maximum value (4460 m). Bottom is lost in the muddy plain east of Zenisu thrust
14 :12: 07	camera reaches the bottom again
14 :12: 07	pelagic mud with numerous burrowings animals holes
16: 15	dark pebbles (>10 cm)
26: 30	worms holes
32: 43	start climbing the mud volcano
33: 12	outcrop of semi- or un-consolidated mudstones unstratified (also 14 : 33 : 36 and 14 : 34 : 24)
35: 30	dredging (?) of pilled-up mudstones blocks
37: 00	smooth muddy bottom
37: 47	semi-consolidated mudstone outcrop
38: 28	outcrop
39: 15	steep slope
45: 00	steep outcrop, dredging
45: 55	outcropping mudstones, flow structures
46: 30	top of the mud volcano, rather smooth
47: 44	small semi-consolidated mudstone block
48: 04	outcrop
50: 50	going smoothly down slope
51: 16	outcrop (also 14 : 51 : 31, 14 : 51 : 52, 14 : 52 : 27, 14 : 52 : 34)
52: 55	nice mudstone outcrop
55: 35	small step (also 14 : 57 : 17)
57: 37	outcrop (also 14 : 57 : 47)
58: 47	outcrop
59: 30	step
15 :00: 20	last outcrop, end of mud volcanopelagic mud with burrowing holes
16 :01: 20	possibly one volcanic clast as approaching a seamount
16 :02: 38	wire up, end of line
18 :00: 00	camera on board

DT-1

Time	Camera			Ship			Cable	Bearing
	Lat (°N)	Lon (°E)	Depth (m)	Lat (°N)	Lon (°E)	Depth (m)	(m)	(°CW)
9: 55	49.83	55.36	2018	49.89	55.73	2135	2284	262.0
10: 00	49.85	55.47	2025	49.89	55.92	2173	2442	266.1
10: 10	49.88	54.85	2061	49.88	56.29	2226	2612	269.8
10: 20	49.92	55.96	2092	49.86	56.64	2392	2750	274.4
10: 30	49.94	56.22	2149	49.83	56.99	2523	2870	276.6
10: 40	49.94	56.77	2206	49.83	57.62	2829	3050	276.3
10: 50	49.91	56.90	2305	49.83	57.78	3056	3128	274.5
11: 00	49.93	57.15	2372	49.88	57.97	3135	3065	273.0
11: 10	49.92	57.38	2456	49.92	58.14	3202	3109	269.9
11: 20	49.91	57.58	2542	49.91	58.31	3199	3112	270.0
11: 30	49.92	57.77	2768	49.90	58.48	3272	3306	271.6
11: 40	49.94	57.96	2932	49.90	58.63	3273	3442	272.6
11: 50	49.95	58.16	3077	49.90	58.78	3313	3546	273.7
12: 00	49.94	58.32	3141	49.86	58.92	3373	3580	276.6
12: 10	49.93	58.47	3188	49.83	59.04	3380	3590	278.6
12: 20	49.93	58.61	3266	49.81	59.14	3400	3634	280.9
12: 30	49.93	58.76	3272	49.79	59.23	3398	3599	283.5
12: 40	49.90	58.92	3317	49.70	59.33	3396	3622	292.1
12: 50	49.85	58.96	3372	49.60	59.41	3390	3655	294.6
13: 00	49.90	59.19	3385	49.61	59.50	3385	3652	307.6
13: 05	49.77	59.24	3396	49.48	59.53	3371	3656	309.9
13: 15	49.70	59.30	3398	49.42	59.57	3354	3644	311.6
13: 20	49.68	59.34	3395	49.38	59.59	3341	3636	315.0
13: 30	49.61	59.33	3394	49.29	59.65	3339	3621	309.1
13: 40	49.52	59.60	3382	49.19	59.77	3335	3603	328.3
13: 50	49.44	59.61	3373	49.15	59.82	3367	3595	319.0
14: 00	49.38	59.71	3352	49.11	59.90	3380	3567	319.5
14: 10	49.31	59.80	3338	49.03	59.98	3382	3555	321.8
14: 20	49.26	59.88	3368	48.98	60.08	3384	3587	318.9
14: 30	49.19	60.00	3383	48.94	60.20	3401	3597	316.1
14: 40	49.14	60.09	3386	48.90	60.33	3420	3609	309.9
14: 50	49.09	60.19	3387	48.83	60.46	3455	3629	308.7
15: 00	49.04	60.31	3390	48.76	60.60	3492	3645	308.9
15: 10	48.99	60.42	3400	48.66	60.72	3544	3673	312.2
15: 20	48.93	60.54	3437	48.56	60.86	3626	3730	314.1
15: 25	48.81	60.60	3468	48.53	60.94	3638	3770	304.2
15: 30	48.86	60.67	3486	48.49	61.00	3677	3795	312.9
15: 40	48.80	60.73	3504	48.42	61.07	3688	3820	312.8
15: 50	48.38	61.16	3539	48.38	61.16	3687	3826	*
16: 00	48.30	61.23	3613	48.30	61.23	3684	3903	*
16: 10	48.26	61.27	3644	48.26	61.27	3681	3907	*
16: 20	48.23	61.40	3677	48.23	61.40	3679	3919	*
16: 30	48.19	62.01	3688	48.19	62.01	3678	3913	*
16: 35	48.11	62.31	*	48.11	62.31	*	3940	*

DT-2

Time	Camera			Ship			Cable	Bearing
	Lat (°N)	Lon (°E)	Depth (m)	Lat (°N)	Lon (°E)	Depth (m)	(m)	(°CW)
10: 00	45.28	54.82	3578	45.27	54.84	3586	3778	294.9
10: 05	45.38	54.68	3581	45.23	54.93	3578	3787	297.0
10: 10	45.35	54.74	3581	45.21	54.99	3554	3792	295.1
10: 15	45.31	54.89	3579	45.22	55.06	3552	3812	293.4
10: 20	45.34	54.85	3581	45.19	55.17	3576	3820	291.0
10: 25	45.32	54.92	3584	45.16	55.29	3610	3844	289.9
10: 30	45.29	55.03	3585	45.15	55.41	3634	3877	287.4
10: 35	45.30	55.08	3585	45.14	55.53	3634	3900	286.3
10: 40	45.11	55.66	*	45.11	55.66	3636	3900	*
10: 45	45.19	55.47	3551	45.09	55.76	3641	3891	285.7
10: 50	45.23	55.43	3534	45.09	55.84	3640	3877	286.0
10: 55	45.25	55.42	3548	45.08	55.96	3638	3908	284.8
11: 00	45.26	55.49	3618	45.07	56.11	3640	4018	284.3
11: 05	45.25	55.45	3631	45.05	56.24	3642	4066	282.0
11: 10	45.22	55.69	3633	45.06	56.31	3644	4060	281.9
11: 15	45.19	55.82	3634	45.05	56.40	3648	4057	281.5
11: 20	45.15	56.01	3635	45.05	56.50	3654	4064	280.0
11: 25	44.81	56.11	3637	45.05	56.58	3653	4067	246.6
11: 30	45.06	56.69	3635	45.06	56.72	3656	4089	277.6
11: 35	45.11	56.65	3639	45.09	56.86	4418	4121	275.0
11: 40	45.12	56.73	3639	45.10	56.97	5247	4131	273.2
11: 45	45.12	56.66	3641	45.08	57.08	3672	4147	274.2
11: 50	45.15	56.46	3642	45.06	57.21	3677	4189	275.9
11: 55	45.16	56.56	3644	45.03	57.34	3684	4210	277.9
12: 00	45.15	56.69	3647	45.02	57.49	3687	4227	277.7
12: 05	45.07	56.78	3646	45.03	57.55	3688	4193	272.4
12: 10	45.08	57.46	3648	45.06	57.59	3688	4169	276.6
12: 15	45.10	57.19	3652	45.05	57.64	3692	4125	275.2
12: 20	45.08	57.54	3655	45.05	57.72	3697	4113	277.0
12: 25	45.05	57.64	3658	45.02	57.83	3698	4123	277.3
12: 30	45.07	57.52	3664	44.98	57.94	3671	4140	279.9
12: 35	45.11	57.35	3673	44.96	58.05	3647	4160	280.3
12: 40	45.12	57.46	3675	44.94	58.15	3685	4165	282.0
12: 45	45.08	57.56	3678	44.91	58.26	3692	4182	281.7
12: 50	45.10	57.66	3682	44.87	58.40	3010	4224	284.2
12: 55	44.92	57.97	3684	44.83	58.54	3932	4262	277.8
13: 00	44.90	58.39	3688	44.79	58.68	3708	4302	287.4
13: 05	44.77	58.74	3691	44.74	58.81	3691	4375	288.6
13: 10	44.81	58.64	3695	44.68	58.95	3706	4400	289.9
13: 15	44.78	58.78	3704	44.65	59.07	3689	4419	290.5
13: 20	44.78	58.79	3685	44.61	59.18	3687	4428	290.2
13: 25	45.02	58.38	3623	44.59	59.27	3696	4331	291.7
13: 30	44.59	59.28	3632	44.55	59.36	3689	4342	291.8
13: 35	44.54	59.40	3695	44.52	59.44	3692	4376	293.2
13: 40	44.56	59.38	3681	44.55	59.42	3690	4267	281.4
13: 45	44.79	58.92	3683	44.59	59.36	3689	4157	290.4
13: 50	44.60	59.34	3688	44.58	59.38	3692	4108	290.7
13: 55	44.69	59.15	3688	44.62	59.32	3691	4030	289.8

14: 00	44.49	58.66	3689	44.59	59.45	3693	4050	264.1
14: 05	44.76	59.44	3689	44.76	59.50	3705	4038	268.8
14: 10	44.90	59.40	3691	44.94	59.49	3711	4050	249.6

DT-3

Time	Camera			Ship			Cable	Bearing
	Lat (°N)	Lon (°E)	Depth (m)	Lat (°N)	Lon (°E)	Depth (m)	(m)	(°CW)
14: 25	45.03	59.34	3693	45.24	59.44	3728	4007	209.3
14: 30	44.83	59.25	3696	45.34	59.43	3733	4023	202.9
14: 35	44.81	59.23	3701	45.42	59.42	3742	4050	201.0
14: 40	45.47	59.39	3705	45.51	59.40	3740	4046	195.6
14: 45	45.25	59.29	3706	45.62	59.34	3727	4087	189.2
14: 50	45.36	59.27	3713	45.74	59.29	3709	4124	182.8
14: 55	45.48	59.25	3718	45.81	59.25	3695	4130	180.0
15: 00	45.61	59.21	3722	45.87	59.20	3695	4122	176.0
15: 05	45.82	59.16	3726	45.92	59.15	3703	4121	173.9
15: 10	45.29	59.20	3730	45.98	59.10	3685	4117	169.9
15: 15	45.71	59.10	3736	46.04	59.04	3687	4115	166.8
15: 20	45.42	59.17	3735	46.10	58.99	3683	4124	162.6
15: 25	46.06	58.97	3740	46.17	58.94	3681	4132	159.9
15: 30	46.11	58.89	3740	46.23	58.84	3680	4149	154.8
15: 35	44.46	59.55	3725	46.31	58.75	3682	4156	152.6
15: 40	45.52	59.03	3719	46.37	58.66	3673	4158	152.1
15: 45	46.27	58.68	3711	46.45	58.58	3670	4173	147.7
15: 50	46.46	58.53	3709	46.51	58.50	3665	4185	147.7
15: 55	46.36	58.55	3702	46.58	58.41	3665	4200	142.3
16: 00	46.39	58.48	3699	46.65	58.31	3665	4207	142.5
16: 05	46.05	58.71	3693	46.70	58.24	3666	4204	139.0
16: 10	46.67	58.21	3688	46.75	58.15	3667	4209	139.8
16: 15	46.16	58.56	3686	46.80	58.07	3667	4203	137.0
16: 20	46.13	58.54	3684	46.87	57.97	3665	4216	136.8
16: 25	46.64	58.12	3681	46.93	57.89	3666	4220	136.2
16: 30	46.77	57.97	3677	46.98	57.80	3665	4224	136.3
16: 35	46.40	58.26	3674	47.03	57.71	3661	4225	133.8
16: 40	46.84	57.84	3654	47.08	57.63	3663	4223	132.8

DT-4

Time	Camera			Ship			Cable	Bearing
	Lat (°N)	Lon (°E)	Depth (m)	Lat (°N)	Lon (°E)	Depth (m)	(m)	(°CW)
9: 55	38.60	31.50	3482	38.60	31.50	3559	3695	*
10: 05	38.90	31.35	3536	38.48	31.51	3575	3795	335.8
10: 10	38.68	31.44	3559	38.41	31.53	3582	3824	337.5
10: 15	38.80	31.40	3561	38.33	31.57	3567	3843	336.5
10: 20	38.71	31.40	3563	38.24	31.58	3600	3856	335.1
10: 25	38.57	31.48	3564	38.14	31.60	3603	3876	341.4
10: 30	38.06	31.62	3569	38.06	31.62	3609	3890	*
10: 35	38.28	31.57	3572	37.99	31.63	3621	3902	346.0
10: 40	38.50	31.51	3578	37.92	31.63	3633	3901	345.7
10: 45	38.44	31.51	3580	37.86	31.63	3649	3903	345.9
10: 50	38.12	31.59	3592	37.77	31.63	3634	3923	351.9
10: 55	38.30	31.55	3603	37.69	31.64	3654	3948	350.1
11: 00	37.80	31.62	3617	37.61	31.65	3662	3967	347.9
11: 05	37.63	31.65	3622	37.54	31.66	3674	3676	350.3
11: 10	38.10	31.58	3622	37.47	31.68	3680	3980	348.8
11: 15	38.04	31.58	3625	37.39	31.73	3667	3992	344.0
11: 20	37.97	31.62	3629	37.32	31.74	3672	3992	348.0
11: 25	37.91	31.61	3633	37.27	31.70	3693	3983	350.3
11: 30	37.82	31.64	3643	37.22	31.69	3685	3975	354.5
11: 35	37.20	31.65	3653	37.16	31.65	3699	3982	357.7
11: 40	37.28	31.64	3658	37.11	31.65	3705	3980	356.3
11: 45	37.61	31.75	3661	37.05	31.65	3710	3985	372.7
11: 50	37.27	31.71	3671	36.98	31.65	3716	3991	373.9
11: 55	37.47	31.63	3677	36.91	31.64	3711	3998	359.3
12: 00	37.43	31.66	3685	36.85	31.67	3724	4001	358.9
12: 05	37.20	31.65	3690	36.79	31.67	3758	4007	356.9
12: 10	37.08	31.67	3695	36.72	31.69	3784	4017	356.1
12: 15	36.69	31.68	3700	36.65	31.69	3795	4025	341.8
12: 20	36.77	31.69	3708	36.58	31.69	3792	4032	359.0
12: 25	36.73	31.68	3718	36.51	31.70	3790	4047	354.6
12: 30	36.70	31.70	3718	36.45	31.71	3797	4052	356.3
12: 35	37.02	31.69	3714	36.40	31.72	3803	4057	357.0
12: 40	36.86	31.69	3717	36.32	31.75	3806	4067	352.3
12: 45	36.58	31.74	3726	36.23	31.77	3814	4080	354.2
12: 50	36.84	31.71	3742	36.15	31.78	3816	4111	353.4
12: 55	36.76	31.73	3778	36.07	31.80	3821	4150	352.6
13: 00	36.66	31.74	3799	35.99	31.83	3827	4182	351.0
13: 05	36.59	32.01	3799	35.93	31.85	3830	4187	376.4
13: 10	36.37	31.94	3800	35.85	31.89	3841	4203	366.4
13: 15	36.00	31.89	3806	35.77	31.92	3850	4218	350.0
13: 20	36.38	31.82	3810	35.69	31.94	3853	4218	348.6
13: 25	36.35	31.84	3813	35.63	31.97	3861	4222	347.7
13: 30	36.27	31.86	3816	35.55	32.00	3865	4232	346.7
13: 35	36.16	31.89	3821	35.48	32.03	3866	4240	346.3
13: 40	36.16	31.91	3822	35.43	32.07	3869	4234	344.9
13: 45	36.08	31.93	3823	35.38	32.09	3873	4224	344.6
13: 50	36.00	31.93	3831	35.32	32.10	3876	4225	343.4
13: 55	35.25	32.13	3838	35.25	32.13	3877	4237	*
14: 00	35.88	31.99	3846	35.17	32.17	3880	4253	343.2
14: 05	35.83	32.16	3855	35.09	32.19	3877	4267	357.3
14: 10	35.71	32.03	3859	35.07	32.22	3879	4240	340.2
14: 15	35.14	32.26	3864	35.14	32.26	3878	4185	*
14: 20	35.62	32.11	3868	35.18	32.32	3876	4167	329.6

DT-5

Time	Camera			Ship			Cable	Bearing
	Lat (°N)	Lon (°E)	Depth (m)	Lat (°N)	Lon (°E)	Depth (m)	(m)	(°CW)
14: 25	35.21	32.07	3880	35.23	32.46	3870	4167	267.5
14: 30	35.24	32.17	3881	35.31	32.57	3866	4179	262.1
14: 35	35.39	32.66	*	35.39	32.66	3858	4167	*
14: 40	35.46	32.75	*	35.46	32.75	3841	4179	*
14: 45	35.53	32.85	3883	35.53	32.85	3810	4203	*
14: 50	35.59	32.97	3882	35.59	32.97	3800	4229	*
14: 55	35.40	32.56	3879	35.63	33.06	3791	4244	248.9
15: 00	35.41	32.63	3878	35.67	33.14	3781	4248	247.0
15: 05	35.44	32.70	3881	35.72	33.22	3765	4267	245.5
15: 10	35.46	32.77	3873	35.77	33.30	3732	4231	243.8
15: 15	35.82	33.41	3869	35.82	33.41	3703	4298	*
15: 20	35.49	32.91	3859	35.86	33.51	3685	4310	243.0
15: 25	35.54	33.01	3841	35.89	33.60	3682	4304	243.8
15: 30	35.55	33.07	3828	35.91	33.68	3650	4292	243.6
15: 35	35.61	33.14	3815	35.94	33.77	3636	4291	246.2
15: 40	35.61	33.22	3811	35.99	33.83	3619	4291	242.6
15: 45	35.65	33.29	3812	36.07	33.90	3604	4303	240.1
15: 50	35.67	33.37	3797	36.12	33.99	3579	4305	238.8
15: 55	35.68	33.45	3781	36.18	34.09	3535	4312	237.1
16: 00	35.73	33.53	3742	36.22	34.18	3500	4307	238.0
16: 05	35.76	33.62	3738	36.28	34.26	3441	4307	235.9
16: 10	35.79	33.69	3719	36.47	34.31	3287	4368	227.5
16: 15	35.84	33.73	3701	36.56	34.33	3201	4342	225.2
16: 20	35.88	33.82	3704	36.63	34.35	3146	4324	220.2

DT-6

Time	Camera			Ship			Cable	Bearing
	Lat (°N)	Lon (°E)	Depth (m)	Lat (°N)	Lon (°E)	Depth (m)	(m)	(°CW)
16: 25	36.70	34.38	3660	36.70	34.38	3083	4272	*
16: 30	35.97	33.91	3632	36.77	34.36	3017	4219	213.9
16: 35	36.04	33.97	3607	36.84	34.35	2969	4166	209.4
16: 40	36.11	34.05	3607	36.91	34.36	2941	4153	205.1
16: 45	36.33	34.12	3542	36.97	34.36	2909	*	204.3
16: 50	36.24	34.12	3481	37.01	34.38	2890	3969	201.9
16: 55	36.34	34.15	3411	37.04	34.39	2880	3858	202.5
17: 00	36.43	34.18	3332	37.06	34.42	2875	3721	204.4
17: 05	37.09	34.44	3263	37.09	34.44	2839	3627	*
17: 10	36.58	34.27	3197	37.13	34.43	2834	3528	199.6
17: 15	36.66	34.29	3122	37.18	34.43	2823	3430	197.9
17: 20	36.75	34.36	3040	37.22	34.44	2797	3329	192.0
17: 25	36.75	34.41	3011	37.25	34.44	2790	3285	184.5
17: 30	36.87	34.18	2778	37.29	34.43	2756	3224	215.8
17: 35	37.33	34.45	*	37.33	34.45	2737	*	*
17: 45	37.06	34.43	2891	37.41	34.45	2713	3105	184.2
17: 50	37.11	34.43	2859	37.46	34.44	2713	3070	182.9
17: 55	37.16	34.44	2837	37.51	34.44	2717	3045	180.2
18: 00	37.21	34.45	2805	37.54	34.45	2727	3009	179.7
18: 05	37.27	34.43	2774	37.58	34.44	2739	2971	182.0
18: 10	37.36	34.44	2750	37.61	34.44	2754	2938	179.5

DT-7

Time	Camera			Ship			Cable	Bearing
	Lat (°N)	Lon (°E)	Depth (m)	Lat (°N)	Lon (°E)	Depth (m)	(m)	(°CW)
9: 48	37.69	54.99	3518	37.72	54.80	4026	3700	96.9
10: 00	37.72	54.87	3974	37.83	54.64	4023	4200	111.9
10: 10	37.74	54.77	4039	37.96	54.51	4026	4026	124.7
10: 20	37.81	54.72	4038	38.13	54.47	3967	3967	136.4
10: 30	37.94	54.63	4040	38.24	54.41	3898	3898	138.2
10: 40	38.12	54.46	4040	38.33	54.32	3822	3822	142.7
10: 50	38.33	54.37	4038	38.45	54.30	3785	3785	145.9
11: 00	38.16	54.47	3986	38.53	54.25	3772	3772	145.3
11: 10	38.25	54.39	3928	38.65	54.16	3763	3763	144.9
11: 20	38.70	54.14	3843	38.80	54.10	3771	3771	154.3
11: 30	38.44	54.27	3790	38.93	54.06	3787	3787	152.6
11: 40	38.56	54.21	3777	39.07	53.98	3779	3779	151.7
11: 50	38.92	54.00	3785	39.18	53.88	3745	3745	150.2
12: 00	38.78	54.10	3764	39.31	53.79	3735	3735	144.9
12: 10	39.37	53.77	3770	39.44	53.71	3751	3751	133.4
12: 20	39.01	53.95	3789	39.59	53.65	3687	3687	148.0
12: 30	39.10	53.89	3756	39.73	53.61	3671	3671	152.3
12: 40	39.24	53.80	3743	39.90	53.52	3673	3673	152.9
12: 50	39.33	53.84	3729	40.07	53.56	3688	3688	155.8
13: 00	39.49	53.69	3738	40.22	53.40	3635	3635	154.3
13: 10	39.63	53.62	3689	40.41	53.34	3538	3538	156.5
13: 20	39.89	53.53	3675	40.57	53.27	3475	3475	155.2
13: 30	40.01	53.47	3682	40.67	53.21	3407	3407	155.1
13: 40	40.21	53.38	3692	40.81	53.14	3317	3317	154.5
13: 50	40.20	53.36	3672	40.96	53.07	3302	3302	155.0
14: 00	40.36	53.30	3570	41.14	53.00	3339	3339	154.9
14: 10	41.12	53.00	3503	41.31	52.93	3381	3381	154.9
14: 20	40.70	53.17	3398	41.47	52.85	3418	3418	153.3
14: 30	40.87	53.09	3301	41.60	52.77	3460	3460	152.2
14: 40	41.47	52.81	3300	41.73	52.69	3471	3471	150.7
14: 50	41.26	52.90	3336	41.87	52.61	3483	3483	150.6
15: 00	41.33	52.87	3372	42.01	52.54	3490	3490	150.2
15: 10	41.97	52.60	3401	42.16	52.51	3494	3494	151.2
15: 20	41.85	52.64	3442	42.28	52.45	3501	3501	152.0
15: 30	42.12	52.48	3469	42.39	52.35	3506	3506	150.0
15: 40	41.91	52.58	3481	42.52	52.25	3507	3507	147.3
15: 50	42.40	52.30	3488	42.66	52.18	3510	3510	149.9
16: 00	42.78	52.11	3497	42.79	52.11	3522	3522	146.3
16: 10	42.33	52.33	3502	42.94	52.03	3511	3511	149.3
16: 20	42.46	52.26	3508	43.10	51.96	3432	3432	150.7
16: 30	42.98	52.01	3508	43.24	51.89	3394	3394	151.8
16: 40	42.98	51.93	3512	43.30	51.79	3343	3343	151.9
16: 50	42.92	51.98	3524	43.53	51.70	3237	3237	151.3
17: 00	43.02	51.92	3493	43.67	51.64	3183	3183	152.4

DT-8

Time	Sonar			Ship			Cable	Bearing
	Lat (°N)	Lon (°E)	Depth (m)	Lat (°N)	Lon (°E)	Depth (m)	(m)	(°CW)
10: 30	38.64	51.15	2861	39.05	51.26	3830	3060	197.6
10: 35	38.94	51.22	3065	39.11	51.26	3811	3270	196.5
10: 40	38.89	51.21	3268	39.17	51.27	3768	3461	195.2
10: 45	39.00	51.20	3363	39.25	51.26	3720	3670	195.3
10: 50	39.38	51.44	3363	39.38	51.44	3692	3870	*
10: 55	39.44	51.66	3362	39.44	51.66	3685	4040	*
11: 00	39.44	51.89	*	39.44	51.89	3718	4220	*
11: 05	39.08	51.44	3728	39.49	52.01	3689	4291	238.8
11: 10	39.11	51.43	3362	39.52	51.91	3673	4150	234.2
11: 15	39.14	51.47	3363	39.53	51.82	3646	4050	227.4
11: 20	39.16	51.48	3650	39.52	51.74	3641	3976	221.4
11: 25	39.21	51.50	3609	39.64	51.71	3574	3920	210.2
11: 30	39.25	51.52	3577	39.77	51.74	3502	3950	207.3
11: 35	39.75	51.98	3570	39.75	51.98	3565	3975	*
11: 40	39.64	52.00	*	39.64	52.00	3626	3935	.*
11: 45	39.47	51.73	3346	39.62	52.19	3685	3931	254.4
11: 50	39.54	51.81	3494	39.56	52.27	3699	3897	268.4
11: 55	39.54	51.86	3404	39.51	52.28	3706	3873	273.0
12: 00	39.56	51.90	3505	39.47	52.28	3708	3824	280.8
12: 05	39.53	51.92	3513	39.42	52.28	3718	3796	284.8
12: 10	39.52	52.02	3507	39.36	52.35	3715	3778	291.6
12: 15	39.51	52.09	3528	39.30	52.42	3704	3810	298.3
12: 20	39.49	52.14	3556	39.25	52.47	3700	3854	301.2
12: 25	39.49	52.20	3574	39.22	52.50	3703	3865	307.2
12: 30	39.47	52.23	3572	39.20	52.49	3705	3838	310.8
12: 35	39.43	52.25	3582	39.14	52.43	3721	3830	323.2
12: 40	39.41	52.31	3581	39.07	52.43	3722	3830	337.0
12: 45	39.36	52.32	3579	38.99	52.42	3738	3837	342.0
12: 50	39.29	52.34	3586	38.91	52.43	3769	3848	344.7
12: 55	39.24	52.41	3580	38.82	52.49	3813	3859	347.4
13: 00	39.17	52.41	3580	38.73	52.51	3847	3872	344.6
13: 05	39.13	52.44	3579	38.61	52.57	3876	3920	343.2
13: 10	39.07	52.48	3579	38.48	52.67	3919	3998	338.8
13: 15	39.02	52.51	3592	38.40	52.74	3926	4040	336.0
13: 20	38.96	52.56	3616	38.29	52.82	3912	4086	335.2
13: 25	38.94	52.60	3623	38.19	52.87	3911	4155	336.7
13: 30	38.84	52.65	3678	38.06	52.86	3936	4211	342.3
13: 35	38.79	52.65	3702	38.02	52.84	3947	4212	343.5
13: 40	38.76	52.68	3686	37.97	52.83	3975	4206	347.1
13: 45	38.70	52.69	3699	37.89	52.81	4008	4204	350.3
13: 50	38.62	52.72	3740	37.79	52.81	4006	4272	353.0
13: 55	38.54	52.73	3773	37.70	52.81	4003	4307	353.4
14: 00	38.46	52.74	3779	37.61	52.83	4003	4325	352.5
14: 05	38.35	52.80	3945	37.52	52.89	4019	4348	352.3
14: 10	37.54	53.03	*	37.54	53.03	4010	4300	*
14: 15	38.14	52.87	3979	37.61	53.18	4017	4228	324.8
14: 20	38.18	52.99	3786	37.71	53.33	4019	4186	318.8
14: 25	38.11	53.05	3770	37.82	53.47	4024	4188	299.9
14: 30	38.06	53.14	3795	37.97	53.64	3997	4220	278.5

DT-9

Time	Sonar			Ship			Cable	Bearing
	Lat (°N)	Lon (°E)	Depth (m)	Lat (°N)	Lon (°E)	Depth (m)	(m)	(°CW)
14: 30	38.06	53.14	3795	37.97	53.64	3997	4220	278.5
14: 35	38.03	53.23	3798	38.07	53.77	3893	4245	266.3
14: 40	38.05	53.37	3979	38.15	53.90	3901	4258	260.7
14: 45	38.01	53.42	4025	38.25	53.99	3837	4284	250.4
14: 50	38.00	53.51	3710	38.38	54.19	3802	4353	245.3
14: 55	38.05	53.67	3932	38.37	54.42	3831	4514	250.3
15: 00	38.05	53.74	3703	38.41	54.62	3832	4570	251.4
15: 05	38.09	53.90	3600	38.51	54.83	3842	4583	249.2
15: 10	38.12	54.01	3546	38.60	55.00	3827	4583	248.0
15: 15	38.21	54.08	3605	38.64	55.08	3809	4583	250.2
15: 20	38.24	54.21	3688	38.59	55.16	3841	4583	252.9
15: 25	38.28	54.23	3689	38.55	55.14	3871	4447	256.1
15: 30	38.36	54.36	3644	38.55	55.20	3871	4366	259.3
15: 35	38.37	54.45	3652	38.58	55.32	3866	4359	258.4
15: 40	38.37	54.55	3643	38.62	55.42	3856	4371	256.7
15: 45	38.41	54.67	3638	38.67	55.54	3857	4356	256.2
15: 50	38.47	54.80	3799	38.69	55.62	3860	4356	257.3
15: 55	38.47	54.93	3797	38.70	55.73	3864	4345	256.7
16: 00	38.52	55.02	3784	38.73	55.82	3863	4331	257.9
16: 05	38.55	55.12	3779	38.73	55.90	3863	4316	259.3
16: 10	38.59	55.22	3853	38.74	55.98	3866	4323	260.4
16: 15	38.62	55.34	3859	38.73	56.10	3863	4325	263.3
16: 20	38.64	55.45	3868	38.76	56.22	3853	4335	262.8
16: 25	38.66	55.59	3887	38.81	56.35	3843	4361	260.4
16: 30	38.62	55.63	3702	38.82	56.43	3844	4364	258.4
16: 35	38.73	55.76	3887	38.85	56.54	3854	4369	262.9
16: 40	38.72	55.89	3851	38.91	56.64	3863	4337	258.0
16: 45	38.75	55.93	3871	38.92	56.65	3864	4314	258.8
16: 50	38.76	56.04	3891	38.92	56.73	3890	4300	259.1
16: 55	38.75	56.12	3752	38.90	56.81	3920	4274	260.0
17: 00	38.79	56.22	3729	38.90	56.92	3914	4256	262.4

DT-10

Time	Camera			Ship			Cable	Bearing
	Lat (°N)	Lon (°E)	Depth (m)	Lat (°N)	Lon (°E)	Depth (m)	(m)	(°CW)
10: 20	42.30	52.20	3499	42.60	52.10	3512	3718	166.4
10: 34	42.40	52.15	3502	42.73	52.00	3522	3769	163.4
10: 40	42.40	52.15	3502	42.73	52.00	3522	3735	163.4
10: 49	42.58	52.06	3510	42.94	51.88	3510	3751	156.4
11: 00	42.59	51.98	2513	43.00	51.86	3466	3764	212.5
11: 10	42.69	51.92	3514	43.13	51.84	3400	3781	171.2
11: 21	42.79	51.85	3509	43.25	51.72	3348	3785	166.4
11: 30	42.80	51.90	3509	43.20	51.70	3348	3795	116.4
11: 40	42.96	51.74	3393	43.44	51.64	3274	3666	169.6
11: 49	43.09	51.70	3340	43.48	51.63	3256	3575	171.0
11: 58	43.20	51.64	3324	43.50	51.67	3233	3524	181.9
12: 09	43.34	51.62	3281	43.67	51.57	3141	3501	176.6
12: 20	43.67	51.57	3281	43.67	51.57	3141	3508	166.5
12: 30	43.45	51.61	3234	43.91	51.45	2971	3509	164.9
12: 39	43.55	51.62	3158	44.18	51.36	2942	3513	160.8
12: 50	43.68	51.52	3144	44.31	51.30	2907	3058	164.0
13: 00	43.78	51.41	3073	44.36	51.28	2914	3370	165.8
13: 10	43.98	51.44	2961	44.66	51.22	2944	3369	167.2
13: 19	44.17	51.44	2937	44.83	51.13	2897	3368	157.6
13: 30	44.27	51.40	2937	44.93	51.09	2847	3402	157.6
13: 39	44.44	51.32	2935	45.16	50.98	2624	3408	160.3
13: 50	44.63	51.24	2945	45.37	50.91	2624	3471	159.7
14: 00	44.90	51.23	2951	45.44	50.89	2624	3468	158.6
14: 10	44.90	51.12	2808	45.76	50.71	2822	3412	158.2
14: 16	45.08	51.03	2548	45.86	50.68	2822	3129	159.3
14: 30	45.20	50.81	2505	45.95	50.47	3069	2960	159.3
14: 40	45.48	50.88	2427	46.20	50.65	2243	2897	165.1
14: 49	45.77	50.81	2368	46.41	50.52	2243	2832	159.6
14: 59	45.93	50.74	2345	46.55	50.47	2243	2757	160.2
15: 10	46.01	50.75	2340	46.56	50.42	2243	2673	158.4
15: 20	46.25	50.62	2321	46.70	50.33	2243	2609	150.9
15: 29	46.44	50.50	2301	46.83	50.25	2243	2555	151.9
15: 40	46.49	50.46	2290	46.88	50.17	2243	2548	148.0
15: 52	46.71	50.27	2242	47.17	49.97	2243	9999	150.2
16: 04	46.94	50.12	2222	47.35	49.85	2243	2518	164.7
16: 11	47.02	50.07	2249	47.44	49.79	2243	2535	149.8
16: 20	47.13	50.01	2252	47.58	49.72	2243	2551	150.4
16: 30	47.29	49.98	2173	47.76	49.61	2243	2486	148.2
16: 40	47.44	49.81	2150	47.98	49.53	2243	2511	156.2
16: 50	47.58	49.73	2107	48.19	49.43	2243	2528	157.6
17: 00	47.76	49.64	2095	48.53	49.34	2243	2655	162.3
17: 09	47.93	49.56	2166	48.78	49.33	2243	2806	167.4
17: 20	48.12	49.48	2327	49.00	49.34	2243	2974	172.9
17: 30	48.20	49.47	2353	49.08	49.32	2243	2924	172.4
17: 40	48.53	49.38	2304	49.30	49.18	2243	2839	167.5
17: 50	48.75	49.34	2314	49.47	49.13	2243	2802	166.8
18: 00	48.90	49.29	2332	49.58	49.08	2243	2784	166.2
18: 11	49.30	49.17	1692	49.79	48.66	2449	*	140.1
18: 24	49.78	48.42	655	49.78	47.71	2533	*	91.1
18: 56	49.62	46.72	0	49.62	46.72	2584	0	*

DT-11

Time	Camera			Ship			Cable	Bearing
	Lat (°N)	Lon (°E)	Depth (m)	Lat (°N)	Lon (°E)	Depth (m)	(m)	(°CW)
9: 50	17.44	5.17	3166	17.95	5.39	3613	3520	226.5
9: 59	17.52	5.21	3563	17.89	5.44	3655	3800	208.6
10: 13	17.60	5.27	3704	18.08	5.48	3600	4003	*
10: 30	17.80	5.31	3654	18.05	5.73	3677	3929	234.0
10: 37	17.87	5.43	3649	18.05	5.85	3708	3929	242.0
10: 47	17.92	5.47	3653	18.06	5.99	3737	3921	250.0
10: 55	17.94	5.55	3665	18.07	6.12	3746	3946	254.0
11: 11	18.00	5.75	3712	18.08	6.34	3804	4002	261.0
11: 22	17.98	5.89	3741	18.04	6.42	3845	4020	263.0
11: 29	18.06	6.54	*	18.06	6.54	3882	4020	*
11: 37	18.02	6.07	3772	18.05	6.72	3931	4082	267.0
11: 50	18.00	6.81	3805	18.01	7.03	4035	9999	200.0
12: 06	18.01	6.79	3878	17.98	7.26	4046	4300	273.4
12: 10	18.00	6.85	3878	17.98	7.33	4048	4304	273.4
12: 14	17.99	6.56	3900	17.99	7.40	4048	4320	270.0
12: 16	17.99	6.60	3926	17.99	7.44	4049	4342	268.9
12: 10	17.99	6.57	3929	17.99	7.44	4047	4352	270.0
12: 20	18.00	6.59	3927	17.99	7.50	4049	4357	269.9
12: 23	18.01	6.63	3930	17.99	7.55	4050	4342	269.6
12: 29	17.99	6.75	3976	17.99	7.65	4049	4430	273.0
12: 41	18.01	6.93	3996	17.99	7.89	4044	4460	271.0
12: 43	17.99	6.90	3997	18.00	7.91	4044	4460	267.0
12: 46	17.99	7.01	4003	18.04	7.94	4043	4460	268.0
12: 50	17.99	7.05	4002	18.08	8.01	4043	4460	264.3
12: 55	18.00	7.11	3999	18.09	8.12	4044	4460	263.0
13: 01	18.01	7.21	3990	18.13	8.20	4044	4465	261.0

DT-12

Time	Camera			Ship			Cable	Bearing
	Lat (°N)	Lon (°E)	Depth (m)	Lat (°N)	Lon (°E)	Depth (m)	(m)	(°CW)
13: 11	18.02	7.39	3919	18.30	8.45	4047	4465	252.0
13: 12	18.02	7.45	3901	18.33	8.48	4047	4465	250.0
13: 15	18.03	7.50	3837	18.43	8.58	4045	4460	246.0
13: 21	18.06	7.56	3734	18.58	8.75	4046	4466	242.0
13: 25	18.09	7.65	3645	18.69	8.89	4019	4466	240.1
13: 31	18.11	7.74	3567	18.81	9.03	3980	4466	238.0
13: 36	18.16	7.83	3571	18.87	9.10	4006	4466	235.0
13: 41	18.23	7.94	3658	18.88	9.12	3998	4465	236.0
13: 46	18.24	7.99	3738	18.88	9.12	3993	4466	235.0
13: 50	18.30	8.10	3808	18.89	9.14	4002	4466	235.0
14: 02	18.41	8.27	3958	18.89	9.16	4011	4466	236.0
14: 10	18.65	8.43	4040	18.91	9.18	4025	4466	236.0
14: 19	18.65	8.60	4060	18.97	9.24	4041	4460	235.3
14: 28	18.66	8.70	4061	19.12	9.40	4049	4474	232.0
14: 31	18.70	8.76	4061	19.15	9.45	4048	4474	232.0
14: 31	18.70	8.76	4061	19.15	9.45	4048	4474	232.0
14: 37	18.74	8.80	4061	19.19	9.50	4048	4474	232.0
14: 38	18.73	8.78	4060	19.20	9.50	4048	4485	232.0
14: 42	18.79	8.89	3966	19.24	9.55	4049	4374	231.0
14: 44	18.79	8.91	3967	19.25	9.57	4048	4374	230.0
14: 49	18.85	8.98	3968	19.28	9.60	4048	4353	230.0
14: 54	18.90	9.04	3997	19.32	9.63	4049	4345	226.0
15: 04	18.98	9.18	4063	19.36	9.72	4048	4379	230.0
15: 07	18.99	9.21	4061	19.37	9.74	4048	4390	230.0
15: 12	19.06	9.28	4061	19.39	9.79	4048	4374	323.0
15: 16	19.09	9.32	4062	19.43	9.85	4044	4373	231.0
15: 20	19.12	9.38	4061	19.47	9.90	4027	4373	230.0
15: 34	19.25	9.52	4060	19.67	10.07	3923	4407	227.0
15: 43	19.28	9.60	4063	19.76	10.18	3866	4427	225.0
15: 59	19.43	9.80	4062	19.88	10.31	3794	4401	224.0
16: 00	19.83	9.81	4061	19.89	10.31	3780	4395	224.7
16: 05	19.52	9.89	3980	19.94	10.40	3742	4302	224.9
16: 10	19.58	9.96	3777	20.04	10.54	3669	4200	227.0

5.4 Discussion and Comments

5.4.1 Discussion (1)

Jacques Boulegue

Several geological settings have been investigated during the R/V Hakuho-Maru cruise KH89-1 at the Kaiko Nankai sites. The accretionary wedge was studied at basal thrust location in the Nankai Trough and immediatly at the East of the mouth of Tenryu Canyon. Upper thrust and fold were also surveyed in the Nankai areas, as well as mud mounds in this same area. In the Zenisu area the basal thrust and a mud volcano were surveyed.

One main result of these surveys is that the clam colonies, and hence inferred deep fluid expulsion, are mostly located in the basal thrust areas, where deformation is younger and where mud slide has had few opportunities of blocking the plumbery. This result helps us generalize the observation made during the Kaiko project. The apex area of fold or its vicinity are also good candidate for fluid expulsion although the amount of observations is more limited.

Location of clam colonies

The largest densities of clam colonies, as well as those of more active aspect (based on black mud surrounding the colony or on shiny white carbonate patches as in Tenryu Canyon) are located in the younger basal thrust areas. This observation is sustained by the dives made in the area of the mouth of Tenryu Canyon and in the Nankai Trough area, east of Tenryu. This observation signifies that the expulsion of nutrient bearing fluid is related in the same way to the pressure head in the decollement plane and the overburden of the sediment. Fluid expulsion seems to be well defined only where the sediment cover is small enough so as to allow upwelling of fluid along the fault.

The majority of the clam colonies are roughly round shaped. This can be related to cylindrical conduit driving the fluid flow, at least in the upper part of the sedimentary column. This observation is in agreement with similar observations on different types of hydrothermal systems. Pervasive expulsion of nutrient bearing fluids seems to be limited. This can be due to the fact that upon contact with the recent organic matter rich upper layer of sediment, bacterial activity will allow oxidation of methane and carbonate deposition. Then the top mud is indurated and

fluid expulsion is prevented, but at places where fracturing will occur, or where the fluid flux is focused.

Clam colonies have also been observed near the apex of a fold in the east of the Nankai area. There intense induration of mud and possibly chimney-like edifice are also observed. This fold is located at about 2000 m depth, well above the CCD. The different expression of fluid expulsion and the presevation of external features such as indurated mudstone blocks and chimny should be related to this location above CCD, which was not the case in the colonies found near the basal thrust (3000 - 4000 m depth). The finding of calm colonies on top of fold well within the wedge shows that this fold is also related to deep plane structure where it can collect enough nutrient bearing fluid.

Observation on the mud mounds in the Nankai area

An almost E-W line patched by several round structure has been observed on the Sea Beam map (Hydrographic Deptartment Japan) of the Nankai area. This direction is not along the local thrust direction (about N 60) or perpendicular to it (N 330). It is rather on a secondary deformation direction.

Only the most eastern structure seems to have developed in a bimodal fashion with two mounds aligned parallel to the direction of the thrust. This general setting suggests that this round structure, that we call mud mounds, should not be related to deep structures or to the main direction of deformation.

The deep-towed observations done on two of these mounds did not show clam activity. The mounds were covered by recent mud. Some of the observations on the slope of the eastern mound showed steep slope and well indurated mudstone. On the slope of the western mound (the first one observed) there was a good density of white filamentous biological structures (sponges); similar biological structures were observed in inactive areas of mud volcanos off Barbados accretionary wedge.

That fluid expulsion has happened at the location of the mud mounds is probable. Their height above the sea floor can only be sustained if connected to some pressure head in the underlying parent mud layer. Methane oxidation may then have led to induration of the mounds.

On the first (western) mud mound, the mud also showed, at the western foot and on top of the structure, very disturbed mud similar to what was observed in the eye of the mud volcano off Barbados (see LePichon et al., 1989). This may be emission centers of the mud. They were covered by more recent pelagic mud, which confirms that mud activity on this mound is probably not active any more.

Observations on the induration of mud

Underneath a small layer of recent pelagic mud, the mud appears to be well consolidated even off active venting areas or off the most active wedge areas. This can be explained by expulsion of pore waters due to the general compaction of the sediment. Pore waters in this area (based on results from Kaiko dives) are enriched in alkalinity, dissolved silica and manganese.

Upon ascent they will arrive at a level where oxygen as well as higher pH is available due to limited diagenesis of organic matter. These conditions can be found in the very top of the sedimentary column. Contact of pore water with this chemical front will yield cementation of the sediment by deposition of calcium carbonate and the apex layer of the indurated mud dissolved Mn will be enriched in MnO_2 due to oxidation of Mn^{2+} . Silica may eventually precipitate although the pH increase at the chemical front is not favorable to such eventuality.

There should be some relation between the extent of this consolidation of the mud and the extent of pore fluid advection as controled by compression and sediment overburden. Such a relation should be used to map these areas based on the deep-towed observations.

Comments on observations made in the Zenisu area

Three different types of area have been observed

(i) the accretionary wedge at the level of the second thrust of the Zenisu area

(ii) the sediment plain

(iii) a mud volcano located between the thrust and a seamount. This mud volcano was the one located during the first Kaiko cruise (1984).

The accretionary wedge above the second thrust have given the following observations: Consolidated mudstone with well developed MnO_2 patina. Some of the mudstone slabs show dissolution features which can be due to the fact that they are under the CCD. At places the bedding can be observed, the strike being quite variable, but mostly towards the slope when approaching the thrust. Pelagic mud covers most of the outcrops. At places pelagic mud seems to be mixed with whitish structures which can be either (i) debris or (ii) scopulate worms. The second possibility is more likely.

Thus, as found in other place like Nankai, the sediment wedge above the second thrust seems to be inactive. The extended induration of the mud shows that pore water should have been strongly expelled.

The sediment plain, which corresponds to the filling of a canyon, is composed of pelagic mud with numerous burrowings corresponding to the biological activity expected in organic rich mud.

The mud volcano is formed by a serial of sediment ledges compared of blocks of slighly indurated mud. The blocks are rounded at places and generally, except on steep scarp, are covered by pelagic mud. A simplified cross-cutting of the mud volcano done on its long axis is given in Fig. 5.4.1.

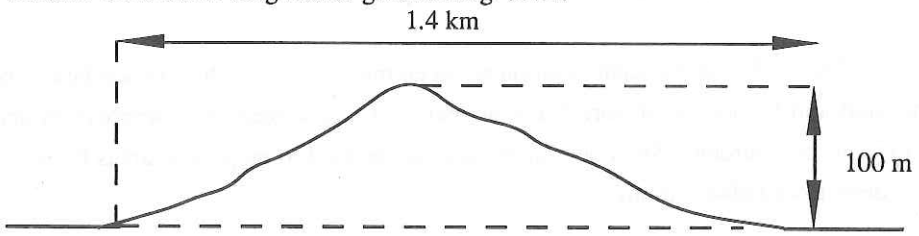

Fig. 5.4.1

Rather than a mud volcano, it should be described as a mud diapir or even as a mud ridge. Its emplacement should correspond to the uplifting of partly indurated mud in an overpressured area. The overall shape of the diapir is an ellipse at its foot level (long axis ≅1.4 km, short axis ≅ 0.7 km). The long axis is almost oriented N-45 which is about the same direction as the thrust 3 km off.

The steep scarp and the numerous boulders covered by pelagic mud evocates a single event of expulsion of mud, with blocks of partly indurated mud rounded by downslope gliding. No trace of life such as clams was found on the mud diapir.

This probably signifies that the overpressured sediment layers from which it is issued have no connection with a methane bearing layer or a decollement plane.

The mud diapir is well covered by pelagic mud, probably several centimeters in the flattest parts. This signifies that, although recent, this is not a young feature. Its age may be several thousands or ten thousands of years. Considering these results the Zenisu area survayed during this deep-towed does not constitute a target for Kaiko Nankai dive.

Conclusion

The deep-towed dives as well as the dive of the side scan sonar have provided good results which provides several targets for the Nankai dive

1) the thrust zone in and east of the mouth of of Tenryu Canyon.
2) The thrust zone in the Nankai trough area covered by the new seabeam map between Kaiko Box 5-1 and 5-2.

5.4.2 Discussion (2)

T. Iiyama

The present tectonic activities in Omaesaki, Tenryu, and Zenisu area are judged from submersible dives and the deep towed TV observation.

The presence of at least two (probably more) major thrusts trending NE-SW direction on the land side wall of the Nankai Trough was recognized during the campains of the Kaiko project (phase I, Sea beam and seismic prospection and phase II, submersible dives). Another two major trusts are present on the south-eastern slope of the Zenisu ridge. It was suggested that the Zenisu ridge was formed by the compressional tectonism in NW-SE direction partly still active at present days. The strongest proof was supplied by the finding during the submersible dives of the phase II of Kaiko project, of the calytogena communities on a narrow step of the south eastern wall of the Tenryu canyon near the estuary of the canyon and the Trough. A small community was observed also on the southern part of the Zenisu basin.

The second proof of the present tectonic activities was furnished by the absence of thick mud deposit except along the trench axis and areas supposed to become already in active.

It may be too early to judge the intensity of the present day tectonic activities in this area from observations covering still rather restricted sea bottom surface. It will however worth while to classify different observed sites according to the features descrived above.

The lowest stage of the accretionary prism of the trough is the most active sties. The Tenryu site 2 along the south eastern wall of the Tenryu wall and the lower part of the Omaezaki site are the examples of this strong active sites. Very frequent presence of the clam colonies, presence of blackish mud, hardened surface of mud cover are strong indication of the activities. The bottom of the Tenryu canyon is covered by a thick deposition of turbidites and the distribution of the colonies became rather scarce in spite of the fact that the canyon traverses the active thrust.

The 3rd strongly active sites may be the southern SSE side of Zenisu ridge. Because of the lack of turbiditic sediments in the deformed pelagic and semipelagic sediments, no sufficient nutrient is present in the venting water. And the

distribution of the clams communities became scarce in the Zenisu basin . The presence of talus deposits and sedimentary rock outcrops uncovered by the recent soft mud are indicative of this activities.

The upper part of the accretionary prisms and the northern part of the south eastern slope of the Zenisu ridge and the Zenisu basin seems to be no more active tectonically.

The presence of thick soft mud deposits, rounded shape of sedimentary rocks exposed and the trace of dissolution of them on the surface are indicative of the present day inactiveness. The presence of fractures, the mud diapirs observed during the campain in this sectors of the surveyed area are indicative presently but very active in the past.

A question remains however: why we could find calyptogena communities at the top of the accretionary prism (point N-1 of the section DT-1) of the off Omaezaki section.

It appears to be interesting to make a numbers of tentatives to determine the age of each deformation fronts of the accretionary prism of the region.

5.5. Summary

K. Kobayashi

Observation of microtopography, outcrops of solidified rocks, distinct color of bottom sediment and biological matters by JAMSTEC deep-towed TV installed on the R.V.Hakuho Maru during leg 2 of this cruise revealed seafloor expression of tectonic features along 200km long tracks across the deformation front and overlying the accretionary prism at the eastern Nankai Trough.

Composite 5 continuous TV lines were obtained by 10 tracks. A track along the frontal scarp provided a deep-towed side-scanning sonar. Two zones of active fluid venting, one at the spur of the Tenryu Canyon, the othre south off Omaezaki were found accompanied with dense bivalve *Calyptogena* colonies on he edge of the frontal thrust at depths of 3,850 to 3,750m. At the crest of fold most probably associated with back-thrust small bivalve communities formed by cold seepage were observed by TV and photographed by a camera. An increase in temperature amounting to 0.05°C was detected by a thermometer towed 3m above the chimney. Mud diapirs found in topographic map of the trough bottom as well as at Zenisu region were proved to be inactive, since no bivalves and color anomaly in sediment were seen around on the diapirs.

These observations helped us selecting the diving sites of French submersible *Nautile* immediately after the present cruise. At Shimizu City before departure of the tendure vessel Nadir the KAIKO-NANKAI scientists examined the photographs and video images taken by the deep-towed cameras very carefully in order to presurvey the proposed diving sites. Our decision was to abandon the revisit of the Tenryu bivalve site and to choose the Omaezaki site, since the latter has clear indication of extremely active venting, whereas the former colonies appear to be less widespread so that return to the exact point of 1985 observation may be difficult. Furthermore, the Omaezaki site has good places for study of back-thrust and diapirs in its adjacent locations. We recognized by the following 24 dives that this conclusion was correct. The French-Japanese KAIKO-NANKAI team owes much to the joint effort in this cruise under the auspices of JAMSTEC for the success in Nautile dives at the Nankai Trough.

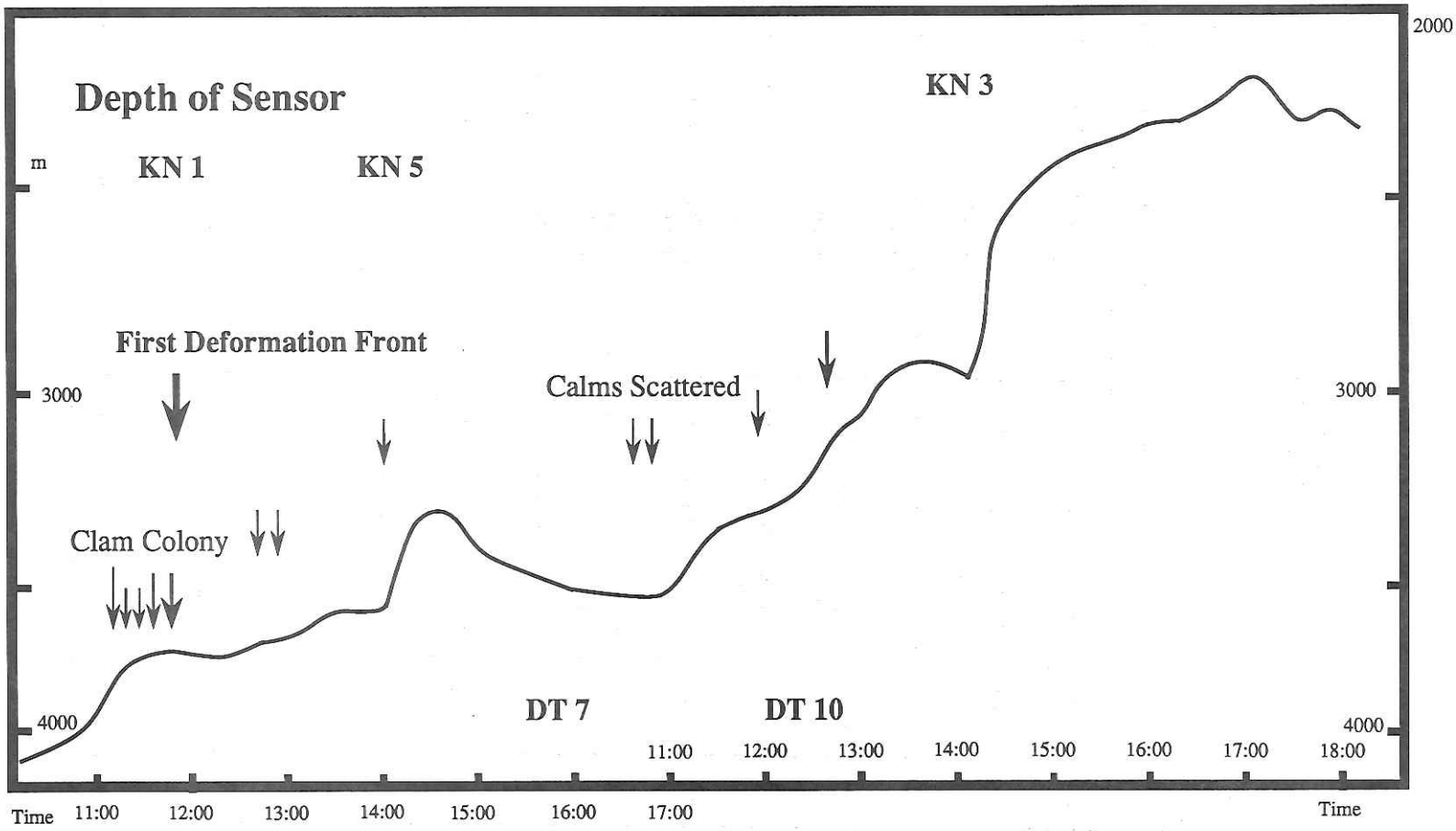
Depth of Sensor
m
KN 1
KN 5
KN 3
First Deformation Front
Calms Scattered
Clam Colony
3000
4000
2000
3000
4000
DT 7
DT 10
11:00
12:00
13:00
14:00
15:00
16:00
17:00
18:00
Time
11:00
12:00
13:00
14:00
15:00
16:00
17:00
Time

DEEP-TOWED SURVEY

R.V. HAKUHO MARU Cruise KH89-1
July 4, 1989 (Yokosuka) ~ July 13, 1989 (yokohama)
Eastern Nankai Trough [KAIKO-NANKAI Site]
by JAMSTEC Deep-Towed TV & Sonar

List of Tracks

DT	Date	Start Time	Start Position	Start Depth	Start Heading	End Time	End Position	End Depth	End Heading
1	05	9:48	33°49'N 137°54'E	2017m	258°	16:34	33°48'N 138°02'E	3678m	122°
2	06	10:01	33°45'N 137°55'E	3579m	86°	14:10	33°45'N 138°00'E	3711m	356°
3	06	14:10	33°45'N 138°00'E	3711m	356°	16:40	33°47'N 137°58'E	3663m	306°
4	07	9:40	33°39'N 137°31'E	3476m	138°	14:23	33°35'N 137°33'E	3876m	126°
5	07	14:23	33°35'N 137°33'E	3876m	40°	16:20	33°37'N 137°34'E	3146m	343°
6	07	16:20	33°37'N 137°34'E	3146m	334°	18:10	33°38'N 137°34'E	2754m	321°
7	08	10:04	33°39'N 137°34'E	4039m	261°	17:00	33°44'N 137°52'E	3493m	284°
8	09	11:35	33°40'N 137°52'E	3570m	171°	14:30	33°38'N 137°54'E	4024m	27°
9	09	14:30	33°38'N 137°54'E	4024m	334°	17:00	33°39'N 137°57'E	3984m	21°
10	10	10:19	33°43'N 137°52E	3499m	166°	18:00	33°50'N 137°49'E	2337m	276°
11	11	10:05	33°17'N 138°05'E	3723m	73°	12:36	33°18'N 138°08'E	3996m	60°
12	12	14:12	33°19'N 138°09'E	4041m	66°	16:03	33°20'N 138°19'E	3990m	67°

Shaded columns indicate survey by Deep-Towed Side-Scanning Sonar with only one limb on shallower side. The others are for TV camera.

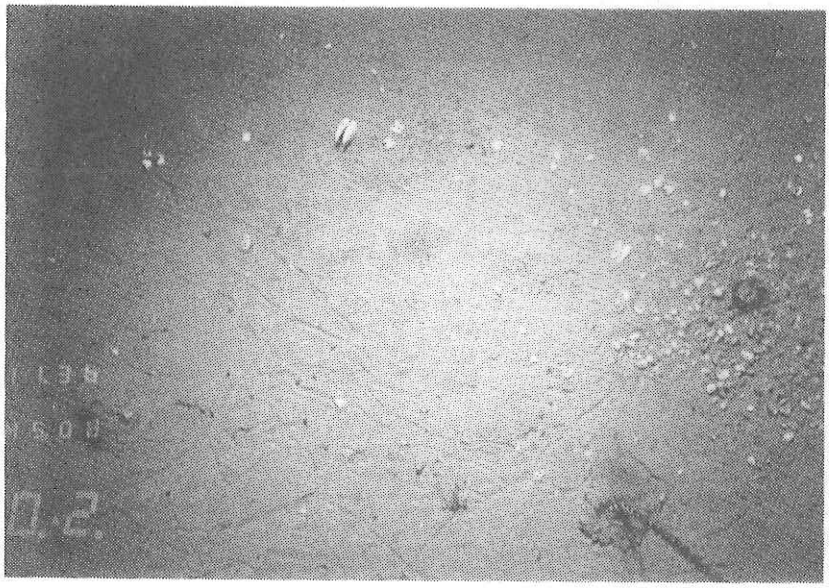

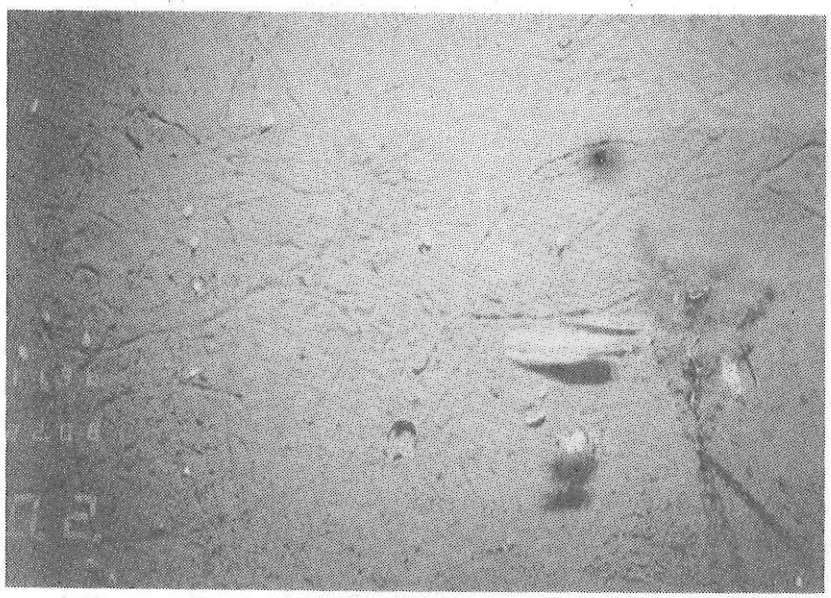

DT 7 Bivalve Colony

Edge of the crest of the 1st deformation front. July 8, 1989, 11:36. D=3783m

Above : Community of Calyptogena & othre animals.

Below : Large Calyptogena with trails on sediment.

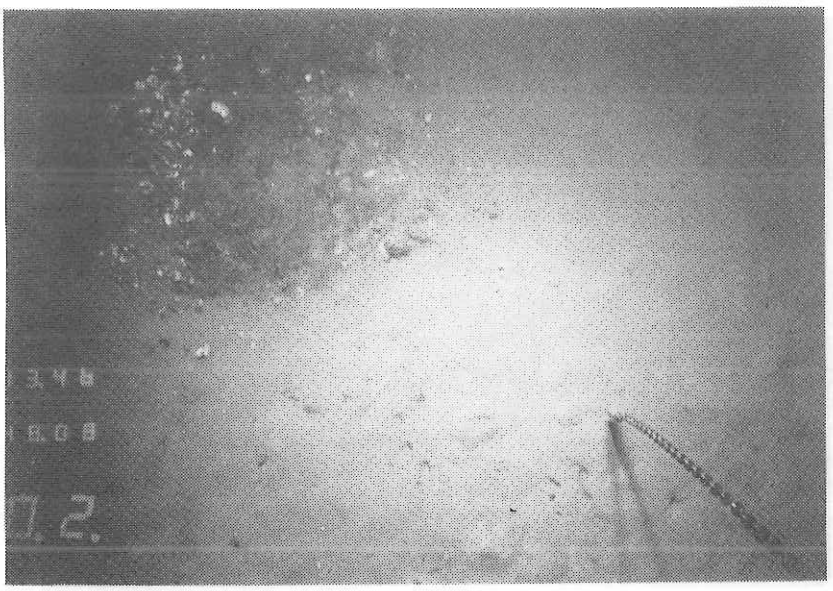

DT 7 Circular Colony of Dark Clams

Crest of the 1st deformation front. July 8, 1989, 13:46. D=3690m

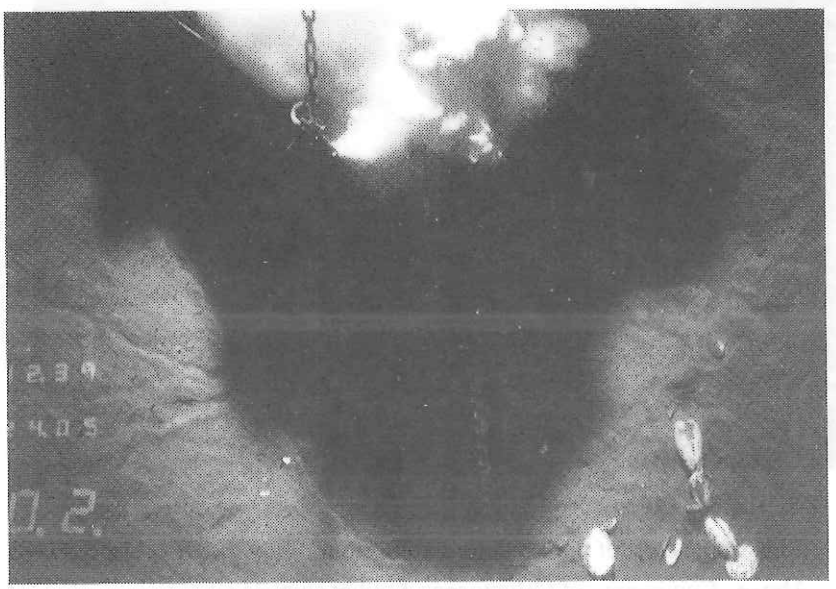

DT 1 Scattered Calytopogena

Flank of the upper "Ridge". July 5, 1989, 12:39. D=3317m

DT 7 Chimney of Cemented Sediment

Flank of deformation front. July 8, 1989, 11:10. D=3900m

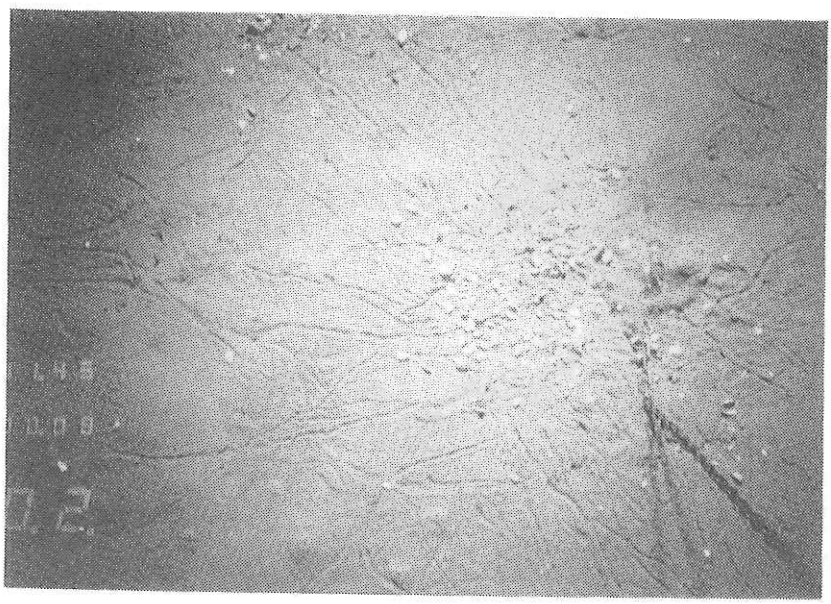

DT 7 Bivalve Colony

Edge of the crest of the 1st deformation front.

July 8, 1989, 11:45. D=3781m

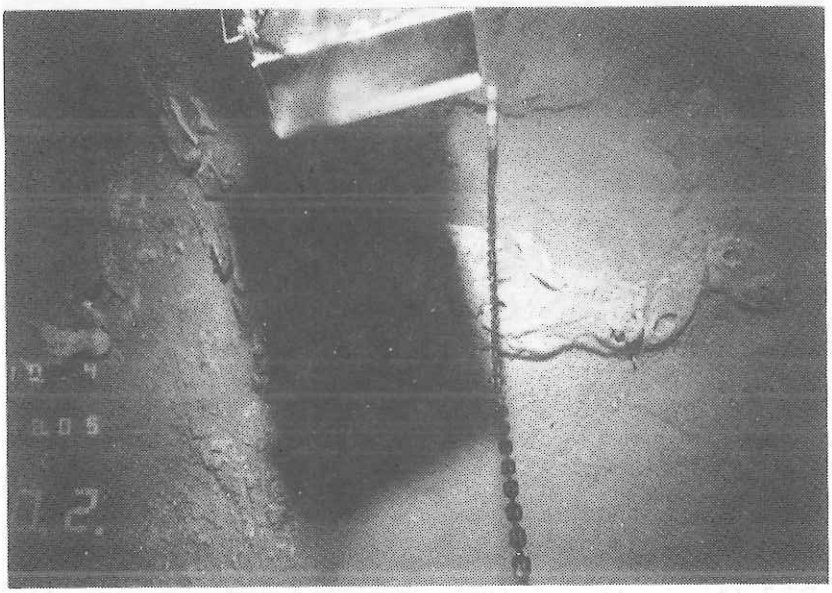

DT 1 Chimney of Cemented Sediment

Crest of the upper "Ridge". July 5, 1989, 10:29. D=2140m

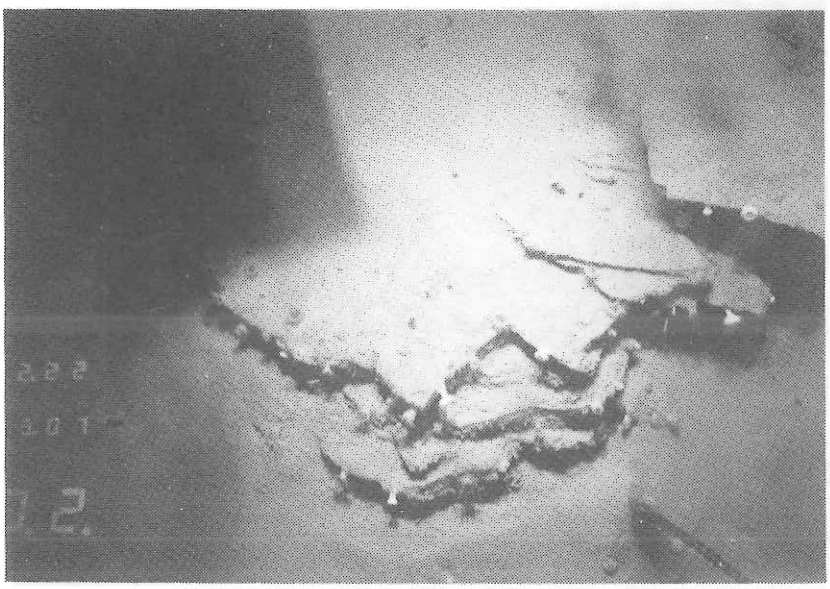

DT 4 Stratified Beds

On faulted scarp slope of the 1st deformation front.

July 7, 1989, 12:22. D=3710m